Proton conducting polymeric materials for hydrogen based electrochemical energy conversion technologies

Aili, David

Publication date:
2011

Document Version
Publisher's PDF, also known as Version of record

Technical University of Denmark

Proton Conducting Polymeric Materials for Hydrogen Based Electrochemical Energy Conversion Technologies

Ph.D. Thesis

David Aili

August 2011

"Water is the coal of the future."

Jules Verne
(1828-1905)

Proton conducting polymeric materials for hydrogen based electrochemical energy conversion technologies

Ph.D. Thesis by David Aili

Energy and Materials Science Group
Department of Chemistry
Technical University of Denmark

Supervisor:

Professor Niels J. Bjerrum

Co-supervisors:

Associate Professor Qingfeng Li
Senior Scientist Erik Christensen
Associate Professor Jens H. von Barner

Date of submission:

12th of August 2011

DTU Chemistry
Department of Chemistry

Abstract

Proton transport is one of the most fundamental phenomena in nature and it also plays key role in proton exchange membrane (PEM) fuel cells and water electrolyzers. Conventionally, a well hydrated membrane of perfluorosulfonic acid (PFSA) such as Nafion® (DuPont) is used as proton conductor and electrode separator in both PEM fuel cells and water electrolyzers. The proton conductivity mechanism of Nafion® is strongly dependent on the presence of water within the membrane nanostructure, which limits the operating temperature to about 80 °C unless the system is pressurized in order to keep the membrane well hydrated. However, some of the main issues of the conventional PFSA based PEM fuel cells and water electrolyzers are directly or indirectly related to their relatively low operating temperature. An elevated operating temperature results in better electrode kinetics in general and improved impurity tolerance of the catalysts, especially for the fuel cell anode. From a system engineering point of view it also allows for simplified cooling and water management and better possibilities for heat recovery. Furthermore, a higher operating temperature is strongly beneficial when the cell is operated in electrolysis mode since it results in a decreased thermodynamic energy requirement for the water splitting reaction. The aiming for an elevated operating temperature has thus resulted in an increasing demand for novel anhydrous proton conducting polymeric materials for both PEM fuel cells and water electrolyzers.

This thesis gives an overview of the principles and the current state-of-the-art technology of the hydrogen based electrochemical energy conversion technologies, with special emphasis on the PEM based water electrolyzers and fuel cells (Chapter 1). The fundamental thermodynamics of water electrolyzers and fuel cells is also explained. A detailed literature review is given that covers proton conducting polymeric materials and composite membrane concepts as well as the mechanisms of proton conduction in these types of structures. The experimental part of this thesis has focused on the development and characterization of polymer based proton conducting membranes for operation at temperatures above 100 °C. The most frequently recurring experimental methods and techniques are described in Chapter 2.

For PEM steam and liquid water electrolysis at temperatures up to 130 °C (Chapter 3 and 4), the presented approaches in this work mainly include chemical modification of the conventional PFSA materials with phosphoric acid or inorganic proton conducting particles such as zirconium phosphate (ZrP) or boron phosphate (BP). A novel methodology for the preparation of homogenous Nafion®/poly[2,2´(*m*-phenylene)-5,5'-bibenzimidazole] (PBI) polymer blends was also developed. The miscibility behavior between Nafion® and PBI was investigated using different Nafion® counter cations. It was demonstrated that NH_4^+ could be used as compatibilizer in the Nafion®/PBI system to give homogenous solution cast blend membranes covering the whole composition range. The strong intermolecular coulomb interactions gave the polymer blends improved mechanical characteristics. However, it allowed for very limited volume swelling in phosphoric acid and therefore a very low acid uptake, which resulted in poor proton conductivity in the 10^{-5}-10^{-3} S cm^{-1} range at 130 °C. The pristine phosphoric acid doped Nafion® and PBI membranes, on the other hand, exhibited proton conductivity in the 10^{-2} S cm^{-1} range at 130 °C, which was superior compared with that of the ZrP or BP composite materials based on Nafion®. Steam electrolysis tests were thus conducted using membrane electrode assemblies (MEAs) based on pristine phosphoric acid doped Nafion® and PBI. The PBI based MEAs suffered from severe durability limitations due to membrane degradation, which was most likely connected to the acid catalyzed hydrolysis of the polymer. The phosphoric acid doped Nafion® based MEAs, on the other hand, exhibited better durability but showed rather high ohmic resistance. The moderate steam electrolysis performance was most likely connected to the poor dimensional stability of Nafion® under the experimental conditions. The mechanical properties of the recast Nafion®

membranes at elevated temperature could be slightly improved by annealing the membrane in order to increase its degree of crystallinity. Short side chain (SSC) PFSA membranes such as Aquivion™ (Solvey Solexis), on the other hand, are generally characterized by a considerably higher degree of crystallinity than Nafion®. The melting point of the large crystalline regions is also considerably higher than that of Nafion®, which allows for better mechanical characteristics at elevated operating temperatures. The low equivalent weight of Aquivion™ also resulted in high phosphoric acid uptake, which allowed for high proton conductivity. The steam electrolysis performance of the Aquivion™ based MEA was thus superior compared with that of the corresponding Nafion® based MEA. The importance of the dimensional stability of the electrolyte material was further demonstrated by reinforcing recast Nafion® with a highly porous polytetrafluoroethylene (PTFE) material. During liquid water electrolysis tests at 120-130 °C (3 bar back pressure), the PTFE reinforced Nafion® based MEA reached as high current density as 2500 mA cm^{-2} at 1.95 V. The conductivity of the reinforced membrane was also demonstrated to be superior over time compared with the commercially available melt extruded Nafion® 117 membrane.

Phosphoric acid doped PBI has emerged as one of the most promising electrolyte materials for high temperature PEM fuel cells operating at temperatures up to about 200 °C during the last 1-2 decades. High phosphoric acid content is the key to achieve high proton conductivity of the membrane, which is of critical importance in order to minimize the ohmic voltage losses in the high current density range. However, the mechanical strength of PBI membranes is strongly correlated to its phosphoric acid content due to the strong plasticizing effect of the dopant. Consequently, the doping level of the membrane has to be a compromise between sufficient mechanical strength for the MEA preparation and maximized proton conductivity. In this work, PBI membranes were crosslinked, either by post-treatment with divinylsulfone or by thermal curing, in order to improve their mechanical characteristics at high acid doping levels (Chapter 5 and 6). In addition to the improved mechanical characteristics of the crosslinked membranes, they also exhibited improved radical-oxidative stability which naturally should improve their long term durability. The feasibility of the crosslinked membranes was demonstrated in fuel cell tests at temperatures up to 180 °C. The MEA based on the cured PBI demonstrated an average voltage decay rate as low as 43 μV h^{-1} during 1800 h of continuous fuel cell operation at 600 mA cm^{-2} at 160 °C. Under these conditions, the average cell voltage decay rate of the MEA based on the non-cured reference membrane (308 μV h^{-1}) was more than 700% higher compared with that of the MEA based on the cured PBI membrane. The results confirmed that the long term durability of phosphoric acid doped PBI based high temperature PEM fuel cells is highly dependent on the membrane characteristics, especially during operation at high current loads.

The thesis is completed by summing up on the results and conclusions (Chapter 7). Further research should be devoted to *ex situ* accelerated membrane degradation tests in combination with *in situ* tests and post mortem analysis in order to unravel and completely understand the membrane degradation mechanisms in the operating electrochemical cells. This knowledge is the key to an intelligent design and synthesis of new, high-performing proton conducting polymer materials with improved long term durability for PEM water electrolyzers as well as PEM fuel cells.

Resumé

Protonoverførsel er et af de mest fundamentale fænomener i naturen og også i protonledende membran (PEM) brændselsceller og vandelektrolysatorer spiller det en nøglerolle. Konventionelt benyttes fuldt hydrerede perfluoro sulfonsyre (PFSA) membraner såsom Nafion® (DuPont) som protonleder og elektrodeseparator i både PEM brændselsceller og vandelektrolyseceller. Protonledningsmekanismen for Nafion® afhænger stærkt af tilstedeværelsen af flydende vand i membranens nanostruktur. Dette begrænser temperaturområdet hvor membranens ledningsevne er tilstrækkelig høj til 80 °C, medmindre systemet tryksættes. Ved tryksætning er det muligt at benytte højere temperaturer og stadig have membranet fuldt hydreret. Imidlertid er flere af problemerne ved konventionelle PFSA baserede PEM brændselsceller og vandelektrolysatorer direkte eller indirekte forbundne med den relativt lave temperatur. Forøget driftstemperatur resulterer i generelt forbedret elektrodekinetik og en forbedret katalysatortolerance overfor urenheder, dette gør sig specielt gældende for brændselscelle anoden. For det samlede system er der flere gevinster ved at hæve driftstemperaturen. Blandt andet opnås simplere køling og kontrol af vandtilførsel og muligheden for varmeudnyttelse forbedres. For elektrolyseceller sænkes den krævede termodynamiske energi for vandsønderdelingen når driftstemperaturen øges og dette gør en hævet temperatur stærkt ønskværdig. Målet om at forøge driftstemperaturen har resulteret i forøgede krav til nye vandfrie protonledende polymer materialer for både PEM brændselsceller og vandelektrolysatorer.

Denne afhandling giver et overblik over de nuværende "state-of-the-art" brintbaserede elektrokemiske energiomdannelsesteknologier med en hovedvægt på PEM vandelektrolysatorer og brændselsceller, samtidig med at en beskrivelse af principperne bag disse gennemgås. Den fundamentale termodynamik gennemgås for elektrolysatorer og brændselsceller. En detaljeret litteraturgennemgang for protonledende polymer materialer og kompositer heraf, såvel som mekanismen for protonledningen af disse strukturer gives i kapitel 1. Den eksperimentelle del af afhandlingen fokuser hovedsageligt på udvikling og karakterisering af polymerbaserede protonledende membraner til driftstemperaturer over 100 °C. De mest brugte eksperimentelle metoder og tekniker benyttet i denne afhandling bliver beskrevet i kapitel 2.

For PEM damp- (kapitel 3) og vand- (kapitel 4) elektrolyse ved driftstemperaturer op til 130 °C, bliver der hovedsageligt anvendt konventionelle PFSA membraner, der bliver kemisk modificerede med fosforsyre eller uorganiske protonledende partikler såsom zirkonium fosfat (ZrP) eller bor fosfat (BP). En ny metode for fremstilling af homogene Nafion®/poly[2,2'(m-phenylen)-5,5'-bibenzimidazol] (PBI) polymer blandinger blev også udviklet. Blandbarheden mellem Nafion® og PBI blev undersøgt under anvendelse af forskellige positive modioner for Nafion®. Det blev vist at med NH_4^+ som modion var det muligt at støbe homogent blandede Nafion®/PBI membraner i hele blandingsforholdsintervallet. De stærke coulombske interaktioner gav blandingspolymeren forbedrede mekaniske egenskaber. Som følge af de forbedrede mekaniske egenskaber var der kun en ringe volumetrisk kvældning, dette medførte meget lav syredopingsgrad med dertilhørende dårlig protonledningsevne i 10^{-5}-10^{-3} S cm^{-1} intervallet ved 130 °C. Derimod udviste de fosforsyre dopede membraner af rent Nafion® og PBI ledningsevner omkring 10^{-2} S cm^{-1} ved 130 °C, disse ledningsevner var overlegne i forhold til Nafion®-baserede kompositmembraner af ZrP eller BP. Dampelektrolyseforsøg blev derfor udført på membranelektrodesamlinger (MEAer) baseret på fosforsyredopede membraner af rent Nafion® og PBI. De PBI baserede MEAer led af alvorlige holdbarhedsbegrænsninger på grund af membrannedbrydning. Membran nedbrydningen skyldes højst sandsynligt den syrekatalyserede hydrolysering af polymerstrukturen. MEAerne baserede på fosforsyredopede Nafion® membraner udviste bedre holdbarhed, men havde større ohmsk modstand. Den beskedne dampelektrolyseydelse kan højst sandsynligt kædes sammen med den dårlige dimensionsstabilitet af Nafion® ved

forsøgsbetingelserne der ligger til grund for denne afhandling. De mekaniske egenskaber af omstøbte Nafion® membraner ved temperaturer over 100 °C kunne forbedres moderat ved udglødning af membranen for a øge dens krystallinitet. PFSA membraner med korte sidekæder (SSC) såsom Aquivion™ (Solvay Solexis) har generelt en betydelig højere krystallinitet end Nafion® membraner. De krystallinske regioner har et betydeligt højere smeltepunkt, det betyder at de mekaniske egenskaber for Aquivion™ ved den undersøgte driftstemperatur er langt bedre. Yderligere har Aquivion™ også lavere ækvivalens vægt end Nafion®, dette betyder at Aquivion™ membraner kan optage større mængder fosforsyre. Den højere dopingsgrad gør protonledningsevnen højere, derfor blev der opnået bedre dampelektrolyse ydelse for MEAer baseret på Aquivion™ end tilsvarende Nafion® MEAer. Betydningen af dimensionsstabiliteten af elektrolytmaterialet blev demonstreret ved et forsøg med en forstærket omstøbt Nafion® membran. Membranen blev forstærket af et højporøst polytetrafluoroethylen (PFTE) materiale. Ved elektrolyse med flydende vand ved 120-130 °C (3 bars total tryk) med en PTFE forstærket Nafion® membran blev der opnået en ydelse på 2500 mA cm^{-2} ved 1.95 V. Yderligere blev det vist at ledningsevnen af en PTFE forstærket membran var overlegen over tid sammenlignet med en kommercielt tilgængeligt ekstruderet Nafion® 117 membran.

Fosforsyre dopet PBI har over de sidste 2 årtier vist sig som et af de mest lovende elektrolytmateriale for højtemperatur PEM brændselsceller ved temperaturer op til omkring 200 °C. Et højt fosforsyre indhold er væsentlig for at opnå høj protonledningsevne af membranen. Den høje protonledningsevne er essentiel for at mindske det ohmske spændingstab ved høje strømtætheder. Dog er den mekaniske stabilitet af PBI membraner stærkt afhængigt af fosforsyreindholdet, da fosforsyre virker som en blødgører på PBI membranen. Konsekvensen af denne modsætning er at det er nødvendigt med et kompromis mellem tilstrækkelig høj mekanisk stabilitet og højst mulig protonledningsevne. I dette arbejde blev PBI membraner krydsbundet ved efterbehandling med divinylsulfon eller ved en termisk hærdning, således at deres mekaniske egenskaber blev forbedret ved selv høje fosforsyredopingsgrader (kapitel 5 og 6). Udover de forbedrede mekaniske egenskaber af krydsbundne membraner, udviste de også en forbedret stabilitet overfor oxidative radikal angreb, dette vil naturligvis også forbedre deres langtidsholdbarhed. De forbedrede egenskaber ved krydsbundne membraner blev vist ved brændselscelle langtidsforsøg ved temperaturer op til 180 °C. MEAer baseret på termisk hærdet PBI havde et gennemsnitligt spændingstab på 43 µV h^{-1} under et 1800 h langtidsforsøg ved 600 mA cm^{-2} og 160 °C. Tilsvarende havde en uhærdet reference MEA under tilsvarende betingelser et gennemsnitlig spændingstab på 308 µV h^{-1}, altså omtrent 7 gange dårligere holdbarhed. Disse resultater bekræftede at langtidsholdbarheden af fosforsyre dopede PBI baserede højtemperatur PEM brændselsceller er stærkt afhængig af membranens egenskaber især ved store strømtætheder.

Afhandlingen afsluttes med en opsummering af de opnåede resultater og konklusioner (kapitel 7). Fremtidig forskning bør helliges accelererede *ex situ* membran holdbarhedsforsøg i kombination med *in situ* forsøg og post mortem analyse for at opklare og fuldt ud klarlægge mekanismen bag membrannedbrydning i elektrokemiske celler. Denne viden er essentiel for et intelligent design og syntese af nye højtydende protonledende polymermaterialer med forbedrede langtidsholdbarhed til såvel PEM vandelektrolyse som PEM brændselsceller.

Preface

The current strong dependence on carbon based fossil fuels is a subject of ever growing concern on a global scale. The enormous environmental impact and the political and economical uncertainties associated with the fossil fuel utilization have resulted in an increasing demand for renewable and sustainable energy sources.

During the last decades, the electrochemical energy conversion technologies have emerged as the central elements in the modern vision of a sustainable energy supply chain. In these devices, the chemically bound energy is converted directly into electrical energy. Analogously, electrical energy can be converted into chemical energy for storage. A completely carbon neutral energy cycle could thus be realized if the energy production from renewable sources is intelligently integrated with efficient electrochemical energy conversion technologies.

The energy society based on the hydrogen and oxygen cycle was proposed as early as 1874 by Cyrus Smith in the classic science fiction novel "The Mysterious Island" by the famous French author Jules Verne.

> *"Yes, my friends, I believe that water will one day be used as fuel, that the hydrogen and oxygen of which it is constituted will be used, simultaneously or in isolation, to furnish an inexhaustible source of heat and light, more powerful than coal can ever be… I believe, then, that once the coal deposits have been exhausted, we will warm our homes and ourselves with water. Water is the coal of the future."*
>
> *"That I´d like to see, said the sailor."*

However, the sailor had solid grounds for his skepticism. The road towards a carbon neutral society is bumpy and crooked and bordered by many highly interconnected hinders. The technological demands are challenging for scientists within many engineering disciplines. Furthermore, political and strong economical interests have a big influence on the direction of the development.

The work presented in this thesis is the result of a Ph.D. project carried out during a period of about three years from August 2008-August 2011 in the Energy and Materials Science group at the Department of Chemistry, Technical University of Denmark. The thesis was written as part of the requirements for obtaining the doctor of philosophy degree and intends to give a glimpse into the present status of the technological achievements on fuel cells and water electrolyzers. The focus is on the development and modification of proton conducting polymeric electrolyte materials for fuel cells and water electrolyzers operating at temperatures above 100 °C.

Chapter 1 aims at giving a general introduction and an overview of the relevant fundamental principles and of the current state-of-the-art technology of fuel cells and water electrolyzers. Chapter 2 briefly describes the background to the most frequently recurring experimental techniques in this work. Chapter 3 and 4 are devoted to hydrogen (and oxygen) production through steam and liquid water electrolysis, respectively. Chapter 5 and 6 are devoted to electrical energy generation in fuel cells. Each of the experimental chapters starts with a literature review in order to give a brief and specific background to the project. The conclusions and the future outlooks are summarized in Chapter 7.

This work would not have been possible without the extensive and invaluable support from a great number of people. I would like to take the opportunity to express my true gratitude to all of them!

First of all I would thank *Professor Niels J. Bjerrum* for believing in me and for giving me the opportunity to get to know a completely new field of chemistry. Furthermore, I would like to dedicate special thanks to *Dr. Qingfeng Li* for all his enthusiasm and strong drive and for sharing all his theoretical and practical knowledge with me. I would also like to acknowledge *Dr. Erik Christensen* for excellent project management and work-coordination, *Dr. Irina Petrushina* for teaching me electrochemistry and *Dr. Jens Oluf Jensen, Dr. Rolf W. Berg* and *Dr. Jens H. von Barner* for their invaluable feed-back.

Thanks to all the present and former members of the Energy and Materials Science group for supporting my work with invaluable experimental data and for creating an inspiring and pleasurable atmosphere; *Chao Pan*, *Aleksey Nikiforov*, *Anastasia Permyakova*, *Antonio Thomás García*, *Jakub Polonsky*, *Dr. Andreas Vestbø*, *Zhuojian Gu, Jingshuai Yang* and *Dr*. *Jianhui Liao*. Special thanks to *Martin Kalmar Hansen* for providing me with the ambient pressure steam electrolysis data, for proof reading this thesis and for helping me with the Danish abstract. Special thanks to *Anton Vassiliev* for helping me with the popular scientific summary in Danish. Special thanks also to *Dr. Lars N. Cleemann* for providing me with the fuel cell test results and the long term durability data.

Dr. Hans Christian Rudbeck, *Dr. Hans Aage Hjuler*, *Dr. Thomas Steenberg, Carina Terkelsen* and *Annika Nielsen* at Danish Power Systems ApS are acknowledged for their great support and for providing materials.

Thanks to all the partners within the WELTEMP project, especially *Dr. Martin Paidar* at ICT Prague for providing me with the conductivity data and the electrolysis test results at elevated temperature and pressure.

The partners within the HyCycle Center for Renewable Hydrogen Cycling are acknowledged for an interesting collaboration. Special thanks to *Professor Eivind Skou* and *Casper Nørgaard* at University of Southern Denmark for interesting discussions about PFSA based composites and to *Dr. Ulla Gro Nielsen* for providing me with the solid state NMR spectral data.

Thanks to all the present and former members of the HyFC academy PhD-programme. Special thanks to *Professor Søren Linderoth* for the excellent management and for organizing the scientific and social events.

Thanks to all the administrative and technical staff for all help; *Kirsten Munkgaard Thomsen*, *Jette Nilsson*, *Mette Hansen*, *Mo Hongling Sønnichen*, *Bodil Fliis Holten*, *Astrid Schøneberg*, *Claus Burke Mortensen, Alex Lisbjerg* and *Steen Blichfeldt*.

Last but definitely not least I would like to thank my family for all the support and for being part of my life.

Thinking big is all about thinking as small as you possibly can. Enjoy!

David Aili

12th of August, 2011
Technical University of Denmark, Kgs. Lyngby

Table of contents

1 General introduction

The fundamental principle that describes the conservation of energy implies that energy can neither be created nor destroyed. This natural law is also known as the first law of thermodynamics. On the other hand, energy can be transformed from one form into another. Energy conversion is also the most fundamental principle on which all life on earth depends on. For example, photosynthetic plants harvest the energy of the sunlight and convert it into chemical energy in the form of hydrocarbons such as starch or glucose. The chemically bound energy of the hydrocarbons can subsequently be released and converted into other forms of energy, such as the mechanical work that is needed to pump the blood into the smallest capillaries in the human body. The energy of the sunlight, in turn, originates from the continuous energy releasing fusion of hydrogen atoms into helium and other heavier species.

Just like the hydrocarbons, hydrogen can be considered as a chemical energy carrier. This also means that energy can be stored in the form of hydrogen and released when needed using electrochemical energy conversion devices.

The aim of this chapter is to give a general introduction to hydrogen as an element, the relevant fundamental thermodynamics and to the hydrogen based electrochemical energy conversion technologies such as fuel cells and water electrolyzers. Special emphasis is devoted to polymer based proton conducting materials and the mechanisms of proton conduction in these types of structures. It will give a fundamental background and motivation to the experimental work carried out during the project.

1.1 Hydrogen

Hydrogen is the lightest and most abundant chemical element in our solar system and was formed in the earliest stages of the universe. It constitutes about 75% of all normal matter in the universe and nearly 90% of all atoms [1]. All other elements originate from merging of the hydrogen atom constituents and fusion into heavier species.

In its most simple form, the hydrogen atom is composed of one proton and one electron. This isotope is also referred to as *protium* (^{1}H). Due to the simplicity of the hydrogen atom, it has been widely used as a model system in quantum mechanical calculations and simulations in the development of the molecular orbital theory. *Deuterium* (^{2}H), which is also known as heavy hydrogen, is the isotope containing one neutron, one proton and one electron. Its natural abundance on earth is about 1 per 6500 hydrogen atoms [1]. Heavier hydrogen isotopes also exist but protium and deuterium are the only known stable hydrogen isotopes under standard conditions. For example, tritium (^{3}H) is a radioactive species that is widely used as radiochemical marker for a wide range of applications.

Based on its similarity with the alkali metals in terms of valence electron configuration, hydrogen has been traditionally placed at the head of group 1 in the periodic table. The chemical and physiochemical characteristics of hydrogen are however very unique. For this reason it has been discussed that hydrogen should appear in period 1, centered in between the alkali metals and the halogens to highlight that it is strikingly different from all the other known elements [2].

The hydrogen cation is the only known cation that completely lacks an electron shell around the nucleus. Hence, the hydrogen cation consists of one single proton, which has a radius r_p of about 8.4×10^{-16} m [3]. This should be compared with the ionic radius of Li^+ (9×10^{-11} m), which is the lightest alkali metal cation with the smallest cationic radius. The charge density of the hydrogen cation H^+ is

thus remarkably high and it strongly interacts with other surrounding electron rich elements or molecule moieties.

At standard temperature and pressure, hydrogen (H_2) is a colorless and odorless diatomic gas with a density of about one-fourteenth that of air. In its pure form, it is however a relatively rarely occurring species on Earth. Here it is mainly found in its oxidized form in water or hydrocarbons of different kinds, which serve as the major building blocks of all life on all levels.

The vast majority of the hydrogen gas produced today comes from reforming of various hydrogen containing fossil fuels such as methane (Equation 1.1 and 1.2), which is the main constituent of natural gas.

$$CH_4\,(g) + H_2O\,(g) \rightleftharpoons CO\,(g) + 3H_2\,(g) \qquad (\Delta H^0 = 206\ \text{kJ mol}^{-1}) \qquad (1.1)$$

$$CO\,(g) + H_2O\,(g) \rightleftharpoons CO_2\,(g) + H_2\,(g) \qquad (\Delta H^0 = -41\ \text{kJ mol}^{-1}) \qquad (1.2)$$

The first step is commonly termed oxygenolysis and is highly endothermic. It is thus carried out at temperatures above 500 °C, normally on supported nickel based catalysts [4]. The gas mixture formed in the oxygenolysis reaction is sometimes called “syngas” and can be used in Fischer-Tropsch synthesis of various heavier liquid hydrocarbons, mainly linear aliphatic alkenes. Further hydrogen can be released if the oxygenolysis reaction is accompanied by a water-gas shift reaction, which is somewhat exothermic.

Steam reforming of hydrocarbons is today the cheapest way to produce hydrogen on a large scale. However, it releases huge amounts of carbon dioxide into the atmosphere [5]. In 2010, the worldwide annual production of hydrogen gas was estimated to be about 50 million metric tons [6]. Assuming that all hydrogen is produced by steam reforming of methane according to Equation 1.1 and 1.2, this number corresponds to an annual carbon dioxide emission of at least 270 million metric tons. The petrochemical industry consumes a large fraction of the produced hydrogen in the processing of hydrocarbons. However, the biggest fraction of the total amount of produced hydrogen is used for nitrogen fixation processes in the synthesis of ammonia or ammonium salts for the fertilizer industry according to the Haber process as shown in Equation 1.3.

$$N_2\,(g) + 3H_2\,(g) \rightleftharpoons 2NH_3\,(g) \qquad (\Delta H^0 = -92\ \text{kJ mol}^{-1}) \qquad (1.3)$$

In 2008, the global production of ammonia was estimated to 133 million metric tons [7]. Hence, the nitrogen fixation process alone should require at least 23.5 million metric tons of pure hydrogen per annum assuming full conversion of hydrogen. This amount of hydrogen thus corresponds to about 50% of the total annual global production.

1.2 The future role of hydrogen

During the last 4-5 decades hydrogen has been identified as one of the most versatile secondary sources of energy in the future energy scenario [8], as also proposed by Jules Verne almost 140 years ago [9]. It plays a key role as the energy carrier in many of the electrochemical energy conversion technologies that are often associated with sustainability and the carbon neutral society [10]. However, the sustainable society based on hydrogen as the secondary source of energy would require that hydrogen gas of high purity can be produced on a large scale and at a low cost from other sources than fossil fuels or nuclear fusion power.

Direct hydrogen production by employing sunlight energy harvesting processes that mimic the photosynthetic mechanisms of plants, algae or certain types of prokaryote bacteria is probably the

ideal concept for achieving that. However, these photobiological, photochemical and photoelectrochemical technologies are still in an early research and development phase on a small laboratory scale [11]. Hydrogen production through water electrolysis, on the other hand, is a considerably more mature and well established technology. Due to its relatively high current cost compared with hydrogen produced by steam reforming of fossil fuels, electrolytic hydrogen is today mainly used for niche applications where hydrogen of high purity is required.

Completely carbon neutral hydrogen production through water electrolysis could thus in principle be achieved if the electrical energy used to electrochemically split water into its constituents comes from a renewable source. Hydrogen production through water electrolysis when the electrical energy production rate is larger than the demand could also be considered as one way to store the excess electrical energy from the renewable sources. Additionally, water electrolysis converts the renewable electrical energy into a portable secondary energy source with very high energy density on a mass basis. Unfortunately, the energy density of gaseous hydrogen on a volume basis is rather low. Efficient and compact hydrogen storage is thus in general rather complicated in many respects [12], especially for portable and automotive applications. Hydrogen storage is, however, beyond the scope of the present work.

As an energy carrier, the inherent energy of the stored hydrogen can be released and converted into electrical energy when needed. This can be done in another type of electrochemical device, which is often referred to as a fuel cell.

1.3 The fundamental thermodynamics of fuel cells and water electrolyzers

1.3.1 The open circuit voltage

As mentioned in the previous sections, the major fraction of the hydrogen on earth is found in its oxidized form. On a mass basis, it constitutes about 11% of the total mass of the water molecule and 25% of the lightest hydrocarbon. The oxidation of hydrogen to form water is a spontaneous and highly exothermic redox process as shown in Equation 1.4 or 1.5.

$$H_2\,(g) + \tfrac{1}{2}O_2\,(g) \rightleftharpoons H_2O\,(l) \qquad (\Delta G^0 = -237\ \text{kJ mol}^{-1},\ \Delta H^0 = -286\ \text{kJ mol}^{-1}) \qquad (1.4)$$

$$H_2\,(g) + \tfrac{1}{2}O_2\,(g) \rightleftharpoons H_2O\,(g) \qquad (\Delta G^0 = -229\ \text{kJ mol}^{-1},\ \Delta H^0 = -242\ \text{kJ mol}^{-1}) \qquad (1.5)$$

The reaction in Equation 1.4 or 1.5 is the overall cell reaction of a H_2/O_2 fuel cell depending on if the product water is condensed to a liquid or if it is in the gas phase, respectively. In electrochemistry, the overall cell reactions are commonly divided into half-reactions in order to distinguish between the discrete reduction and oxidation processes that occur at the electrodes.

The overall H_2/O_2 fuel cell reaction can thus be divided into the oxidation of hydrogen and the reduction of oxygen. For example, the fuel cell anode and cathode half reactions in an acidic media corresponding to Equation 1.4 can be described by Equation 1.6 and 1.7, respectively.

Oxidation of hydrogen (anode):

$$H_2\,(g) \rightleftharpoons 2H^+ + 2e^- \qquad (E^0_{anode} = 0.00\ \text{V}) \qquad (1.6)$$

Reduction of oxygen (cathode):

$$\tfrac{1}{2}O_2\,(g) + 2H^+ + 2e^- \rightleftharpoons H_2O\,(l) \qquad (E^0_{cathode} = 1.23\ \text{V}) \qquad (1.7)$$

The electrochemical dissociation of hydrogen (Equation 1.6) is almost reversible on a platinized platinum electrode. Hence, the standard potential for the oxidation of hydrogen and the reduction of protons on platinum is taken as 0.00 V by definition at all temperatures. Conventionally, all standard reduction potentials are determined and tabulated relative to the standard hydrogen electrode. The standard reduction potential is a measure of a species tendency to acquire electrons under standard conditions. The standard oxidation potential, on the other hand, is simply the negative of the standard reduction potential.

The cell voltage of a Galvanic cell (E_{cell}) is determined by the potential difference between the cathode and anode reactions and can thus be described by Equation 1.8 where $E_{cathode}$ and E_{anode} are the reduction potentials of the cathode and anode half-cell reactions, respectively.

$$E_{cell} = E_{cathode} - E_{anode} \tag{1.8}$$

E_{cell} is commonly referred to as the theoretical reversible voltage, open circuit voltage (OCV) or electromotive force (EMF). The reversible cell voltage E^0_{cell} of the overall H_2/O_2 fuel cell reaction shown in Equation 1.4 under standard conditions is thus 1.23 V, as calculated based on the standard reduction potentials shown in Equation 1.6 and 1.7 according to Equation 1.8.

However, Equation 1.8 only applies when the current through the cell is negligible. Under these conditions, the reversible cell voltage E_{cell} is correlated to the Gibbs free energy difference ΔG according to Equation 1.9, where n is the number of electrons participating in the electrochemical process and F is the Faraday constant. ΔG is in turn calculated according to Equation 1.10, where ΔH is enthalpy difference, T is the absolute temperature and ΔS is the entropy difference.

$$E_{cell} = \frac{-\Delta G}{nF} \tag{1.9}$$

$$\Delta G = \Delta H - T\Delta S \tag{1.10}$$

ΔG can thus be defined as the maximum chemical energy of a fuel cell reaction that is available to do external work. A negative ΔG results in a positive E_{cell}, which implies that the overall cell reaction is thermodynamically favorable. In a Galvanic cell such as a fuel cell, this energy is used as the driving force to conduct electrons through an external circuit and load. ΔG is also the minimum energy that is required to reverse the H_2/O_2 fuel cell reaction, i.e. the minimum energy requirement for splitting water into its constituents.

As can be seen from Equation 1.10, ΔG is obviously a function of $T\Delta S$, which implies that the reversible voltage E_{cell} changes with the temperature. Additionally, ΔH and ΔS are strongly dependent on the phase of the reactants and products, which is also naturally reflected in the ΔG. For example, at 200 °C the ΔG value of the H_2/O_2 fuel cell reaction (Equation 1.5) is -220 kJ mol^{-1} assuming that the product water is in the gas phase. According to Equation 1.9 and 1.10 it corresponds to a theoretical reversible cell voltage E_{cell} of 1.14 V.

Consequently, an elevated temperature is advantageous when the cell is operated in water electrolysis mode since the reversible voltage and thus the thermodynamic energy requirement of the water splitting reaction decreases with increasing temperature. If enough energy is supplied in the form of heat, water spontaneously dissociates to its constituents in a process called thermolysis. However, extremely high temperatures are required to reduce the Gibbs free energy of the water splitting reaction to zero, which makes water thermolysis practically difficult [13].

When the conditions deviate from the standard conditions in terms of temperature, partial pressure or reactant activity the theoretical reversible voltage E can be calculated from the Nernst equation

(Equation 1.11), where Q is the reaction quotient and E_{cell} is the theoretical reversible cell voltage at the temperature of interest (Equation 1.9) whereas R, T, n and F have their usual meanings.

$$E = E_{cell} - \frac{RT}{nF} lnQ \tag{1.11}$$

The Nernst equation can be derived from the fundamental chemical equilibrium thermodynamics and it gives the theoretical reversible cell voltage under certain defined conditions.

In the typical H_2/O_2 fuel cell reaction as shown in Equation 1.4 or 1.5 the reaction quotient Q would be as shown in Equation 1.12, where a is the specific activity of each component. If all the reactants and products are in the gas phase, a can be defined as the respective partial pressure P of each component since the mole volume of all gaseous substances is close to equal assuming that the Dalton´s law for an ideal gas mixture applies.

$$Q = \frac{a_{H_2O}}{a_{H_2} \times a_{O_2}^{\frac{1}{2}}} \tag{1.12}$$

For example, according to the Nernst equation the theoretical reversible cell voltage of a fuel cell operating on humidified air and hydrogen at ambient pressure at 200 °C would be 1.14 - 0.04 V = 1.10 V (Equation 1.13), assuming that the relative humidity of both feed gases is 4% and given that the saturated vapor pressure of water at 200 °C is 15.5 bar [14].

$$E = E_{cell} - \frac{RT}{nF} ln \frac{P_{H_2O}}{P_{H_2} \times P_{O_2}^{\frac{1}{2}}} V = E_{cell} - \frac{RT}{nF} ln \frac{0.62}{0.38 \times 0.08^{\frac{1}{2}}} V = E_{cell} - 0.04\,V \tag{1.13}$$

1.3.2 The polarization curve

In a H_2/O_2 fuel cell with an acidic electrolyte the hydrogen is catalytically oxidized at the anode to protons and electrons according to Equation 1.6. The released electrons are conducted through an external circuit and a load whereas the protons are transported through the electrolyte to the fuel cell cathode. At the fuel cell cathode the electrons and protons are catalytically recombined with oxygen to give off water according to Equation 1.7. As also indicated by the positive E_{cell}, this is a spontaneous process and only applies when the cell voltage is lower than the OCV.

On the other hand, if the cell voltage is raised above the OCV through external control, the electrochemical process can be reversed. The polarity of the respective electrode is thus also reversed and the current flows in the opposite direction. The result is a catalytic splitting of water at the electrolyzer anode to give off oxygen, protons and electrons. The protons are transported through the electrolyte to the electrolyzer cathode where they are electro-catalytically reduced to hydrogen gas. This process requires the input of energy in terms of electricity and is referred to as water electrolysis.

Figure 1.1 shows an idealized illustration of the current-voltage relationship of a proton exchange membrane (PEM) based electrochemical cell operating in fuel cell mode (solid line) and in electrolysis mode (dashed line). This type of plot is often referred to as a polarization curve. The current density represents the rate of the overall electrochemical reaction at a certain cell voltage.

Region A of the polarization curve is the activation overvoltage. It is connected to the voltage losses in the electro-catalyst layers, especially for the water splitting reaction in electrolysis mode (anode) [15, 16] and for the oxygen reduction reaction in fuel cell mode (cathode) [17]. Hence, the appearance of the polarization curve in this region is mainly determined by the oxygen electrode. The magnitude of the activation loss is dependent on the nature of the catalyst in terms of the so called exchange current density i_0. It can be obtained by plotting the logarithm of the current density against the overpotential

in a Tafel plot and extrapolating the linear regression of the high current density range of the curve to zero overpotential. The OCV can be recorded when the cell current is close to 0. The obtained OCV is generally somewhat different from the theoretical reversible voltage calculated from the Nernst equation (Equation 1.11). This is mainly due to the formation of various metal oxides on the oxygen electrodes depending on the nature of the catalyst. For example, the platinum based electrocatalysts normally used as cathode material in fuel cells with acidic electrolytes are not completely inert in the acidic media. Various oxidized platinum species such as PtO_x or $Pt(OH)_y$ are thus formed on the surface of the catalyst crystallites, which naturally affect the reversible cell voltage [18]. Additionally, the reactant cross-over through the electrolyte causes a mixed electrode potential that negatively affects the reversible voltage of the fuel cell.

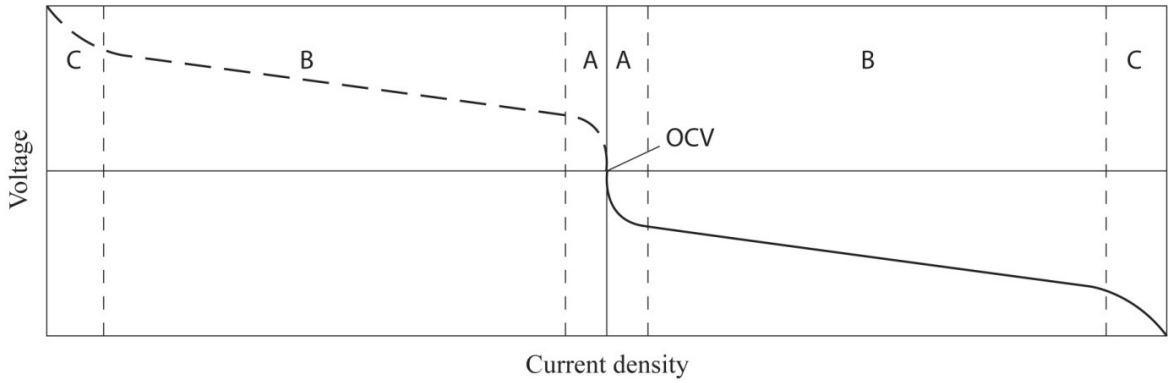

Figure 1.1 *Idealized illustration of the current-voltage relationship of a PEM electrochemical cell operated in fuel cell mode (solid line) and water electrolysis mode (dashed line).*

Region B of the polarization curves is of ohmic nature since the current-voltage relationship appears linear. The extent of the total *iR* drop is determined by for example the ohmic resistances in the cell hardware and catalyst layers or by the interfacial contact resistances between different cell components. However, the major part of the *iR* drop is normally connected to ohmic resistance in the electrolyte. Hence, the total ohmic resistance in the cell can be considerably reduced by reducing the area specific resistance by decreasing the thickness of the electrolyte layer and/or by improving its ionic conductivity.

The third region, region C, is connected to mass transfer limitations. It is determined by how fast the fuel or the oxidant can be supplied to the catalytically active sites in the electrodes and how fast the products can be removed. The point where no current increase is observed when the cell voltage is lowered (fuel cell mode) or increased (water electrolysis mode) is called the limiting current i_L.

1.3.3 Efficiency

Efficiency is a parameter that is directly associated with the investment as well as the operational cost of fuel cells as well as water electrolyzers. However, system efficiency is generally quite poorly defined which makes it difficult to make comparisons between different technologies. In principle, each step in the hydrogen supply chain including production and storage must be considered in order to calculate the overall efficiency of the energy conversion. It is thus important to specify all the considered variables in the efficiency calculations.

The difference in the ΔH value between Equation 1.4 and 1.5 corresponds to the vaporization energy of water, ΔH_{vap}. The condensation of water is an exothermic process, which is reflected in Equation 1.4 by a considerably more negative ΔH. In order to distinguish between the thermodynamic variable ΔH in

Equation 1.4 and 1.5, it is commonly referred to as the higher heating value (HHV) and the lower heating value (LHV), respectively.

Hence, the vaporization (or condensation) energy of water must be taken into consideration when the efficiency (ε) of the hydrogen based electrochemical energy conversion technologies is calculated. If the calculation should be based on the LHV or the HHV depends on if the heat generated by the product water condensation can be used. Assuming 100% current efficiency, the fuel cell efficiency at a certain current density is often defined as the product of the thermodynamic efficiency ($\varepsilon_g = \Delta G/\Delta H$), the voltage efficiency ($\varepsilon_v = voltage/OCV$) and the fuel utilization fraction (α) according to Equation 1.14 [19].

$$\varepsilon = \varepsilon_g \varepsilon_v \alpha \tag{1.14}$$

The overall efficiency of a fuel cell is thus dependent on the load and to what extent the evolved heat can be recovered. For example, fuel cells in combined heat and power (CHP) units are generally more efficient than fuel cells for automotive applications due to the better possibilities for the waste heat utilization.

However, the maximum theoretical efficiency of a fuel cell is, unlike that of the conventional internal combustion engines, not limited by the Carnot cycle which means that in principle all the available energy (ΔG) of the fuel can be converted into electrical energy [20].

1.4 Hydrogen based electrochemical energy conversion technologies

The different types of fuel cells and water electrolyzers are normally named after the nature of the electrolyte. The different types are also suitable for different applications due to the large variations in terms of for example operating temperature, startup time, reactant purity requirements, compactness, robustness, lifetime and cost. The most common types will be briefly described in Chapter 1.4.1 and 1.4.2 with special emphasis on the proton exchange membrane (PEM) based systems.

1.4.1 Fuel cells

The battery dates back to an invention by Alessandro Volta more than 200 years ago [21]. It utilizes the potential difference between two redox couples for the generation a direct electrical current. Two major types of batteries have reached broad commercial utilization for many household and industrial applications. The *primary* battery is disposable and is thus discarded after use whereas the *secondary* battery can be recharged by externally applying a voltage in order to reverse the discharging reaction. However, one thing the two types of batteries have in common is that they are closed systems and that limited amounts of reactants are stored in the electrodes.

Fuel cells, on the other hand, are electrochemical power generating devices just like batteries and work according to the same basic principles. The major difference is that a fuel cell is continuously supplied with reactants. It means that it in principle can operate as long as the electrodes are fed with sufficient amounts of fuel and oxidant.

Several different types of fuel cells have been developed throughout the years. The most common types are summarized in Table 1.1 and briefly described below [19, 22, 23] with special emphasis on the proton exchange membrane (PEM) fuel cell. The cathode and anode reactions of each fuel cell type are summarized in Table 1.2.

The alkaline fuel cell (AFC) was invented by Sir Francis Bacon in the 1960s at the General Electric company [24]. The electrolyte is generally composed of a concentrated aqueous KOH solution due to its superior conductivity compared with aqueous solutions of other alkali metal hydroxides. The concentrated aqueous KOH electrolyte can either be statically held in a matrix between the electrodes or circulated by pumping through heat exchangers and purification units. However, extensive CO_2 removal from the feed gases is generally required in order to prevent precipitation of potassium carbonate in the cell, which otherwise unavoidably would cause severe system failure. A big advantage with the alkaline fuel cell technology is the low overpotential of the oxygen reduction reaction (ORR) at the cathode. It is also possible to use electrodes made of non-noble and relatively cheap materials such as nickel or nickel based compounds. This is strongly beneficial since the prize of the noble metal electrocatalyst materials that are generally used in the fuel cell systems with acidic electrolytes normally contributes to a large fraction of the total system investment cost.

Table 1.1 *The most common types of fuel cells.*

Fuel cell type	Mobile ion	Operating temperature (°C)	Electrode material
Alkaline (AFC)	OH^-	50-200	Pt, Ni
Proton exchange membrane (PEMFC)	H^+	30-200	Pt
Phosphoric acid (PAFC)	H^+	150-200	Pt
Molten carbonate (MCFC)	CO_3^{2-}	650	Ni based compounds
Solid oxide (SOFC)	O^{2-}	500-1000	Ni, ceramics

Phosphoric acid is a thermally stable triprotic inorganic acid with very low vapor pressure and high proton conductivity at temperatures up to 200 °C. The phosphoric acid fuel cell (PAFC) thus normally operates in the 150-200 °C temperature range. The liquid electrolyte is normally immobilized in a porous and highly corrosion resistant ceramic matrix such as silicon carbide (SiC). Due to the high activity and good impurity tolerance of the platinum electrocatalysts as a result of the relatively high operating temperature, the fuel cell anode can be fed with hydrocarbon fuel reformate containing up to 5% CO. However, the strong adsorption of dissociated phosphoric acid on the platinum surface and the relatively high corrosion rate of the carbon catalyst support limit the efficiency as well as the lifetime of the systems. Fuel cells of this type operating on natural gas reformate have reached limited commercial viability since the beginning of the 1990s and have mainly been installed as backup power units on the 200 kW scale.

The molten carbonate fuel cell (MCFC) electrolyte is based on a molten mixture of carbonate salts of alkali metal cations such as lithium, sodium and potassium. At the anode, the fuel is catalytically oxidized whereas carbon dioxide is reduced to carbonate in the presence of oxygen at the cathode. The high operating temperature at about 650 °C allows for non-noble metal electrode materials, thermal integration with fuel processing units, good tolerance to reactant impurities as well as high efficiencies. Unfortunately, it also limits the construction and sealing materials that can be used.

Table 1.2 *The cathode and anode reactions of the different fuel cell types.*

Fuel cell type	Cathode reaction	Anode reaction
Alkaline (AFC)	$O_2 + 4e^- + 2H_2O \rightleftharpoons 4OH^-$	$2H_2 + 4OH^- \rightleftharpoons 4H_2O + 4e^-$
Proton exchange membrane (PEMFC)	$\frac{1}{2}O_2 + 2e^- + 2H^+ \rightleftharpoons H_2O$	$H_2 \rightleftharpoons 2H^+ + 2e^-$
Phosphoric acid (PAFC)	$\frac{1}{2}O_2 + 2e^- + 2H^+ \rightleftharpoons H_2O$	$H_2 \rightleftharpoons 2H^+ + 2e^-$
Molten carbonate (MCFC)	$O_2 + 2CO_2 + 4e^- \rightleftharpoons 2CO_3^{2-}$	$2H_2 + 2CO_3^{2-} \rightleftharpoons 2H_2O + 2CO_2 + 4e^-$
Solid oxide (SOFC)	$O_2 + 4e^- \rightleftharpoons 2O^{2-}$	$2H_2 + 2O^{2-} \rightleftharpoons 2H_2O + 4e^-$

The solid oxide fuel cell (SOFC) utilizes a solid ceramic electrolyte material based on for example sintered yttria or scandia stabilized zirconia. These types of materials are dense and exhibit high oxide

ion conductivity at temperatures around 1000 °C. The high operating temperature opens the possibility to feed the fuel cell with varying hydrocarbon based fuels such as natural gas, alcohols, petroleum or diesel. Additionally, noble metal based catalyst materials can be circumvented due to the high catalytic activity of alternative metallic or ceramic materials as a result of the high temperature. Much research effort is currently devoted to reducing the operating temperature of the SOFC, ultimately to around 500 °C in order to simplify the design of the fuel cell hard-ware, reduce the start-up time and to enhance the number of possible construction and sealing materials.

A schematic illustration of a proton exchange membrane (PEM) fuel cell membrane electrode assembly (MEA) is given in Figure 1.2. The membrane is depicted as a shaded grey rectangle in the center whereas the catalyst layers are depicted as small unfilled circles on each side of the membrane.

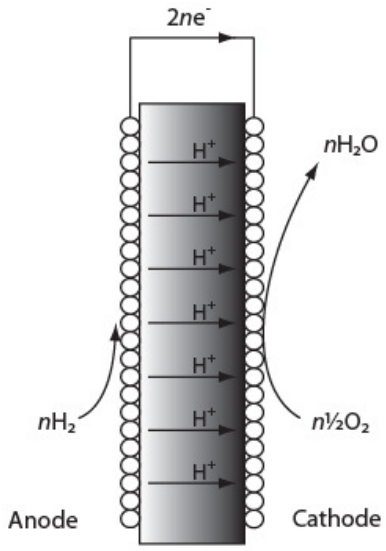

Figure 1.2 *Schematic illustration of a H_2/O_2 PEM fuel cell MEA.*

The first proton exchange membrane fuel cell was developed and patented by William Grubb at the General Electric company in the late 1950s [25, 26]. It found its first practical application in the NASA Gemini space program as on-board electrical power generator and water producer. However, the PEMFC technology was later abandoned in the NASA Apollo space program in benefit for the alkaline fuel cell technology.

Today, the PEM fuel cell technology has been recognized as an efficient and environmentally benign concept for electrical power generation, especially for portable and automotive applications [27-29]. The environmental impact of PEM fuel cells at the point of use in terms of for example air pollution and noise is generally negligible compared with that of the conventional vehicle propulsion systems based on internal combustion. PEM fuel cells can be operated at high power densities which means that the total active area of the MEAs can be minimized, allowing for a compact design of the fuel cell stack. Additionally, PEM fuel cells rapidly respond to load changes and have fairly short startup times, which are characteristics of particular importance for the automotive applications.

The conventional PEM fuel cell technology is based on perfluorosulfonic acid (PFSA) membranes, such as Nafion® from DuPont. The proton conduction mechanism of PFSA membranes is generally strongly dependent on the presence of water, which will be further described in Chapter 1.7. However, the strong dependence on liquid water in the polymer matrix generally limits the operating temperature of the PFSA based PEM fuel cells to around 80 °C at ambient pressure. For conventional H_2/O_2 PEM fuel cells based on PFSA membranes, high current densities above 1000 mA cm^{-2} at a practical cell voltage of 0.6-0.7 V can be obtained under optimal operating conditions [30].

Alternatively, PEM fuel cells can be fed with methanol, which is mainly advantageous from fuel infrastructure and storage points of view, since methanol is a liquid at room temperature and at ambient pressure. However, PFSA membranes are generally characterized by high methanol permeability. The high methanol cross-over rate results in poor overall performance and low efficiency of direct methanol PEM fuel cells due to the mixed cathode potential and the low fuel utilization coefficient α (Equation 1.14) [31].

Unfortunately, the conventional PFSA membrane based PEM fuel cell technology suffers from drawbacks thath are directly or indirectly related to the relatively low operating temperature. An operating temperature above 100 °C has thus been identified as a solution to meet some of the technological challenges of PEM fuel cells [32]. The advantages with an elevated operating temperature include improved electrocatalyst impurity tolerance [33] and the possibility to operate the PEM fuel cell on methanol reformate without further CO removal [34]. Additionally, due to the higher operating temperature the water management and cooling systems can simplified and the heat recovery can be facilitated [35].

Despite extensive research and development activities devoted to the improvement of PEM fuel cells and their components, cost and lifetime are two strongly interrelated parameters which have to be further addressed in order to strengthen the competitiveness and the commercial viability of the technology [36].

1.4.2 Water electrolyzers

The history of water electrolysis dates back to the end of the 18th century and the beginning of the 19th century [37, 38]. In 1789 Adriaan Paets van Troostwijk and his friend Johan Rudulph Deiman observed that evolution of an explosive gas occurred during electrical discharging between two gold wires which were submerged in a water filled glass tube. However, William Nicholson and Anthony Carlisle are often ascribed as the inventors of water electrolysis. They used Alessandro Volta´s Voltaic pile [21] to generate a continuous direct current through a pair of platinum electrodes submerged in water and discovered that hydrogen gas was evolved from the cathode whereas oxygen was evolved from the anode.

Today, hydrogen produced by water electrolysis has been identified as one of the central and most versatile secondary energy sources in a future decentralized energy system based on renewable energy [39]. Just like fuel cells, the different types of water electrolyzers are commonly referred to according to the type of electrolyte. The most common types of water electrolyzers are summarized in Table 1.3 and further described below with special emphasis on the PEM technology. The type of electrolyte in the different water electrolysis systems determines the electrochemistry at the electrodes. The anode and cathode reactions of the different types of electrolyzers are summarized in Table 1.4.

Table 1.3 *The most common types of water electrolyzers.*

Water electrolyzer type	Mobile ion	Operating temperature (°C)	Electrodes
Alkaline (AEC)	OH^-	80	Ni
Proton exchange membrane (PEMEC)	H^+	80	Pt, Ir based compounds
Solid oxide (SOEC)	O^{2-}	500-1000	Ni, ceramics

Alkaline water electrolysis is the most mature technology for electrochemical production of hydrogen on an industrial scale. It has also been used in space missions for on-board generation of hydrogen and oxygen from water [40]. Like in alkaline fuel cells, a highly concentrated aqueous KOH solution is used as electrolyte. It is circulated between the electrodes and pumped through heat exchangers and

purification units in order to ensure optimal chemical composition of the electrolyte. The electrodes are usually separated by an asbestos diaphragm in order to limit the product gas cross-over rate. A major advantage with the alkaline approach is that the electrodes can be made of relatively cheap and non-noble materials such as nickel or nickel based compounds. This is naturally of more importance for the widespread commercial viability and competitiveness of the technology than for special and less cost dependent niche applications on a small scale.

Solid oxide electrolyzers are typically operating at temperatures up to 1000 °C. Like in the SOFC technology, the high operating temperature is required to provide sufficient oxide ion conductivity of the electrolyte material. Due to the high operating temperature, a substantial fraction of the energy required for the water splitting reaction is provided as heat rather than as electric power since E_{cell} (ΔG) is obviously a function of temperature (Equation 1.10) [41, 42]. Naturally, the electrode kinetics is also governed by the high operating temperature. The solid oxide water electrolysis technology could thus be an attractive solution for stationary hydrogen production where waste heat from other heat generating industrial processes can be recovered through the generation of high temperature steam.

Table 1.4 *The cathode and anode reactions of different water electrolysis types.*

Water electrolyzer type	Cathode reaction	Anode reaction
Alkaline (AEC)	$2H_2O + 2e^- \rightleftharpoons H_2 + 2OH^-$	$2OH^- \rightleftharpoons H_2O + ½O_2 + 2e^-$
Solid oxide (SOEC)	$H_2O + 2e^- \rightleftharpoons H_2 + O^{2-}$	$O^{2-} \rightleftharpoons ½O_2 + 2e^-$
Proton exchange membrane (PEMEC)	$2H^+ + 2e^- \rightleftharpoons H_2$	$H_2O \rightleftharpoons 2H^+ + ½O_2 + 2e^-$

PEM water electrolysis offers several advantages in terms of hydrogen production rate, energy efficiency and compactness compared with the conventional alkaline technology [39, 43]. This makes the technology particularly well suited and attractive for on-board or remote production of hydrogen and oxygen of high purity on a relatively small scale.

A schematic illustration of a PEM water electrolyzer MEA is given in Figure 1.3. The membrane is depicted as the shaded grey rectangle in the center whereas the electrocatalyst layers are depicted as unfilled circles on each side of the membrane.

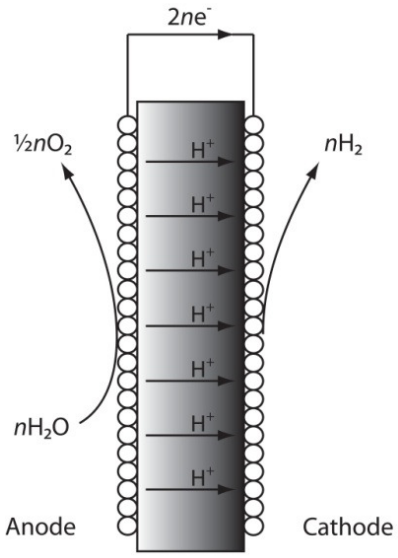

Figure 1.3 *Schematic illustration of a PEM water electrolyzer cell MEA.*

Just like the conventional PEM fuel cell technology, the state-of-the-art PEM water electrolysis technology is based on PFSA membranes. This technology was developed and established by the Asea Brown Boweri (ABB) corporation in the 1980s [44]. However, post mortem analysis of the cells after continuous operation at a current density of 1000 mA cm^{-2} for more than 20000 h revealed considerable membrane thinning as a result of oxidative membrane degradation [45].

For PEM water electrolyzers elevated operating temperatures [42] or pressures [46] offer several advantages from thermodynamic, kinetic and engineering points of view. At higher operating temperatures the electrode kinetics will be improved and therefore the overpotentials at both electrodes will be reduced. At ambient pressure and at temperatures above 100 °C, the water is fed as steam which naturally results in a decreased thermodynamic energy requirement of the water splitting reaction [41]. For example, the total process energy requirement (ΔH) is about 284 kJ mol^{-1} for liquid water electrolysis at 80 °C but only about 242 kJ mol^{-1} for steam electrolysis at 200 °C. The reversible voltage E_{cell} is 1.23 V at room temperature but only 1.14 V at 200 °C when water is supplied as steam (Equation 1.9 and 1.10). Of course this part of the energy saving should be compensated for by extensive heat supply, which could eventually be covered by the waste heat from the cell as a consequence of the unavoidable heat generating ohmic losses. For example, the excess heat could be used for evaporation and preheating of the feed water. From an engineering point of view this may further simplify the intensive cooling of the electrolyzer stacks, especially when the cell is operated at higher current densities.

1.5 The membrane electrode assembly

The general principle of the construction of a single cell PEM water electrolyzer or fuel cell is depicted as an exploded view in Figure 1.4. The MEA is the heart of the cell and it consists of the membrane together with the catalyst layers and eventually the gas diffusion layers depending on the specific engineering of the electrodes.

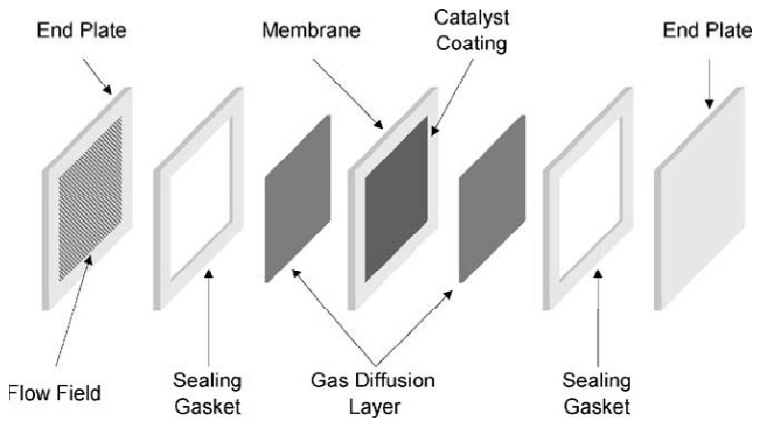

Figure 1.4 *Exploded view of a typical PEM fuel cell or water electrolyzer single cell. The illustration is reproduced from [30].*

The conceptual design of the membrane electrode assembly (MEA) and the single cell is more or less identical for PEM fuel cells and water electrolyzers. However, the considerably higher oxygen electrode potential when the cell is operated in electrolysis mode compared with in fuel cell mode limits the number of available construction materials [47].

The catalyst layers and the membrane electrode interfaces are generally rather complex structures [48]. In the electrode and in the membrane electrode interface, a so called triple-phase boundary has to be generated where a protonic conducting phase intersects with a gas filled pore that is in direct

contact with a catalytically active site on a catalyst particle. In order to maximize the electrochemically active surface area per mass unit of noble metal, the diameter of the catalyst particles is minimized and is generally below 10 nm. The gas diffusion layers and the catalyst particles together with their supporting materials must provide good electronic conductivity in the electrode to ensure that electrons can effectively be transported to and from the catalytically active sites. A certain amount of a proton conducting material is also required in the catalyst layers to ensure that the protons can be effectively transported between the bulk membrane and the catalytically active sites in the electrodes. Additionally, the catalyst layers have to be highly porous in order to facilitate an efficient and rapid transport of gaseous or liquid reactants and products to and from the electrochemically active sites of the catalyst particles.

The gas diffusion layers and the flow fields in the end plates ensure an even distribution of reactants over the catalyst layers. The end plates are also used as current collectors in fuel cells or for current supply in water electrolyzers. If several cells are stacked in bigger units, the end plates function as interconnecting bipolar plates. To ensure that the cell is virtually completely gas tight, sealing gaskets of poly(tetrafluoroethylene) (PTFE) such as Teflon® or fluoroelastomers such as Viton® are normally used. The sealing gaskets also ensure electrical insulation between the end plates or the bipolar plates and thus prevent short circuiting of the cell.

In PEM fuel cells, both catalyst layers are generally made of nanocrystalline platinum which is finely dispersed on a high surface area supporting material with high electronic conductivity, such as carbon black [28, 49]. The carbon supported nanocrystalline platinum catalyst is subsequently applied onto a highly porous carbon substrate, either by spraying or by tape-casting, to give a gas diffusion electrode with a typical platinum loading of around 1 mg cm^{-2}. The gas diffusion electrodes are subsequently hot-pressed to the membrane in order to achieve good interfacial contact and high proton conductivity between the electrode and the membrane. The prohibitive high cost of platinum is one of the major factors hampering the widespread commercial utilization of PEM fuel cells. Hence, non-noble metal based electrocatalytically active materials are under active development [50], especially for the oxygen reduction reaction on the fuel cell cathode which normally requires the highest platinum loading.

Like in PEM fuel cells, the electrocatalytically active materials in PEM water electrolyzers are generally based on noble metals. Nanocrystalline platinum is normally used as catalyst for the hydrogen evolution reaction (HER) due to its superior catalytic activity and low overpotential [51]. Like in the state-of-the-art PEM fuel cell technology, the nanocrystalline platinum is finely dispersed on highly porous carbon black and applied on a porous carbon gas diffusion substrate. However, due to high corrosion rate of platinum in acidic media at the high operating potentials on the anode side, IrO_2 [52] or Ir based oxide mixtures [53] are generally used as catalysts for the oxygen evolution reaction (OER). Due to the high anode potential in PEM water electrolyzers, carbon materials cannot be used as catalyst support, gas diffusion layers or flow fields on the oxygen side [47, 54]. Hence, titanium has evolved as the state-of-the-art construction material for PEM water electrolyzers operating at temperatures up to about 80 °C. Unfortunately, the corrosion rate of titanium in acidic media at temperatures above 100 °C is rather high, which limits the construction material scope to more corrosion resistant and more expensive materials such as tantalum.

1.6 Proton exchange membrane materials

The proton exchange membrane is one of the key materials in both PEM fuel cells and water electrolyzers that partly determines the overall efficiency, cost and lifetime of the systems and thus their commercial viability and competitiveness relative to the more conventional technologies. Hence, the chemical, physiochemical and economical more or less interconnected requirements on the proton exchange membrane material are rather extensive in many respects, as also summarized in Table 1.5 below.

Table 1.5 *Summary of the fundamental requirements on the proton exchange membrane material [32, 55].*

Requirement	Motivation
High proton conductivity	Proton conductivity above 10^{-2} S cm^{-1} is required in order to minimize the ohmic voltage losses, especially at high current densities.
Negligible electronic conductivity	The membrane has to be electronically insulating in order to avoid short circuit of the cell.
Low reactant permeability	The membrane has to be a good barrier for the reactants. Reactant cross-over results in poor fuel utilization and voltage losses in fuel cells. High cross-over rate might also be connected with safety issues due to the formation of explosive gas mixtures.
Mechanical strength and flexibility	The mechanical strength and the flexibility of the membrane are important parameters in the membrane processing and production of MEAs. Thermal cycling of the electrochemical cell will induce stresses in contact points between different cell components, which ultimately might lead to physical membrane failure.
Durability	The membrane has to be tolerant to the harsh oxidative conditions in the operating cell. For example the polymer matrix has to withstand aggressive radicals, high potentials, extreme pH and eventually high temperatures.
Compatibility	The proton conductor has to be chemically compatible with the cell hardware as well as the electrode materials in order to allow for good reaction kinetics.
Availability	In order to reach widespread commercial utilization of the PEM technology the cost of the membrane material has to be minimized.

1.6.1 Sulfonated polymers

The first proton exchange membranes for PEM fuel cell applications were based on sulfonated crosslinked polystyrene [25]. Today, PFSA membranes have emerged as the state-of-the-art membrane materials for PEM fuel cells [30, 49] and water electrolyzers [56] operating at temperatures below the boiling point of water due to their superior chemical stability and hydrous proton conductivity. The development of membranes based on PFSA was initiated in the 1960s in the search for a novel separator and cation conductor for the electrolytic industrial scale production of alkali metal hydroxides, chlorine and hydrogen. The PFSA membrane based chloroalkali technology is now gradually evolving as the state-of-the-art process as the old conventional mercury based Castner-Kellner technology is being phased out [57].

Nafion® is today the most well known polymer in the PFSA family of materials. It consists of a perfluorinated polymer backbone and perfluorinated ether branches with sulfonic acid terminal groups, as shown in Figure 1.5.

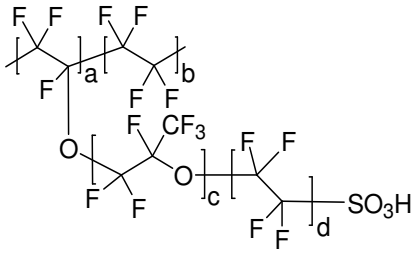

Figure 1.5 *Chemical structure of Nafion®.*

It is typically synthesized by copolymerizing tetrafluoroethylene with perfluorinated vinyl ether co-monomers [30]. The average molecular weight of the resulting ionomer has been estimated to be in

the 100-1000 kDa range [58]. The concentration of sulfonic acid groups in the polymer is normally expressed as the equivalent weight (EW), which is defined as the dry polymer mass per mole number of sulfonic acid groups. Typically, the equivalent weight of the commercially available Nafion® membranes is around 1100 g eq^{-1} as a compromise between high ion exchange capacity and mechanical stability in water [58]. Due to the highly electron deficient characteristics of the perfluorinated polymer backbone, the PFSA polymers are classified as superacids and their pK_a value has been calculated to around -6 [31].

Membranes of PFSA, such as Nafion®, are generally prepared by melt extrusion or by casting from a true solvent solution or from a dispersion of PFSA in a mixture of water and light alcohols. The casting technique and the thermal history of the membrane are directly related to the degree of crystallinity of the polymer and hence the physiochemical properties of the membrane. A certain degre of crystallinity of the PFSA based membranes is crucial in order to achieve a water insoluble and mechanically strong film [59].

The perfluorinated polymer backbone is highly hydrophobic whereas the sulfonic acid end groups are highly hydrophilic. The extremely ambivalent polarity of PFSA polymers results in phase separation on the nanoscale, as confirmed by various X-ray and neutron diffraction techniques [58, 60]. During hydration of the membrane, a self assembled nanostructured network of interconnected hydrophilic and highly acidic domains is developed through which the proton transport can occur. This cluster-network structure is a well established model to describe the nanoscale morphology of hydrated PFSA membranes [31]. The dimensions of the hydrophilic clusters and the interconnecting hydrophilic channels in well hydrated PFSA membranes have been determined to be in the 1-4 nm range.

The phase separation on the nanoscale of most membrane types based on sulfonated polymers is also the key to their proton conduction mechanism [31], as will be further discussed in section 1.7. When membranes based on sulfonated polymers dehydrate the sophisticated nanostructure collapse. The dehydration subsequently results in dramatic proton conductivity decay of up to several orders of magnitude.

Due to the relatively high cost of PFSA membranes, alternative PEM materials based on sulfonated non-fluorinated or partially fluorinated aliphatic or aromatic polymers or multiblock copolymers are under active development [31, 61]. These include sulfonated poly(etheretherketone) (sPEEK) or sulfonated polysulfone (sPSF) as schematically shown in Figure 1.6.

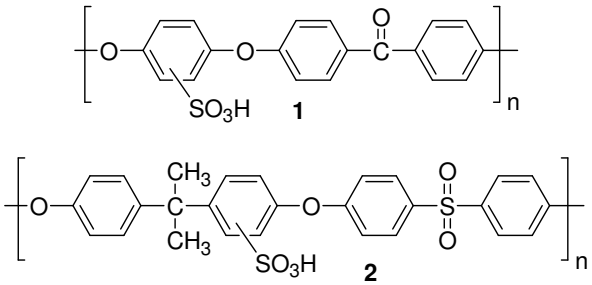

Figure 1.6 *Chemical structure of sPEEK (1) and sPSF (2).*

However, the nanoscale phase separation and thus the proton conduction pathway after hydration of these materials is generally less well developed as compared with PFSA based membranes. This is mainly due to the less hydrophobic characteristics of the polymer backbone and the weaker acidity of the sulfonic acid groups due to the less electron deficient nature of the main chain.

As discussed in the previous sections, an elevated operating temperature of PEM fuel cells and water electrolyzers is advantageous from both thermodynamic as well as system engineering points of view. Consequently, during the last 1-2 decades much research has been devoted to the development of new

polymer based electrolyte systems capable of maintaining high proton conductivity under anhydrous conditions [32].

Low equivalent weight PFSA membranes with short side chains such as Aquivion™ (Figure 1.7) and Hyflon® Ion (Solvay Solexis) or Dow 840™ (Dow Chemical Company) have recently received attention as promising membrane materials for PEM fuel cells operating at elevated temperatures [62-64]. These types of materials have considerably higher concentration of sulfonic acid groups compared with the conventional Nafion® membranes. Normally, the equivalent weight ranges from about 750-850 g eq^{-1}.

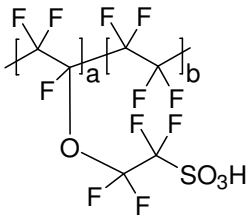

Figure 1.7 *Chemical structure of Aquivion*™.

The short side chain structure of the polymer results in a membrane with a more coherent structure compared with the conventional Nafion® membranes. The higher degree of crystallinity also prevents the membranes from completely dissolving in water as the equivalent weight is reduced to as low as around 700 g eq^{-1} [64]. The short side chain PFSA membranes also exhibit superior dimensional stability and elastic modulus which might be the sole reason for their better PEM fuel cell performance compared with Nafion® in general [63]. It has also been demonstrated that the short side chain PFSA membranes exhibit significantly better water retention characteristics and thus higher proton conductivity under dehydrating conditions compared with the conventional PFSA membranes, which should further facilitate the PEM fuel cell operation at elevated temperatures [62].

Another approach to improve the hydration characteristics of PFSA based membrane materials at elevated temperatures is to prepare composite membranes with a second phase of inorganic hygroscopic and/or proton conducting particles [65]. Replacement of water in the PFSA membrane matrix with less volatile proton solvents such as ionic liquids [66] or phosphoric acid [67] has also been suggested.

1.6.2 Polybenzimidazoles

Phosphoric acid doped poly[2,2´(*m*-phenylene)-5,5' bibenzimidazole] (PBI, Figure 1.8) was first suggested as electrolyte material for proton exchange membrane fuel cells in the middle of the 1990s [68]. It was originally proposed as electrolyte material for direct methanol PEM fuel cells due to its very low methanol permeability. The proton conduction mechanism of phosphoric acid doped PBI membranes is, in contrast to the conventional PFSA membranes, not dependent on the presence of water molecules within the membrane matrix. Hence, phosphoric acid doped PBI has emerged as one of the most promising proton exchange membrane materials for operation in the 100-200 °C temperature range during the last 1-2 decades [32, 55].

PEM fuel cells of this type have demonstrated durability exceeding 6000 h [69]. The average voltage decay rate during continuous H_2/O_2 fuel cell operation at a current density of 200 mA cm^{-2} was determined to around 5 μV h^{-1}. On the other hand, when the fuel cell was operated in start/stop cycling mode with a maximum load of 200 mA cm^{-2} the average cell voltage decay rate was found to be considerably higher (10 μV h^{-1}).

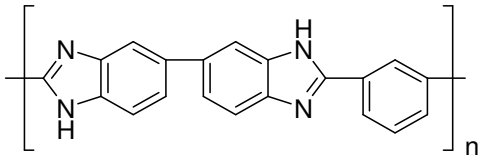

Figure 1.8 *Chemical structure of PBI.*

Since Wainright *et al.* [68] demonstrated the proof of concept for phosphoric acid doped PBI as electrolyte material in high temperature PEM fuel cells in 1995 extensive research activities within the field have been carried out. For example, a large number of PBI structure analogues have been synthesized and evaluated aiming at improving the membrane characteristics, as recently reviewed by Mader *et al.* [70], Li *et al.* [55] and Asensio *et al.* [71].

The polybenzimidazoles are a family of thermally stable and oxidation resistant engineering plastics. The first polybenzimidazoles were described and patented by DuPont de Nemours in 1959 [72]. In a classic full paper from 1961, Vogel and Marvel [73] reported synthetic routes to a wide range of different polybenzimidazoles accompanied by systematic and extensive physiochemical characterization of the novel materials. The polybenzimidazoles were synthesized by melt condensation polymerization from aromatic tetraamines and aromatic dicarboxylic acids. The various structure analogues were obtained by varying the chemical structure of the aromatic tetraamines and dicarboxylic acids in the melt condensation reaction.

However, the melt condensation polymerization process failed to provide well defined polybenzimidazoles, as reviewed by Neuse [74]. Additionally, the polymers obtained were difficult to process by standard techniques other than spinning and film casting. Hence, in order to handle the limited processability of the polybenzimidazoles, pre-polymers of low molecular weight were generally prepared which were further polymerized in a later stage.

Today, the polybenzimidazoles used for proton exchange membranes are generally synthesized in polyphosphoric acid (PPA) as polycondensation solvent, as first described by Iwakura *et al.* [75] in 1964 and shown in Scheme 1.1. The homogenous solution polymerization in PPA at 170-200°C gives a better control of the reaction, which also results in a more well defined polymer in terms of reduced polydispersity index as well as minimized side reactions such as branching and/or crosslinking.

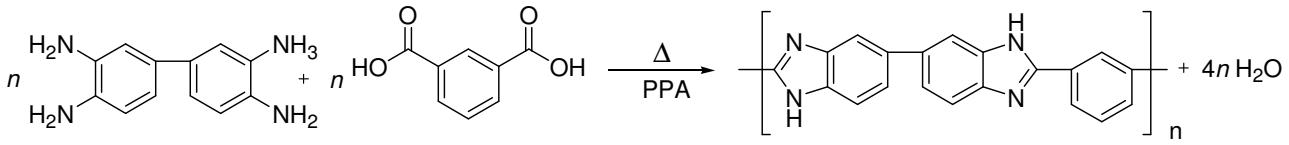

Scheme 1.1 *Synthetic route to PBI [75].*

A limited number of highly polar aprotic organic solvents are capable of solubilizing the polymer by breaking the relatively strong intermolecular hydrogen bonds present in the dry and pure PBI. These include N,N-dimethylacetamide (DMAc), N,N-dimethylformamide (DMF), N-methyl-2-pyrrolidone (NMP) and dimethylsulfoxide (DMSO). DMAc is probably the most widely used organic solvent and was originally chosen in the 1960s as the preferred solvent due to the proper viscosity of the solution for dry-spinning of PBI fibers, as reviewed by Chung [76]. A few weight percents of lithium chloride is often added to the PBI/DMAc solutions in order to facilitate the dissolution and to prevent the polymer from phasing out during storage [77].

The glass transition temperature T_g of PBI is close to the thermal decomposition temperature, which excludes membrane casting by melt extrusion. Hence, phosphoric acid doped PBI membranes are generally prepared according to a multiple step procedure by solution casting from any of the

available organic solvents [68] or from mixtures of aqueous solutions of alkali metal hydroxides or alkoxides and light alcohols [78] followed by extensive washing in water, drying and phosphoric acid imbibing. Phosphoric acid doped PBI membranes can also be prepared directly from the polyphosphoric acid polycondensation solvent [79] or from a mixture of trifluoroacetic acid (TFA) and phosphoric acid [80]. BASF fuel cell has chosen the preparation of phosphoric acid doped PBI membranes directly from the polyphosphoric acid polycondensation solvent for their industrial production process of PBI based MEAs for high temperature PEM fuel cells [81]. When the polyphosphoric acid hydrolyses to phosphoric acid, the polymer precipitates to form a gel-like membrane with very high phosphoric acid content and superior proton conductivity at temperatures up to 200 °C [79].

1.7 Proton conductivity

Ion exchange is one of the most fundamental and essential phenomena in nature. Proton exchange serves a vital role in pH regulation in all living cells and it is the power source of the biosynthesis of the intracellular energy transferring molecule adenosine triphosphate (ATP) [82].

The majority of the hydrogen based energy conversion technologies are also dependent on proton exchange processes. In PEM fuel cells and water electrolyzers, high proton conductivity of the membranes and in the electrodes as well as in the membrane electrode interfaces is essential in order to reach good performance and to minimize the voltage losses that are associated with ohmic resistance.

The importance of proton conduction in general has been highlighted by the implementation of the concept *protonics* [83], analogous to *electronics* but with focus on the conduction of positively charged hydrogen nuclei rather than negatively charged electrons. Even though the proton is remarkably small compared with other cations, it is considerably larger than an electron. For example, the mass of one proton is nearly 2000 times larger than the mass of one electron [14]. Naturally, the several orders of magnitude higher mass of the proton makes proton transport a more energy demanding process compared with for example the conduction of electrons in a metallic material.

Proton conduction is dependent on various types of charge carriers and it is also mechanistically very different from electronic conduction in many respects. The proton conduction mechanism is thus dependent on the nature of the charge carrier, which can also be thought of as a proton solvent.

The proton transport in a proton exchange membrane can follow two major mechanisms depending on the conditions and on the type of matrix in which it occurs. The two types of proton conductivity mechanisms are commonly referred to as the vehicle mechanism and the Grotthuss mechanism, as will be further described below.

1.7.1 The vehicle mechanism

As indicated by its name, the vehicle mechanism involves proton transport assisted by different types of carrier molecules. In an aqueous media the proton carriers are water molecules. The protons are transported in the form of different hydrated complexes such as hydronium cations (H_3O^+), Zundel cations ($H_5O_2^+$) or Eigen cations ($H_9O_4^+$) [84]. The net transport of water molecules in the proton transport direction is referred to as the electro-osmotic drag, which is normally expressed as the water drag coefficient ξ. The proton transport is also accompanied by a continuous counter diffusion of water molecules in the opposite direction due to the emerging concentration gradient through the membrane cross-section.

The vehicle mechanism is the dominating proton conductivity mechanism of well hydrated membranes made of PFSA and other sulfonated polymers [31, 84]. Hence, PFSA membrane based PEM fuel cells require sophisticated water management systems in order to keep a well balanced

humidification of the electrolyte and to avoid flooding of the electrodes. Electrode flooding effectively blocks the supply of reactants to the electrodes which results in a reversible fuel cell failure.

Since the proton transport mechanism of membranes based on PFSA and other sulfonated polymers relies on water molecules as carriers the conductivity is highly dependent on the water content of the membrane. The water uptake of these types of materials is often expressed as the hydration number λ, which is defined as the mole number of water molecules absorbed per mole number of sulfonic acid groups according to Equation 1.14.

$$\lambda = \frac{n_{H_2O}}{n_{SO_3^-}} \tag{1.14}$$

The conductivity of PFSA materials generally increases with increasing hydration number λ [85]. Under fully hydrous conditions at 80 °C the proton conductivity of PFSA membranes can exceed 0.1 S cm^{-1}, as also shown in Figure 1.11. However, the saturated vapor pressure of water increases dramatically with temperature and exceeds 1 bar at temperatures above 100 °C, as shown in Figure 1.9. Hence, one way to circumvent the complete dehydration of PFSA based membranes and thus the dramatic proton conductivity decay in PEM water electrolyzers [86-88] or fuel cells [62] operating at temperatures above 100 °C is to pressurize the system in order enhance the water activity (fuel cell mode) or to keep the feed water in the liquid phase (water electrolysis mode).

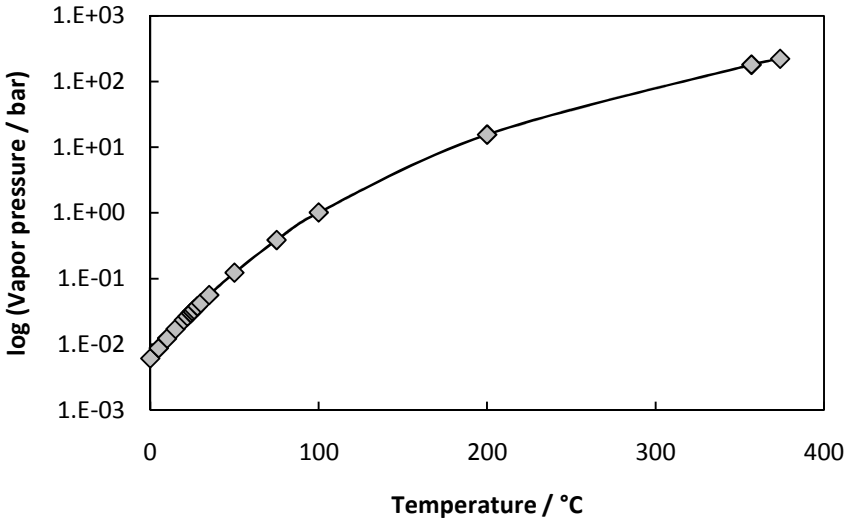

Figure 1.9 *Saturated vapor pressure of water as a function of temperature [14].*

Although pressurized operation of PEM water electrolyzers would facilitate the subsequent gas compression of hydrogen and oxygen, it is associated with engineering issues due to the increased gas cross-over rate [89, 90] as well as increased cost of the cell hardware and various balance of plant components such as valves, compressors and tubing.

1.7.2 The Grotthuss mechanism

In the Grotthuss mechanism, protons are transported by a continuous and fast reorganization of different hydrogen bond network structures [91]. This implies that the protons are more or less delocalized and mobile within the media, which is also the fundamental principle of the Grotthuss type

proton transport mechanism. Hence, the Grotthuss mechanism does not involve any net transport or counter flow of carrier molecules in contrast to the vehicle mechanism.

The Grotthuss mechanism is the dominating proton conductivity mechanisms in most anhydrous proton conducting materials based on various acid doped polymeric materials, such as different types of membranes based on polybenzimidazoles [92, 93]. This has also been confirmed by various NMR techniques [94, 95].

An idealized illustration of the continuously reorganizing hydrogen bond network of a phosphoric acid doped PBI matrix is schematically depicted in Figure 1.10.

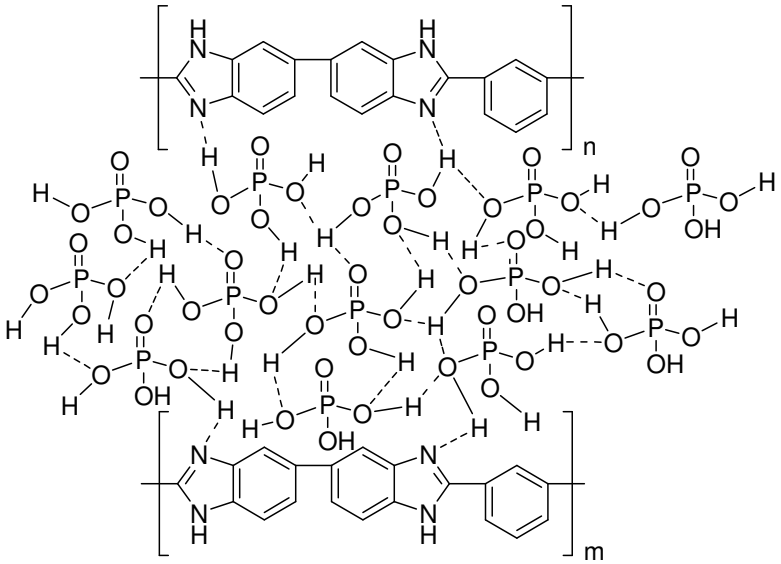

Figure 1.10 *Schematic illustration of the hydrogen bond network of a phosphoric acid doped PBI membrane.*

A wide range of liquid inorganic or organic acids have been investigated as dopants for PBI, including H_2SO_4 [92, 96, 97], $HClO_4$ [97], HBr [92], HCl [96], HNO_3 [97], CH_3SO_3H and $CH_3CH_2SO_3H$ [96]. The relative proton conductivity of PBI membranes doped in different acids has been determined as H_2SO_4 > H_3PO_4 > HNO_3 > $HClO_4$ > HCl [97]. Although H_2SO_4 doped PBI exhibits higher conductivity than phosphoric acid doped PBI [92], phosphoric acid is of special interest for elevated temperature applications due to its excellent thermal stability and low vapor pressure.

Since the proton transport is mainly mediated by the phosphoric acid molecules in phosphoric acid doped PBI, the proton transport is not completely dependent on the presence of water as charge carrier. However, water molecules can participate in the continuously reorganizing hydrogen bond network. The presence of water generally improves the conductivity of phosphoric acid doped PBI membranes since the rate of proton transfer between one phosphoric acid molecule and one water molecule is higher than the rate of proton transfer between two phosphoric acid molecules. When PBI is doped with excess phosphoric acid the proton transport has been proposed to be mediated along either the $H_2PO_4^-$ - H^+ - $H_2PO_4^-$ chain or the $H_2PO_4^-$ - H^+ - H_2O chain depending on the water content of the membrane [98]. The rate of proton transfer between different species present was determined as H_3PO_4 and $H_2PO_4^-$ to H_2O > H_3PO_4 to $H_2PO_4^-$ > N-H^+ to $H_2PO_4^-$ and N-H^+ to H_2O > N-H^+ to N-H. However, under completely anhydrous conditions at temperatures around 160-170 °C the orthophosphoric acid condenses to pyrophosphoric acid or higher oligomers that are less proton conductive [99].

Analogously to the hydration number λ of membranes based on sulfonated polymers, the phosphoric acid content of PBI membranes is often expressed as the acid doping level (DL). It is normally

expressed as the mole number of phosphoric acid molecules per mole number of PBI repeating units according to Equation 1.15.

$$DL = \frac{n_{H_3PO_4}}{n_{PBI_{RU}}} \tag{1.15}$$

The proton conductivity of PBI or PBI structure analogue based membranes of different phosphoric acid doping levels prepared according to different procedures are summarized in Figure 1.11. The proton conductivity of 100% H_3PO_4 and of well hydrated Nafion® 117 is also included for comparison.

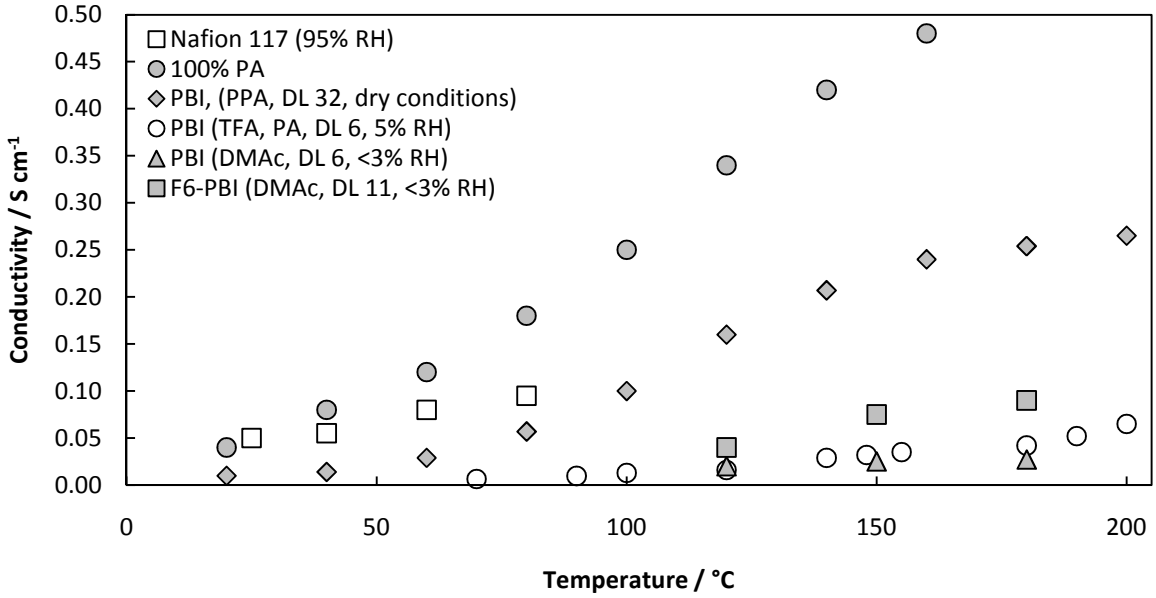

Figure 1.11 *Proton conductivity of Nafion® 117 [55], 100% phosphoric acid (PA) [55], PBI cast directly from PPA [79], PBI cast from a TFA/PA mixture [98], PBI cast from DMAc [100] and F6-PBI cast from DMAc [101]. The phosphoric acid doping levels (DL) and the relative humidity (RH) are indicated in the figure legend.*

Just like the conductivity of sulfonated polymers increases with the hydration number λ, the conductivity of an acid doped PBI membrane increases with increasing acid doping level [98, 102]. At a phosphoric acid doping level equal to or less than 2, virtually all the doping acid is ionically bound to the polymer which results in very low proton conductivity. For example, a PBI membrane with a phosphoric acid doping level of 1.9-2.0 exhibits proton conductivity in the 10^{-9}-10^{-5} S cm^{-1} range [92, 96]. In order to obtain sufficient proton conductivity for any practical use as electrolyte material in for example PEM fuel cells it is thus of great importance that as large excess as possible of the doping acid is present in the membrane.

Under completely anhydrous conditions at 180 °C, the PBI membrane with a high phosphoric acid doping level of 32 exhibits about one order of magnitude higher proton conductivity compared with the membrane with an acid doping level of around 6, which further illustrates the strong correlation between the acid doping level and the resulting proton conductivity. The proton conductivity of the PBI membrane with an acid doping level of 32 at 120-200 °C (0.16-0.27 S cm^{-1}) is also considerably higher than that of the well hydrated Nafion® 117 membrane measured at 80 °C (0.1 S cm^{-1}).

1.8 Scope of the present work

This thesis is devoted to the development of new proton conducting polymer based materials for PEM fuel cells and water electrolyzers operating at temperatures above 100 °C. The overall aim is to improve the membrane characteristics in terms of for example mechanical strength, oxidative stability and hydrous or anhydrous proton conductivity. The approaches covered include:

- Development of composite membranes based on Nafion®, PBI and their blends as well as various phosphoric acid doped PFSA membranes for PEM steam electrolysis (Chapter 3).
- Development of PFSA based composite membranes for liquid water PEM electrolysis at elevated temperatures and pressures (Chapter 4).
- Chemical modification and thermal treatment of PBI based membranes for high temperature PEM fuel cells (Chapter 5 and 6).

Membrane preparation procedures are presented together with chemical and physiochemical characterization of the novel materials. Fuel cell and water electrolysis tests of MEAs based on selected membrane materials were further conducted as ultimate tests of the novel membrane types.

The optimization of the gas diffusion electrodes, MEA preparation procedures as well as cell operating conditions and parameters are beyond the scope of the present work.

2 Description of experimental techniques

The aim of this chapter is to give an overview and a basic theoretical introduction to the most frequently recurring experimental methods and materials characterization techniques used in Chapter 3-6.

2.1 Synthesis and molecular weight determination of PBI

The PBI used in the present work was supplied by Danish Power Systems ApS. It was synthesized by homogenous solution polymerization from tetraaminobiphenyl and isophtalic acid in polyphosphoric acid as polycondensation solvent at about 200 °C according to Scheme 1.1. The polymer was subsequently precipitated in water and extensively washed with dilute aqueous ammonia or sodium hydroxide. The dry polymer powder was thereafter dissolved in DMAc from which the membranes were cast by solvent evaporation at elevated temperatures.

Molecular weight values generally depend on the method of measurement. The number average molecular weight $\overline{M}_n$ is defined according to Equation 2.1, where N_i is the mole number of polymer chains having molecular weight M_i.

$$\overline{M}_n = \frac{\sum N_i M_i}{\sum N_i} \tag{2.1}$$

$\overline{M}_n$ is obtained from methods that depend on the colligative properties of the polymer, i.e. techniques that measure the number of molecules in a given volume rather than the chemical or physiochemical properties of the polymer solution. These include for example end-group analysis, mass spectrometry, freezing-point depression, boiling point elevation and membrane or vapor pressure osmometry measurements.

The molecular weight determination through light scattering or ultracentrifugation experiments gives the weight average molecular weight $\overline{M}_w$, which is defined according to Equation 2.2.

$$\overline{M}_w = \frac{\sum N_i {M_i}^2}{\sum N_i} \tag{2.2}$$

The average molecular weight $\overline{M}$ of a polymer can thus be expressed according to Equation 2.3, where a is equal to 0 and 1 for $\overline{M}_n$ and $\overline{M}_w$, respectively.

$$\overline{M} = \frac{\sum N_i M_i^{a+1}}{\sum N_i M_i^{a}} \tag{2.3}$$

The ratio between the weight average molecular weight $\overline{M}_w$ and the number average molecular weight $\overline{M}_n$ of the polymer is often called the polydispersity index. It is a measure of the molecular weight distribution of the polymer chains.

Solution viscosity measurements are the most widely used techniques for estimating molecular weights of polymers. However, the viscosity measurements have to be used in conjunction with a technique that measures the absolute average molecular weight of the fractionized polymer. The viscosity average molecular weight $\overline{M}_v$ is defined according to Equation 2.4, where α is a constant which depends on the specific polymer-solvent system.

$$\overline{M}_v = \left(\frac{\sum N_i M_i^{\alpha+1}}{\sum N_i M_i^{\alpha}}\right)^{1/\alpha} \tag{2.4}$$

The molecular weights of PBI reported in the present work were obtained from single concentration viscometry measurements using an Ubbelohde capillary viscometer and concentrated sulfuric acid as solvent. The inherent viscosity η_{inh} (logarithmic viscosity number) can subsequently be calculated according to Equation 2.5, where t_0 and t_c are the flow times of the pure solvent and the polymer solution at a given concentration c, respectively.

$$\eta_{inh} = \frac{\ln {t_c}/{t_0}}{c} \tag{2.5}$$

The inherent viscosity η_{inh} determined at one single concentration is often used as an approximate value of the intrinsic viscosity [η] [103]. The intrinsic viscosity [η] (limiting viscosity number) is the viscosity of the solution at infinite dilution and can be obtained by plotting the specific viscosity ($(t_c-t_0)/t_0$) of the solution as a function of concentration followed by extrapolation of the linear regression to $c=0$. Mathematically, it can be derived from the Huggins equation as shown in Equation 2.6, where k is a positive constant known as the Huggins coefficient.

$$\frac{{(t_c-t_0)}/{t_0}}{c} = [\eta] + k[\eta]^2 c \tag{2.6}$$

The single point method seems to give a rather accurate estimation of the intrinsic viscosity [η] of PBI in sulfuric acid, especially at relatively low polymer concentrations [104]. In the present work, the inherent viscosity η_{inh} is thus used as an approximate value of the intrinsic viscosity [η] in the molecular weight calculations.

The intrinsic viscosity [η] is in turn correlated to the viscosity average molecular weight $\overline{M}_v$ of the polymer according to the Mark Houwink Sakurada expression as shown in Equation 2.7, where K and α are empirical constants which depend on the particular system.

$$[\eta] = K M_v^{\alpha} \tag{2.7}$$

By plotting log[η] versus $\log \overline{M}_n$ or $\log \overline{M}_w$ of a series of fractionized polymer samples, a linear relationship is obtained as shown in Equation 2.8.

$$\log[\eta] = \log K + \alpha \log \overline{M} \tag{2.8}$$

In the present work, the empirical constants K = 1.94 × 10^{-4} dL g^{-1} and α = 0.791 were used. The constants are based on early light scattering measurements by Buckley *et al.* [105] and relate the intrinsic viscosity [η] of PBI in sulfuric acid to the weight average molecular weight $\overline{M}_w$ as as shown in Figure 2.1.

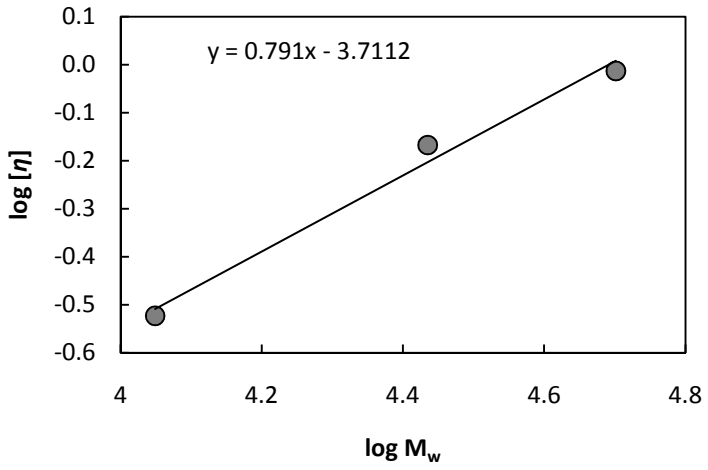

Figure 2.1 *The relation between the intrinsic viscosity [η] and the linear weight average molecular weight $\overline{M}_w$ of PBI [105].*

2.2 Conductivity measurements

Various techniques are available for proton conductivity measurements. AC impedance spectroscopy or high frequency square wave current techniques are commonly used. However, measuring proton conductivity data is not completely straightforward and no general standardized procedure has been established. An accurate proton conductivity measurement requires knowledge about eventual anisotropy present in the membrane, compensation for ohmic losses in the hardware as well as instantaneous data about parameters such as sample dimensions and hydration level or acid content. It can thus be difficult to compare reported conductivity data from different laboratories. This problem was recently highlighted by Cooper *et al.* [106], who discussed some of the difficulties in recording accurate, reproducible and reliable through-plane proton conductivity data of proton exchange membrane materials.

In this work the in-plane proton conductivity measurements were conducted using a four electrode square wave current technique. The high frequency square wave current was supplied through platinum foils connected to the membrane. The in-plane voltage drop was measured between two platinum probes which were connected to the membrane and separated at a fixed distance. The membrane conductivity was subsequently calculated according to Equation 2.9, where I is the applied current, V is the voltage and d is distance between the electrodes from which V is recorded. A is the membrane cross-sectional area through which the current was assumed to be homogenously distributed.

$$C = \frac{I}{V} \times \frac{d}{A} \tag{2.9}$$

The conductivity cell was placed in a furnace for temperature regulation. The relative humidity was controlled by pumping water into an evaporator. The steam was converged with a mass-flow controlled airflow and transported to the conductivity cell interior through heated stainless steel and PTFE tubing. A combined temperature and relative humidity sensor was used to monitor the conditions inside the conductivity cell.

The through-plane conductivity measurements were conducted by sandwiching the membrane between two gas diffusion electrodes, consisting of a layer of Pt/C catalyst and a porous carbon

substrate as described elsewhere [107]. The relative humidity was controlled by pumping water into a steam generator by means of an infusion pump and converged with an air flow passing through both sides of the MEA in the conductivity cell. The conductivity was subsequently calculated according to Equation 2.9.

2.3 Fenton test

In the Fenton test, hydroxyl and perhydroxyl radicals are generated by transition metal ion catalyzed decomposition of hydrogen peroxide according to Equation 2.10 and 2.11, as reviewed by Wardman and Candeias [108]. The reaction is a one-electron transfer process and normally the Fe^{2+}/Fe^{3+} redox couple is used as the catalytic system.

$$H_2O_2 + Fe^{2+} + H^+ \rightleftharpoons Fe^{3+} + {}^{\bullet}OH + H_2O \quad (2.10)$$

$$H_2O_2 + {}^{\bullet}OH \rightleftharpoons {}^{\bullet}OOH + H_2O \quad (2.11)$$

The Fenton chemistry is commonly used in for example waste water treatment to oxidize a wide range of organic compounds.

In membrane research, the Fenton test is used as an accelerated degradation test to evaluate the relative radical-oxidative chemical stability of different membrane materials. In PEM research the Fenton chemistry is commonly used in order to simulate the harsh radical-oxidative conditions in operating electrochemical cells [109-111]. A typical Fenton solution used in PEM research constitutes of a 3-30 wt.% aqueous H_2O_2 solution containing about 3-30 ppm Fe(II). A slightly elevated temperature is normally used in order to further enhance the decomposition rate of hydrogen peroxide and thus the rate of the radical generation.

2.4 Mechanical strength

The tensile properties of the membranes were recorded using a modified universal materials testing machine (Testometric Micro 350). The membrane samples, together with grips, were contained in a metallic chamber equipped with heating elements for temperature regulation. The grips were separated at a rate of 10.00 mm min^{-1}.

The mechanical data were subsequently extracted from the stress-strain curves. The engineering tensile stress (σ) and the tensile strain (ε) were calculated according to Equation 2.12 and 2.13, respectively, where F is the force in Newton, A is the cross-sectional area of the sample, ΔL is the linear dimension change of the sample and L^0 is the initial sample length.

$$\sigma = \frac{F}{A} \quad (2.12)$$

$$\varepsilon = \frac{\Delta L}{L^0} \times 100\% \quad (2.13)$$

The Young´s modulus (or elastic modulus) E is defined as the initial slope of the stress-strain curve and gives information about a material´s resistance to deformation. It can be derived from the linear regression equation of the stress-strain curve in the elastic low strain region according to Equation 2.14.

$$E = \frac{\sigma}{\varepsilon} \quad (2.14)$$

The Young´s modulus E and the engineering tensile stress σ are normally expressed in the SI unit pascal (Pa) whereas the tensile strain ε is generally reported in percent.

The dog-bone shaped membrane samples were prepared by stamping using a hydraulic press. The samples were 30 mm long and 2 mm wide and the thicknesses varied between typically 50-150 µm.

The reported mechanical data are the average values of 4-5 samples and the reported errors are the standard deviations.

2.5 Thermal analysis

The weight change of a sample in relation to changes in the temperature can be measured by thermogravimetric analysis (TGA). It can thus be used to determine the thermal or thermo-oxidative degradation temperature of a material depending on the atmosphere. It can also provide information about for example water content and the total amount of non-volatile inorganic material in the sample. Simultaneous differential thermal analysis (DTA) or differential scanning calorimetry (DSC) can further provide information about endothermic or exothermic transitions in the material such as crosslinking temperatures and different types of morphological changes such as the glass transition temperature T_g.

In this work, TGA was used to determine the water uptake of different membrane materials. It was also used to measure the loading of non-volatile inorganic material in different types of composite membranes. The onset temperature of the major thermal decomposition of the different membrane types was obtained from the intersection of the linear regression of the TGA curve just before and after the initiation of the major decomposition. Thermal and thermo-oxidative stability could be evaluated by controlling the atmosphere in the chamber.

3 Composite membranes based on PFSA, PBI and their blends for PEM steam electrolysis

The following chapter is devoted to the membrane development for a PEM steam electrolyzer operating at temperatures up to about 130 °C. Parts of the data and discussion presented in the chapter are also available in Paper I. The MEA preparation and the water electrolysis tests were conducted by Martin Kalmar Hansen at Technical University of Denmark, Kgs. Lyngby, Denmark.

3.1 Background

One strong motivation for steam electrolysis is, as already discussed in Chapter 1, the thermodynamically lower energy requirement of the electrochemical splitting of water when it is supplied as steam instead of as a liquid. The required energy can thus partly be supplied as heat, which results in a reduced ΔG and therefore a lowered reversible voltage E.

The conventional PEM electrolysis technology relies on well hydrated PFSA membranes as electrolyte materials since they exhibit superior characteristics in terms of proton conductivity, mechanical stability and oxidative resistance. However, due to the complete absence of liquid water in a PEM steam electrolyzer an electrolyte material which is less dependent on water as proton solvent is required.

The amount of literature available concerning PEM steam electrolysis is, however, rather limited. Until today´s date, relatively few types of electrolyte materials have been reported for these types of applications. Linkous *et al.* [112] evaluated a wide range of sulfonated polymers as potential electrolyte materials for PEM steam electrolyzers. At 100 °C, a cell based on sPEEK was operated at a rather moderate current density of 60 mA cm^{-2} at a cell voltage of 1.8 V. PBI was also considered but was found to be susceptible to hydrolysis at high temperatures under a steam atmosphere, especially at temperatures above 200 °C [113]. Furthermore, Antonucci *et al.* [87] operated a steam fed Nafion®-SiO_2 composite membrane based MEA in electrolysis mode at 120 °C. Under similar operating conditions Baglio *et al.* [88] used a MEA based on a composite membrane of Nafion®-TiO_2. However, relatively poor performances in terms of high ohmic resistances were obtained due to the severe dehydration of the membranes and the concomitant dramatic proton conductivity decay. On the other hand, the performance of the SiO_2 and TiO_2 composite membrane based MEAs was slightly better compared with that of the MEAs based on pristine Nafion®-115 due to their somewhat better hydration characteristics and better water retention capability.

More work has been devoted to the development of PFSA based high temperature electrolyte materials for PEM fuel cells. For example, composite membranes of Nafion® and hygroscopic oxides such as TiO_2 or SiO_2 have been reported to exhibit better performance in PEM fuel cells under dehydrating conditions compared with their pristine Nafion® counterparts [114, 115]. Furthermore, Nafion® based composite membranes containing hygroscopic inorganic proton conductors such as zirconium phosphates, ($Zr(HPO_4)_2 \cdot nH_2O$, ZrP) [65, 116-126], zirconium sulfophenylphosphates [127] and heteropolyacids [65] have been developed and tested.

The most thoroughly investigated PFSA based composite systems for PEM fuel cell are probably those based on Nafion® and ZrP. The inorganic filler is generally loaded into the membrane by cation exchange in an aqueous solution of a Zr(IV) salt such as $ZrOCl_2$, followed by *in situ* precipitation of the ZrP in dilute phosphoric acid [122]. Even though the PFSA based ZrP composite membranes often show better performance in fuel cell tests under anhydrous conditions compared with their pristine

PFSA membrane counterparts [117-119], the *ex situ* proton conductivity of the PFSA based ZrP composite membranes is generally inferior compared with that of the corresponding pristine PFSA membranes [119, 124].

On the other hand, the inorganic fillers reduce the segmental motion of the polymer chains within the membrane, which generally results in a mechanical toughening of the composite. This could in turn facilitate the operation at temperatures above the softening temperature of the corresponding membrane based on the pristine polymer.

In addition to the PFSA based composite membranes with inorganic fillers, membranes based on polymeric blends of acidic and basic polymers have been widely investigated as electrolyte materials for PEM fuel cells during the last decade [128]. These types of materials form ionically crosslinked network structures due to the rapid and almost entirely irreversible proton transfer from the acidic polymer to the basic polymer.

For example, the severe embrittlement of membranes based on sPEK under anhydrous conditions dramatically affects the robustness of the PEM systems based on these types of materials. This motivated Kerres *et al.* [129] to improve the anhydrous mechanical properties of sPEK by preparing acid-base blend membranes based on sPEK as the acidic component and for example diaminated polysulfone (PSF) or PBI as the basic constituents. The acid-base blend membranes exhibited excellent thermal stability which, from a mechanical stability point of view, naturally should facilitate the operation at elevated temperatures and under anhydrous conditions. However, the acid-base reaction between the two polymers resulted in partial neutralization of the blend membrane which considerably reduced the ion exchange capacity and the number of available proton charge carriers and thus the proton conductivity.

Polymer blending is a common concept in polymer chemistry, which aims at tuning the properties of the individual polymers [103]. It often results in new materials with unique properties depending on the type of blend as well as the composition and the blend homogeneity. Due to the poor physical attraction at the phase boundaries in materials of immiscible polymer blends, complete phase separation might occur under stress, which generally results in poor mechanical characteristics.

The miscibility between different types of polymers is generally poor due to their inherent differences in terms of for example polarity and density [103]. In order to obtain a completely miscible polymer blend, the mixing has to be thermodynamically favorable which implies that the Gibbs free energy of mixing (ΔG_m, Equation 3.1) has to be negative.

$$\Delta G_m = \Delta H_m - T\Delta S_m \tag{3.1}$$

The miscibility between polymers can thus be improved by increasing the temperature. It can also be improved by adding a compatibilizer to the mixture, which chemically helps binding the immiscible phases together.

However, it is often difficult to evaluate the homogeneity of a polymer blend and several polymer-polymer miscibility criteria have been established [130]. Most of them rely on visual judgement based on microscopy images of thin films of the blends. The polymer-polymer miscibility is also often evaluated by studying thermal transitions. For example, completely homogenous polymer blends should ideally show only one single glass transition temperature T_g.

Numerous reports describing different approaches to prepare PBI or PBI structure analogue based polymer blend membranes with a wide range of acidic polymers have been published during the last decade, mainly for hydrogen or direct methanol PEM fuel cell applications. The different approaches are summarized in Table 3.1.

Table 3.1 *Acid-base polymer blend membrane concepts having PBI or PBI structure analogues as the basic constituents.*

Basic polymer	Acidic polymer	Remarks	Reference
PBI	sPEK	DMFC, low MeOH permeability	[129, 131-140]
Sulfonated poly(benzimidizole-co-diphenyl hexafluoropropane)	sPEK	10^{-2} S cm^{-1} at 80 °C and 90% RH	[141]
PBI	sPSF	10^{-2} S cm^{-1} at up to 160 °C after PA doping	[34, 129, 131, 142-146]
PBI	pyridine containing PSF copolymers[1]	0.07 S cm^{-1} at 160 °C and 30% RH (PA doped), permeable to steam	[147, 148]
p-O-PBI	sPAES	0.201 S cm^{-1} at 80 °C, low MeOH permeability	[149]
O-PBI	sFPSO	0.11 S cm^{-1} at room temperature and 100% RH	[150]
PBI	sFPAES	Specific resistance and water uptake dependent on the acidic co-polymer composition as well as the ratio between the two polymers	[151]
PBI	sPAE	H_2/O_2 fuel cell test at 80 °C (1000 mA cm^{-2} at 0.55-0-65 V)	[152, 153]
PBI	sFPAE	40 MEAs based on PA doped blend membranes tested in a 2 kW stack	[152, 154, 155]
SO_2-PBI, F_6-PBI	sFPAE	Good mechanical properties at high PA doping levels, fuel cell tests at 125-200 °C	[101]
PBI	sPPO	H_2/O_2 fuel cell test at room temperature, proton diffusion coefficient determined	[156-158]
PBI	sPOP	0.005-0.08 S cm^{-1} at room temperature, 100 h DMFC test	[159]
PBI	sPAS	0.12-0.22 S cm^{-1} at room temperature	[160]
sPBI	sPASS	Up to 0.1 S cm^{-1} at 85 °C and 85% RH	[161]
p-sPBI, sPAEB copolymers	sPES	0.049-0.108 S cm^{-1} at room temperature, H_2/air fuel cell and DMFC tests at 70 °C	[162]
ABPBI	PSSA	10^{-3} S cm^{-1} at 100-150 °C	[163]
ABPBI	PVPA	10^{-3} S cm^{-1} at 20 °C and 50% RH	[164]
PBI	PFSA	720 h H_2/O_2 fuel cell durability test at 150 °C at constant load (700 mA cm^{-2}) using PA doped membrane	[165-168]

[1] Basic polymer

Deimede *et al.* [142] throughly investigated the miscibility behaviour between PBI and sulfonated polysulfone (sPSF). The sPSF-Na ionomeric salt form was employed to prepare blends of sPSF and PBI throughout the whole composition range. The miscibility between the two polymers was evaluated by estimating the glass transition temperature T_g using dynamic mechanical analysis (DMA). The miscibility between the two polymers was found to be highly dependent on the sulfonation degree of the sPSF. Miscible or partially miscible blends were obtained at degrees of sulfonation above 10 mole %. The ternary phosphoric acid doped PBI-sPSF blend membranes were subsequently characterized with respect to chemical as well as physiochemical properties by Hasiotis *et al.* [143, 144] and tested in a methanol reformate fed fuel cell operating at temperatures up to 200 °C by Li *et al.* [34]. Furthermore, the miscibility behaviour between basic pyridine containing polysulfone copolymers and PBI was investigated by Daletou *et al.* [147]. Based on the single glass transition temperature T_g

criterion, completely miscible or immiscible blends were obtained depending on the copolymer and blend composition. The blend membranes showed good thermal and oxidative stability and high phosphoric acid uptake, which resulted in excellent anhydrous proton conductivity.

Blend membranes of partially fluorinated sulfonated arylene polyethers (sFPAE) and excess PBI were recently reported to show improved oxidative resistance compared with the pristine PBI membrane in the Fenton test [154]. The ternary phosphoric acid doped blend membranes were also characterized and evaluated in fuel cells tests [155]. Phosphoric acid doping levels as high as 11-12 were obtained resulting in anhydrous proton conductivity exceeding 0.1 S cm^{-1}. Despite the high acid doping levels the membranes maintained sufficient mechanical strength for the MEA preparation. Similarly, blend membranes of sFPAE and PBI structure analogues having electron deficient -$S(O)_2$- and -$C(CF_3)_2$- groups incorporated into the main chain were recently prepared. Improved mechanical strength allowed for higher phosphoric acid doping levels and thus higher anhydrous proton conductivity and reduced ohmic losses during PEM fuel cell operation, especially in the high current density range [101].

Recently, Feng *et al.* [149] suggested a sulfonated poly(arylene ether sulfone) (sPAES) - *p*-O-PBI blend as electrolyte for DMFC applications, whereas Acar *et al.* [163] prepared poly(styrene sulfonic acid) (PSSA) - ABPBI blends with good thermal stability and moderate proton conductivity of 0.02 S cm^{-1} at ambient temperature and at 50% relative humidity.

Methanol cross-over over from the anode to the cathode is a big issue for PFSA membrane based direct methanol PEM fuel cells, as also discussed in Chapter 1. One approach to reduce the methanol permeability of PFSA based membranes is to prepare composite membranes containing an inorganic solid phase within the confines of the hydrophilic regions in order to physically block the methanol permeation, as reviewed by Alberti and Casciola [65]. Hobson *et al.* [165], on the other hand, coated Nafion® membranes with a thin layer of PBI in order to reduce its methanol permeation rate. The layered Nafion® based membrane with a thin methanol barrier of PBI on each side showed, as expected, considerably lower methanol permeability compared with the pristine Nafion® membrane. The significantly reduced methanol permeation rate was also illustrated by a dramatically improved OCV in direct methanol PEM fuel cell mode. The work inspired further investigations devoted to the PBI-Nafion® polymer blend system for direct methanol PEM fuel cells [166, 167]. Furthermore, although on a relatively short time scale, Zhai *et al.* [168] reported improved durability of a ternary phosphoric acid doped PBI-Nafion® (4/1 wt. ratio) blend membrane based MEA compared with a MEA based on pure phosphoric acid doped PBI.

In this work the miscibility between Nafion® and PBI was investigated by using different salt forms of the Nafion® ionomer. Membranes covering the whole composition range were prepared based on the NH_4^+ cation exchanged Nafion® ionomer and the membranes were extensively characterized with respect to chemical and physiochemical properties including water uptake, ZrP loading, phosphoric acid doping, proton conductivity and thermal, mechanical and chemical stability. Furthermore, ambient pressure steam electrolysis tests were conducted at elevated temperatures. In order to further improve the electrolysis performance, alternative PFSA based materials were investigated.

3.2 Experimental

3.2.1 Membrane preparation

3.2.1.1 Membranes of Nafion®, PBI and their blends

The Li^+, Na^+, K^+, NH_4^+, $N(CH_3)_4^+$, Rb^+ and Cs^+ ionomers of Nafion® were prepared by neutralization of the as received Nafion® dispersion (DuPont) with aqueous solutions of the corresponding hydroxides.

After solvent evaporation at 90 °C *in vacuo*, the solid residues were collected and dissolved in DMAc (Merck) to give solutions with concentrations of about 5 wt.%. PBI with an average molecular weight of 66 kDa was supplied by Danish Power Systems ApS and dissolved in DMAc by refluxing to obtain a 5 wt.% solution after filtering.

For the Nafion® ionomer screening, the Nafion®/PBI wt. ratio was 88/12. For the systematic membrane characterization, the DMAc solution of the Nafion®-NH_4 ionomer was mixed with the PBI/DMAc solution to give polymer blends with Nafion®/PBI weight ratios of 97/3, 94/6, 88/12, 82/18, 70/30, 40/60, 5/95. The polymer blend solutions were sonicated for 1 h, followed by solution casting on pre-heated Petri-dishes (95 cm^2) and drying in a pre-heated furnace at 120 °C. Pure Nafion® and PBI membranes were prepared according to the same procedure. The membranes were subsequently boiled in 0.1 mol L^{-1} aqueous H_2SO_4 for 1 h in order to restore the protonated form of Nafion® and finally boiled in demineralized water for 4 h.

The obtained blend membranes are hereafter referred to as Mxxx according to the corresponding Nafion® contents in wt.%. For example, the blend membrane containing 88 wt.% Nafion® and 12 wt.% PBI is referred to as M088. The pure Nafion® and PBI membranes are referred to as M100 and M000, respectively.

3.2.1.2 Commercially available PFSA membranes

The commercially available PFSA membranes were pre-treated according to a standard procedure in 3% aqueous H_2O_2 at 80 °C for 1 h in order to oxidize and wash out impurities and eventual solvent residuals. The membranes were subsequently boiled in demineralized water for 2 h and in 0.5 mol L^{-1} aqueous H_2SO_4 for 1 h. Finally the membranes were rinsed and boiled in demineralized water for several hours and stored in demineralized water until they were used.

3.2.1.3 ZrP loading

The membranes of high Nafion® contents (M082-M100) were refluxed in a MeOH:H_2O, 1:1 (v/v) mixture at 80 °C for 1 h to extensively swell the membranes in order to facilitate the consecutive cation exchange step. The swollen membranes were submerged in aqueous $ZrOCl_2$ hydrochloric acid solutions with Zr(IV) concentrations ranging from 0.1-0.4 mol L^{-1} for 1 h up to 3 days at 80 °C. The ZrP was then precipitated *in situ* by submerging the membranes in 1.0 mol L^{-1} aqueous H_3PO_4 at 80 °C for 12 h. The membranes were subsequently boiled in water in order to remove excess phosphoric acid and eventual ZrP which had been precipitated on the membrane surfaces.

3.2.1.4 Phosphoric acid doping

Phosphoric acid doping was achieved by submerging the membranes in 85% H_3PO_4 at temperatures ranging from 50-150 °C for at least 16 h. The membranes were dried until constant weight at 100 °C *in vacuo* before and after acid doping. The H_3PO_4 contents after doping were calculated based on the weight gains according to Equation 3.2 on the dry membrane basis.

$$PA\ content = \frac{m_{doped\ membrane} - m_{undoped\ membrane}}{m_{doped\ membrane}} \times 100\% \quad (3.2)$$

3.2.2 Characterization

Fourier Transform Infra-Red (FTIR) spectra were recorded using a Perkin-Elmer 1710 Infrared Fourier Transform spectrometer under ambient atmosphere. The pre-dried membrane samples were 5-10 μm thick. The spectra were integrated using Perkin-Elmer Spectrum 2.0 software in order to obtain the relative peak areas of the 810 cm^{-1} and 530 cm^{-1} absorption bands.

Thermogravimetric analysis (TGA) was performed using a Netzsch STA 409 PC equipped with a Netzsch QMS 403 C mass spectrometer. Synthetic air was used as purge gas and the samples were heated from room temperature to 1000 °C at a heating rate of 10 °C min^{-1}. The ZrP loadings were calculated based on the residual masses after complete thermal oxidation of the polymer matrixes, assuming that the zirconium hydrogen phosphate initially present was condensed to zirconium pyrophosphate during the measurement, according to Equation 3.3.

$$Zr(HPO_4)_2 \rightleftharpoons ZrP_2O_7 + H_2O \quad (3.3)$$

Wide angle X-ray diffraction (WAXD) patterns were recorded using a Huber D670 diffractometer equipped with a Cu-K α X-ray source.

Thermograms of the pure Nafion®, PBI and their blends were also recorded under inert atmosphere (N_2 5.0) from room temperature to 500 °C at a heating rate of 3 °C min^{-1}.

For evaluation of the relative chemical stability, membrane samples (approximately 1 g) were submerged in 100 mL 3% H_2O_2 (Merck) aqueous solutions containing 4 ppm Fe(II) (added as $(NH_4)_2Fe(SO_4)_2 \cdot 6H_2O$) at 68 °C. After a certain period of time (maximum 20 h), the membrane samples were collected, rinsed with demineralized water and dried at 110 °C for at least 5 h. The dry weights were recorded and the membrane samples were submerged in freshly prepared Fenton solution for continuation of the experiment. The reported results are the average numbers of two parallel samples.

Stress-strain curves were recorded at 130 °C without active humidity control or monitoring.

The in-plane proton conductivity was measured using a four-probe conductivity cell. The symmetric square wave current was supplied in the 5-10 kHz frequency range through platinum foils and the voltage drop was measured via platinum probes fixed at a distance of 1.0 cm apart. The through-plane conductivity was calculated from the measured voltage drop trough the membrane when a symmetric square wave current was supplied in the 6-7 kHz frequency range. The conductivity was subsequently calculated according to Equation 2.9.

3.2.3 Electrolysis tests

The anode catalyst (IrO_2) was prepared according to the Adam fusions method, as described by Marshall *et al.* [53] but scaled up to 10 times the amount of the precursor salt ($H_2IrCl_6 \cdot 4H_2O$). The calcination time of the salt-oxide mixture was extended to 5 hours at 500 °C. The cathode catalyst (Pt/C) was prepared by chemical reduction of H_2PtCl_6 by formic acid in the presence of Vulcan XC-72R powder (Cabot) [17]. The final composition of the cathode catalyst powder was about 40 wt.% Pt on carbon.

The anodes were prepared for each MEA by spraying a catalyst ink directly to the gas diffusion layers (GDLs). The GDLs were made of tantalum coated (Tantaline®) stainless steel felts (Swiit Metallic Fiber Co. Ltd). The catalyst was manually sprayed onto the substrate at 130 °C from an ink consisting of IrO_2, Nafion® dispersion (DuPont) and ethanol. The IrO_2 loadings were in the 1-4 mg cm^{-2} range. For the cathode, a 600 cm^2 sheet was prepared by spraying the catalyst ink (Pt/C, PBI, PA and formic acid) onto a non-woven carbon cloth GDL (Freudenberg). The catalyst loading was 0.7 mg Pt cm^{-2}.

The tests were performed in a round single cell with an active electrode area of 10 cm^2. The flow pattern was an asymmetric spiral with inlet and outlet in the outer perimeter. The flow plates were made of tantalum coated stainless steel (Tantaline®) and fixed to aluminum end plates containing heating elements.

The electrolysis tests were performed at temperature ranging from 80-140 °C at ambient pressure. At cell temperatures above 100 °C, the steam was fed through an evaporator at 180 °C. The cell and the

evaporator were first heated to the operating temperatures before steam was supplied to the cell in order to avoid condensation of water in the cell and the concomitant wash-out of phosphoric acid. The polarization curves were recorded using current step potentiometry. The steady-state potential was recorded about 10 minutes after each current was set.

3.3 Results and discussion

3.3.1 Ionomer screening

Polymer miscibility is often strongly dependent on the present cations. The cations can sometimes function as compatilizers by affecting the polymer-polymer interactions. Specific intermolecular interactions can thus be governed, which reduce the Gibbs free energy of mixing ΔG_m so that the mixing becomes thermodynamically favorable. For example, Lu and Weiss [169] showed that the miscibility between Nylon-6 and sulfonated polystyrene was very sensitive to the counter cation of the ionomer. The Zn^{2+} ionomer gave a completely miscible polymer blend throughout the whole composition range according to the single glass transition temperature T_g criteria.

When Nafion® in its protonated form (Nafion®-H) was mixed with the PBI/DMAc solution in the present study, a turbid suspension of insoluble polymeric salt was formed in the mixture as a result of the instant proton transfer from Nafion® (pK_a -6 [31]) to PBI (pK_{aH} 5.5 [98]).

In order to improve the miscibility characteristics between the two polymers, a set of experiments was designed where the Nafion® counter cation was systematically varied during the membrane casting. Membrane composition M088 was used as model system for the ionomer counter cation screening. The resulting membranes were subsequently evaluated according to their visual appearances as listed in Table 3.2. Optical microscope images of the membranes are shown in Appendix 1.

Table 3.2 *Visual appearances of M088 (88 wt.% Nafion® and 12 wt.% PBI) prepared from different cation exchanged Nafion® ionomers.*

Nafion® ionomer	H^+	Li^+	Na^+	K^+	NH_4^+	$N(CH_3)_4^+$	Rb^+	Cs^+
Membrane visual appearance	N/A	Texture	Texture	Poor	Homogeneous	Poor	Poor	Poor

Complete phase separation occurred during the membrane casting when any of the K^+, $N(CH_3)_4^+$, Rb^+ or Cs^+ Nafion® ionomer forms were used. The resulting membranes had relatively large agglomerates of PBI dispersed in a continuous opaque Nafion® phase. The Na^+ and Li^+ ionomers gave transparent blend membranes. However, texture and irregularities were observed in the membranes indicating miscibility limitations.

As the ionic radius increases from H^+, Li^+ and Na^+ to K^+, Rb^+ and Cs^+, the Lewis acidity and therefore the charge coordination ability of the cations decreases. The H^+-form of Nafion® instantaneously transfers its proton to PBI to form an insoluble polymeric salt from which a membrane cannot be cast. The K^+, Rb^+ or Cs^+ Nafion® ionomers are completely non-acidic and thus form stable solutions when mixed with PBI in DMAc. However, when the solvent was evaporated during membrane casting complete phase separation occurred between the two polymers. Compared with K^+, Rb^+ and Cs^+, Li^+ and Na^+ are weakly acidic which allows for limited charge coordination and thus stabilization of the Nafion®/PBI blends by functioning as intermolecular compatibilizers.

In this context, the NH_4^+ cation is special. It has an ionic radius similar to that of K^+ but is significantly more acidic (pK_{aH} 9.2). In addition, NH_4^+ has the inherent capability to form bridging hydrogen bonds with imine groups in the benzimidazole rings of PBI and O atoms in the sulfonic acid groups of

Nafion®. The modification and tuning of intermolecular hydrogen bond interactions is a well established tool to reduce the Gibbs free energy of mixing ΔG_m for polymer blends in general [103]. Favorable hydrogen bonding can reduce the overall ΔG_m by reducing enthalpy of mixing ΔH_m.

The combination of the weak acidity of the ammonium cation and its ability to form bridging hydrogen bonds seemed to facilitate the coordination between Nafion® and PBI during the membrane casting. Phase separation could thus be circumvented since the ammonium cations made the polymer-polymer mixing thermodynamically favorable. The polymer blends were also soluble and stable in DMAc for extended periods of time (at least 2 days) which further facilitated the processing of the polymer blend.

The discussion seems further supported by the observation that complete phase separation occurred during the membrane casting when the $N(CH_3)_4^+$ ionomer was employed. $N(CH_3)_4^+$ is a completely non-acidic and aprotic cation, which means that it lacks the most fundamental characteristics that makes the ammonium cation a good compatibilizer in the Nafion®/PBI polymer blend system.

3.3.2 Membrane preparation

Based on results from the ionomer screening, blend membranes covering the whole composition range could easily be cast from the Nafion®-NH_4 ionomer and its DMAc mixtures with PBI. After casting, the membranes were boiled in dilute aqueous H_2SO_4 and treated with boiling water in order to wash out NH_4^+ and to restore the protonated form of Nafion® to give an ionically crosslinked blend membrane. A schematic illustration of the ionically crosslinked structure is given in Figure 3.1.

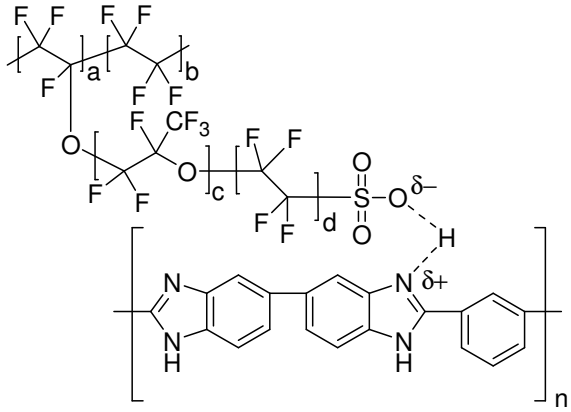

Figure 3.1 *Schematic illustration of the ionically crosslinked Nafion®/PBI complex.*

The negative and positive charges on Nafion® and PBI, respectively, were probably fully developed since the acidic protons were assumed to be completely transferred to the basic sites. This result in strong coulombic forces between the two polymers and the complex can thus be described as a polymeric salt.

The ratio between the acidic and basic groups was logically dependent on the blend membrane composition. For example, the membrane composition M097 corresponds to about 9 sulfonic acidic groups per PBI repeating unit. Similarly, the mole number of acidic groups per mole number of PBI repeating unit of the blend membranes throughout the whole composition range can be calculated according to Equation 3.4, where 1100 corresponds to the equivalent weigh of Nafion® and 308 corresponds to the mole weight of one PBI repeating unit.

$$Acidic\ groups\ per\ PBI_{RU} = \frac{Wt.fraction\ Nafion^{®}/_{1100}}{Wt.fraction\ PBI/_{308}} \quad (3.4)$$

The number that is obtained from Equation 3.4 is analogous to the acid doping level, which is often used to define the phosphoric acid content of PBI membranes. The membrane composition M088 thus corresponds to an acid doping level of 2 according to the acid doping level terminology, which implies that the amount of acidic groups from Nafion® equals the amount of basic groups from PBI. Hence, M088 corresponds to the completely charge neutral membrane composition. It should be remembered that each PBI repeating unit has 2 available basic sites. Hence, the membrane compositions M094, M097 and M100 are acidic whereas the membrane compositions M082, M060, M030, M005 and M000 have an excess of basic groups.

The blend membrane casting procedure based on Nafion®-NH_4 and its mixtures with PBI could without modifications be scaled up to prepare at least 800 cm^2 homogeneous membranes throughout the whole composition range.

3.3.3 ZrP incorporation

Zr(IV) was loaded through cation exchange within the confines of the hydrophilic regions of the membranes. The ZrP was subsequently precipitated *in situ* by treatment in dilute phosphoric acid according to a procedure that was originally developed by Grot and Rajendran [122]. This process has been well established and is known to give a homogeneous and even distribution of ZrP throughout the whole cross-section of PFSA based membranes according to EDX analysis and elemental mapping [116, 120, 124]. The obtained ZrP contents in the present study were calculated from the thermogravimetric curves (Figure 3.2) based on the remaining masses at 250 °C and 800 °C.

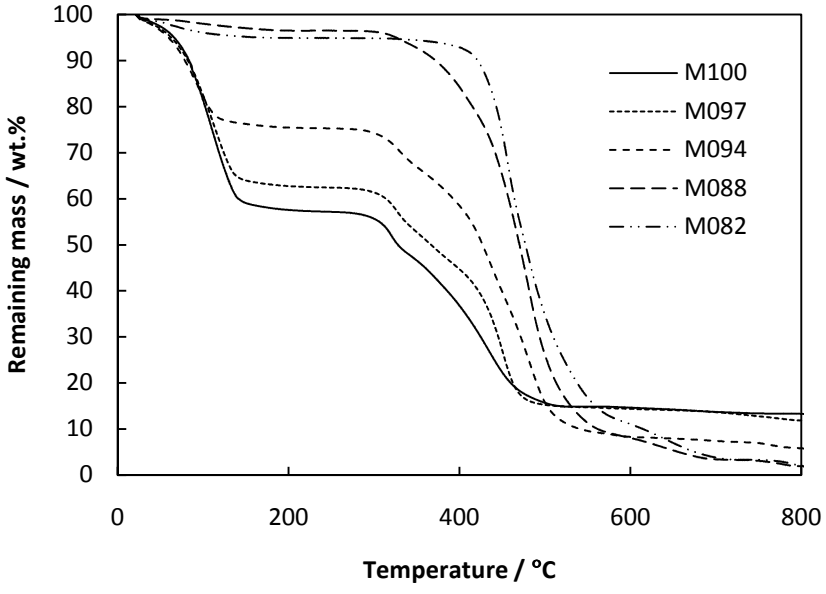

Figure 3.2 *Representative thermogravimetric curves of the ZrP composite membranes based on M082-M100.*

For the membranes with high Nafion® contents (membrane M094, M097 and M100) the obtained ZrP content increased dramatically with the weight fraction of Nafion®. Increased Nafion® content resulted in a less coherent polymer matrix and more available vacant acidic sites for Zr(IV) incorporation

through cation exchange. When the pre-swollen membranes were soaked in a 0.2 mol L^{-1} $ZrOCl_2$ solution for 16 h at 80 °C prior to the *in situ* precipitation of ZrP in dilute phosphoric acid, ZrP contents of 25, 20 and 8 wt.% were obtained for the membranes based on M100, M097 and M094, respectively. By increasing the $ZrOCl_2$ concentration to 0.4 mol L^{-1}, ZrP contents as high as 40 wt.% could be obtained for M100. However, the composite membranes having high ZrP contents were extremely brittle, which naturally limited their practical usefulness as electrolyte materials. A high ZrP content of PFSA based composites is also known to reduce the proton conductivity of the material [119, 124].

According to Equation 3.4, the basic groups of all membranes with higher PBI contents than 12 wt.% were in excess which resulted in complete neutralization the Nafion® sulfonic acid groups. Since the ZrP incorporation process relied on cation exchange, the basic membranes could not be incorporated with ZrP according to this procedure. The small remaining mass at 800 °C of blend membrane M088 and M082 could possibly be explained by ZrP which had been precipitated on the membrane surface.

An alternative procedure for ZrP incorporation based on a soluble ZrP precursor, which was developed by Alberti *et al.* [127], could eventually allow for ZrP incorporation of the blend membranes with an excess of PBI. It could also give a more precise control of the ZrP content and the distribution of the filler throughout the membrane cross-section.

3.3.4 Water uptake

Water uptake data of the pristine membranes covering the whole composition range and of the ZrP composite membranes of high Nafion® contents are plotted versus the membrane composition in Figure 3.3.

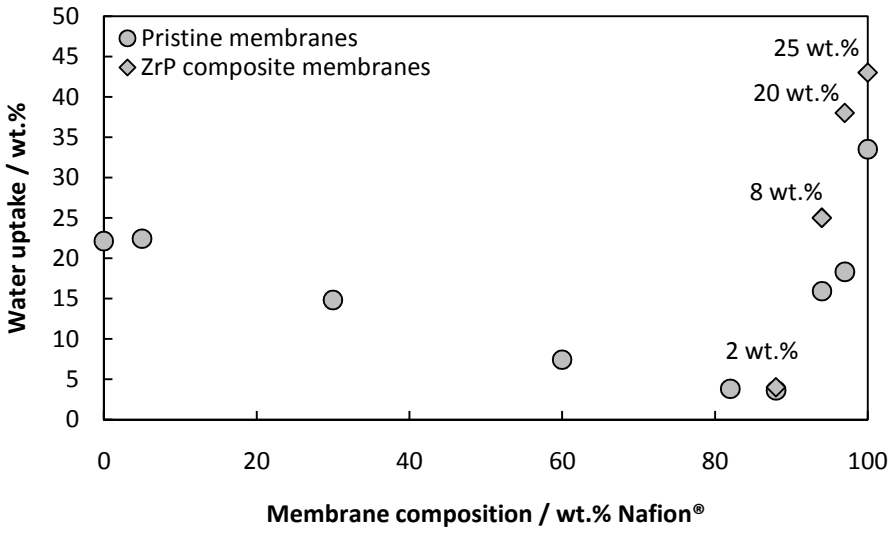

Figure 3.3 *Water uptake of the pristine membranes covering the whole composition range and of the ZrP composites of high Nafion® contents. The corresponding ZrP contents in wt.% are indicated in the figure.*

Mass-spectrometry confirmed that the major weight loss at temperatures up to 250 °C was due to evaporation of water. Therefore, the water uptake was calculated based on the total weight loss at 250 °C on the dry membrane basis.

In this work water uptakes of about 22 wt.% and 33 wt.% were obtained for PBI and recast Nafion®, respectively. It is also in good agreement with previously reported results for solution cast PBI and melt extruded Nafion® 117 [170]. The high hydrophilicity of PBI and Nafion® originates from the

strong hydrogen bond interaction between water molecules and the nitrogen atoms in the benzimidazole moieties in PBI [171] and the sulfonic acid terminal groups in Nafion® [85].

The water uptake of the Nafion® membrane M100 in the present study corresponded to a hydration number λ of about 20. The water uptake of the blend membranes of high Nafion® contents decreased from 33 wt.% for M100 to around 18 wt.% for M097. It reached a minimum at the neutral composition (M088) which could possibly be explained by reduced hydrophilicity of the completely ionically crosslinked polymer matrix. The membranes close to the neutral composition should also exhibit a high resistance to swelling which naturally should result in a reduced water uptake. For the membranes of high PBI contents and thus an excess of basic groups (membranes M082-M000) the water uptake gradually increased as the Nafion® content decreased. This was obviously due to the gradual increasing concentration of hydrophilic N or N-H sites available for hydrogen bond interaction with water and the gradual increasing swelling ability.

The higher water uptakes in general of the ZrP composite membranes based on M094-M100 compared with their pristine counterparts were probably not directly related to the high hygroscopicity of ZrP. It was more likely a consequence of morphological or structural changes induced by the *in situ* precipitation of the inorganic filler [124].

3.3.5 Phosphoric acid doping

3.3.5.1 Phosphoric acid doping of the pristine membranes

Phosphoric acid doping of the membranes covering the whole composition range was performed in 85% H_3PO_4 for at least 16 h at temperatures ranging from 50-150 °C. The obtained phosphoric acid contents on the dry membrane basis after doping at different temperatures as calculated according to Equation 3.2, are summarized in Figure 3.4.

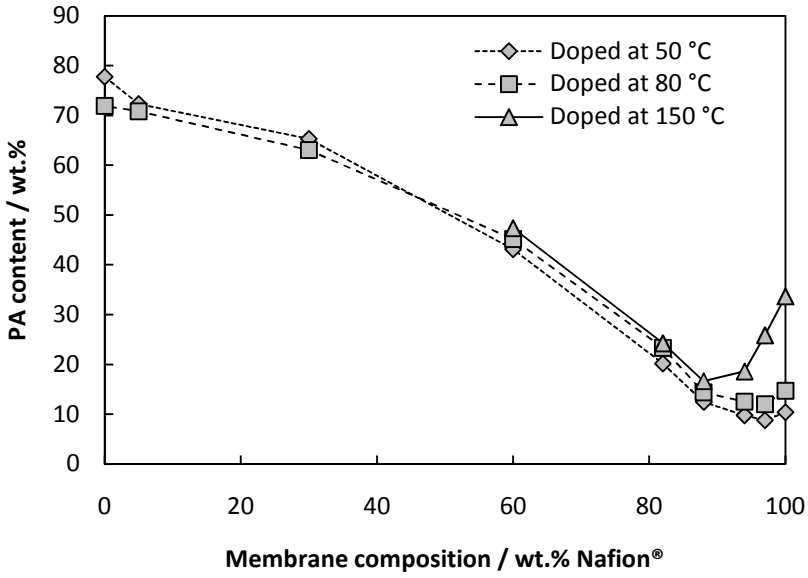

Figure 3.4 *The phosphoric acid uptake of Nafion®, PBI and their blends. The membranes were doped in 85% H_3PO_4 for at least 16 h at 50-150 °C.*

The membranes of high PBI contents and thus a large excess of basic groups (M030-M000) were partially soluble in the orthophosphoric acid at temperatures higher than 50 °C, as also indicated by a

slightly colored doping solution. Due to the partial dissolution of the PBI-rich membranes slightly lower apparent phosphoric acid contents were obtained when the doping temperature was increased from 50 °C to 80°C.

The phosphoric acid uptake of membrane M000 (pure PBI) doped at 50 °C corresponds to an acid doping level of around 11. Furthermore, the phosphoric acid uptake of membrane M100 (pure recast Nafion®) doped at 150 °C corresponds to around 5 H_3PO_4 molecules per sulfonic acid group. These results are in good agreement with previously reported results for pristine phosphoric acid doped PBI [171] and Nafion® [67] membranes which were doped under similar conditions.

Phosphoric acid doping of PBI is generally accompanied by extensive membrane swelling and polymer chain separation. Covalently crosslinked PBI membranes are naturally more coherent compared with their linear counterparts and they exhibit considerably higher resistance to swelling. Hence, elevated temperatures are required in order to reach sufficient acid doping levels for any practical use in for example PEM fuel cells [100, 172]. This also seems to be valid for various types of ionically crosslinked PBI based blend membranes [101, 144, 155].

Analogously to the water uptake data in the present study (Figure 3.3), a phosphoric acid uptake minimum was observed for M088. Since the terminal sulfonic acid groups in Nafion® are considerably more acidic compared with phosphoric acid, the ionic interaction between Nafion® and PBI is stronger than the corresponding ionic interaction between phosphoric acid and PBI. Hence, due to the strong coulombic forces between Nafion® and PBI, the blend membranes were extremely dimensionally stable which allowed for very limited volume swelling in phosphoric acid. For example, even after doping at 150 °C the phosphoric acid uptake of M088 was as low as about 17 wt.%.

3.3.5.2 Phosphoric acid doping of the ZrP composites

The wide angle X-ray diffractograms (WAXD) of the pristine and phosphoric acid doped blend membrane M094 with an initial ZrP content of 25 wt.% are shown in Figure 3.5. The membrane was doped in 85% H_3PO_4 at 50 °C for 16 h.

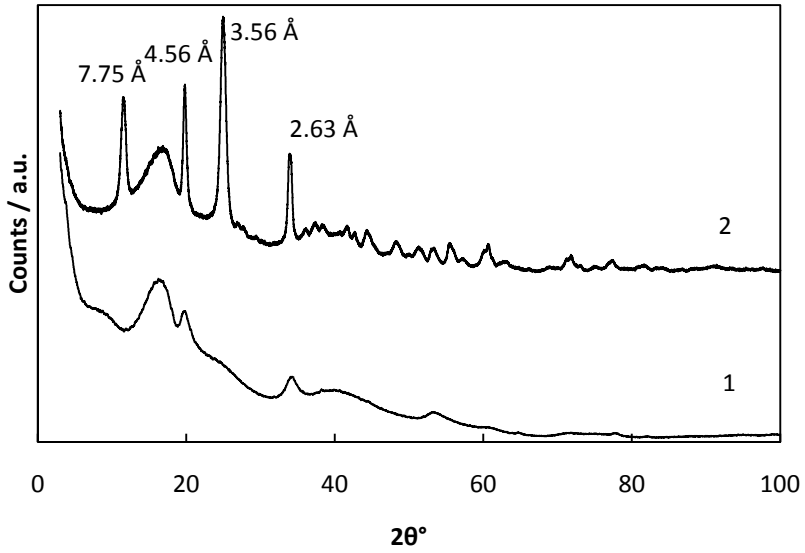

Figure 3.5 *X-ray diffractograms of M094+25 wt.% ZrP before (1) and after (2) PA doping.*

The broad reflection centered at about 16° 2θ which was present in both X-ray diffractograms is attributed to convolution of crystalline and amorphous scatterings of the Nafion® perfluorinated

backbone [173]. The diffraction pattern of the non-doped M094 based ZrP composite membrane in the present study fits well with previously reported X-ray diffraction patterns of ZrP containing Nafion® membranes which were prepared according to the cation exchange methodology [118, 123].

The single lamella structure of α-ZrP is shown in Figure 3.6. Each phosphate is bonded to three different Zr atoms to form a crosslinked covalent network. The interlayer zeolitic cavities in the structure can effectively host water molecules, which is the major reason for the high hygroscopicity and water the retention capability of the material.

According to the literature data, morphologically pure and crystalline α-$Zr(HPO_4)_2 \cdot nH_2O$ prepared by refluxing a Zr(IV) precursor in 14 mol L^{-1} H_3PO_4 shows characteristic and sharp reflections at *d*-spacings of 7.75 Å, 4.48 Å, 3.57 Å and 2.63 Å [174]. However, the characteristic sharp interlayer reflection at a *d*-spacing of 7.75 Å is normally missing in the X-ray diffractograms of Nafion® based ZrP composite membranes prepared according to the cation exchange procedure [118, 121]. It has thus been suggested that a monolayered and exfoliated amorphous or semi-crystalline phase of ZrP rather than a pure crystalline phase of α-$Zr(HPO_4)_2 \cdot nH_2O$ is formed within the confines of the hydrophilic regions during the *in situ* precipitation of ZrP in Nafion®.

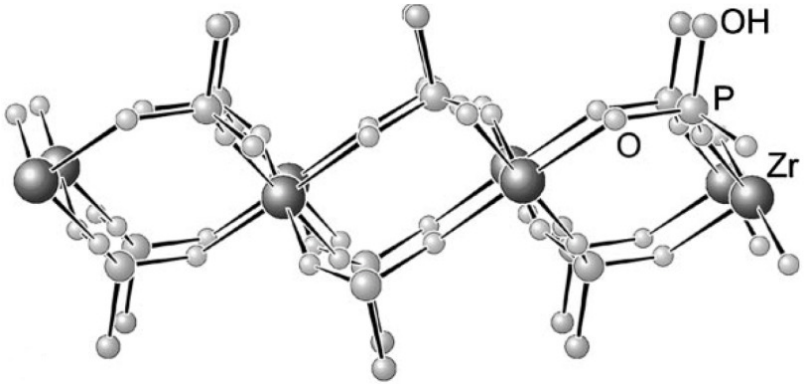

Figure 3.6 *Single lamella structure of α-ZrP. The illustration is reproduced from [65].*

The proton conductivity of α-$Zr(HPO_4)_2 \cdot nH_2O$ is mainly a surface process. Hence, the proton conductivity is decreasing with increasing crystallite size. From a proton conductivity point of view, an amorphous or semi-crystalline ZrP should thus be preferred since crystalline α-$Zr(HPO_4)_2 \cdot nH_2O$ is known to exhibit lower proton conductivity than amorphous or semi-crystalline ZrP due to its lower surface area [65].

During doping of the ZrP composite membrane based on M094 in 85% H_3PO_4 a crystalline phase of α-$Zr(HPO_4)_2 \cdot nH_2O$ was developed. The X-ray diffraction pattern of the phosphoric acid doped composite membrane was in good agreement with the reference diffraction data of crystalline α-$Zr(HPO_4)_2 \cdot nH_2O$. Based on the four sharp reflections at *d*-spacings of 7.75 Å, 4.56 Å, 3.56 Å and 2.63 Å the mean particle size was estimated to 16 nm using the Debye-Scherrer equation with correction for instrumental effects. This is about 4 times larger than the average diameter of the hydrophilic domains of a well hydrated and pure Nafion® membrane [60], which naturally should result in a considerable distortion of the original polymer morphology.

It has previously been proposed that the gradual crystallization of amorphous ZrP to pure α-$Zr(HPO_4)_2 \cdot nH_2O$ in concentrated phosphoric acid goes via a continuous digestion-recrystallization mechanism [175]. According to the literature, ZrP is also sparingly soluble in warm phosphoric acid in the higher concentration range. The solubility of ZrP in 15 mol L^{-1} (85%) phosphoric acid at 50 °C was reported to about 0.7-0.8 wt.%. Hence, it is probable that the major fraction of the ZrP in the composite membrane was dissolved and recrystallized as pure α-$Zr(HPO_4)_2 \cdot nH_2O$ during the doping. The digestion-recrystallization mechanism should thus result in a continuous loss of the ZrP to the

phosphoric acid bulk solution over time, as also confirmed by TGA of the membrane after doping for extended periods of time.

3.3.6 FTIR

The FTIR spectra of the pristine membranes covering the whole composition range were recorded at room temperature and are shown in Figure 3.7. The absorption band assignments are also summarized in Table 3.3.

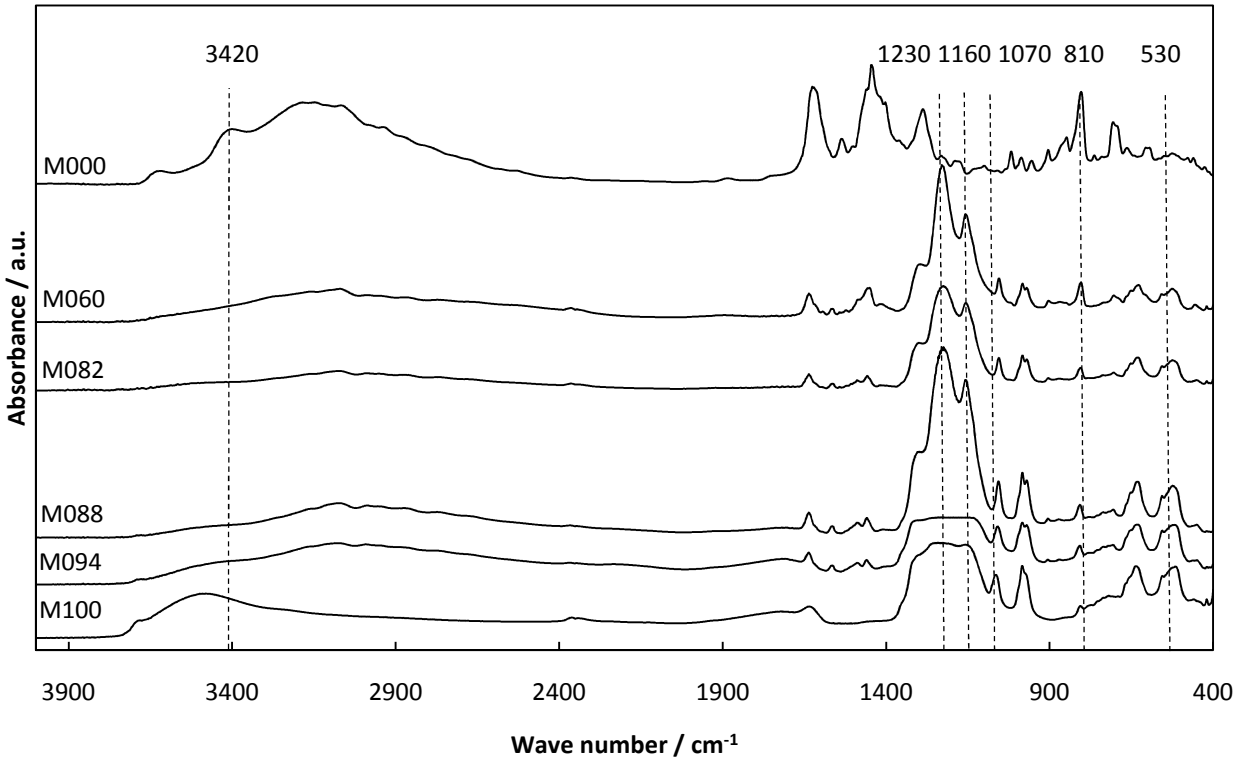

Figure 3.7 *FTIR spectra of the membranes based on Nafion®, PBI and their blends.*

A broad absorption band in the 1100-1370 cm^{-1} region was observed in the FTIR spectrum of the M100 and M094 membranes, which was assigned to overlapping C-F and sulfonic acid end group stretching. Two distinct absorption peaks were developed at 1230 cm^{-1} and 1160 cm^{-1} in the spectrum of the neutral membrane (M088) and of the blend membranes with an excess of basic groups (M082 and M060). The appearance and the exact location of these absorption bands are known to be highly dependent on the local environment of the sulfonate groups [142, 169]. The changed visual appearance of the absorption bands in this region of the spectrum could thus be connected to the formation of ionic sulfonate as a consequence of the complete proton transfer from Nafion® to PBI.

One characteristic absorption band for each of the two polymers in the FTIR fingerprint region (810 cm^{-1} for PBI and 530 cm^{-1} for Nafion®) was identified and integrated in order to obtain the relative peak areas. The peak area of the 810 cm^{-1} absorption band relative to the total peak area of the 810 cm^{-1} and 530 cm^{-1} absorption bands calculated for each spectrum according to Equation 3.5 are plotted versus the membrane composition in Figure 3.8.

$$Relative\ peak\ area = \frac{A_{810\ cm^{-1}}}{A_{810\ cm^{-1}} + A_{530\ cm^{-1}}} \tag{3.5}$$

A linear correlation between the relative peak area and the membrane composition was obtained, which further confirmed the blend membrane composition homogeneity after the casting and washing procedure.

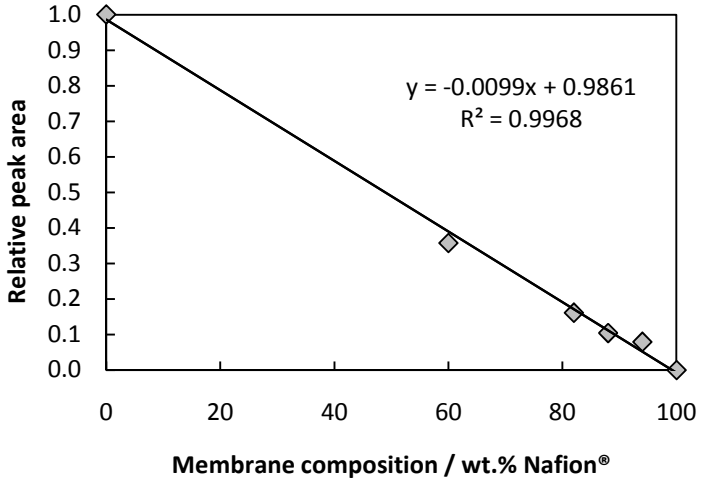

Figure 3.8 *Relative peak area of the FTIR absorption bands at 810 cm^{-1} and 530 cm^{-1} in Figure 3.7 as calculated according to Equation 3.5.*

The high frequency FTIR of M000 showed an absorption band at 3420 cm^{-1}, which was assigned to non-hydrogen bonded N-H stretching. It has previously been reported that this absorption band experiences a slight red shift to lower frequencies when PBI is blended with an acidic polymer, such as sPSF [142]. This red shift could thus be connected to the polymeric salt formation as a consequence of the acid-base interaction between the two polymers. Additionally, the characteristic S-O stretching at around 1070 cm^{-1} originating from the sulfonic acid end groups of Nafion® experienced a slight red shift to lower frequencies when the PBI content was increased (M94-M60), further indicating the strong interactions between the two polymers.

Table 3.3 *FTIR assignments of Nafion®, PBI and their blends.*

Wave number (cm^{-1})	**Assignment**		
	Nafion® [176, 177]	**PBI [142, 177-180]**	**Blends [177]**
530	CF_2-O-CF_2		
640	CF_2-O-, -CF_2-		
710		Benzene ring C-H bending	
810		Benzene ring C-H bending	
980 (s)	C-F stretching (-CF(CF_3)) C-O-C stretch		
1070 (m)	S-O stretch		
1100-1370 (s, broad)	CF_2 and CF_3 stretch, S-O stretch		
1160 (s, broad)			Ionic sulfonate
1230 (vs, broad)			Ionic sulfonate
1300 (s)		N-H	
1450 (vs)		Aromatic C-C stretch	
1630 (vs)		C=C/C=N imine stretch	
3160 (broad)		Hydrogen bonded N-H	
3420 (broad)		Non hydrogen bonded N-H	
3500 (broad)	O-H stretch		

The intensity of the 3420 cm^{-1} absorption band of all the Nafion®/PBI blend membranes in the present study (M094-M060) was very low while the 3160 cm^{-1} absorption band was still present. This indicates, just like expected, that the fraction of "free" non-hydrogen bonded N-H protons was very low in the Nafion®/PBI blends due to the polymeric salt formation [180].

3.3.7 Radical-oxidative stability

The relative chemical stability of the membranes was evaluated in an accelerated degradation test (Figure 3.9 and Figure 3.10), commonly referred to as the Fenton test. The polymer samples were submerged in aqueous solutions of hydrogen peroxide (3 wt.%) and 4 ppm Fe(II) in order to catalyze the decomposition of hydrogen peroxide into hydroxyl and perhydroxyl radicals according to Equation 2.10 and 2.11.

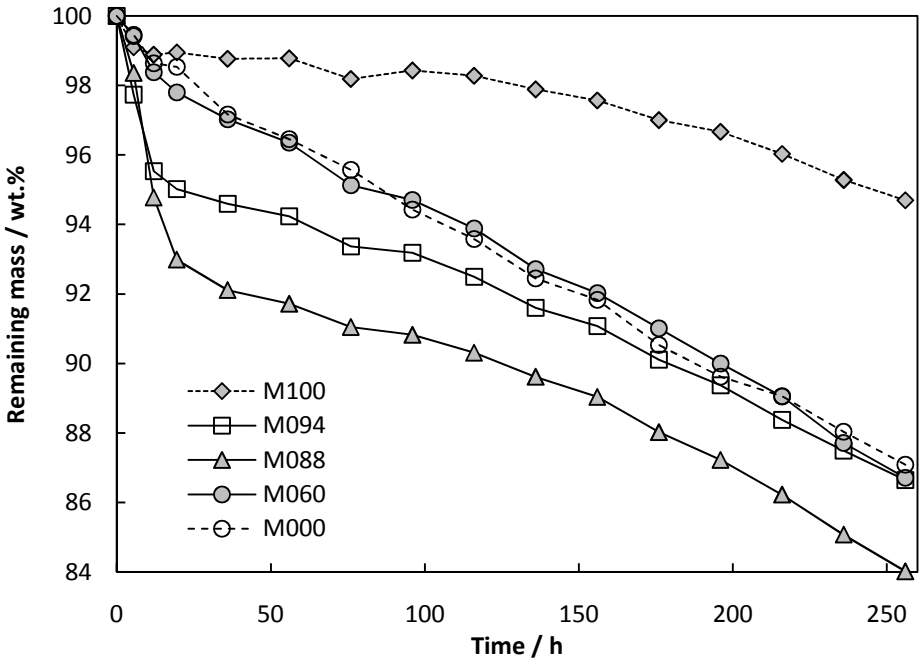

Figure 3.9 *Chemical degradation expressed as the membrane remaining mass after certain durations of the Fenton test.*

It is interesting to note that the highest initial rate of weight loss in the Fenton test was observed for the membrane with equimolar amounts of acidic and basic groups (M088). During the first 20 h of the Fenton test, the rate of weight loss was about 0.35 wt.% h^{-1} for M088, whereas it was only about 0.075 wt.% h^{-1} for the pure Nafion® and PBI membranes (M100 and M000). After 20 h of Fenton test, the rate of weight loss was stabilized at about 0.05 wt.% h^{-1} for M094-M000 and slightly lower for the pure Nafion® membrane (about 0.03 wt.% h^{-1}).

The chemical degradation of Nafion® in an oxidative environment has been the subject for extensive research since it has been identified as one of the most important factors that partly determine the long term durability of the conventional PFSA membrane based PEM fuel cells [181] and water electrolyzers [45]. The oxidative membrane degradation during fuel cell operation is often monitored by measuring the fluoride and sulphate ion emission rate in the effluent water using ion chromatography.

One possible starting point in the radical induced oxidative degradation of Nafion® is the radical attack on the sulfonic acid end groups, accompanied by a successive unzipping mechanism of the side chains according to Equation 3.6 and 3.7 [111].

$$-(CF_2)SO_3^- + R^\bullet \rightleftharpoons -(CF_2)SO_3^\bullet + R^- \quad (3.6)$$

$$-(CF_2)SO_3^\bullet \rightleftharpoons -(CF_2)^\bullet + SO_3 \quad (3.7)$$

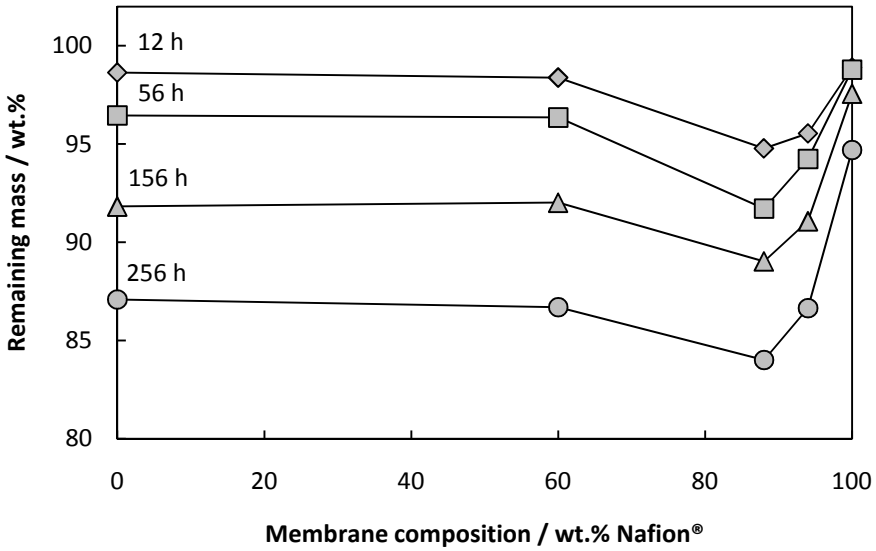

Figure 3.10 *Remaining membrane mass of M000, M060, M088, M094 and M100 after 12 h, 56 h, 156 h and 256 h of Fenton test.*

According to the proposed degradation mechanism in Equation 3.6 and 3.7, sulfur trioxide (SO_3) should be the degradation product that is released first. However, SO_3 does not exist as a discrete species in an aqueous solution. It will instantaneously form adducts ($^+OH_2\bullet SO_3^-$) with water followed by water assisted deprotonation to give aqueous sulfuric acid according to Equation 3.8.

$$SO_3 + H_2O \rightleftharpoons H_2SO_4\,(aq.) \quad (3.8)$$

Analogously, SO_3 has been demonstrated to form zwitterionic adducts with ammonia ($^+NH_3\bullet SO_3^-$) with relatively low energy barrier of formation [182]. Similarly, the electron donating sites in PBI may form adducts with SO_3 in the same manner as ammonia and thus promote the radical induced oxidation of Nafion® by shifting the reaction coordinate towards the SO_3 formation.

In this way PBI could function as a catalyst for the initiation of the radical induced oxidation of the sulfonic acid terminated side chains. This could also explain why the highest initial rate of weight loss was observed for the completely neutral membrane M088 having an equimolar amount of acidic and basic groups. As a result of the good homogeneity of the polymer blend, the sulfonic acid end groups should be positioned in proximity to the electron donating and the potential adduct forming basic sites in PBI. The high initial weight loss of M088 could thus be assigned to the decomposition of the sulfonic acid terminated side chains of the Nafion® component in the blend.

On the other hand, Kerres *et al.* [154] reported improved chemical resistance of ionically crosslinked blend membranes of PBI and sFPAE in the Fenton test. These contradicting results could possibly be explained by a major distinction in the degradation mechanism between Nafion® and the sFPAE.

3.3.8 Thermal and thermo-oxidative stability

The residual membrane mass at 500 °C under an inert atmosphere is plotted versus the pristine membrane composition in Figure 3.11. The membranes were heated from room temperature to 500 °C at a rate of 3 °C min^{-1}.

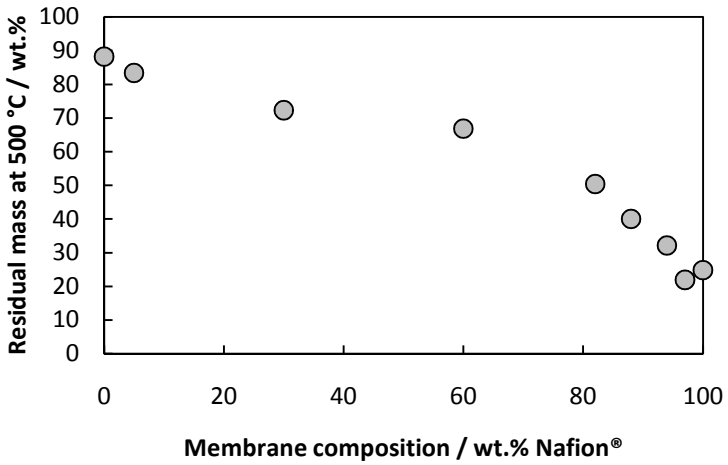

Figure 3.11 *Membrane residual masses at 500 °C under N_2 atmosphere.*

It shows a gradual increase of the remaining mass from about 25 wt.% to 88 wt.% as the PBI content of the membrane increased from 0 wt.% (M100) to 100 wt.% (M000). No signs of thermal incompatibility between the two polymers were observed and the gradual increase of the remaining mass was obviously connected to the gradually increased weight fraction of PBI, since PBI exhibits considerably better thermal stability than Nafion®.

The onset temperatures of the thermal induced major decomposition under air and nitrogen of the membranes covering the whole composition range are presented in Figure 3.12. The data were extracted from the thermogravimetric curves recorded using synthetic air and nitrogen as purge gases at heating rates of 10 °C min^{-1} and 3 °C min^{-1}, respectively.

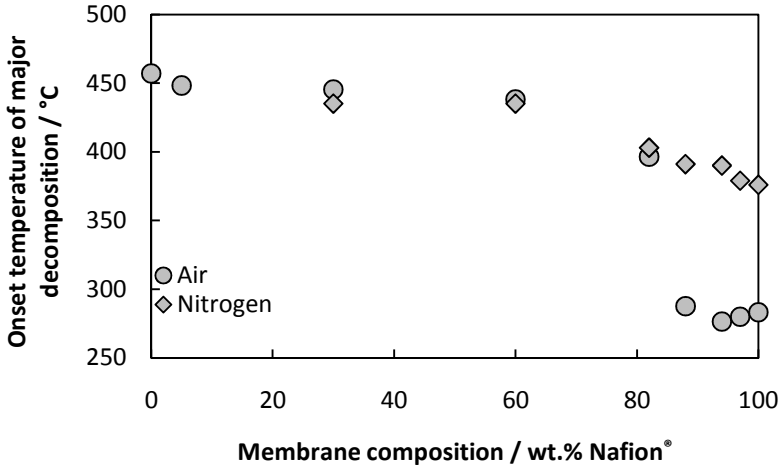

Figure 3.12 *Onset temperature of major decomposition of membranes covering the whole composition range.*

As seen in Figure 3.13, the thermal induced oxidation of Nafion® (M100) occurred in two major steps. The weight loss in the 280-400 °C region was connected to the thermo-oxidative degradation of the side chains of the polymer, whereas the weight loss above 400 °C was connected to thermal induced oxidation of the polymer backbone [125].

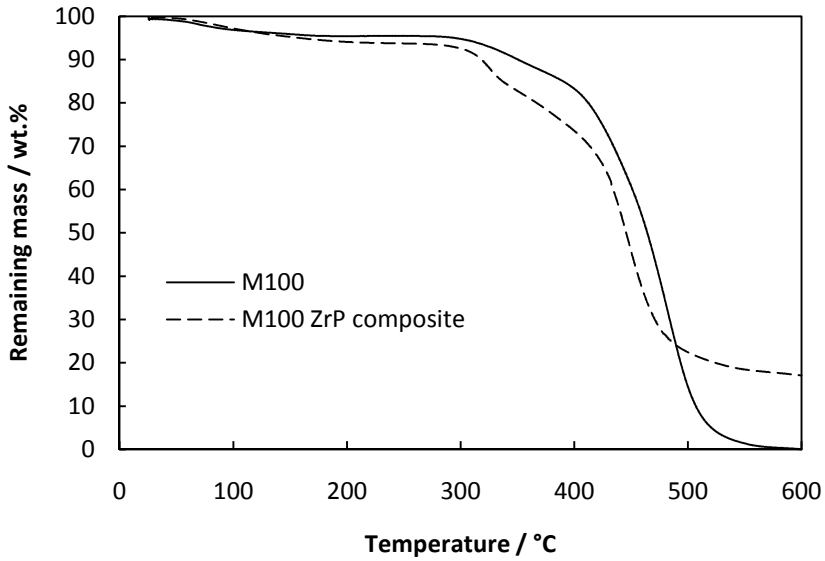

Figure 3.13 *Thermogravimetric curves of M100 and a ZrP composite membrane based on M100*.

A similar two-step thermo-oxidative degradation was observed for all the membranes having an excess of acidic groups (M100-M094). The first onset temperature of decomposition of these membranes under air was around 280 °C, as shown in Figure 3.12. The neutral membrane (M088) showed one single onset temperature of major decomposition at around 290 °C. Similary, all the membranes having an excess of basic groups (M082-M000) showed a single step thermo-oxidative decomposition. However, the onset temperature was shifted to above 400 °C.

Under nitrogen atmosphere, the thermal stability of the membranes in the high Nafion® content range (M088-M100) was dramatically improved even though the heating rate was lower, which should allow for a more efficient heat transfer to the sample. No onset temperature of major decomposition within the measured temperature range was observed for the membranes of high PBI contents (M000 and M005) under nitrogen.

On the other hand, the ZrP composite membranes based on M100-M094 exhibited slightly lower thermo-oxidative stability compared with their pristine counterparts, as exemplified in Figure 3.13. The onset temperature of major decomposition of the M100 based ZrP composite membrane was essentially the same as that of the pristine M100 membrane. However, the decomposition rate of the polymer matrix in the ZrP composite was higher than that of the pristine membrane, especially in the 280-400 °C temperature range. This phenomenon was most likely connected to thermochemical incompatibility between the polymer membrane and the inorganic filler [125].

3.3.9 Mechanical strength

Important mechanical data parameters of the pristine and the phosphoric acid doped membranes based on Nafion®, PBI and their blends covering the whole composition range are summarized in Table 3.4. Mechanical data of the ZrP composite membranes based on M100-M094 of varying ZrP

contents are also summarized. All stress-strain curves were recorded at 130 °C and without active relative humidity control which implies that that the relative humidity was close to zero.

Table 3.4 *Summary of Young´s modulus, elongation at break and engineering tensile stress at break of membranes and composites based on Nafion®, PBI and their blends. The stress-strain curves were recorded at 130 °C and at ambient relative humidity. The ZrP and phosphoric acid contents are indicated in the table.*

	Young´s modulus (MPa)		**Elongation at break (%)**		**Engineering tensile stress at break (MPa)**	
Membrane	Pristine	PA doped	Pristine	PA doped	Pristine	PA doped
M100 (34% PA)	2.9 ± 0.5	5.5 ± 0.8	> 800	732 ± 49	≈ 0	2.3 ± 0.2
M100 + 4 wt.% ZrP	10	N/A	65	N/A	3	N/A
M100 + 25 wt.% ZrP	30	N/A	7	N/A	1	N/A
M097	20	-	434	-	5	-
M097 + 5 wt.% ZrP	80	N/A	34	N/A	5	N/A
M097 + 18 wt. % ZrP	90	N/A	28	N/A	2	N/A
M094 (19% PA)	64.5 ± 8.7	59.0 ± 3.4	70.8 ± 9.9	192 ± 29.3	5.1 ± 0.9	3.6 ± 0.4
M094 + 7 wt.% ZrP	171	N/A	9	N/A	8	N/A
M088 (17% PA)	313 ± 12.4	200 ± 13.7	14.1 ± 2.1	19.8 ± 5.0	16.9 ± 0.3	9.1 ± 0.7
M082 (24% PA)	722 ± 25.6	272 ± 11.7	9.3 ± 1.7	64.5 ± 11.0	30.9 ± 2.7	13.2 ± 0.5
M060 (43% PA)	1596 ± 145	127 ± 15.8	16.4 ± 6.5	109 ± 8.8	68.7 ± 3.4	8.4 ± 0.6
M000 (78% PA)	2708 ± 510	5.8 ± 1.7	39.8 ± 8.6	113 ± 17.8	126 ± 16.9	1.8 ± 0.2

The resistance to deformation of the non-doped pristine membranes was improved as the PBI content of the membranes increased, indicated by a Young´s modulus increase from 2.9 MPa for M100 (pure Nafion®) to about 2.7 GPa for M000 (pure PBI). The engineering tensile stress at break data followed the same trend and increased gradually from about 0 for M100 to about 126 MPa for M000, which is in good agreement with previously reported mechanical data for PBI membranes [183].

The measuring temperature was above what is commonly referred to as the glass transition temperature T_g of Nafion® [184], which explains the very poor mechanical properties of M100. However, the extreme softening of Nafion® in this temperature range is not a true glass transition in the physical meaning. It has been assigned to the melting point of large crystallites in the material which causes the membrane to almost completely lose its dimensional stability [184, 185].

The elongation at break exceeded 800% for M100 and dropped to around 9% for M082 and then increased to about 40% for M000. The brittleness and the strong resistance to plastic deformation of the membranes close to the neutral composition further confirm the strong coulombic intermolecular forces between Nafion® and PBI.

Stress-strain curves were also recorded of the phosphoric acid doped membranes covering the whole composition range. M100, M094, M088 and M082 were doped in 85% H_3PO_4 at 150 °C whereas M060 and M000 were doped at 50 °C. The resulting acid contents are given in Figure 3.4 and are also indicated in parenthesis in Table 3.4.

It is well known that PBI membranes suffer from poor mechanical stability at high acid doping levels due to the strong plasticizing effect of phosphoric acid [183]. This was also confirmed in the present investigation and illustrated by a dramatic decrease of the Young´s modulus as well as the engineering tensile stress at break and an increase of the elongation at break, especially for the pristine phosphoric acid doped PBI membrane (M000). In order to highlight the mechanical properties dependence on the membrane composition, the Young´s modulus and the elongation at break of the phosphoric acid doped membranes covering the whole composition range are plotted in Figure 3.14.

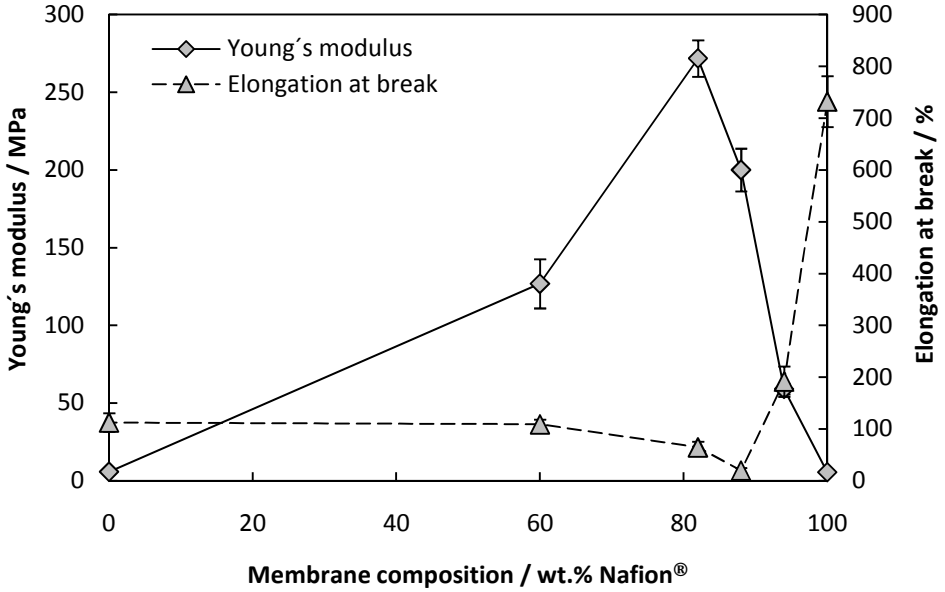

Figure 3.14 *Young´s modulus and elongation at break of phosphoric acid doped M100, M094, M088, M082, M060 and M000. The corresponding phosphoric acid contents are given in Table 3.4.*

The mechanical properties of the pure recast Nafion® membrane (M100) were improved after acid doping. This could eventually be connected to a shift in the softening temperature after the doping. After acid doping, an elongation at break minimum and a Young´s modulus and engineering tensile stress at break maximum was observed close to the neutral composition. This could primarily be explained by the low phosphoric acid contents of these membranes, which result in limited plasticizing effects. On the other hand, the lower phosphoric acid contents of these membranes were directly related to the strong intermolecular coulomb interactions between the two polymers, which should thus be the major reason for their limited volume swelling and their high dimensional stability after acid doping.

Furthermore, the ZrP composite membranes based on M100-M094 showed increased Young´s modulus and decreased elongation at break as well as engineering tensile stress at break compared with their pristine counterparts. It is well known that inorganic fillers such as ZrP improve the elastic modulus of Nafion® membranes by reducing the segmental motion of the polymer chains within in the structure [126]. The extent of the improvement is dependent on the amount of filler as well as the hydration number λ. In the present study, the membranes of high ZrP contents were fragile and brittle, as illustrated by a relatively high Young´s modulus and a very low engineering tensile stress at break.

The mechanical characteristics of PFSA membranes [126] and PBI membranes [155] are also known to be highly dependent on the water contents since the water molecules reduce the intermolecular hydrogen bond forces. However, under the present experimental conditions the plasticizing effect of water can most likely be neglected due to the very low water activity.

3.3.10 Proton conductivity

3.3.10.1 M100, M097 and M094 and their composites with ZrP

The in-plane proton conductivity of the pristine blend membranes of high Nafion® contents (M100, M097 and M094) and of the ZrP composite membranes based on M100, M097 and M094 was

measured at 130 °C and at relative humidity (RH) ranging from about 18-37%. The conductivity data are summarized in Figure 3.15.

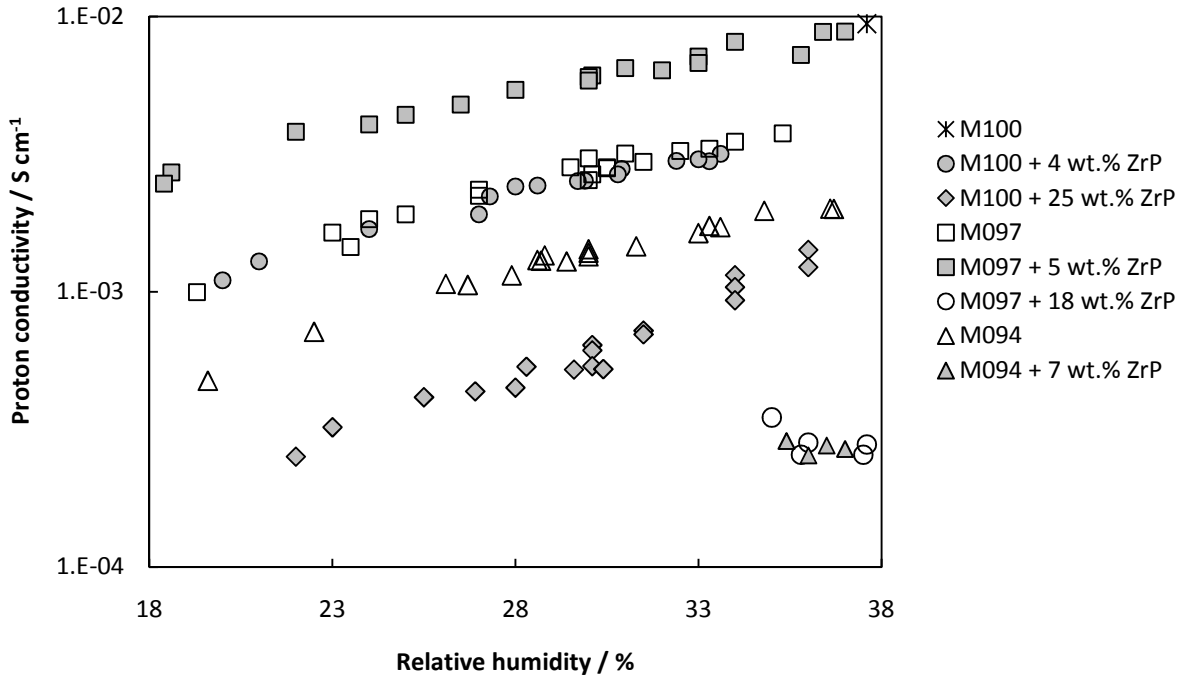

Figure 3.15 *In-plane proton conductivity of M100, M097 and M094 and of the ZrP composite membranes based on M100, M097 and M094 at 130 °C as functions of relative humidity.*

The conductivity of the pristine membranes having an excess of basic groups (M088-M000) was out of the range of the conductivity measurement hardware and was estimated to be below 10^{-4} S cm^{-1}. Pure PBI (M000) has been reported to exhibit proton conductivity in the 10^{-4} S cm^{-1} range [186], i.e. at least 2-3 orders of magnitude too low for any practical use as electrolyte material in PEM water electrolyzers or fuel cells.

The pure recast Nafion® membrane (M100) exhibited proton conductivity of about 10^{-2} S cm^{-1} at 130 °C and 37% RH. However, due to the poorly defined sample dimensions of M100 under the experimental conditions the conductivity data must be considered as rather uncertain. However, a PEM fuel cell operated under these conditions would suffer from severe reactant starvation due to the high partial pressure of steam. It means that no current can be drawn even though the membrane conductivity might be sufficient. On the other hand, the high water activity should be beneficial when the cell is operated in water electrolysis mode.

At 130 °C and 30% RH, the conductivity of the composite membrane based on M100 with a ZrP content of 4 wt.% was about 2×10^{-3} S cm^{-1}. When the ZrP content was increased to 25 wt.%, the conductivity dropped to around 6×10^{-4} S cm^{-1}. For comparison, proton conductivity of 5×10^{-3} S cm^{-1} at 120 °C and 45% RH was recently reported for a composite membrane based on Nafion® 115 with a ZrP content of 7.8 wt.% [124]. When the ZrP content was increased to 16 wt.%, the conductivity dropped to 1×10^{-3} S cm^{-1}.

The conductivity of the pristine membrane M097 (3×10^{-3} S cm^{-1} at 30% RH) was comparable to that of membrane M100 with a ZrP content of 4 wt.%. By slightly increasing the PBI content of the blend membrane (membrane M094) the conductivity decreased to 1×10^{-3} S cm^{-1}, most likely due to the reduced fraction of “free” acidic groups within the membrane and thus the reduced ion exchange

capacity. According to Equation 3.4 the number of acidic groups per PBI_{RU} is around 9.0 and 4.5 for membrane M097 and M094, respectively. It implies that M094 should exhibit 50% lower ion exchange capacity compared with M097, which naturally should result in reduced proton conductivity.

The highest in-plane proton conductivity (6×10^{-3} S cm^{-1} at 30% RH) was obtained for the composite membrane based on M097 with a ZrP content of 4 wt.%. On the other hand, the composite membrane based on M097 with a ZrP content of 18 wt.% exhibited proton conductivity as low as in the 10^{-4} S cm^{-1} range even at relative humidity as high as 35%.

3.3.10.2 Phosphoric acid doped membranes

The conductivity of the phosphoric acid doped membranes was measured through the membrane cross-section due to the considerable surface bleeding of phosphoric acid from the acid doped membranes of high Nafion® contents. In this way the surface effects connected to proton conduction in the thin phosphoric acid layer on the membrane surface could be avoided. The through-plane conductivity data are shown in Figure 3.16. The measurements were carried out at 130 °C and the relative humidity was controlled at about 16-18%.

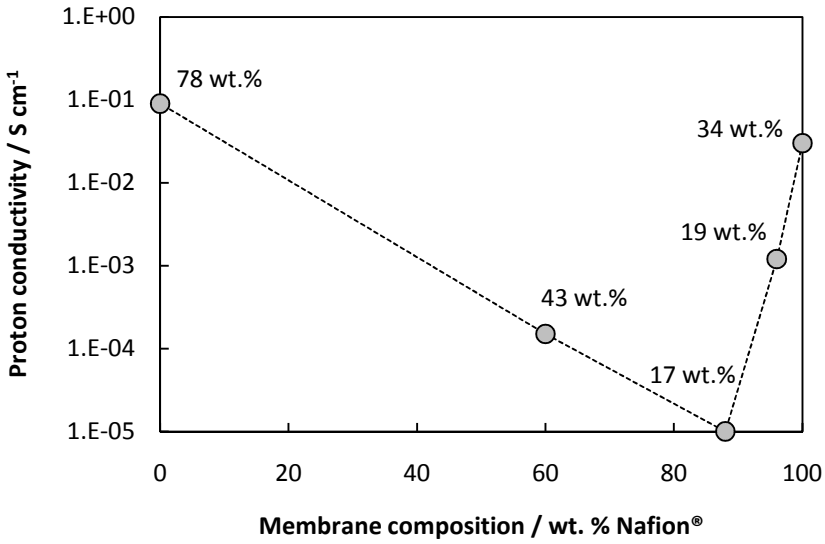

Figure 3.16 *Proton conductivity of the phosphoric acid doped membranes covering the whole composition range at 130 °C and relative humidity of 16-18%. The corresponding phosphoric acid contents of the membranes are indicated in the figure as also indicated in Table 3.4.*

The blend membranes with Nafion® contents of 88 wt.% (M088), 94 wt.% (M094) and 100 wt.% (M100) were doped in 85% H_3PO_4 at 150°C for about 16 hours, whereas the blend membranes with Nafion® contents of 0 wt.% (M000) and 60 wt.% (M060) were doped in 85% H_3PO_4 at 50 °C overnight. The phosphoric acid contents of these membranes are indicated in the figure, also as shown in Figure 3.4 and Table 3.4.

It should be remembered that it is not straightforward to compare these results because of the large discrepancies in terms of the total phosphoric acid contents. The conductivity of M000 having an acid content of 78 wt.%, corresponding to an acid doping level of around 11, was about 0.09 S cm^{-1}. The phosphoric acid doped pure Nafion® membrane (M100) with an acid content of 34 wt.% exhibited proton conductivity of 0.03-0.04 S cm^{-1}. Both were in good agreement with the previously reported literature data [67, 101].

However, the conductivity of the phosphoric acid doped blend membranes was considerably lower. This was most likely a direct consequence of the low phosphoric acid contents of these membranes and thus indirectly a consequence of the strong intermolecular ionic interactions between the two polymers. On the other hand, the reduced ion exchange capacity of the blend membranes should also negatively influence the conductivity.

3.3.11 Steam electrolysis tests

It is well known that a membrane proton conductivity of at least 10^{-2} S cm^{-1} is required for high temperature PEM fuel cells in order to obtain reasonable performance at high current densities [55]. The membrane thickness can in principle be reduced in order to lower the area specific resistance and thereby compensate for slightly lower membrane conductivity. However, the proton conductivity requirement should also be valid when the cell is operated in electrolysis mode since there is logically a limitation in how thin the membrane can be made from mechanical strength and gas permeability points of view.

In order to evaluate the membranes as electrolyte materials, water electrolysis polarization curves of MEAs based on M100 and a composite membrane based on M097 with a ZrP content of about 5 wt.% were recorded. Polarization curves were also recorded of the MEAs based on the phosphoric acid doped M100 and M000 membranes. The single cells were assembled directly from anode, cathode and membrane without previous hot-pressing.

3.3.11.1 M100 and the ZrP composite based on M097

The pure M100 membrane showed better performance compared with the M097 based ZrP composite membrane at 80 °C as well as at 120 °C, as illustrated by the polarization curves in Figure 3.17.

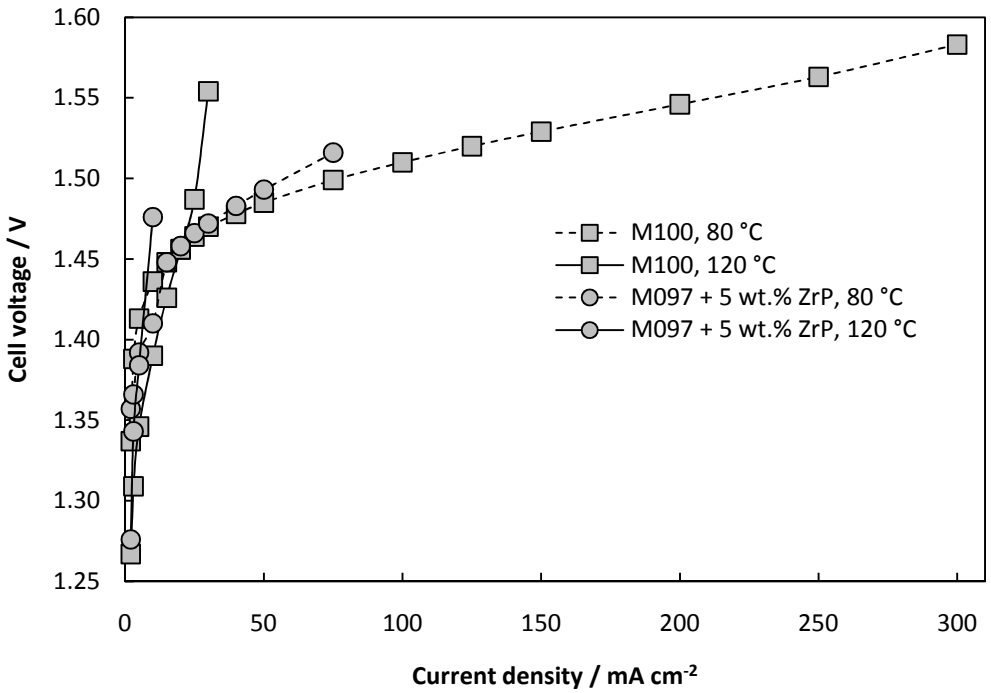

Figure 3.17 *Polarization curves at 80 °C and 120 °C of the MEAs based on M100 and M097 + 5 wt.% ZrP.*

Based on the conductivity data in the high relative humidity range in Figure 3.15 and assuming a membrane thickness of 50 μm, the M097 based composite membrane with a ZrP content of 4 wt.% would give a voltage loss of about 200 mV at a current density of 200 mA cm^{-2} and about 1000 mV at a more practical current density of 1000 mA cm^{-2} if operated at 130 °C. The membrane contribution to the overall voltage loss is thus about one order of magnitude higher than the demands in terms of efficiency and gas production rate normally can allow for.

However, the performance of the MEA based on pure recast Nafion® (M100) operating at 80 °C was considerably lower than what can be expected for a MEA based on this membrane type operating under fully hydrous conditions.

For example, assuming a proton conductivity of 0.1 S cm^{-1} for a membrane of this type (M100) under fully hydrous conditions at 80 °C and a membrane thickness of 50 μm, the membrane contribution to the overall voltage loss would be 10 mV at a current density of 200 mA cm^{-2} and about 50 mV at a current density of 1000 mA cm^{-2}. For comparison, a Nafion® 115 based MEA was recently reported to operate at about 500 mA cm^{-2} at a cell voltage of 1.6 V at 80 °C [87]. 67% higher current density was thus reached at similar cell voltage of the MEA based on a similar electrolyte material, even though the membrane was considerably thicker.

The performance loss in the present investigation was mainly found in the linear region of the polarization curve. It indicates that it should be a substantial contribution to the overall ohmic resistance from the cell hardware, catalyst layers or from the membrane electrode interface apart from the pure membrane resistivity, as also discussed by Millet *et al.* [56]. Poor contact in the membrane electrode interface could also result in hot-spots. Hot-spot formation should severely affect the membrane chemically as well as physiochemically at high current density and ultimately lead to complete membrane failure.

3.3.11.2 Phosphoric acid doped membranes

Based on the results from the through-plane conductivity measurements it was obvious that only the pure phosphoric acid doped Nafion® (M100) and PBI (M000) membranes could fulfill the membrane conductivity requirements. Representative polarization curves of a set of MEAs based on pure PBI (M000) and Nafion® (M100) doped in 85% H_3PO_4 at 50 °C and 150 °C, respectively, are shown in Figure 3.18.

It can be seen that at low current densities (up to about 30 mA cm^{-2}) the cell voltage of the phosphoric acid doped M000 and M100 based MEAs were more or less identical. It indicates that the major difference in the cell performance was not related to differences in the catalytic activity of the electrodes.

Furthermore, it can be seen that the current density reached at the same cell voltage of the MEAs based on the phosphoric acid doped M000 and M100 were generally substantially higher than that of the MEAs based on the membranes of pure recast Nafion® (M100) and the M097 composite membrane with a ZrP content of 5 wt.%. Even though the cell temperature was 10 °C higher, the ohmic voltage losses of the phosphoric acid doped membrane based cells were lower due to the conductivity mechanism´s reduced water dependence. Additionally, the phosphoric acid should allow for a lower contact resistance in the membrane electrode interface, which naturally results in a lower overall ohmic resistance and thus better steam electrolysis performance of the MEA in the high current density range.

The current density of the MEA based on phosphoric acid doped M100 reached 300 mA cm^{-2} at 1.75 V. However, the current density at 1.75 V was significantly higher for the MEA based on phosphoric acid doped M000 (500 mA cm^{-2}). This is comparable with the current density of about 450 mA cm^{-2} at 1.75 V, which was reported by Antonucci *et al.* [87] for a Nafion®-SiO_2 composite membrane based steam fed cell operated at 120 °C at ambient pressure. Under similar operating conditions, Baglio *et al.* [88]

reached a current density of about 650 mA cm^{-2} at 1.75 V using a MEA based on a Nafion®-TiO_2 composite membrane. However, the better performances in general of the MEAs based on the Nafion®-SiO_2 and Nafion®-TiO_2 composite membranes compared with the cell based on the phosphoric acid doped M100 membrane in the present study could most likely partly be connected to their lower activation overvoltages due to better catalytic activity of the anodes. This also becomes obvious when the non-linear parts of the polarization curves in the low current density range are compared.

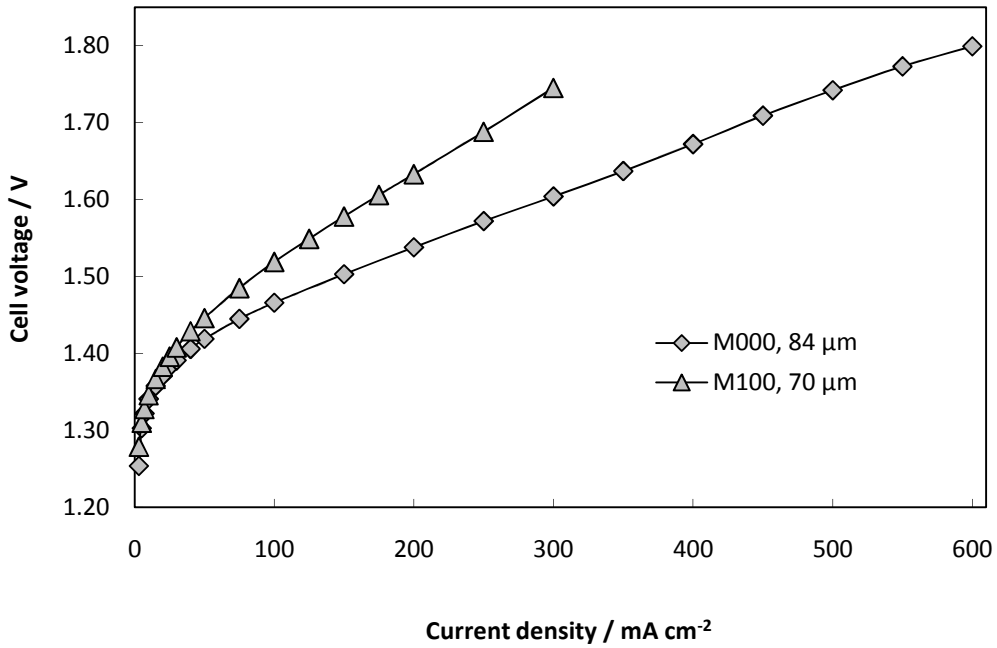

Figure 3.18 *Polarization curves at 130 °C of the steam electrolysis MEAs based on PA doped M100 and M000. The type of membrane and the corresponding membrane thickness is indicated in the legend.*

Unfortunately, the MEAs based on phosphoric acid doped PBI (M000) suffered from severe durability limitations. Most of the tested MEAs based on this membrane type lasted only for a couple of hours. The durability problems were apparently connected to severe membrane failure which resulted in short circuiting of the cell. This was illustrated by a gradual decrease of the cell voltage when it was operated at constant current density. The voltage decay was also accompanied by a reduction of the gas (both hydrogen and oxygen) evolution rate. For comparison, high temperature PEM fuel cell tests with MEAs based on phosphoric acid doped PBI membranes have demonstrated durability of more than 10000 h with an average cell voltage decay rate of about 5-10 µV h^{-1} [55, 69].

The phosphoric acid doped Nafion® (M100) membranes, on the other hand, exhibited considerably better durability in water electrolysis mode. For example, during a continuous operation test for about 90 hours the current density at a constant cell voltage of 1.7 V was recorded as a function of time, as shown in Figure 3.19.

The current density was found to vary with temperature and steam pumping rate. However, no evident membrane degradation was observed from the polarization data or with respect to the hydrogen and oxygen production rates.

Although the time scale was relatively short, the stable performance of the phosphoric acid doped M100 membrane demonstrated the proof of concept as electrolyte material for operation at elevated temperature and at ambient pressure. It should thus be possible to improve the cell performance by

further increasing the total phosphoric acid content of the membrane and by improving for example the cell components and their interfaces.

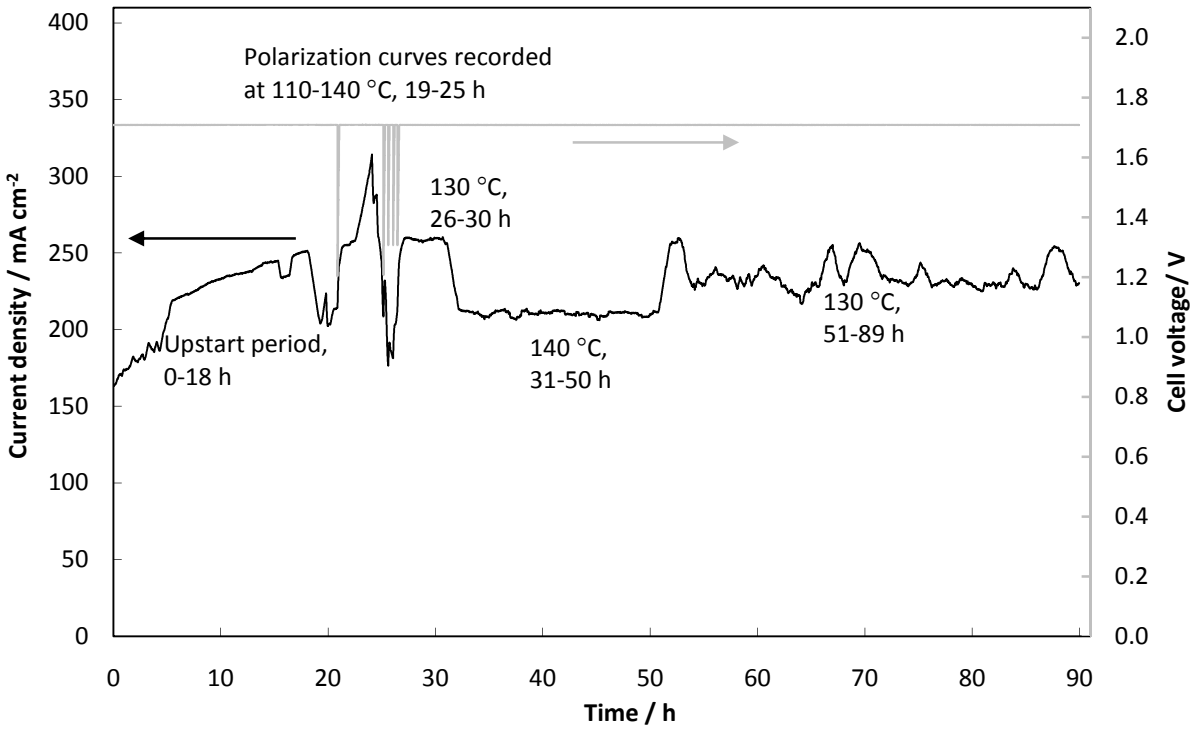

Figure 3.19 *Performance of an electrolysis cell based on phosphoric acid doped M100 under a constant cell voltage. The variation of the cell temperature is indicated in the figure.*

The degradation mechanism of the phosphoric acid doped PBI membranes (M100) under the electrolysis conditions has not been further investigated but might involve hydrolysis, as suggested by Linkous [113]. PBI was found to be thermo-hydrolytically stable at 200 °C under a steam containing atmosphere for at least 24 h. However, under steam atmosphere at 300 °C the material was found to be severely degraded after 24 h.

Imine hydrolysis is an acid catalyzed reaction and the hydrolytic resistance of PBI could thus be dramatically reduced by the phosphoric acid. The acid catalyzed hydrolysis of PBI is thus simply the reverse of the polycondensation reaction (Scheme 1.1) and is schematically depicted in Scheme 3.1. The protonation of the imine enhances the electrophilicity of the carbon atom linking the benzimidazole moieties and the adjacent benzenoid rings which should facilitate the polymer hydrolysis.

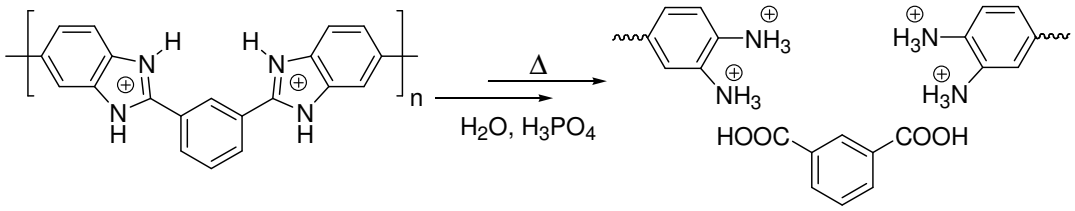

Scheme 3.1 *The acid catalyzed hydrolysis of PBI.*

In addition to the considerably higher water activity, the potentials are also significantly higher when the cell is operated in water electrolysis mode compared with in fuel cell mode which eventually also could affect the membrane long term durability and eventually the acid catalyzed hydrolysis reaction coordinate.

3.4 Towards improved steam electrolysis performance

Although the pure phosphoric acid doped Nafion® (M100) membrane showed promising results in the steam electrolysis tests at 130 °C, the performance was rather poor. The relatively poor performance was suspected to be partly connected to the limited dimensional stability of the membrane under the operating conditions. Additionally, the total phosphoric acid content of the M100 was relatively low which was suspected to be one of factors limiting the proton conductivity since phosphoric acid apparently was the major contributor to the proton conductivity under anhydrous conditions.

In order to further improve the electrolysis performance, alternative phosphoric acid doped PFSA membranes were considered. These included different types of melt extruded and solution or dispersion cast PFSA membranes of varying equivalent weights.

3.4.1 Phosphoric acid doping

The phosphoric acid contents after doping of different melt extruded and solution or dispersion cast PFSA based membrane types of varying equivalent weights from different manufacturers are summarized in Table 3.5.

Table 3.5 *Obtained phosphoric acid contents of different PFSA membrane types after doping. Unless otherwise noticed, the doping was performed in 85% H_3PO_4 at 150 °C for 16 h.*

Entry	PFSA membrane type	Phosphoric acid content (wt.%)
1	Nafion® 105	27.1
2	Nafion® 112	27.1
3	Nafion® 212	19.5
4	Nafion® 212 (pre-swollen in MeOH)	27.1
5	Nafion® 115	25.7
6	Nafion® 115 (100% PA, 150 °C)	27.1
7	Nafion® 115 (100% PA, 180 °C)	27.5
8	Hyflon™-ion	38.2
9	Aquivion™	43.9
10	50 µm recast Nafion®	36.6
11	120 µm recast Nafion®	33.8
12	120 µm recast Nafion® (pre-swollen in MeOH)	40.4

For the different types of commercially available melt extruded or solution/dispersion cast Nafion® membranes (105, 112, 115) the total phosphoric acid content after doping in 85% H_3PO_4 at 150 °C was about 25 wt.%. According to Equation 3.9, it corresponds to a relative phosphoric acid content of about 4 phosphoric acid molecules per sulfonic acid group. Increased doping temperature or increased concentration of the phosphoric acid doping solution did not result in increased phosphoric acid uptake of the Nafion® 115 membrane (Table 3.5, Entry 6-7).

$$Relative\ acid\ content = \frac{n_{H_3PO_4}}{n_{SO_3^-}} \tag{3.9}$$

On the other hand, the recast Nafion® membranes displayed a somewhat higher phosphoric acid content of about 34-37 wt.%, corresponding to about 5-6 phosphoric acid molecules per sulfonic acid group (Table 3.5, Entry 10-11). In order to further increase the phosphoric acid content and thus the proton conductivity, membranes of recast Nafion® and Nafion® 212 were pre-swollen in a 1:1 (v/v) water:MeOH mixture at 70 °C for 1 h in order to expand the polymer matrix before the acid doping (Table 3.5, Entry 4 and 12). By this methodology, the phosphoric acid contents of Nafion® 212 and the recast Nafion® membrane could be increased from 19.5% to 27.1% and from 33.8% to 40.4%, respectively.

The melt extruded membranes based on short side chain PFSA membrane types (Hyflon™-ion and Aquivion™) showed the highest total phosphoric acid uptakes (Table 3.5, Entry 8-9). The equivalent weights of the Hyflon™-ion and Aquivion™ membranes used in the present study were about 850 g eq^{-1} and 790 g eq^{-1}, respectively. Hence, the phosphoric acid contents of the Hyflon™-ion and Aquivion™ membranes after doping corresponded to about 5-6 phosphoric acid molecules per sulfonic acid group.

Conclusively, the maximum number of phosphoric acid molecules per sulfonic acid group that could be obtained was about 5-6. This number was in agreement with or slightly higher than previously reported data for Nafion® 117 doped in 85% H_3PO_4 at 150 °C [67]. However, even though the number of phosphoric acid molecules per sulfonic acid group was maximum 5-6, the total amount of phosphoric acid absorbed by the short side chain PFSA based membranes was higher, apparently due to the considerably lower equivalent weight compared with Nafion®.

3.4.2 Mechanical strength

It is well known that a certain degree of crystallinity of a PFSA based membrane is crucial in order to make it mechanically stable and insoluble in water. Hence, the membranes prepared by melt extrusion casting are generally characterized by better mechanical properties compared with the solution cast membranes due to their more well developed crystallinity.

3.4.2.1 Annealing of recast Nafion®

Annealing is thus generally required for recast PFSA membranes in order to develop crystalline regions and to obtain insoluble films with sufficient mechanical strength for the MEA preparation. For example, small angle X-ray diffraction (SAXS) measurements revealed that annealing of recast Nafion® films in the salt forms at temperatures up to 200 °C increases the lamellar crystallite size, improves the internal order and develops long-range order [59, 185]. Completely amorphous PFSA membranes prepared at low temperatures are extensively swollen or even dissolved in water, resulting in a complete loss of its dimensional stability.

Annealing should thus result in a membrane with a higher degree of crystallinity and thus a morphology resembling that of the commercially available melt extruded Nafion® 115 and 117 membranes.

In order to evaluate how the thermal history affects the mechanical properties of recast Nafion®, a set of recast Nafion® membranes was annealed at temperatures ranging from 120-160 °C. The membranes were annealed in the Nafion®-NH_4 form in order to avoid the self acid-catalyzed ether hydrolysis of the sulfonic acid terminated branches. The membranes were subsequently treated in hot H_2SO_4 and boiled in demineralized water in order to restore the protonated form of the ionomer. Stress-strain curves were recorded at 130 °C and the mechanical data are summarized in Table 3.6.

Table 3.6 *The annealing effect on the mechanical properties of recast Nafion®. The annealing time was 6 h and the annealing temperatures are indicated in the table. The stress-strain curves were recorded at 130 °C.*

Annealing temperature	Young´s Modulus (MPa)	Elongation at break (%)	Engineering tensile stress at break (MPa)
120 °C (standard)	2.9 ± 0.5	< 800	≈ 0
140 °C	6.5 ± 2.1	771 ± 104	0.1 ± 0.1
160 °C	14.6 ± 3.8	874 ± 152	0.2 ± 0.2

The increased degree of crystallinity after annealing was illustrated on a macroscopic scale by increased toughness. For example, the Young´s modulus of the membrane which had been annealed at 160 °C was about 400% higher compared with that of the membrane which had been annealed at 120 °C.

For conventional Nafion® membranes, an equivalent weight of around 1100 g eq^{-1} has been a well established compromise between high ion exchange capacity and good mechanical properties in water [63]. Nafion® membranes of lower equivalent weights tend to soften or even dissolve completely after hydration due to their limited degree of crystallinity.

The equivalent weight of a PFSA based membrane with a certain chemical structure thus directly affects the physiochemical characteristics of the membrane. The interrelated membrane characteristics can be summarized according to Scheme 3.2 below.

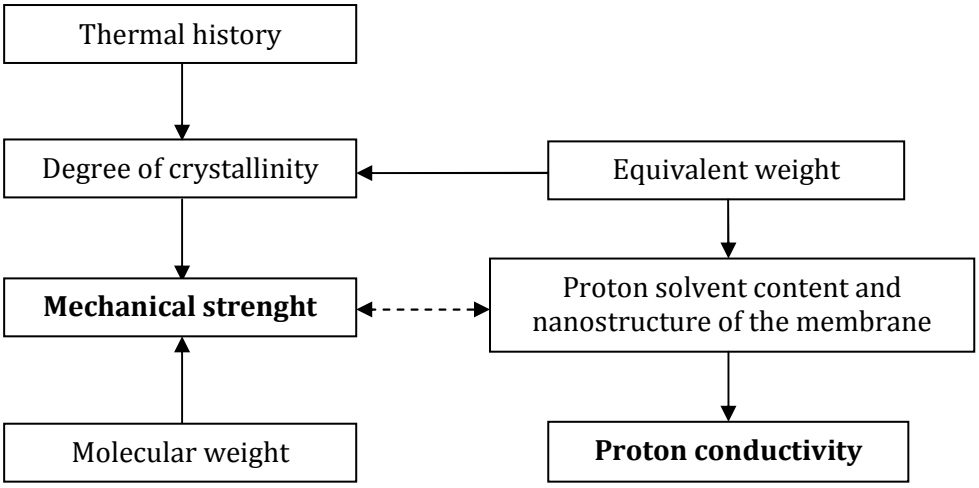

Scheme 3.2 *Schematic illustration of the relationship between the equivalent weight of a PFSA membrane with a certain repeating chemical structure and some of the physiochemical properties of the corresponding membranes.*

The most important parameters for the practical use of the membranes material that are connected to the equivalent weight are probably the mechanical strength and the proton conductivity, as also highlighted in Scheme 3.2.

The proton conductivity of the membrane is directly related to the proton solvent content of the membrane. The proton solvent content of the membrane is mainly determined by the equivalent weight. The proton solvent uptake also affects the mechanical characteristics of the membrane since proton solvent normally act as plasticizer, unless the proton solvent is a solid inorganic proton

conductor such as ZrP. On the other hand, poor mechanical strength of the membrane should allow for high volume swelling and thus high proton solvent uptake and high proton conductivity.

The equivalent weight also determines the degree of crystallinity of the membrane, which is also highly dependent on its thermal history. The degree of crystallinity is in turn strongly correlated to the mechanical characteristics of the membrane. The mechanical strength of the membrane can also be improved by increasing the molecular weight of the polymer.

3.4.2.2 Membranes based on short side chain PFSA

Membranes based on short side chain PFSA are known to exhibit considerably higher melting temperatures of the large crystalline regions (commonly referred to as T_g) compared with Nafion® [187]. Consequently, they can maintain their dimensional stability at higher temperatures which naturally makes them more suitable than for example Nafion® as electrolyte materials for applications at elevated temperatures.

Typical stress-strain curves of phosphoric acid doped membranes based on recast Nafion® (M100) and the commercially available melt extruded Aquivion™ E79-05S (Figure 1.7), which is a short side chain PFSA based membrane with an equivalent weight of about 790 g eq^{-1}, are shown in Figure 3.20. The phosphoric acid contents were as shown in Table 3.5.

Depending on the equivalent weight and the thermal history of the short side chain PFSA membrane the crystalline melting temperature varies between 150-180 °C [63, 64], compared with about 100-120 °C for Nafion® [184]. The higher crystalline melting temperatures in general of the short side chain PFSA membrane has been attributed to the closer and more well ordered polymer chain packing due to the reduced plasticizing effect of the shorter side chains.

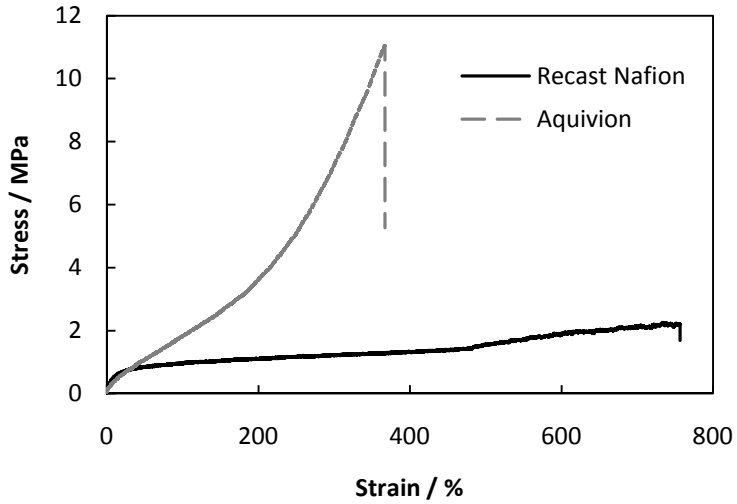

Figure 3.20 *Representative stress-strain curves at 130 °C of phosphoric acid doped Nafion® and Aquivion™ with phosphoric acid contents of 34 wt.% and 44 wt.%, respectively,*

Superior H_2/O_2 fuel cell performance (2500 mA cm^{-2} at 0.5 V) was achieved during operation of the MEAs based on short side chain PFSA membranes as early as 1990 [188]. For comparison, the current density at the same cell voltage of the Nafion® 117 based MEA was about 1000 mA cm^{-2}. Kreuer *et al.* [63] have identified the superior dimensional stability and the high elastic modulus of the short side chain PFSA membranes as the main factors responsible for their excellent fuel cell performance.

As also summarized in Table 3.7, the phosphoric acid doped Aquivion™ membrane showed considerably higher Young´s modulus and engineering tensile stress at break at 130 °C compared with the phosphoric acid doped recast Nafion® membrane. The Aquivion™ membrane also showed a significantly higher resistance to plastic deformation.

Table 3.7 *Summary of the mechanical data at 130 °C of pristine and phosphoric acid doped Nafion® and Aquivion™.*

	Recast Nafion®	Aquivion™	PA doped recast Nafion®	PA doped Aquivion™
Young´s Modulus (MPa)	2.9 ± 0.5	113.7 ± 24.3	5.5 ± 0.8	8.8 ± 1.5
Engineering tensile stress at break (MPa)	≈ 0	13.8 ± 2.9	2.3 ± 0.2	10.0 ± 0.8
Elongation at break (%)	< 800	166 ± 14	732 ± 49	347 ± 13

The Young´s modulus of the Aquivion™ membrane was dramatically reduced after phosphoric acid doping whereas it was slightly increased for the phosphoric acid doped recast Nafion® (M100) membrane. This could eventually be connected to the considerably higher total phosphoric acid content of the Aquivion™ membrane.

3.4.3 Phosphoric acid doped Aquivion™ as electrolyte in steam electrolysis

Steam electrolysis mode polarization curves were recorded at 120-130 °C of a MEA based on a phosphoric acid doped Aquivion™ membrane as shown in Figure 3.21.

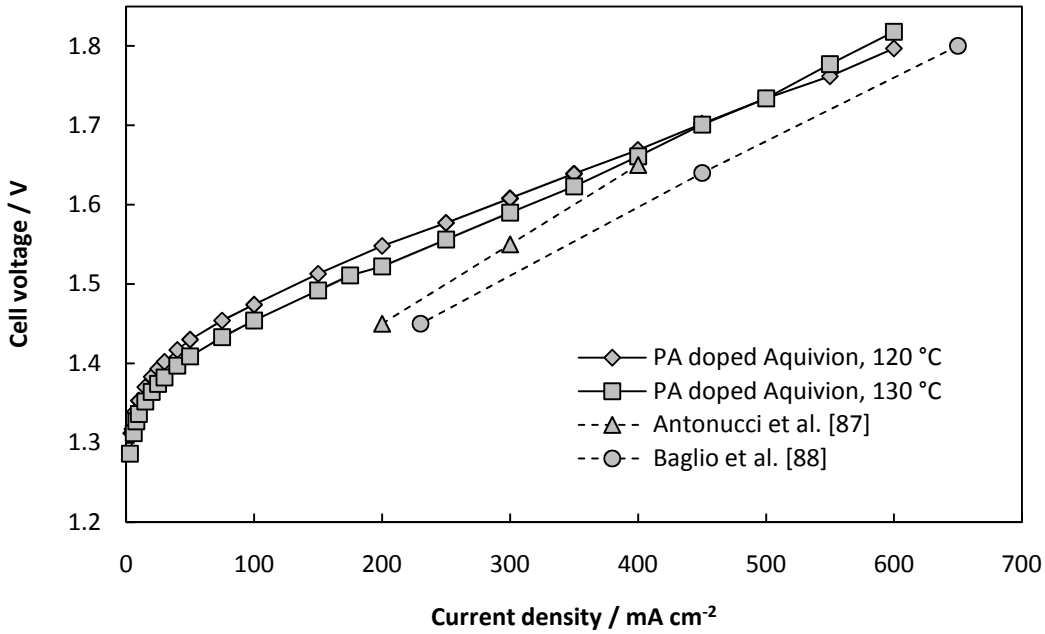

Figure 3.21 *Steam electrolysis polarization curves at 120 °C and 130 °C of the MEA based on phosphoric acid doped Aquivion™. The high current parts of the polarization curves of the MEAs based on the Nafion®-SiO_2 composite (Antonucci et al. [87]) and the Nafion®-TiO_2 composite (Baglio et al. [88]) which were recorded at 120 °C at ambient pressure are included for comparison.*

The MEA which was based on the phosphoric acid doped Aquivion™ membrane showed superior performance compared with the MEA based on phosphoric acid doped recast Nafion® (M100, Figure 3.18). For example, at a cell voltage of 1.75 V a current density of 500 mA cm^{-2} was reached. This should be compared with about 300 mA cm^{-2} for the MEA based on a phosphoric acid doped recast Nafion® (M100) membrane of comparable thickness.

For comparison, the slope of the polarization curve of the MEA based on the phosphoric acid doped Aquivion™ in the linear high current range at 120 °C was slightly lower than the slope of the corresponding polarization curves of the MEAs on the Nafion®-SiO_2 composite (Figure 1b in Antonucci *et al.* [87]) and the Nafion®-TiO_2 composite (Figure 6 in Baglio *et al.* [88]) which were recorded under similar conditions. This indicates that the ohmic resistance of the phosphoric acid doped Aquivion™ based MEA was slightly lower. On the other hand, the activation overvoltage which is mainly determined by the activity of the anode catalyst was obviously considerably higher which resulted in poorer performance in low current density range.

At 130 °C, slightly better performance was obtained in the low current density range compared with at 120 °C. It might be connected to improved electrode kinetics due to the higher temperature. However, the slope of the linear region of the polarization curve was increased with the increased temperature, indicating limitations in the membrane anhydrous proton conductivity. Hence, in the higher current density range (above 500 mA cm^{-2}) slightly better performance was obtained at 120 °C.

The superior steam electrolysis performance of the phosphoric acid doped Aquivion™ membrane compared with the phosphoric acid doped recast Nafion® membrane (M100) was most likely connected to the short side chain structure and low equivalent weight of Aquivion™ [63]. It allowed for higher phosphoric acid contents due to the increased concentration of sulfonic acid groups, as discussed in Chapter 3.4.1.

Additionally, the better dimensional stability of the Aquivion™ membrane at elevated temperatures helped preserving the sophisticated morphology of the membrane electrode interface, which is critical for the overall cell performance [48, 63]. It is likely that the large ohmic resistance in addition to the membrane resistance observed during polarization of the MEA based on the recast Nafion® membrane (M100) originates from limited proton conductivity in the membrane electrode interface. The high contact resistance in the membrane electrode interface could be due to the very limited dimensional stability of the Nafion® membrane under the experimental conditions.

3.5 Summary

Homogeneous Nafion®/PBI blend membranes were prepared from DMAc solutions of PBI and Nafion®-NH_4. The inherent special features of the NH_4^+ ionomer counter cation, e.g. its moderate acidity of combination with the ability for hydrogen bond formation, made it a good compatibilizer in the present system and could thus prevent phase separation between the two polymers during membrane casting.

The homogeneity of the blend membranes throughout the whole composition range was confirmed by FTIR. FTIR further indicated a decreased fraction of non-hydrogen bonded N-H groups in the Nafion®/PBI blend membranes.

The water as well as the phosphoric acid uptake of the blend membranes was strongly dependent on the composition of the binary blends. The water and phosphoric acid uptake dependence on the membrane composition was directly related to the intermolecular coulomb interactions between the two polymers. Hence, a water uptake as well as phosphoric acid uptake minimum was observed for membrane M088, which represented the completely neutral composition. Furthermore, the ZrP composite membranes based on the membranes with an excess of acidic groups (M100-M094) showed increased water uptake compared with the pristine membranes. During doping in hot H_3PO_4,

the major fraction of the ZrP in the composite membranes was dissolved and washed out according to a digestion-recrystallization mechanism.

At 130 °C, the Young´s modulus and the engineering tensile stress at break of the pristine membranes showed a gradual increase as the PBI content increased. After acid doping, the membranes close to the neutral composition (M088 and M082) exhibited the highest Young´s modulus and engineering tensile stress at break. ZrP loading of the membranes of high Nafion® contents was found to increase the Young´s modulus by reducing the segmental motions of the polymer chains within the structures.

The composition corresponding to the neutral blend membrane showed the highest total weight loss as well as the highest initial rate of weight loss in the Fenton test. This indicated a chemical incompatibility between the two polymers in the presence of oxidative radicals. The onset temperature of major decomposition in air was found to increase from about 280 °C for M100 to about 450 °C for M000.

The proton conductivity of the ZrP composites based on the membranes of high Nafion® contents (M100-M094) as well as that of the pristine membranes was insufficient for efficient steam electrolysis at 130 °C. The phosphoric acid doped membranes based on pure Nafion® (M100) and PBI (M000), on the other hand, exhibited proton conductivity in the 10^{-2} S cm^{-1} range at 130 °C.

Steam electrolysis tests were further conducted at 130 °C. As expected based on the conductivity data, poor performances were obtained during operation of the MEAs based on pure Nafion® as well as the composite membrane based on M097 with a ZrP content of 5 wt.%. However, the overall ohmic loss when the Nafion® based MEA was operated in electrolysis mode at 80 °C under fully hydrous conditions was considerably higher than what could be expected based on the membrane conductivity data. It indicated a considerable ohmic resistance in the cell in addition to the membrane contribution. This ohmic loss was most likely due to high interfacial contact resistance in the membrane electrode interface or due to poor electronic or protonic conductivity in the catalyst layers.

The MEA based on phosphoric acid doped PBI showed the best performance but suffered from severe long term durability limitations. On the other hand, reasonable performance and stability was demonstrated for the MEAs based on the phosphoric acid doped recast Nafion® (M100) membranes. Additionally, the phosphoric acid helped preserving a good interfacial contact between the membrane and the electrodes.

In order to further improve the electrolysis performance, a set of recast and melt extruded PFSA membranes of varying equivalent weights were evaluated as electrolyte materials. The commercially available melt extruded short side chain PFSA membrane Aquivion™ showed high phosphoric acid uptake as well as good mechanical properties at 130 °C. The higher phosphoric acid uptake and the better mechanical characteristics of the Aquivion™ membrane compared with the recast Nafion® (M100) was a direct consequence of the lower equivalent weight and the higher degree of crystallinity, respectively.

The MEA based on phosphoric acid doped Aquivion™ showed improved performance in steam electrolysis tests compared with the MEA based on the phosphoric acid doped recast Nafion® membrane. At 130 °C the current density reached 600 mA cm^{-2} at a cell voltage of 1.8 V. The improved performance was most likely connected to the higher phosphoric acid content and better dimensional stability of Aquivion™ compared with Nafion®.

4 Composites for PEM water electrolysis at elevated temperature and pressure

The following chapter is devoted to the development of PFSA based composite materials for PEM water electrolysis with a liquid water feed at temperatures above 100 °C.

The solid state NMR measurements were conducted by Dr. Ulla Gro Nielsen at University of Southern Denmark, Odense. The conductivity measurements at elevated temperatures and pressures and the water electrolysis tests were conducted by Dr. Martin Paidar at the Institute of Chemical Technology, Prague, Czech Republic.

4.1 Background

PEM water electrolysis at elevated pressure is a considerably more mature and well established technology compared with PEM steam electrolysis. For example, a 12 cell stack with a total active area of 250 cm^2 with the possibility to operate at back pressures up to 50 bar and at temperatures in the 100-150 °C range was developed within the GenHyPEM research program which was supported by the European Commission [86]. Stable performance was recorded over 10000 h at an operational current density of 1000 mA cm^{-2}, however, at a stack temperature well below 100 °C.

Accumulation of evolved H_2 and O_2 within the electrodes has been identified as one of the major contributors to the overall ohmic loss in PEM water electrolyzers [56]. Hence, a moderate pressurization the system might be beneficial since it will reduce the the total volume of the evolved gases in the cell. Pressurized operation of PEM water electrolyzers at up to 130 bar is advantageous since it offers the possibility to store the product gases directly in pressurized vessels. On the other hand, it is associated with safety risks due to the relatively high permeation rate of hydrogen and oxygen through the most commonly used electrolyte materials at high pressures [89, 90].

The most widely used electrolyte materials for PEM water electrolyzers with a liquid water feed operating at ambient [44] or elevated pressure [46, 189] are based on membranes of the PFSA type. It has evolved as the state-of-the-art type of electrolyte material since the PEM water electrolysis technology was born in the 1980s [190]. The superior proton conductivity of PFSA based membranes under fully hydrous conditions results in an acceptable contribution to the overall ohmic loss in the high current density range, which also allows for high efficiencies.

A limited number of alternative electrolyte materials for PEM electrolysis with a liquid water feed have been investigated throughout the years. For example, Masson *et al.* [191] developed a sulfonated polyethylene based composite membrane and operated the MEA in electrolysis mode at a current density of 200 mA cm^{-2} for 3000 h without any apparent degradation. Sawada *et al.* [192] prepared membranes based on post-sulfonated styrene-graft crosslinked PTFE. At 80 °C a rather low current density of 40 mA cm^{-2} at 2 V was obtained. The poor performance was attributed to high interfacial resistance between the membrane and the electrode in the MEA.

Linkous *et al.* [112] operated a liquid water fed electrolysis cell based on sPEEK at a current density of 100 mA cm^{-2} at 2.1 V at 60 °C. Furthermore, phosphotungstic acid composite membranes based on sPEEK have been thoroughly characterized and evaluated as electrolyte for PEM water electrolysis at temperatures up to 80 °C [193-195]. Wei *et al.* [196] reached a current density of 1600 mA cm^{-2} at a cell voltage of 2 V using a MEA based on a blend membrane of 30% poly(ether sulfone) and 70%

sPEEK. The electrolysis performance was found to be highly dependent on the type of ionomer used in the catalyst layers.

Antonucci *et al.* [87]operated a PEM liquid water or steam fed electrolyzer cell based on a Nafion®-SiO_2 composite membrane at 80-120 °C at pressures up to 3 bar. The membrane showed better hydration characteristics and thus better electrolysis performance compared with the pristine Nafion® 115 membrane. The steam fed cell based on the Nafion®-SiO_2 composite membrane reached a moderate current density of 450 mA cm^{-2} at a cell voltage of 1.75 V. On the other hand, the performance was considerably boosted by increasing the pressure to 3 bar in order to keep the feed water in the liquid phase and to keep the membrane well hydrated. Under these conditions a maximum current density of 2100 mA cm^{-2} at a cell voltage of 1.9 V was recorded. Using a similar membrane type (but considerably thinner), Xu *et al.* [197] operated a liquid water fed electrolyzer at a current density of 1000 mA cm^{-2} at a cell voltage as low as 1.51 V at 130 °C. Furthermore, a Nafion®-TiO_2 composite membrane based electrolyzer cell was evaluated by Baglio *et al.* [88]. Just like the Nafion®-SiO_2 composite membrane based electrolyzers, the Nafion®-TiO_2 composite membrane based electrolyzer showed better performance at 80-120 °C at pressures up to 3 bar compared with the pristine Nafion®-115 based cell due to its better hydration and water retention characteristics. At 120 °C the cell based on the Nafion®-TiO_2 composite membrane reached a current density of about 600 mA cm^{-2} and about 1000 mA cm^{-2} at a cell voltage of 1.75 V when it was fed with steam at ambient pressure and liquid water at a pressure of 3 bar, respectively.

As discussed in the previous chapter, the amount of available literature concerning polymer based membrane materials and composites for PEM fuel cell applications is considerably more comprehensive in general. Different types of PFSA based composite membranes with a broad range of inorganic fillers have been prepared, characterized and evaluated as electrolyte materials for PEM fuel cells, as reviewed by Alberti and Casciola [65].

Boron orthophosphate (BP) is an inorganic polymeric material with the empirical formula BPO_4. Depending on the degree of crystallinity, it is known to exhibit water mediated proton conductivity as high as 10^{-2} S cm^{-1} at room temperature [198] and close to 10^{-1} S cm^{-1} at 100-150 °C [199]. The high hydrous proton conductivity of BP has resulted in an increasing interest for using it as inorganic component in different types of proton conducting polymer based composite membrane materials.

Based on sPEEK, a series of composite membranes with BP as the inorganic component was prepared and the membranes were evaluated for various applications [200, 201]. The proton conductivity of the BP composite membranes was found to exceed that of the pure polymers with up to about one order of magnitude. Analogously, BP composite membranes based on PFSA [202] and sPEEK/PBI acid-base blends [137] have been prepared and characterized. These composite materials were prepared by solvent evaporation casting from a polymer solution with fine particles of pre-formed BP dispersed in it to give membranes of different polymer/BP weight ratios.

On the other hand, Krishnan *et al.* [203] developed a one-step sol-gel procedure for preparing BP composite membranes based on sPEEK. The polymer solution was mixed with a boron precursor (e.g. $B(OC_3H_7)_3$) and H_3PO_4 in equimolar amounts to give a homogenous solution from which the membranes were solution cast at 120 °C. The procedure was subsequently optimized by tuning the reaction conditions to give *in situ* formed BP particles of different diameter [204]. Analogously, the sol-gel methodology has been employed for preparing BP composite membranes based on sulfonated poly(phtalazinone ether nitrile) (sPPENK) [205] as well as sPES [206].

In this work, PFSA-BP composite membranes were developed and characterized. In order to provide further mechanical strength, composite membranes reinforced with highly porous PTFE were developed. The composite membranes were subsequently evaluated as electrolyte materials for water electrolysis with a liquid water feed at temperatures above 100 °C.

4.2 Experimental

4.2.1 Membrane preparation

The as-received 5 wt.% Nafion® dispersion (DuPont) was neutralized with dilute aqueous ammonium hydroxide. The solvent was subsequently evaporated *in vacuo* at 80-90 °C and the solid residue was dissolved in DMAc to give a 5 wt.% solution. To an amount of Nafion® solution corresponding to about 1 g of the ionomer, $B(OEt)_3$ and H_3PO_4 (100%) were added in stoichiometric amounts to give theoretical BP contents ranging from 0-20 wt.%. The mixtures were stirred at room temperature until homogenous, colorless and transparent solutions were obtained. The membranes were prepared by solution casting on 95 cm^2 Petri-dishes at temperatures up to 120 °C. The resulting membranes were subsequently peeled off in demineralized water and treated in 1 mol L^{-1} H_2SO_4 at 80 °C for 1 h and in demineralized water at 90 °C for 2 h.

The membranes are hereafter referred to as Mxx according to their theoretical initial BP contents in wt.%, i.e. M05 for a membrane prepared from a solution corresponding to a theoretical BP content of 5 wt.%. The pure recast Nafion® membrane is referred to as M00.

The PTFE reinforced composite membranes were prepared by casting the membranes according to the same procedure on top of a highly porous PTFE film (Yeumiflon® ePTFE) with a thickness of about 5 µm that was fixed at the bottom of the Petri-dishes.

4.2.2 Characterization

The water uptake and volume swelling data in liquid water were measured by submerging the membrane samples in water at different temperatures. The membranes were pre-dried *in vacuo* at 100 °C before the measurement. The water uptake and the volume swelling were calculated according to Equation 4.1 and 4.2, respectively. Four parallel samples of each composition were used and the water droplets on the surfaces were carefully wiped off with tissue paper.

$$Water\ uptake = \frac{mass_{wet} - mass_{dry}}{mass_{dry}} \times 100\% \quad (4.1)$$

$$Volume\ swelling = \frac{volume_{wet} - volume_{dry}}{volume_{dry}} \times 100\% \quad (4.2)$$

Attenuated Total Reflectance Fourier Transform Infrared Spectroscopy (ATR-FTIR) measurements were conducted using a Perkin Elmer Spectrum One FTIR spectrometer equipped with a universal ATR sampling accessory. The membrane samples were pre-dried at 100 °C *in vacuo* before the spectra were recorded.

Wide Angle X-ray Diffraction (WAXD) patterns were recorded using a Huber D670 diffractometer equipped with a Cu-K α X-ray source.

SEM-EDX measurements were made using a Carl Zeiss EVO MA10 scanning electron microscope equipped with an INCA EDX system from Oxford Instruments. The membrane cross-sections were obtained either by cryogenically fracturing the membranes in liquid nitrogen or by hot pressing the membrane between two pieces of carbon cloth followed by ion milling. The membrane cross-sections were subsequently carbon coated by vacuum sputtering in order to enhance the electronic conductivity of the surfaces.

Thermogravimetric curves were recorded at a heating rate of 10 °C min^{-1} using synthetic air as purge gas. The differential thermal analysis (DTA) data were acquired at a heating rate of 3 °C min^{-1} and instrumental nitrogen 5.0 was used as purge gas.

Stress-strain curves were recorded at 20 °C or 130 °C under ambient atmosphere.

The in-plane proton conductivity at ambient pressure was measured at temperatures ranging from 100-140 °C under a steam atmosphere. The symmetric square wave current was supplied in a frequency range from 5-10 kHz. The conductivity of four different samples of each composition was recorded.

The in-plane conductivity measurements at elevated temperatures and pressures were conducted by Dr. Martin Paidar at the Institute of Chemical Technology, Prague, Czech Republic (ICTP). The conductivity was measured in a four platinum electrode conductivity cell made of PTFE, using an electrochemical impedance spectroscopy technique. The ohmic resistance of the membranes was extracted from the Nyquist plots as the high frequency intercept on the real axis. The conductivity cell was placed in a furnace for temperature control and water was supplied using a high pressure pump. The pressure was controlled using a back pressure valve on the outlet of the cell. The conductivity was subsequently calculated according to Equation 2.9.

The water electrolysis tests were conducted by Dr. Martin Paidar at ICTP. The anodes were prepared by spraying a suspension containing IrO_2/TiO_x and Nafion® onto a Tantalum coated stainless steel felt (Tantaline®). The anode catalyst loadings varied between 0.5-3.1 mg cm^{-2}. The cathodes were prepared by spraying a suspension containing Pt/C and Nafion® onto a porous carbon substrate. The Pt loadings were about 0.5-1.0 mg cm^{-2}. The thicknesses of all membranes used in the electrolyzer tests were about 100 μm.

4.3 Results and discussion

4.3.1 Membrane preparation

The Nafion®-BP composites were prepared according to a sol-gel methodology that was originally developed by Krishnan *et al.* [203] and used for the preparation of BP composites based on sPEEK. The methodology was inspired by an early work by Moffat and Neelman [207], who prepared boron phosphates of high surface area at relatively low temperatures. Based on a model system reaction, the inorganic solid phase was assumed to develop *in situ* during the membrane casting according to Equation 4.3 below.

$$B(OEt)_3 + H_3PO_4 \rightleftharpoons BPO_4 + 3EtOH \quad (4.3)$$

Analogously, Nafion®-BP composite membranes with theoretical initial BP contents up to 20 wt.% were prepared in the present study according to Scheme 4.1 below.

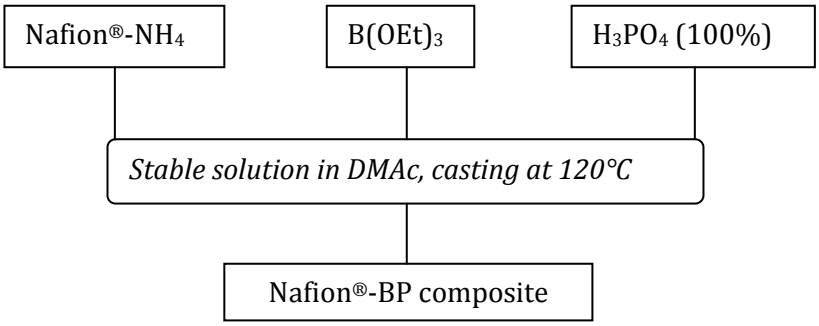

Scheme 4.1 *Schematic description of the Nafion®-BP membrane preparation procedure.*

The resulting composite membranes were homogenously bright white and non-transparent. However, a network of small interconnected cracks was observed in the composite membrane with an initial theoretical BP content of 20 wt.% (M20).

The M00-PTFE membrane was completely homogenous and transparent after casting, showing that the solid Nafion® phase was continuously developed within the porous PTFE network. The physiochemical characteristics of the perfluorinated backbone of Nafion® resemble those of PTFE, which should allow for a good interfacial adhesion between the two materials.

After casting, all membranes were submerged in hot dilute H_2SO_4 in order to restore the protonated form of Nafion®.

4.3.2 Water uptake and volume swelling

The water uptakes of the non-PTFE reinforced membranes M00-M20 at 20 °C and 70 °C calculated according to Equation 4.1 are plotted in Figure 4.1.

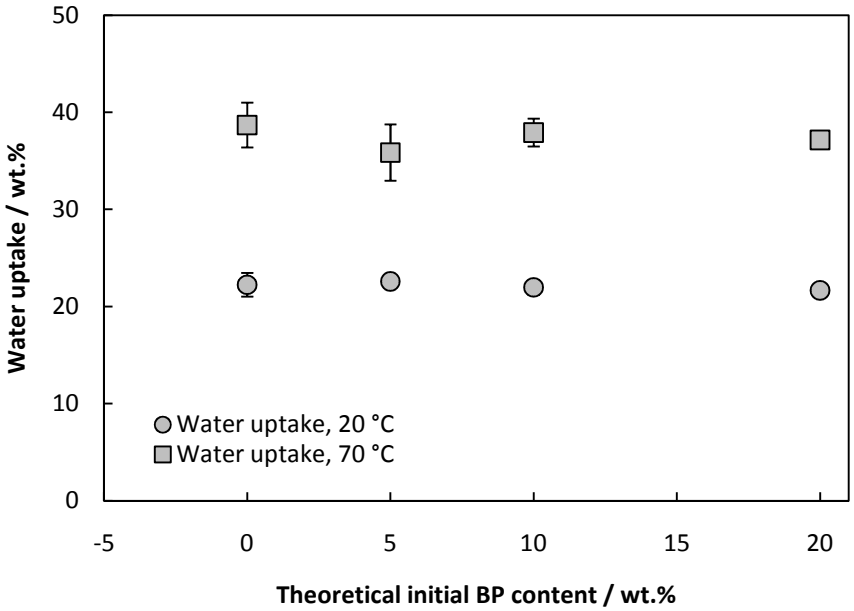

Figure 4.1 *Water uptake at 20 °C and 70 °C.*

The water uptake or hydration number λ is normally strongly correlated with the proton conductivity as well as the mechanical properties of PFSA based membranes [31, 85]. BPO_4 is highly hygroscopic and can retain water at temperatures up to 300 °C [208], which in turn should improve the hydration characteristics of the BP composite membranes.

The introduction of BP into the polymer matrix is known to increase the water uptake of sPEEK based composite membranes prepared according to the sol-gel procedure [203] as well as for BP composite membranes based on sPEEK prepared by casting by solvent evaporation from a sPEEK-BP suspension [200]. The water uptakes were generally found to increase with increasing BP contents.

On the other hand, the total water uptake of a PFSA based BP composites was found to be relatively unaffected by the inorganic BP phase [202]. This was also confirmed in the present study. However, the specific water uptake, i.e. the water uptake calculated on the dry Nafion® fraction basis of the membrane based on the theoretical BP content, increased linearly with increasing theoretical BP content.

The water uptake was found to be constant at about 22 wt.% at 20 °C and 38 wt.% at 70 °C throughout the whole investigated composition range. This corresponds to a hydration number λ of 13.6 and 23.6 for M00 at 20 °C and 70 °C, respectively. The water uptake of the recast Nafion® membrane (M00) used in the present study was slightly higher compared with the water uptake of melt extruded Nafion® 117 membranes having a similar thermal history [85].

The total volume swelling of the membranes calculated according to Equation 4.2 was found to be relatively constant throughout the whole investigated composition range as shown in Figure 4.2.

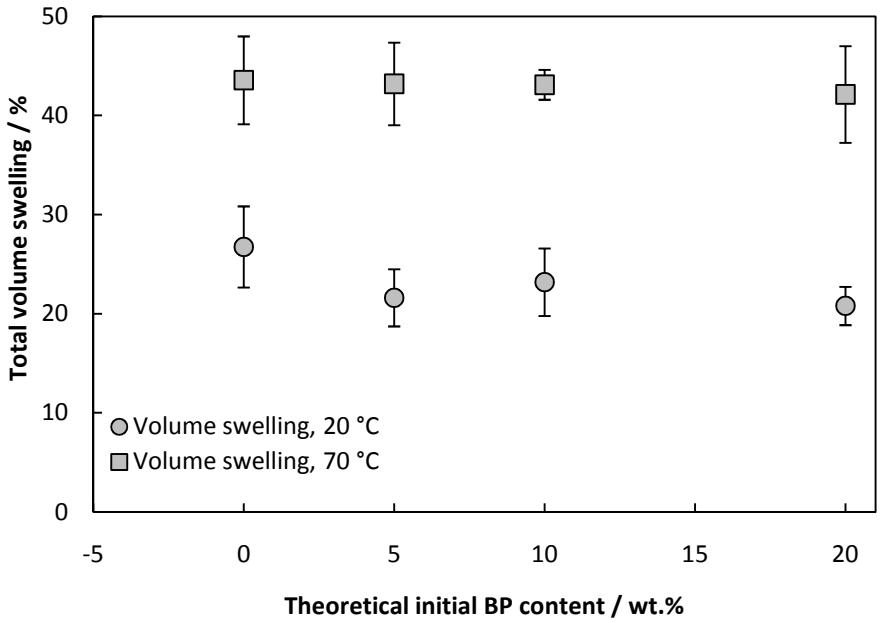

Figure 4.2 *Total volume swelling at 20 °C and 70 °C.*

This is reasonable since the total volume swelling should be strongly correlated with the water uptake. The volume swelling data of the pure recast Nafion® membrane M00 was in good agreement with previously reported data for a Nafion® 117 membrane in the Li^+ form [209]. The literature data further confirmed that the solvent uptake and the concomitant volume swelling of Nafion® in almost any solvent is highly dependent on the temperature.

Melt extruded PFSA membranes such as Nafion® 115 or 117 are often more of less anisotropic which implies that they normally show slightly different volume swelling in different directions during hydration. For example, Gebel *et al.* [59] reported that the melt extruded PFSA membranes exhibited considerably higher swelling perpendicular compared to parallel to the laminating direction. On the other hand, the recast PFSA membranes were found to be more isotropic and thus showed a more homogenous swelling.

In the present study the swelling of the pure recast Nafion® membrane M00 was found to be completely isotropic. The swelling in water in all three directions was highly dependent on the temperature and the data were in good agreement with the literature data for pure recast Nafion® [59]. It was about 9% at 20 °C and 13% at 70 °C and equal in all directions, as shown in Figure 4.3. The swelling data of the composite membranes M05-M20 were slightly less consistent. For example, at 20 °C the composite membrane M20 showed a considerable lower thickness swelling compared with in the length and width directions, which indicates anisotropy effects.

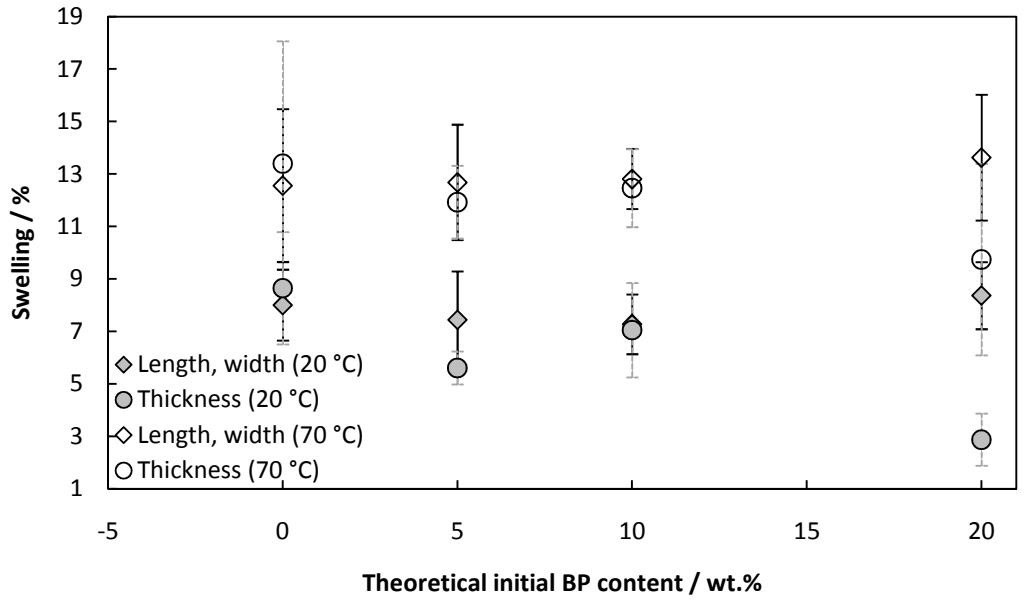

Figure 4.3 *Swelling in different directions at 20 °C and at 70 °C. The error bars corresponding to the length and width swelling are solid and black whereas the error bars corresponding to the thickness swelling are dashed and grey.*

4.3.3 Spectroscopic characterization

The ATR-FTIR spectra of M00-M20 are shown in Figure 4.4. The strong FTIR absorption band which was centered at around 1060 cm^{-1} was assigned to the characteristic sulfonic acid group absorption of Nafion® [176]. The absorption bands which were centered around 1150 and 1210 cm^{-1} were assigned to overlap of the strong C-F symmetric (1150 cm^{-1}) and asymmetric (1210 cm^{-1}) [176] stretching and S-O absorption [177].

The two strong absorption bands which were centered around 1150 and 1210 cm^{-1} in the spectrum of the pure recast Nafion® membrane (M00) were gradually blue shifted to higher frequencies as the theoretical initial BP content of the membrane was increased. In the spectrum of M20 these absorption bands were centered around 1155 and 1220 cm^{-1}, respectively, indicating a change of the local environment of the perfluorinated polymer backbone or the sulfonic acid terminal groups [142]. A similar blue shift of the absorption bands centered at about 1150 and 1200 cm^{-1} in the FTIR spectrum of the sPPENK based composite membranes with increasing BP contents was also observed [205]. However, the origin of the absorption frequency shift was not discussed. It could eventually be connected to a shift of the sulfonic acid group absorption due to their interaction with the BP component.

Alentiev *et al.* [210] studied the chemical aging of Nafion® under dry conditions at 95 °C using FTIR. Furthermore, Collette *et al.* [211] investigated the thermal and hygrothermal aging of Nafion® at 80 °C using FTIR and solid state NMR. The ageing under hydrous as well as anhydrous conditions was illustrated by a dramatic decrease of the water uptake as well as the proton conductivity. Both proposed aging mechanisms involved condensation of two sulfonic acid groups to sulfonic acid anhydride. The developed sulfonic acid anhydrides showed a strong absorption band centered around 1440 cm^{-1}. Hence, the gradual development of an absorption band at 1465 cm^{-1} in the FTIR spectrum of M05-M20 might originate from the development covalent sulfonate bonds. The development of covalent sulfonate bonds could also explain the gradual blue shift of the absorption bands which were centered around 1150 and 1210 cm^{-1} in the FTIR spectrum of M00.

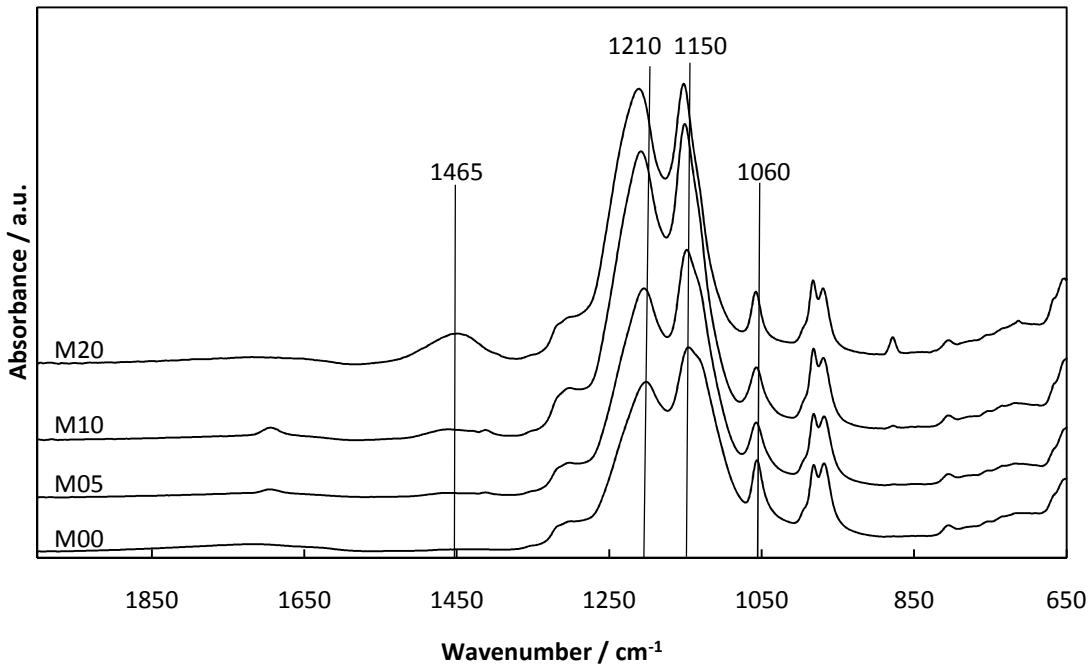

Figure 4.4 *ATR-FTIR spectra of M00-M20.*

In order to confirm the presence of BP in the composite membranes, ^{11}B and ^{31}P solid state NMR experiments were conducted. However, no resonance signal for any of these two nuclei could be recorded (see Appendix 2). It suggests that a large fraction of the BP filler might have been dissolved and washed out during the membrane treatment after casting. Amorphous BP is known to be relatively soluble in water [198] and even crystalline BP can hydrolyze to soluble or volatile species at higher temperatures under steam atmosphere [199].

The complete absence of ^{11}B and ^{31}P signals in the solid state NMR spectrum of M20 proved that the actual BP contents of the resulting composite membranes were much lower than the theoretical initial BP loadings. On the other hand, the FTIR spectra of the BP composites indicated that the membranes were chemically or morphologically different compared with the pristine recast Nafion® membrane M00. Eventually, a small fraction of covalently attached boron containing species remained in the membrane after the membrane treatment in dilute acid and water. The remaining boron containing species in M05-M20 might have been covalently attached to the terminal sulfonic groups to give a structure resembling that of the superacidic boron Nafionates (Figure 4.5) synthesized from Nafion® and boron halides by Olah [212]. It could also explain the development of FTIR absorption band centered around 1465 cm^{-1}, which was assigned to covalent Nafion® sulfonates by Alentiev *et al.* [210] and Collete *et al.* [211].

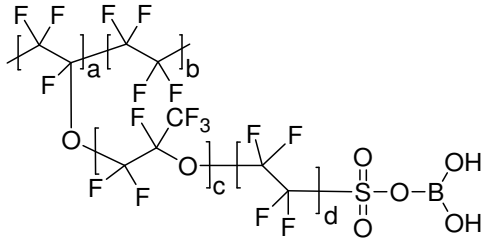

Figure 4.5 *Structure of the boron Nafionate as proposed by Olah [212].*

Assuming an equimolar amount of sulfonic acid and boron as shown in Figure 4.5 and an equivalent weight of Nafion® of 1100 g eq^{-1}, the total amount of boron in the membrane would be less than 0.1 wt.% which was below the solid state NMR detection limit.

4.3.4 X-Ray diffraction

The crystallinity as well as the crystallite size of BP is known to increase with the calcination temperature [198]. BP composite membranes based on sPEEK/PBI blends [137] or PFSA [202] prepared from pre-calcined BP by casting from a dispersion showed the characteristic X-ray diffraction pattern of pure crystalline BP which confirmed the presence of the inorganic component in the resulting membranes.

The wide angle X-ray diffractograms of M00-M20 are shown in Figure 4.6. The broad reflections at about 16° 2θ and 40° 2θ are characteristic for Nafion® and originate from diffraction caused by the crystalline regions in the perfluorinated polymer backbone [118].

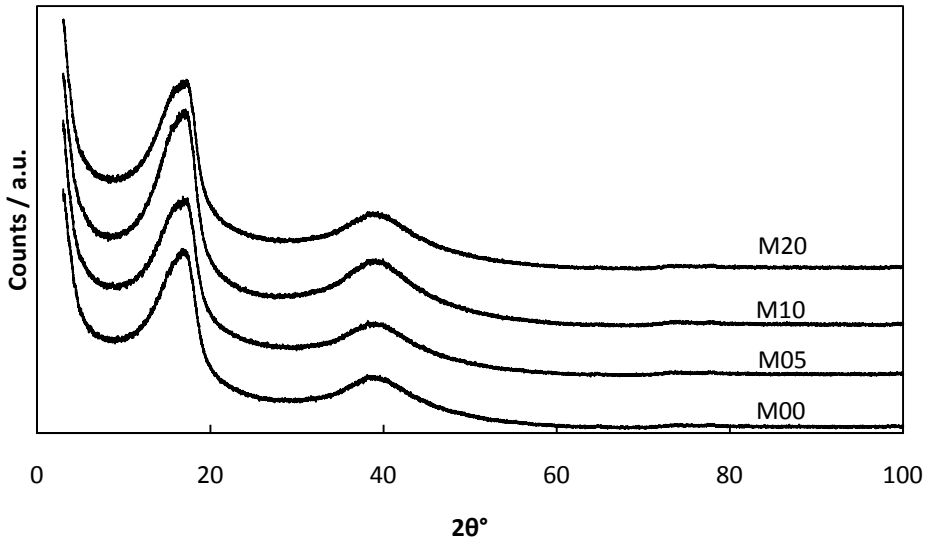

Figure 4.6 *X-ray diffractograms of M00-M20.*

However, according to literature the BP prepared *ex situ* at 120 °C is completely amorphous and shows a broad amorphous halo in the 2-40° 2θ range [203]. Hence, only reflections originating from the polymer matrix could be observed in the X-ray diffractograms of the sPEEK [203] or sPPENK [205] based BP composites which were prepared according to the sol-gel procedure.

The X-ray diffraction measurement could thus not confirm the presence of the inorganic filler within the polymer matrix. Similarly, no crystalline phase of BP could be identified within the PFSA based composites prepared in the present study according to the sol-gel methodology.

4.3.5 SEM

4.3.5.1 The Nafion®-BP composites

The cross-sectional micro structures of the of the BP composite membranes in the present study were very similar to that of of the BP composite membranes based on sPEEK [203, 204], sPPENK [205] or sPES [206] which had been prepared according to similar *in situ* sol-gel procedures. Wen *et al.* [206]

also confirmed the presence of BP in the sPES based composite membranes by EDX mapping with respect to B and P. The SEM-EDX analysis also confirmed that the microstructure as well as the BP elemental distribution was homogenous throughout the whole membrane cross-section.

In the present study, the cross-sectional morphology of the pure recast Nafion® membrane (M00) was smooth and even as shown in Figure 4.7a. In contrast, the cross-sectional structures of M05-M20 were featured by homogenously distributed pores with diameters of up to about 500 nm as shown in Figure 4.7b-d.

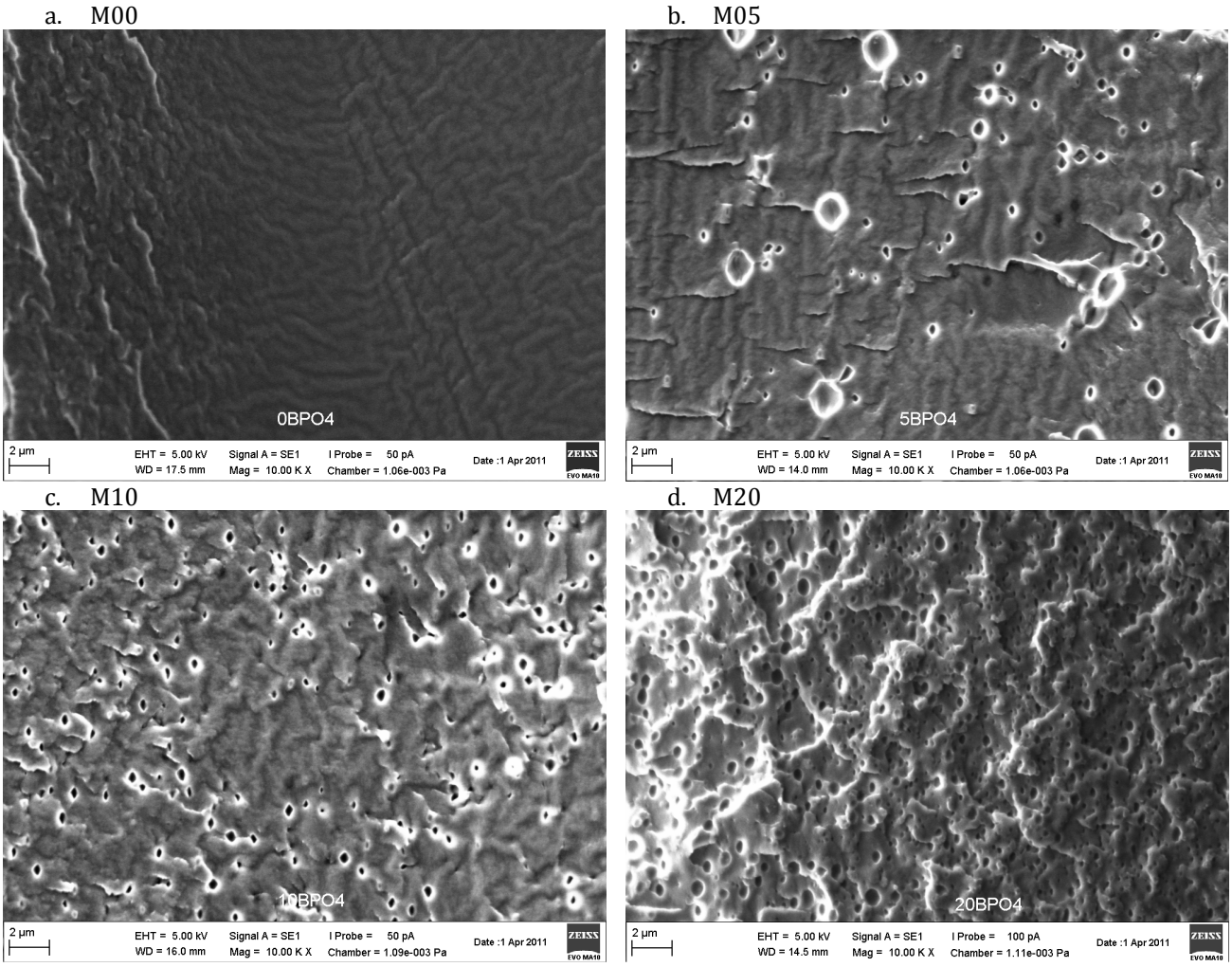

Figure 4.7 *Cross-sectional SEM micrographs of M00-M20. The scale bars represent 2 µm.*

The number of pores per unit area was also found to increase with increasing theoretical initial BP content of the membranes. In the composite with the highest initial theoretical BP content (M20) a nearly interpenetrating network of pores was developed.

The porous structures were most likely a result of the dissolution of the major fraction of the BP particles during the membrane treatment with dilute acid and water after casting. No phosphorous signals were detected by elemental EDX mapping of the cross-sections which further supports that the major fraction of the BP component was dissolved and washed out during the membrane treatment after casting.

4.3.5.2 The Nafion®-PTFE composite

The SEM micrographs of the PTFE reinforced M00 membrane cross-sections are shown in Figure 4.8 and Figure 4.9. The membrane was fixed between two pieces of carbon cloth and can be seen as the dark grey area in the center of Figure 4.8.

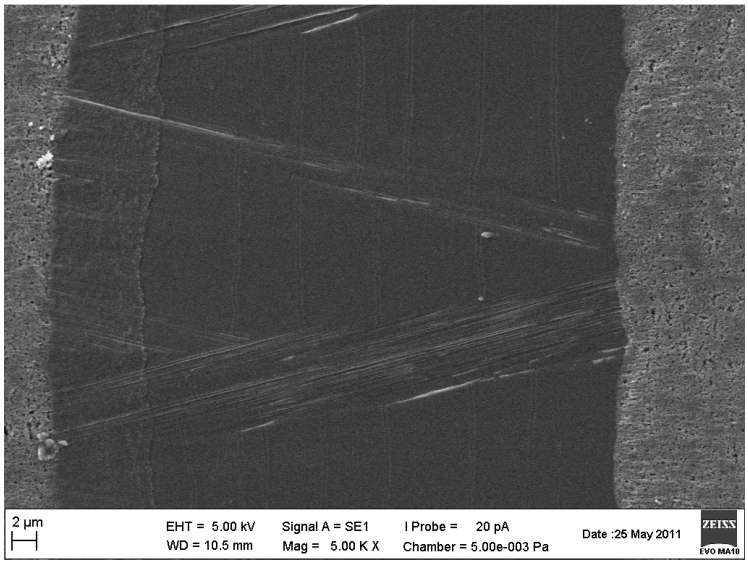

Figure 4.8 *SEM micrograph of the complete M00-PTFE composite membrane cross-section. The scale bar represents 2 µm.*

The cross-section of the PTFE reinforced M00 membrane appeared to be highly asymmetric, which obviously was a direct consequence of the membrane casting procedure where the Nafion® phase was solution cast on top of the porous PTFE film. The porous PTFE layer can be seen in Figure 4.8 as a diffuse delimited area on the left side of the membrane cross-section. The thickness of the porous PTFE layer was about 5 µm.

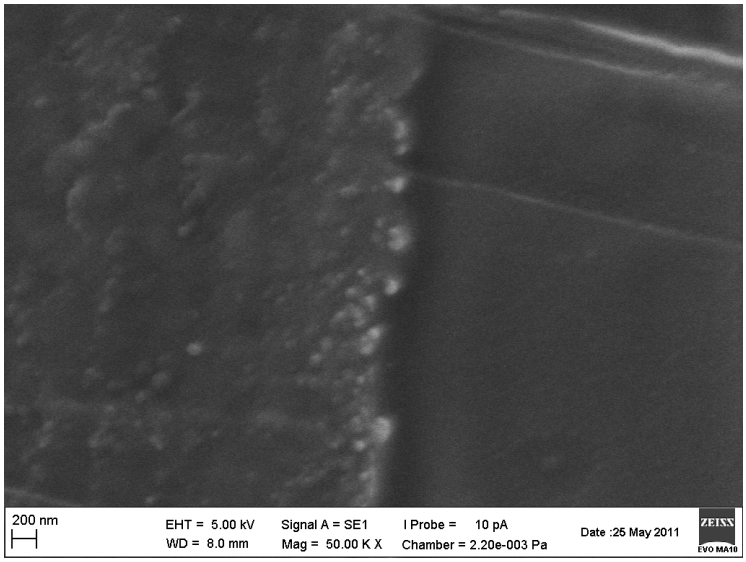

Figure 4.9 *SEM micrograph of the cross-sectional interface between the bulk Nafion phase and the porous PTFE of the PTFE reinforced M00 membrane. The scale bar represents 200 nm.*

The high magnification SEM micrograph in Figure 4.9 shows the interface between the bulk Nafion® phase (right) and the porous PTFE reinforced layer (left). It shows a rather homogenous morphology and good interfacial compatibility between the two phases. The extreme hydrophobicity of the perfluorinated Nafion® backbone and PTFE should allow for good interfacial adhesion between the two phases. Hence, a continuous Nafion® phase was developed within the porous PTFE structure which is naturally of critical importance for the complete through-plane proton conduction pathway.

4.3.6 Thermal analysis

Although it is well known that BP can hydrolyze into volatile species at high temperatures in the presence of steam [199], it has been confirmed that BP is thermally stable under anhydrous conditions and crystallizes to a completely insoluble material after annealing at 1000 °C [198].

The BP composites based on sPEEK [203, 204], sPPENK [205] or sPES [206] showed varying residual mass in the thermogravimetric curves after the thermal oxidation of the polymer, corresponding to the mass of the inorganic component in the composite membrane. The extent of the residual mass after the thermal oxidation of the polymer was naturally dependent on the amount and the relative stoichiometry of the boron phosphate precursors which were used in the sol-gel reaction and thus the composition of the resulting composite membranes.

In the present study, the thermogravimetric curves of M00-M20 were practically identical as shown in Figure 4.10. No remaining mass was observed at temperatures higher than about 510 °C, further illustrating that the major fraction of the BP filler was washed out during the membrane treatment after casting. The total weight loss of all membranes at 270 °C (about 5 wt.%) was assigned to the evaporation of water. Furthermore, the weight loss in the 300-400 °C region was connected to the decomposition of the side chains of the polymer whereas the weight loss above 400 °C was connected to the thermal oxidation of the Nafion® backbone [125].

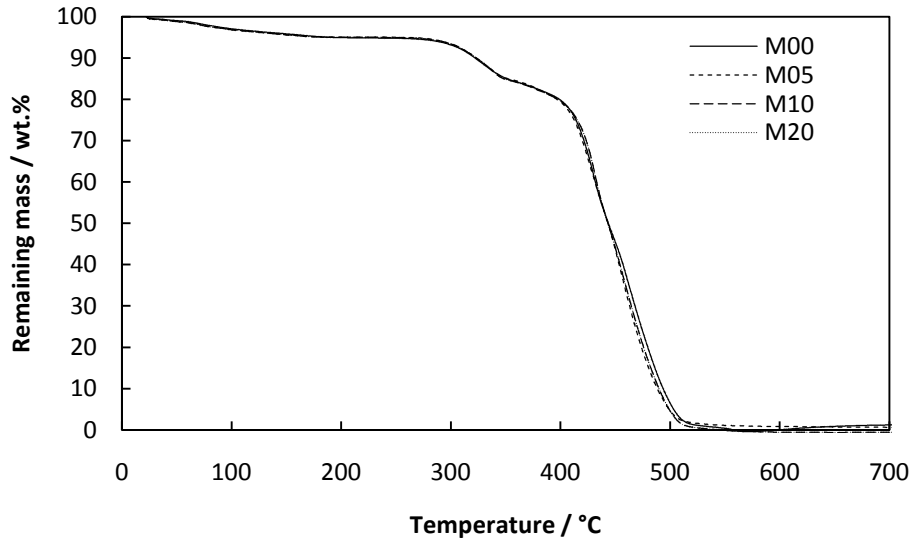

Figure 4.10 *Representative thermogravimetric curves of M00-M20 recorded at a heating rate of 10 °C min^{-1} under air atmosphere.*

Although the TGA curves of the composite membranes M00-M20 under air atmosphere were practically identical, the DTA data which were acquired under inert atmosphere (N_2) indicated some special features of the BP composites compared with the pristine recast Nafion® membrane M00, as shown in Figure 4.11.

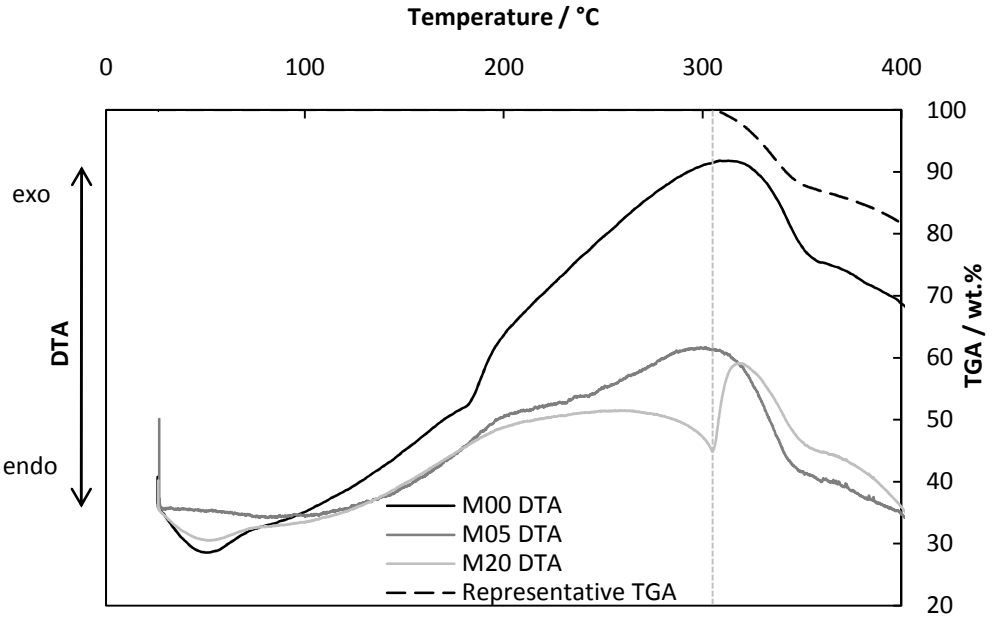

Figure 4.11 *DTA of M00, M05 and M20 recorded at a heating rate of 3 °C min^{-1} under nitrogen atmosphere. The onset temperature of the first major decomposition is indicated by the grey dotted line.*

For example, the M20 composite membrane showed, in contrast to M00, an endotherm at 300 °C where the decomposition of the sulfonic acid terminated end groups is known to start [125]. This could eventually indicate that the chemical and/or morphological environment of the sulfonic acid end groups of the BP composite membranes was slightly different compared with that of the pristine Nafion® membrane M00, especially in the high theoretical initial BP content range.

The characteristic thermal transition of pure of Nafion® at around 100 °C is often termed α relaxation and originates from the melting of large crystalline regions in the polymer backbone [185], as also discussed in Chapter 3.3.9. Although the α relaxation is not a true glass transition temperature T_g in the physical meaning, it is highly interconnected with the macroscopic mechanical characteristics of the material and is often confused with the glass transition temperature T_g [184].

In principle, the glass transition temperature T_g of an amorphous polymer [213] and the crystalline melting temperature as well as the degree of crystallinity [214] of a crystalline or semicrystalline polymer can be determined from the DTA curves recorded at different heating rates. The thermal transition data should be plotted versus the heating rate followed by extrapolation of the linear regression to a heating rate of 0 °C min^{-1} in order to compensate for thermal conductivity limitations in the sample. However, the thermal transitions can often be rather diffuse which makes it difficult to extract quantitative data from the DTA curves.

The changed appearance of the DTA curves in the present study could thus likely be connected with a shift of the melting temperature of the crystalline regions in the membranes.

4.3.7 Mechanical strength

The mechanical data of M00-M20 are summarized in Table 4.1. The stress-strain curves were recorded at 20 °C and 130 °C without active relative humidity control. The mechanical data of the M00-PTFE composite and the Aquivion™ membrane are included for comparison.

The Young´s modulus of the membranes throughout the whole composition range M00-M20 was around 115-120 MPa at room temperature. At 130 °C the Young´s modulus of M00 dropped to about 3

MPa whereas it was slightly higher for the BP composite membranes M05-M20. The generally higher elastic modulus at 130 °C in general of the composite membranes M05-M20 compared with the pure recast Nafion® membrane M00 could eventually be explained by the slightly higher crystalline melting temperatures of the composite membranes as discussed in the previous section. This was also illustrated by slightly higher tensile stress at break and decreased elongation at break in general of the M05-M20 composite membranes compared with the pure recast Nafion® membrane M00.

For comparison, Wen *et al.* [206] observed a mechanical strength improvement of the of BP composites based on sPES at 20 °C as well as at 100 °C as compared with the pristine sPES membrane. The improvement was assumed to be connected with the decreased segmental motion of the polymer chains within the membrane due to the presence of the inorganic phase.

Table 4.1 *Summary of the mechanical data of M00-M20, M00-PTFE and Aquivion™.*

	Young´s Modulus (MPa)		**Engineering tensile stress at break (MPa)**		**Elongation at break (%)**	
	20 °C	130 °C	20 °C	130 °C	20 °C	130 °C
M00	116.5 ± 5.7	2.9 ± 0.5	8.0 ± 1.0	≈0	256 ± 60	>800
M05	121.6 ± 13.1	15.8 ± 3.7	10.6 ± 1.2	1.9 ± 0.9	201 ± 48	631 ± 103
M10	122.4 ± 11.9	7.5 ± 1.2	9.5 ± 2.8	0.5 ± 0.4	170 ± 69	663 ± 63
M20	116.8 ± 12.5	8.6 ± 4.4	7.8 ± 2.4	1.1 ± 0.7	139 ± 54	571 ± 262
M00-PTFE	172.2 ± 16.8	11.0 ± 3.3	18.9 ± 1.0	1.8 ± 0.2	199 ± 17	796 ± 102
Aquivion™	-	113.7 ± 24.3	-	13.8 ± 2.9	-	166 ± 14

The Young´s modulus of the PTFE reinforced M00 membrane was considerably higher than that of the pure M00 membrane at 20 °C as well as at 130 °C. On the other hand, the Aquivion™ membrane showed about 40 times higher Young´s modulus at 130 °C compared with the recast Nafion® M00 membrane.

The superior dimensional stability of the Aquivion™ membrane under the experimental conditions could primarily be explained by its considerably higher crystalline melting temperature, which in turn originates from the close polymer chain packing due to the short side chain structure [187]. Representative stress-strain curves of M00, M00-PTFE and Aquivion™ at 130 °C are shown in Figure 4.12.

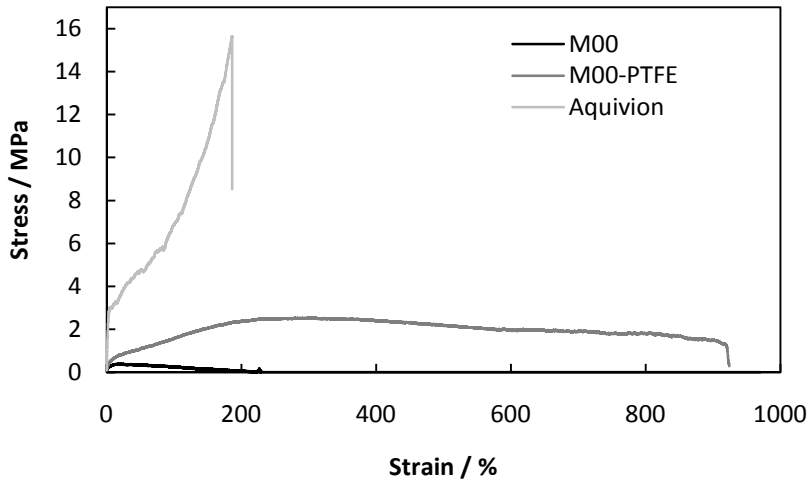

Figure 4.12 *Representative stress-strain curves at 130 °C of M00, M00-PTFE and Aquivion™.*

The engineering tensile stress at break of M00 was practically 0 at 130 °C and the elongation at break reached close to 1000%. At the same temperature, the PTFE-reinforced M00 membrane showed an ultimate strength of about 2.5 MPa at 200% strain which probably corresponded to the breaking point of the PTFE reinforcement.

4.3.8 Proton conductivity

4.3.8.1 Conductivity under steam atmosphere

It has previously been reported that BP composites based on for example sPEEK [203, 204], sPES [206] or sPPENK [205] which were prepared according to the sol-gel procedure exhibit high proton conductivity in the 10^{-2}-10^{-1} S cm^{-1} range under fully hydrous conditions at temperatures below 100 °C. Generally, the conductivity increased with increasing BP content.

The in-plane proton conductivity of M00-M20 in the present study at 100-140 °C under hydrous conditions at a steam pressure of 1 bar is shown in Figure 4.13.

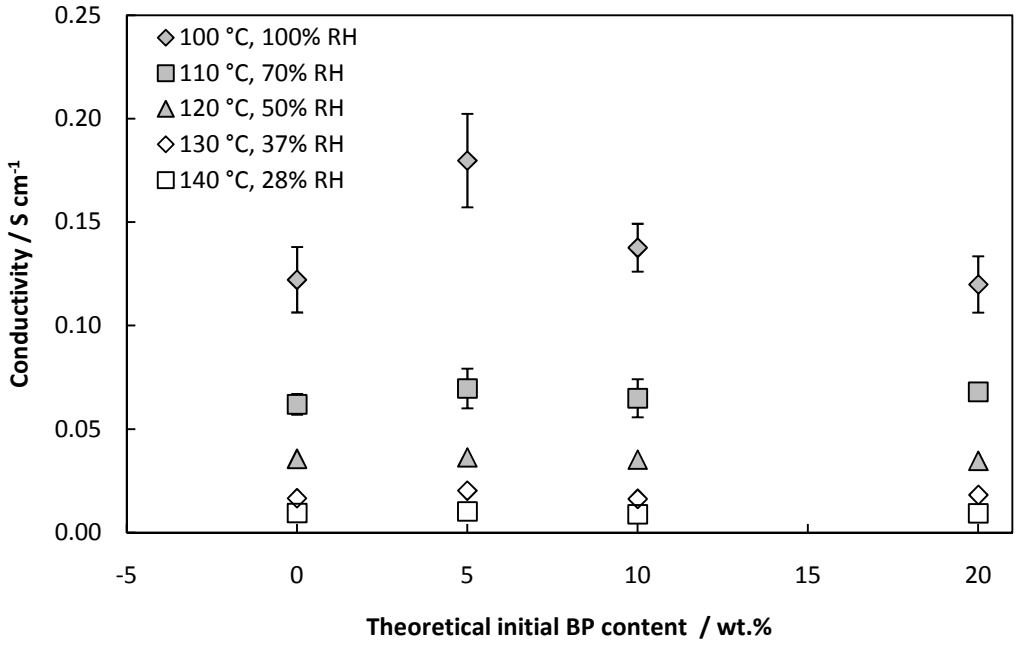

Figure 4.13 *In-plane proton conductivity of M00-M20 at 100-140 °C and ambient pressure. The corresponding relative humidity (RH) is indicated in the figure.*

The M05 composite membrane exhibited a proton conductivity maximum of about 0.18 S cm^{-1} at a relatively low temperature of 100 °C. At higher temperatures and thus lower water activities, the conductivity of all the membranes decreased gradually. At 110 °C and 70% relative humidity all membranes exhibited proton conductivity of about 0.06-0.07 S cm^{-1}.

The conductivity of all membranes M00-M20 was, just like that of the conventional and commercially available melt extruded Nafion® membranes [85], obviously strongly dependent on the presence of water. At 130-140 °C the conductivity of all the membranes M00-M20 was about 10^{-2} S cm^{-1}. However, in this temperature range the conductivity data were rather uncertain due to the limited dimensional stability of the membranes which resulted in poorly defined sample dimensions.

4.3.8.2 Conductivity in liquid water

The in-plane conductivity of M00, M10, M00-PTFE and M05-PTFE at 150 °C was measured as functions of time at 6 bar back pressure in order to keep the water in the liquid phase and the membranes well hydrated, as shown in Figure 4.14. The conductivity of Nafion® 117 was measured according to the same procedure for comparison.

The conductivity of the pure recast Nafion® membrane M00 decreased from about 0.35 to 0.08 S cm^{-1} during the first 50 h of the experiment. The conductivity decay continued and when the experiment was terminated after about 250 h the conductivity was around 0.05 S cm^{-1}. The conductivity of the M10 membrane was initially recorded at 110 °C. After about 150 h the temperature was increased to 150 °C followed by a conductivity drop to about 0.08 S cm^{-1}. The conductivity of the M10 composite gradually decreased to 0.07 S cm^{-1} after 320 h.

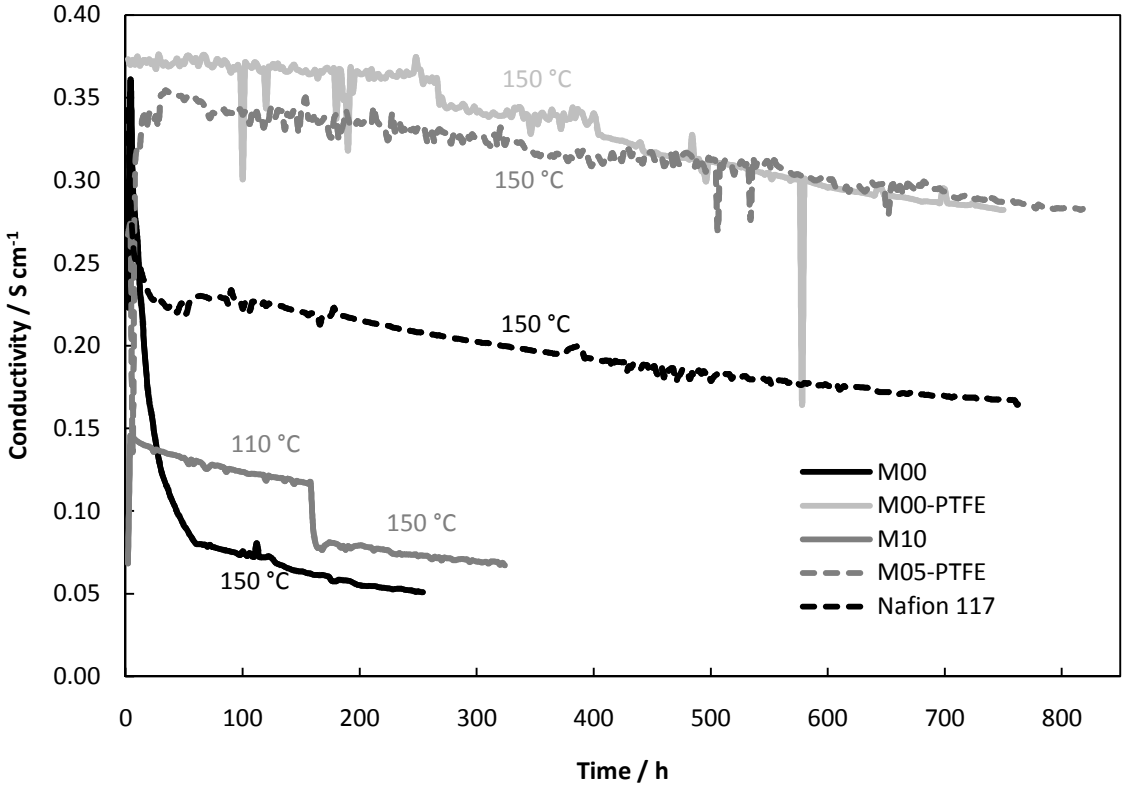

Figure 4.14 *The in-plane proton conductivity of M00, M10, M00-PTFE and Nafion® 117 at a general temperature of 150 °C and 100% RH (6 bar).*

The PTFE reinforced M00 membrane (M00-PTFE) exhibited a high and stable conductivity of about 0.35 S cm^{-1} during the first 250 h of the experiment. However, a gradual conductivity decay was observed after 250 h. When the experiment was terminated after about 750 h the conductivity was about 0.29 S cm^{-1}. For comparison, the commercially available Nafion® 117 exhibited proton conductivity of about 0.16 S cm^{-1} after 750 h. The proton conductivity decay rate of the PFTE reinforced M05 membrane (M05-PTFE) was almost identical with that of the pure PTFE reinforced M00 membrane (M00-PTFE).

The conductivity results of the PTFE reinforced membranes further illustrated the importance of the dimensional stability. The melting of the large crystalline regions within the polymer should result in complete loss of the mechanical strength of the membrane and thus a collapse of the sophisticated

cluster-network which is of critical importance for its proton conductivity mechanism, as also schematically illustrated in Scheme 3.2.

Although the absolute conductivity data must be considered as relatively uncertain due to the poorly defined sample dimensions under the experimental conditions, the importance of the dimensional stability of the PFSA based membrane seems further supported by the direct correlation found between the elastic modulus of the PFSA membrane and the PEM fuel cell performance, as reported by Kreuer *et al.* [63].

4.3.9 Water electrolysis tests

Water electrolysis tests were conducted at 120 °C at 2-3 bar back pressure in order to keep the feed water in the liquid phase. Representative polarization curves of the MEAs based on M00, M05 and M05-PTFE are shown in Figure 4.15.

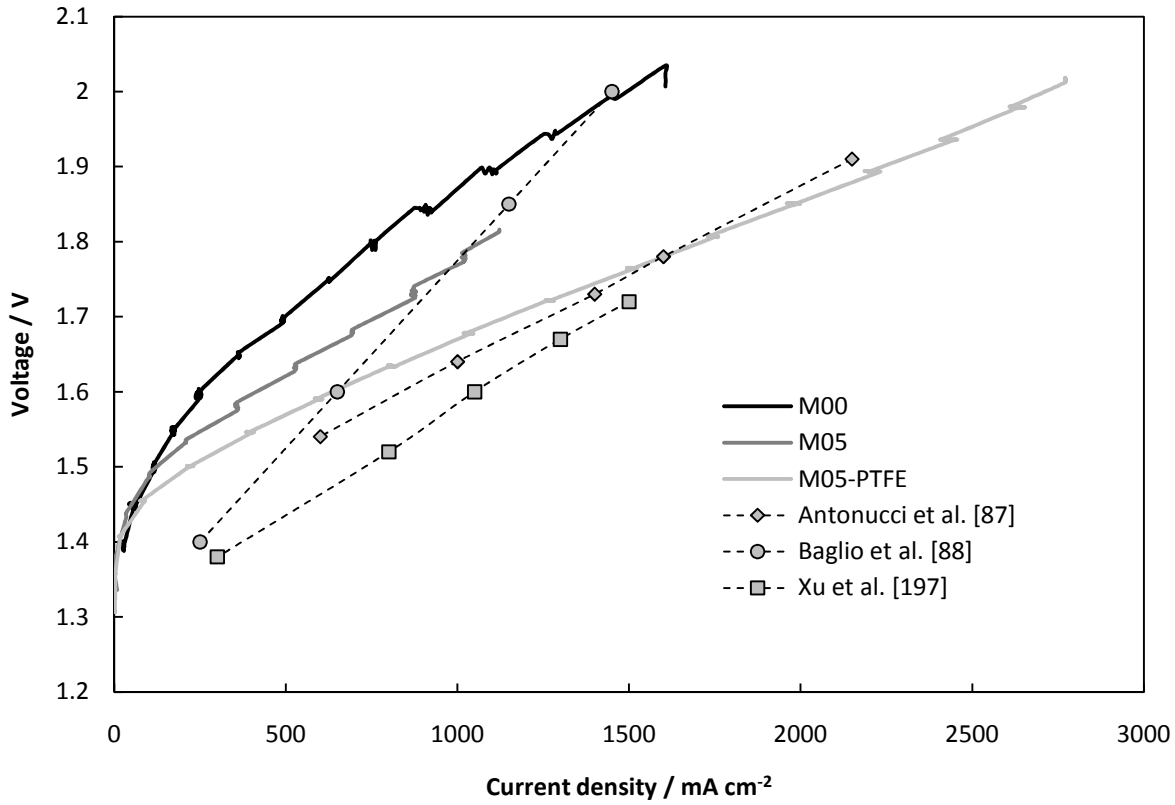

Figure 4.15 *Representative polarization curves of the MEAs based on M00, M05 (3 bar) and M05-PTFE (2 bar) at 120 °C and 100% RH. The high current parts of the polarization curves of the MEAs based on the Nafion®-SiO_2 composite (Antonucci et al. [87], 120 °C, 3 bar), Nafion®-TiO_2 composite (Baglio et al. [88], 120 °C, 2 bar) and the PFSA-SiO_2 composite (Xu et al. [197], 120 °C, 3 bar) are included for comparison.*

The anode catalyst loadings of the MEAs based on M00, M05 and M05-PTFE were 0.6 mg cm^{-2}, 3.1 mg cm^{-2} and 0.8 mg cm^{-2}, respectively, which could explain the differences observed between the polarization curves in the non-linear low current density range.

In the higher current density range, on the other hand, the slope of the polarization curves is mainly determined by the total ohmic resistance in the cell. At 1000 mA cm^{-2} the cell voltages of the MEAs

based on M00, M05 and M05-PTFE were 1.86 V, 1.77 V and 1.66 V, respectively. All the membranes were of comparable thickness so the differences in the higher current density range should originate from variations in the area specific resistance.

Generally, the area specific resistance and thus the slope of the polarization curve in the linear region is mainly determined by the proton conductivity of the membrane. The total ohmic loss is also partly determined by the electronic or protonic resistance in the catalyst layers and limitations in the interfacial contact between the membrane and the electrode due to limited dimensional stability of the membrane [48, 56].

The MEA based on the M05-PTFE composite membrane reached a current density as high as 2500 mA cm^{-2} at a cell voltage of 1.95 V at 120 °C and 2 bar back pressure in order to keep the feed water in the liquid phase and thus the membranes well hydrated. Under similar operating conditions (120 °C, 3 bar), the MEAs based on the Nafion®-SiO_2 [87] or Nafion®-TiO_2 [88] composite membranes reached a current density of about 2200 mA cm^{-2} and 1300 mA cm^{-2} at 1.9 V, respectively. For comparison, the cells based on the pristine Nafion® 115 membrane reached a more moderate current density of about 700 mA cm^{-2} at a cell voltage of 1.9 V. The improved performance of the Nafion®-SiO_2 and Nafion®-TiO_2 based cells was assigned to the considerably better hydration and water retention characteristics of the composite membranes compared with the pristine Nafion® 115 membranes. The inorganic fillers should also reduce the segmental motion of the polymer chains within the membrane which mechanically stabilizes the structure which also should help preserving the sophisticated proton conducting nanostructure at elevated temperatures.

Using a similar but considerably thinner PFSA-SiO_2 type composite membrane, Xu *et al.* [197] operated a liquid water fed electrolyzer at 120 °C and 130 °C at back pressures of 2 and 3 bar, respectively. The cell voltages at a current density of 1000 mA cm^{-2} were 1.58 V and 1.51 V at 120 °C and 130 °C, respectively. For comparison, the corresponding cell voltage at a current density of 1000 mA cm^{-2} at 120 °C and 2 bar back pressure of the MEA based on the M05-PTFE membranes in the present study was about 1.65 V.

The linear regression of the polarization curve of the M05-PTFE composite based MEA in the 1040-2451 mA cm^{-2} current density range corresponds to an area specific resistance of 184 mΩ cm^2. Given that the membrane thickness was 100 μm and assuming that the total ohmic loss originated solely from the membrane resistance, it corresponds to a membrane conductivity of about 0.05-0.06 S cm^{-1}. For comparison, the linear regression of the polarization curve at 120 °C of the MEA based on the 60 μm thick PFSA-SiO_2 composite membrane (Figure 13 in Xu *et al.* [197]) in the 350-1450 mA cm^{-2} current density range results in an area specific resistance of 264 mΩ cm^2. Assuming that the total ohmic loss originated solely from the membrane resistance it corresponds to a membrane conductivity of 0.03 S cm^{-1}.

The better electrolysis performance of the MEAs based on the PFSA-SiO_2 [87, 197] or PFSA-TiO_2 [88] composite membranes in the low current density range compared with the MEA based on PTFE reinforced M05 composite in the present study should thus not be connected to better membrane characteristics of the PFSA based SiO_2 or TiO_2 composite membranes, as also indicated in Figure 4.15. For example, the better performance of the PFSA-SiO_2 composite membrane based MEA (Xu *et al.* [197]) was apparently directly related to the considerably lower activation overvoltage of the $Ru_{0.7}Ir_{0.3}O_2$ anode catalyst compared with the IrO_2/TiO_x based anode catalyst which was used in the present study. The linear extrapolation of the polarization curve of the PFSA-SiO_2 composite membrane based MEA (Xu *et al.* [197]) to higher current densities intersects with the polarization curve of the M05-PTFE based MEA in the present study at a current density of about 1700 mA cm^{-2}. It should thus be room for a substantial electrolysis performance improvement of the PTFE reinforced PFSA based membranes used in the present study by optimizing the anode catalyst and the membrane electrode interface.

4.4 Summary

A set of Nafion®-BP composite membranes was prepared by solution casting according to a sol-gel methodology. Composite membranes having theoretical initial BP contents of up to 20 wt.% were prepared.

The water uptake of the membranes was found to be independent on the membrane composition and the membrane swelling in water of M00-M10 was found to be completely isotropic. The M20 membrane, however, showed a higher swelling in the length and width dimensions compared with in the thickness direction.

The spectroscopic characterization with ATR-FTIR showed a gradual blue shift of the two strong absorption bands which were centered around 1150 and 1210 cm^{-1} in the spectrum of M00 when the theoretical initial BP content increased. In the spectrum of the M20 composite these absorption bands were shifted to 1155 and 1220 cm^{-1}, indicating a change of the local environment of either the perfluorinated polymer backbone or the sulfonic acid groups. No ^{11}B or ^{31}P signals were observed in the solid state NMR spectra of M20, suggesting that the major fraction of BP was dissolved and washed out during the membrane treatment with dilute acid and boiling water after casting. On the other hand, a gradual development of an absorption band which was centered around 1465 cm^{-1} in the ATR-FTIR spectrum was observed as the theoretical initial BP content increased, eventually indicating the formation of covalent Nafion® sulfonates such as boron Nafionates. The X-ray diffraction data further confirmed that no crystalline BP phase was present in any of the membranes.

The TGA curves of M00-M20 were basically identical, further confirming that the major fraction of the BP inorganic filler was dissolved and washed out during the membrane treatment. However, the DTA data eventually indicated that the crystalline melting temperatures of the BP composite membranes were somewhat higher compared with the pristine recast Nafion® membranes.

Stress-strain curves were recorded at 20 °C and at 130 °C. At 130 °C, the composite membranes M05-M20 showed slightly better mechanical stability compared with the pure recast Nafion® membrane (M00). This could eventually be attributed the slightly higher crystalline melting temperatures of the BP composite membranes. In order to further improve the mechanical strength and the dimensional stability of the membranes at elevated temperatures, a novel procedure was developed for preparing Nafion® based composite membranes which were reinforced with highly porous PTFE.

The cross-sectional SEM micrographs showed a micro-porous structure of M05-M20. The size of the pores was about 0.5 µm in diameter and the number of pores gradually increased with increasing theoretical initial BP loading. The cross-sectional SEM micrographs of the PTFE reinforced membrane (M00-PTFE) showed a rather asymmetric structure of the membrane, which was a direct consequence of the membrane preparation procedure. It also showed a good distribution of ionomer within the porous PTFE which is of critical importance for the through-plane proton conductivity of the membrane.

The in-plane proton conductivity of all membranes was found to be strongly dependent on the presence of water. At 100 °C and 100% relative humidity a conductivity maximum of 0.18 S cm^{-1} was recorded for M05. At 150 °C in liquid water (6 bar back pressure) the conductivity of the BP composite membrane M10 was slightly higher compared with that of the pure recast Nafion® membrane (M00). The conductivity of both membranes declined over time. However, the absolute conductivity values must be considered as relatively uncertain due to the poor dimensional stability of the membranes which results in poorly defined sample dimensions.

The PTFE reinforced M00 and M05, on the other hand, showed superior proton conductivity over time in liquid water at 150 °C compared with the pure M00 and M05 membranes as well as Nafion® 117. It was about 0.34 S cm^{-1} after 250 h and 0.29 S cm^{-1} after 750 h.

In order to demonstrate the feasibility of the developed membranes, electrolysis tests were conducted at 120 °C with a liquid water feed and at 2-3 bar back pressure. Although the anode catalyst loadings varied between the MEAs, the performances in the higher current density range gave indicative information about the membrane characteristics.

The highest current density was reached (2500 mA cm^{-2} at 1.95 V) using the PTFE reinforced BP composite membrane. The considerably better performance of the MEA based on the PTFE reinforced membrane compared with the MEAs based on M00 and M05 membranes could primarily be explained by the better dimensional stability of the reinforced membrane. The better mechanical stability should help preserving the nanostructure of the membrane which is crucial for its proton conductivity mechanism. Additionally, it probably reduces the membrane-electrode interfacial contact resistance, which is critical for the overall cell performance.

However, the anode activation overvoltage was found to be relatively high compared with the literature data which implies that it should be room for a considerable performance improvement by improving the catalyst activity.

5 Crosslinking of PBI membranes for high temperature PEM fuel cells

The following chapter is devoted to the development of an operationally simple post crosslinking procedure of PBI membranes for high temperature PEM fuel cells. The major parts of the data and discussion are also available in paper II.

5.1 Background

When PBI is doped with phosphoric acid, the intermolecular cohesion within the polymer matrix is reduced due to the strong plasticizing effect of phosphoric acid. The mechanical characteristics of phosphoric acid doped PBI membranes are thus strongly correlated with the acid doping level. At doping levels below 2, the strong coulomb interactions between the polymer and the acid has been demonstrated to enhance the molecular cohesion within the membrane, as indicated on a macroscopic scale by increased elastic modulus and toughness [78, 183]. On the other hand, when the doping level is higher than 2 and excess acid is present in the membrane the mechanical strength is dramatically reduced with increasing acid doping level.

As previously discussed in Chapter 1.7.2, a high acid doping level is desirable from a proton conductivity point of view. However, a highly doped PBI membrane generally suffers from extremely poor mechanical stability which limits its usability as PEM material. Therefore, a compromise between a high acid doping level and the mechanical stability of the membrane is generally inevitably made. Based on these two variables, an acid doping level of 3.5-7.5 has been suggested as a reasonable compromise between the mechanical strength and the proton conductivity of thin PBI membranes prepared by solution casting followed by acid imbibing for high temperature PEM fuel cells [170].

A high linear molecular weight of the polymer to be used for the membrane preparation is often advantageous from a mechanical strength perspective [183]. However, it is often problematic from a material processing point of view due to the limited solubility of the high molecular weight fraction of the polymer and the high viscosity of the obtained solutions.

Mechanical reinforcement with for example surface functionalized carbon nanofibers results in PBI composites with superior mechanical strength [215], which allows for higher acid doping levels and thus higher proton conductivity. However, carbon nanofibers are electronically conducting which might cause short circuit of the cell. Therefore, mechanical reinforcement of phosphoric acid doped PBI membranes with porous PTFE might be a better solution since the PTFE is electronically insulating. Since it improves the mechanical characteristics of the phosphoric acid doped membrane it also allows for reduced membrane thickness and thus reduced area specific resistance [216, 217].

Ionic crosslinking between PBI and an acid polymer, as discussed in Chapter 3, is one way to tailor the membrane properties. For example, blend membranes of PBI and partially fluorinated and sulfonated arylene polyethers have recently been reported to exhibit improved chemical stability compared with the pristine PBI membrane. They also exhibited sufficient mechanical strength for the MEA preparation even at as high acid doping levels as 10-13 [154, 155]. A complete list of different reported PBI based acid-base polymer blend membrane concepts for hydrogen based electrochemical energy conversion technologies is available in Table 3.1.

Another efficient approach to toughen polymeric materials in general is crosslinking. In a covalently crosslinked membrane the polymer chains are chemically bridged by covalent bonds. Crosslinking of a

polymer dramatically increases the molecular weight and turns the thermoplastic polymer into a thermoset which makes processing after crosslinking almost impossible. Hence, the crosslinked membrane preparation procedure has to be intelligently designed in order to circumvent the extremely poor solubility which is a fundamental characteristic of crosslinked polymers.

Covalently crosslinked and phosphoric acid doped PBI membranes are generally mechanically stronger and tougher than their linear counterparts of a similar acid doping levels. Naturally, this allows for higher doping levels without sacrificing the mechanical strength. Better fuel cell performance can thus be expected and eventually better durability due to the enhanced oxidative stability of the crosslinked structures. Several different crosslinking agents are available for PBI. Most of them rely on conventional S_N2 type reactions or Michael additions and employ the rather high nucleophilicity of the imine groups in the benzimidazole moieties.

For example, dichloro-*p*-xylene has been employed for the preparation of crosslinked PBI nanofiltration membranes [179, 218]. Recently, dibromo-*p*-xylene [100] and dichloromethyl phosphinic acid [172] were demonstrated to crosslink PBI after heat treatment at temperatures up to 300 °C. Yu *et al.* [219] prepared a crosslinked membrane based on 2OH-PBI according to the PPA process. Phosphate bridges were developed during the synthesis as confirmed by a low molecular weight model system reaction. Furthermore, pendant amino groups on the PBI backbone were recently introduced and used as handles for further crosslinking reactions [220]. Han *et al.* [221] recently reported a crosslinking procedure of PBI for high temperature PEM fuel cells using 4,4´-diglycidyl(3,3´,5,5´-tetramethylbiphenyl) epoxy resin as the crosslinking agent. The crosslinking reaction was initiated by heat treatment at temperatures exceeding 160 °C, as confirmed by DSC. Additionally, several patents describing PBI functionalization or crosslinking procedures for varying applications have been granted throughout the years [222-226]. Furthermore, a covalent network polymer membrane based on PBI and polyvinylphosphonic acid has been commercialized by BASF fuel cell for DMFC applications under the trade name Celtec-V [227, 228]. In general, the covalently crosslinked membranes exhibited superior chemical, mechanical and dimensional stability compared with their linear counterparts.

Divinylsulfone (DVS) was first suggested as a crosslinking agent for PBI in a US patent which was filed in 1987 [229]. The crosslinking reaction was assumed to be a Michael type addition and alkali metal alkoxides or quaternary ammonium hydroxides were employed as base catalysts in order to further enhance the nucleophilicity of the nitrogen atoms in the benzimidazole moieties in PBI.

However, the covalent crosslinking chemistry of PBI has yet not been studied in detail and generally complete reaction between the crosslinking agent and two active sites in the polymer is assumed when the degree of crosslinking is calculated.

In this work, a novel methodology for the crosslinking of preformed PBI membranes with DVS was developed. The crosslinking chemistry was studied and optimized using a low molecular weight model system reaction. The crosslinked membranes were subsequently characterized with respect to chemical and physiochemical properties. The feasibility of the crosslinked membranes was demonstrated by high temperature PEM fuel cell testing.

5.2 Experimental

5.2.1 Model system reaction

All chemicals were used as received without further purification. The reactions were performed under ambient atmosphere. The NMR spectra were recorded on a Varian Mercury 300 spectrometer, using DMSO-d_6 as solvent. The chemical shifts are given in ppm relative to the solvent residual peaks at 2.50 ppm (^{1}H) and 39.52 ppm (^{13}C). The peak assignments were accomplished by coupling pattern and

integrals. Thin layer chromatography (TLC) was performed on Merck precoated aluminium TLC plates coated with silica gel 60 F_{254} and visualized in UV light (254 nm). Purification of products was achieved using flash column chromatography with silica gel (0.04-0.063 mm). Evaporation and concentration refer to the use of a rotatory evaporator under reduced pressure. The reported yields are isolated yields calculated on the dry mass basis.

Reaction in MeOH

Benzimidazole (359.8 mg, 3.05 mmol (Table 5.1, Entry 1), 358.8 mg, 3.04 mmol (Table 5.1, Entry 2)) was dissolved in MeOH (20 mL). DVS (174.8 mg, 1.48 mmol (Table 5.1, Entry 1), 353.1 mg, 2.99 mmol (Table 5.1, Entry 2)) was added at room temperature under stirring. After stirring at 50 °C for 70 h the reaction mixture was concentrated and purification was achieved using flash column chromatography (SiO_2, 19:1, CH_2Cl_2:MeOH) to give product **1** as a white solid (R_f: 0.27) and product **2a** as a colorless oily liquid (R_f: 0.33). The yields are listed in Table 5.1.

Reaction in aqueous KOH

Benzimidazole (379.5 mg, 3.21 mmol) was dissolved in 1 mol L^{-1} aqueous KOH (20 mL). DVS (187.3 mg, 1.59 mmol) was added at room temperature, resulting in instant precipitation of a white solid. The reaction mixture was further stirred at room temperature for 1 h. Product **1** was isolated from the mother liquor as a white solid (153.9 mg, 27%) by filtration.

NMR spectral data

1 (1-[2-(2-(1*H*-benzimidazoyl)-ethanesulfonyl)-ethyl]-1*H*-benzoimidazole) δ_H: (300 MHz, DMSO-d_6) 8.21 (2H, s), 7.64 (2H, dd, *J* = 7.8, 0.9 Hz), 7.57 (2H, dd, *J* = 7.2, 1.2 Hz), 7.23 (4H, m), 4.69 (4H, t, *J* = 7.0 Hz), 3.77 (4H, t, *J* = 7.0 Hz); δ_C: (75 MHz, DMSO-d_6) 145.9, 144.0, 134.0, 123.2, 122.4, 120.2, 111.1, 52.2, 49.9

2a (1-[2-(2-methoxy-ethanesulfonyl)-ethyl]-1*H*-benzoimidazole) δ_H: (300 MHz, DMSO-d_6) 8.23 (1H, s), 7.65 (1H, dd, *J* = 8.4, 0.6 Hz), 7.61 (1H, dd, *J* = 7.8, 0.9 Hz), 7.24 (2H, m), 4.69 (2H, t, *J* = 6.6 Hz), 3.68 (2H, t, *J* = 6.6 Hz), 3.66 (2H, t, *J* = 5.1 Hz), 3.41 (2H, t, *J* = 5.1 Hz), 3.21 (3H, s); δ_C: (75 MHz, DMSO-d_6) 145.0, 144.1, 134.0, 123.1, 122.4, 120.2, 111.0, 66.1, 58.8, 53.4, 49.9, 38.2

5.2.2 Membrane preparation and phosphoric acid doping

PBI powders with average molecular weights of about 23 kDa and 44 kDa were supplied by Danish Power Systems ApS. The PBI powders were dissolved in DMAc at 80 °C to give solutions with concentrations of about 5 wt.% after filtering. The PBI membranes were subsequently cast from the PBI/DMAc solutions on glass substrates by solvent evaporation and dried at temperatures up to 120 °C. The residual solvent was removed by boiling the membranes in water and methanol for several hours followed by drying at 200 °C for at least 15 h.

For the post crosslinking the dry membranes were weighed and submerged in methanol with a fixed PBI:MeOH mass ratio. Varying amounts of DVS was subsequently added to the solutions to give DVS:PBI_{RU} molar ratios of 0, 1, 5 and 10. The reaction mixtures were stirred at 50 °C for typically 70 h. The membranes were thereafter treated with pure and warm MeOH and boiling demineralized water for several hours followed by drying at 200 °C and weighing. From the weight gains the apparent degrees of crosslinking were calculated.

Phosphoric acid doping of the pristine and the crosslinked PBI membranes was achieved by submerging the membranes in 85% H_3PO_4 at different temperatures and for different durations.

5.2.3 Membrane characterization

Elemental analysis (H, N, C, S) was performed on three parallel samples by Mikroanalytisches Laboratorium, Universität Wien.

The FTIR spectra were recorded on a Perkin-Elmer 1710 Infrared Fourier Transform spectrometer under ambient atmosphere. The membranes were pre-dried at 200 °C for 20 h and stored in sealed containers in order to avoid moisture absorption. The spectra were integrated using Perkin-Elmer Spectrum 2.0 software in order to obtain the relative peak area of the 3420 cm^{-1} and 810 cm^{-1} absorption bands.

TGA was performed on a Netzsch STA 409 PC equipped with Netzsch QMS 403 C mass spectrometer. Synthetic air 5.0 was used as the purge gas and the samples were heated up to 1000 °C at a heating rate of 10 °C min^{-1}.

Membrane samples (30-40 μm thick) were submerged in a 3% H_2O_2 (Merck) aqueous solution containing 4 ppm Fe(II) (added as $(NH_4)_2Fe(SO_4)_2 \cdot 6H_2O$) at 68 °C. Every 20 h, the membrane samples were collected, rinsed with demineralized water and dried at 120 °C for at least 5 h. The dry weight was recorded and the membrane samples were submerged in freshly prepared Fenton solution for continuation of the test.

The stress-strain curves were recorded at 20 °C and 180 °C under ambient atmosphere without any active humidity control.

The in-plane conductivity was measured at ambient pressure at 150 °C and 180 °C at relative humidity ranging from 1-20% and 3-10%, respectively. The symmetric square wave current was supplied in a frequency range from 5-10 kHz. The phosphoric acid doped membrane samples were pre-dried at 180 °C for 2 h before the dimensions were measured.

For the fuel cell tests, gas diffusion electrodes were made by spraying Pt/C onto non-woven gas diffusion layers made of carbon cloth. The platinum catalyst was supported on carbon black (Vulcan 72R, Cobat) and was prepared by a solution reduction method. It had a composition of about 40 wt.% Pt and 60 wt.% carbon. The catalyst powders were subsequently dispersed in a mixture of formic acid, H_3PO_4 and PBI (0.5 wt.%). The ink was sonicated for 30 minutes before spraying. On the final gas diffusion electrodes the Pt loading was about 0.7 mg Pt cm^{-2}. The PBI loading was about 0.14 mg cm^{-2}, and the catalyst layer was doped with phosphoric acid at a level of 1.2 mg cm^{-2}. The pristine and the crosslinked (8% apparent degree of crosslinking) PBI membranes were typically 70 μm thick and they were doped in 85% H_3PO_4 at 20 °C and 50 °C, respectively, for at least 24 h to give acid doping levels of about 10. The membranes were sandwiched between two pieces of gas diffusion electrodes and hot-pressed under a pressure of about 10 MPa for 10 minutes. The hot-pressing temperature of the linear PBI membrane based MEA was 150 °C. The phosphoric acid doped crosslinked PBI membrane was stiffer than the membranes based on its linear counterpart and it exhibited a much higher Young´s modulus. The hot-pressing temperature was therefore elevated to 200 °C in order to achieve good interfacial contact between the membrane and the electrodes. However the hot-pressing procedure was not systematically optimized. The size of the active electrode area of the MEAs was typically 4 cm^2. Dry hydrogen and air at flow rates of 100 and 200 mL min^{-1}, respectively, were supplied to the fuel cell without pre-humidification. The polarization curves were obtained using a current step potentiometer. The steady state potentials were recorded about two minutes after each current was set.

Even at the maximum current densities reached during polarization of the MEAs, the gas flow rates were much higher than the reactant consumption. By using a considerable over-stoichiometry, the fuel cell tests were performed in order to evaluate the materials but not to optimize the cell operating parameters.

5.3 Results and discussion

5.3.1 Model system reaction

A low molecular weight model system reaction was designed in order to study the key step of the crosslinking reaction, i.e. the linking of two benzimidazole moieties with DVS, in detail. The model system reaction is illustrated in Scheme 5.1.

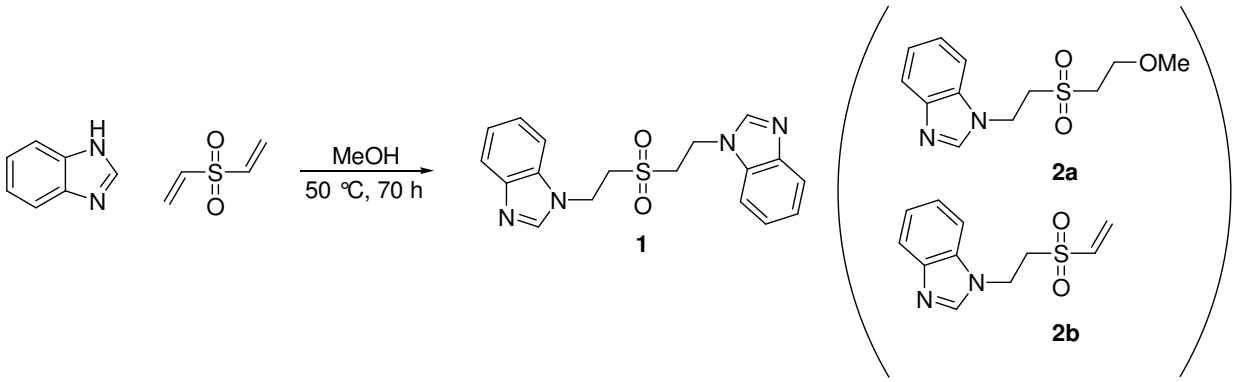

Scheme 5.1 *Model system reaction in MeOH.*

When benzimidazole was reacted with DVS in stoichiometric amounts the reaction preceded smoothly and the desired product **1** could be isolated in 83% yield (Table 5.1, Entry 1). On the other hand, when DVS was added in excess (Table 5.1, Entry 2) **2a** was the major product and was isolated in 58% yield.

Table 5.1 *Yields and products of the model system reaction in MeOH.*

Entry	Benzimidazole (eq.)	DVS (eq.)	Yield (1)	Yield (2a + trace amounts of 2b)
1	1	0.5	83%	7%
2	1	1	36%	58%

When the concentration of DVS is high, the probability that **2a** or **2b** should react with another free benzimidazole molecule to give **1** is logically lower than the probability that one free DVS molecule should react with one free benzimidazole molecule to give one more molecule of either **2a** or **2b**. It also indicates that grafting of 2-methoxy-ethanesulfonyl groups on the polymer backbone could be the favored reaction rather than the crosslinking if excess DVS is present during the post-treatment, since the crosslinking per definition requires that each DVS molecule reacts with PBI twice.

Just like the benzimidazole moieties in PBI, MeOH is somewhat nucleophilic which means that the solvent was competing with benzimidazole as nucleophile in the present study. It is thus likely that the reaction between one DVS molecule and two benzimidazole molecules goes via a dimethoxylated sulfone intermediate, followed by two sequential substitution reactions. It also explains why **2a** and not **2b** was the major by-product and main product in Entry 1 and 2, respectively.

However, it must be remembered that the model system reaction is very different from the PBI membrane post treatment reaction in terms of for example the local concentration of benzimidazole moieties. Additionally, the degrees of freedom of the benzimidazole moieties in the polymer membrane are very much limited compared with the degrees of freedom of the benzimidazole molecules in solution.

PBI doped with KOH has previously been demonstrated to exhibit ionic conductivity in the 10^{-2} S cm^{-1} range [230], which makes it an interesting electrolyte for alkaline PEM fuel cell applications. When a stoichiometric amount of DVS was added to benzimidazole in aqueous KOH, product **1** was formed and precipitated from the mother liquor in 27% yield after 1 h at room temperature. The results from the alkaline model system reaction indicate that it might be possible to combine an operationally simple and fast post crosslinking procedure of PBI membranes with alkaline doping in one single step.

5.3.2 Post crosslinking of PBI membranes

A schematic illustration of the crosslinking procedure of the PBI membranes by post-treatment with DVS is given in Scheme 5.2.

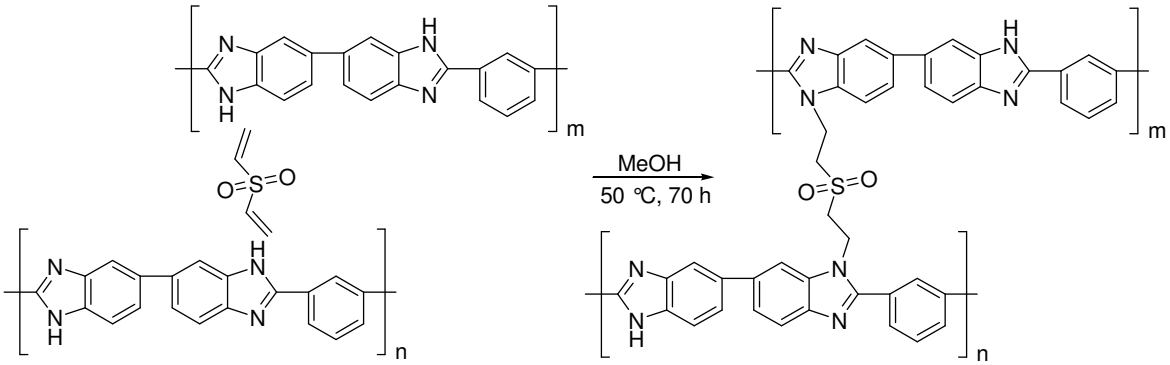

Scheme 5.2 *Schematic illustration of the PBI crosslinking procedure by post-treatment with DVS.*

After the post-treatment with DVS, the membranes were visually homogenous and almost completely insoluble in DMAc at 80 °C. The membrane solubility in terms of remaining undissolved mass after certain submersion times in DMAc at 80 °C is shown in Figure 5.1.

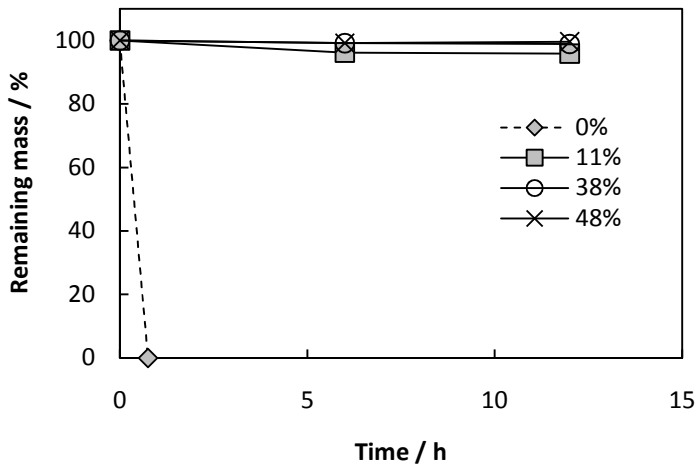

Figure 5.1 *Membrane solubility in DMAc at 80 °C. The apparent degrees of crosslinking are indicated in the figure.*

From the weight gains after the DVS treatment the weight percentages of sulfur in the membranes were calculated. As seen from Table 5.2, the calculated results were in good agreement with the sulfur contents determined by elemental analysis. However, the post crosslinking reaction time was

decreased to 16 h meaning that the membrane weight gains and thus the calculated sulfur contents based on the weight gains were considerably lower compared with that of the membranes which were post-treated for 70 h.

Table 5.2 *Calculated and found sulfur contents of the crosslinked membranes.*

Initial DVS:PBI$_{RU}$ molar ratio	**1**	**5**	**10**
Calculated sulfur content from weight gain, wt.%	0.060	0.43	0.99
Found sulfur content, wt.% (elemental analysis)	0.053	0.45	0.94

As already discussed in Chapter 5.3.1, the complete crosslinking requires that one molecule of DVS reacts with PBI twice. Naturally, it also requires that the DVS molecule reacts with two separate PBI molecules and not two reactive sites within the same PBI chain.

The risk for mono-addition of DVS was identified in the model system reaction when DVS was added in excess. Hence, it is probable that the post-treated membranes contain a certain amount of grafted 2-methoxy-ethanesulfonyl groups in addition to the developed crosslinks. On the other hand, it should be probable that a vinylsulfone or 2-methoxysulfone which has been attached to one benzimidazole moiety reacts with another benzimidazole moiety since the local concentration of benzimidazole moieties should be high within the PBI membrane.

However, the apparent degree of crosslinking calculated based on the membrane weight gain according to Equation 5.1 could thus be different from the real degree of crosslinking. The fraction of the graft 2-methoxy-ethanesulfonyl groups is thus unknown. It would obviously be higher at higher initial DVS:PBI$_{RU}$ molar ratios during the membrane post-treatment.

$$Apparent\ CL = 2 \times \frac{n_{DVS}}{n_{PBI_{RU}}} \times 100\% \tag{5.1}$$

The apparent degrees of crosslinking reached after the DVS treatment of 30 µm thick PBI membranes are plotted versus the initial DVS:PBI$_{RU}$ molar ratios in the post-treatment reactions in Figure 5.2.

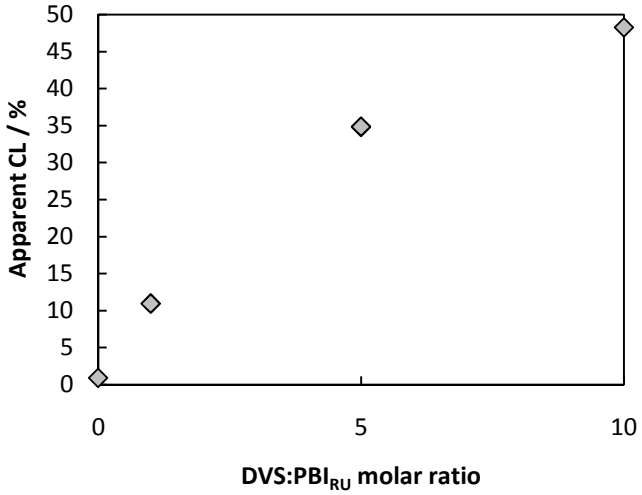

Figure 5.2 *Apparent degree of crosslinking as a function of the initial DVS:PBI$_{RU}$ molar ratio. The membrane thickness was 30 µm.*

Assuming complete reaction between one DVS molecule and 2 PBI reactive sites, the DVS:PBI_{RU} ratio of 1 during the post-treatment reaction would give a theoretical degree of crosslinking of 200% and a membrane weight gain of 38%. The crosslinking degree of PBI can theoretically be higher than 100% since each repeating unit of PBI has two reactive sites which are available for Michael addition.

However, the measured weight gain after the DVS treatment under the given conditions was 2.1%, which corresponds to an apparent degree of crosslinking of about 11%. For the membranes treated with DVS at higher initial DVS:PBI_{RU} molar ratios the apparent degrees of crosslinking were considerably higher. The membrane which was treated with DVS at an initial DVS:PBI_{RU} molar ratio of 10 obtained an apparent degree of crosslinking as high as close to 48%.

It is well known that PBI membranes are dense and exhibit very low gas permeability [231]. That is of course an advantage when PBI is used as electrolyte material in for example PEM fuel cells. However, due to the presumed rather low permeation coefficient of DVS in PBI, the reaction between DVS and PBI should start on the membrane surface during the membrane post treatment. In that case, the obtained apparent degree of crosslinking would be dependent on the membrane thickness. This was studied by treating a set of membranes with varying thicknesses in a solution with a fixed initial DVS:PBI_{RU} molar ratio of 1, as shown in Figure 5.3.

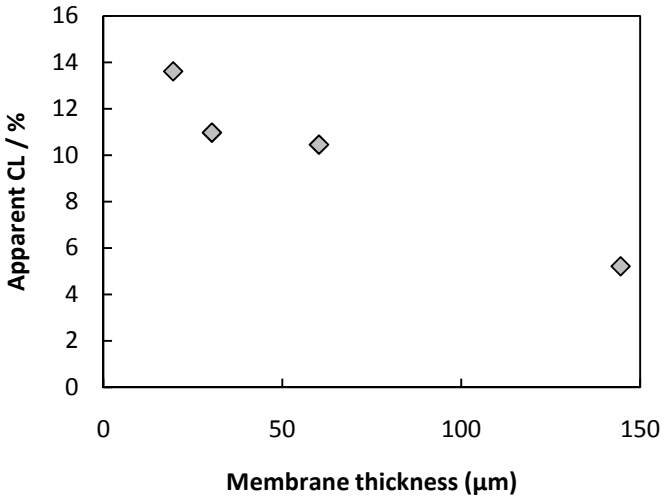

Figure 5.3 *Apparent degree of crosslinking as a function of the membrane thickness for a constant initial DVS:PBI_{RU} molar ratio of 1.*

It revealed a correlation between the membrane thickness and the apparent degree of crosslinking obtained. The apparent degree of crosslinking was increased from about 5% for a 150 µm thick membrane to about 13% for a 20 µm thick membrane. It indicates that the diffusion of DVS into the bulk membrane is limiting the possibilities to obtain a homogeneous distribution of the crosslinking density throughout the membrane cross-section. As a result, the crosslinking density should be higher near the membrane surface. Additionally, it is likely that it depends on the morphology of the membrane.

5.3.3 Phosphoric acid doping

An acid doping level of around 11 is normally obtained during doping of linear PBI membranes in 85% H_3PO_4 at room temperature [171]. This was confirmed in the present study, as summarized in Table 5.3. However, during doping at 50 °C the linear reference membrane was partially dissolved as also indicated by a slightly colored doping solution.

Table 5.3 *Phosphoric acid doping of PBI membranes of different apparent degrees of crosslinking in 85% H_3PO_4.*

Initial DVS:PBI_{RU} molar ratio (apparent CL degree in parenthesis)	**0 (0 %)**		**1 (11 %)**		**5 (35 %)**		**10 (48 %)**	
Doping temperature (°C)	20	50	20	50	20	50	20	50
Doping level (PA/PBI_{RU})	10.6	-	3.2	8.3	0.7	7.4	0.4	6.0
Volume swelling (%)	143	-	33	110	5	71	6	62
Specific swelling (Volume swelling/Doping level)	13.5	-	10.3	13.3	7.1	9.6	15	10.3

In 85% H_3PO_4 at room temperature, the obtained acid doping level of the crosslinked membrane with an apparent degree of crosslinking of 35% was as low as 0.7. The corresponding volume swelling was about 5%. By further doping the membrane at 50 °C the doping level could be increased to 7.4, accompanied by a volume swelling of 71%. As also well documented in the literature [100, 172], the covalently crosslinked PBI membranes had to be doped at elevated temperatures in order to obtain sufficient phosphoric acid doping levels (and thus anhydrous proton conductivity) for any practical use in PEM fuel cells.

This should be a direct consequence of the improved dimensional stability and thus the enhanced resistance to swelling of the covalently crosslinked structures. The doping acid solutions remained clear and uncolored during the phosphoric acid doping of the crosslinked membranes, which further confirmed the limited solubility of the DVS post-treated membranes due to the dramatic molecular weight increase.

5.3.4 FTIR

The FTIR spectra of the non-doped membranes of varying apparent degrees of crosslinking are shown in Figure 5.4. The pristine PBI membrane showed all characteristic featured absorption bands, as also summarized in Table 3.3.

In addition, the DVS post-treated membranes showed two new absorption bands which were centered around 1140 cm^{-1} and 1324 cm^{-1}. These bands were assigned to sulfone group absorption [177] and obviously originated from the divinylsulfone molecules which had reacted with the polymer. They could be present either as grafted groups or in the form of complete crosslinks. Furthermore, the absorption bands of the membranes which had been post-treated in solutions of higher initial DVS:PBI_{RU} molar ratios were more pronounced and intense. As expected, it indicates a gradual increase of the sulfone group concentration within the membranes which had been post-treated in solutions of increasing initial DVS:PBI_{RU} molar ratio which implies that the apparent degree of crosslinking increased.

Furthermore, an obvious decrease of the 3420 cm^{-1} absorption band intensity was observed in the FTIR spectra of the membranes with very high apparent degrees of crosslinking. This absorption band is associated with non-hydrogen bonded or “free” N-H stretching vibrations in the imidazole moieties [179]. As new N-C bonds were developed during the post-treatment as a result of the Michael addition of DVS to the benzimidazole moieties, the total amount of “free” N-H bonds in the membrane was reduced. Since the intensity of the absorption band is proportional to the concentration of non-hydrogen bonded N-H groups in the sample, the intensity decrease of the 3420 cm^{-1} absorption band should be more pronounced for the samples of high apparent degree of crosslinking.

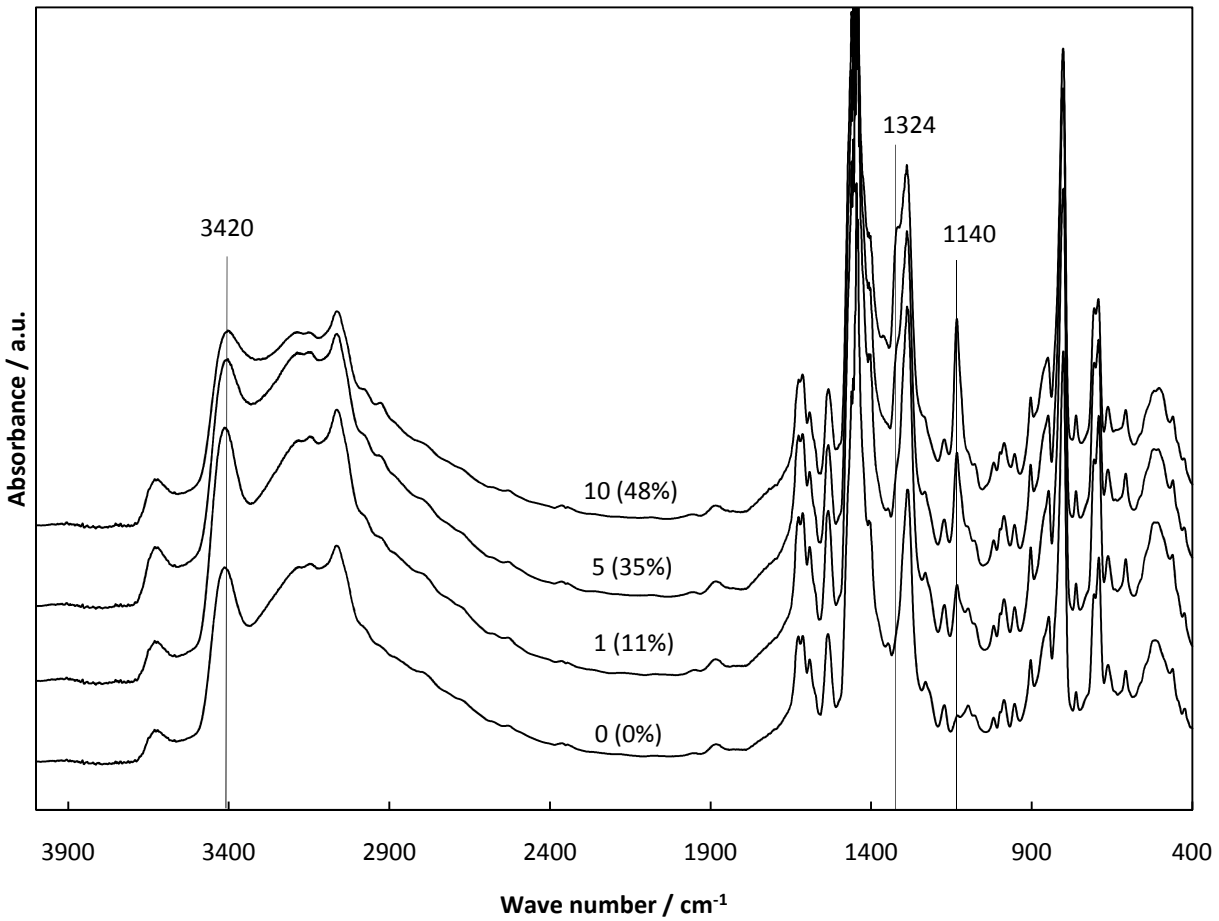

Figure 5.4 *FTIR spectra of pristine PBI and PBI membranes post-treated with DVS. The initial DVS:PBI$_{RU}$ molar ratios were as indicated. The apparent degrees of crosslinking calculated based on the weight gains are shown in parentheses.*

This was also confirmed by comparing the relative peak area of the 3420 cm^{-1} absorption band and the 810 cm^{-1} absorption band for each sample. The area under the 810 cm^{-1} absorption band should remain unaffected by the DVS treatment since it originates from benzene ring C-H bending, as also shown in Table 3.3. The peak area of the 3420 cm^{-1} absorption band relative to the peak area of the 810 cm^{-1} absorption band as calculated for each spectrum according to Equation 5.2 decreased with increasing apparent degree of crosslinking.

$$Relative\ peak\ area = \frac{A_{3420\ cm^{-1}}}{A_{810\ cm^{-1}}} \tag{5.2}$$

It was 2.10, 2.01, 1.85 and 1.25 for the membranes with an apparent degree of crosslinking of 0%, 11%, 35% and 48%, respectively, as also illustrated in Figure 5.5.

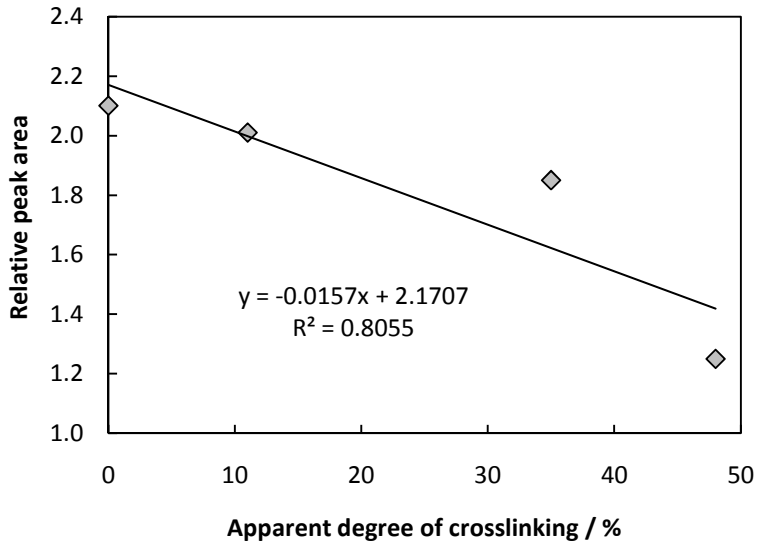

Figure 5.5 *The relative peak area of the FTIR absorption bands at 3420 cm^{-1} and 810 cm^{-1} in Figure 5.4 as calculated according to Equation 5.2.*

5.3.5 Radical-oxidative stability

The relative chemical stability of the membranes with apparent degrees of crosslinking of 0%, 11%, 35% and 48% was evaluated in a Fenton test. In the Fenton test hydroxyl and perhydroxyl radicals are generated by Fe(II) catalyzed decomposition of hydrogen peroxide according to Equation 2.10 and 2.11 in Chapter 2, respectively.

Membrane degradation by radical induced oxidation has been identified as one of the major long term durability limitations of the conventional PFSA based PEM fuel cells [111] as well as of the phosphoric acid doped PBI [232] based high temperature PEM fuel cells. For PFSA based PEM fuel cells, the generation of hydroxyl and perhydroxyl radicals has been suggested to occur on platinum which has been deposited within the membrane. The so called platinum band which is formed within the membrane is a consequence of the rather high corrosion rate of platinum in acidic media at the relatively high fuel cell cathode operational potentials, especially during fuel cell idling at OCV [181].

Chain scission of the polymer backbone has been identified as the starting point in the radical induced oxidative degradation of PBI membranes [109, 110]. The cleavage was proposed to start by hydroxyl or perhydroxyl radical attack at the carbon atoms linking the benzenoid and imidazole rings. Additionally, the chain scission was reported to generate new fragments which were highly susceptible to further endpoint oxidation reactions. Chain scission should naturally dramatically decrease the average molecular weight of the polymer, which was also confirmed by size exclusion chromatography measurements [109]. The dramatically decreased average molecular weight of the polymer should also result in reduced mechanical strength of the membrane, which ultimately might lead to severe membrane failure or pinhole formation.

In the present study, the linear PBI reference membrane started to spontaneously disintegrate after 140 h in the Fenton test solution after a 20% weight loss as shown in Figure 5.6. In contrast, the membrane with an apparent degree of crosslinking of 11% lasted for 280 h and could tolerate a 29% weight loss before it spontaneously started to disintegrate in the Fenton solution. The corresponding result for the membrane with an apparent degree of crosslinking of 35% was 440 h and 35% weight loss. When the experiment was terminated after 440 h, the membrane with an apparent degree of crosslinking of 48% was still in one piece.

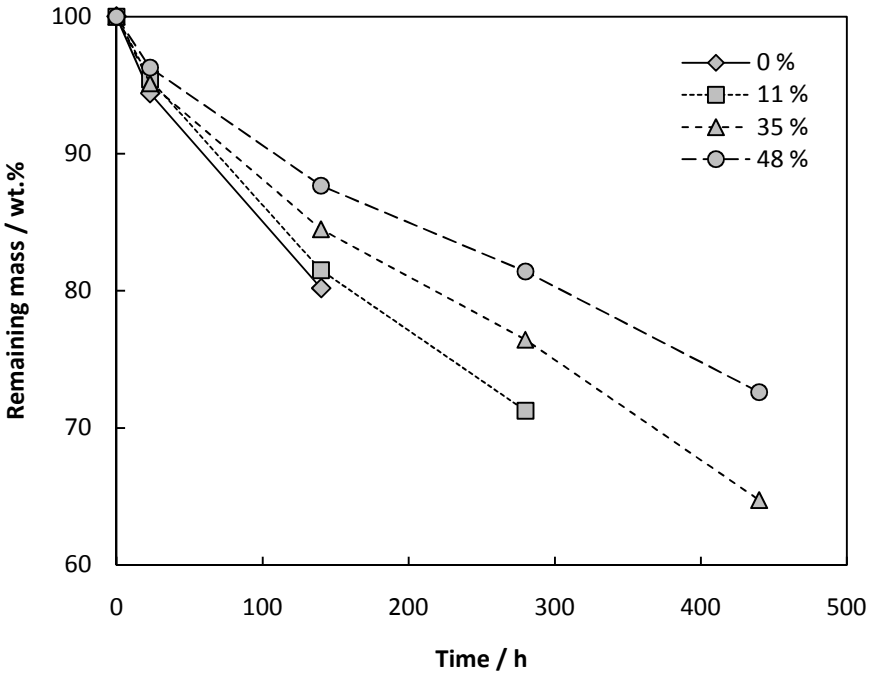

Figure 5.6 *Remaining membrane mass during the Fenton test of membranes of varying apparent degrees of crosslinking.*

The average rate of weight loss decreased with increasing degree of apparent crosslinking, which was in agreement with previously reported results for covalently crosslinked PBI membranes [100, 172]. The average rates of weight loss in the present study were 0.13, 0.10, 0.08 and 0.06 wt.% h^{-1} for the membranes with apparent degrees of crosslinking of 0%, 11%, 35% and 48%, respectively.

The network structure which is a fundamental characteristic of the crosslinked membranes should reduce the probability that low molecular weight degradation fragments are generated which are volatile or soluble in the aqueous Fenton solution.

5.3.6 Thermo-oxidative stability

Water, carbon oxides and nitric oxides have been reported as the major decomposition products when phosphoric acid doped PBI is thermally oxidized in air [233]. For pure PBI, a thermo-oxidative degradation mechanism has been postulated where the oxidation is initiated by hydrogen abstraction from the imine groups in the benzimidazole moieties [180]. Various oxidized PBI species are most likely formed in this process. At a certain temperature, the thermal oxidation results in polymer chain scission and ultimately complete weight loss due to the evaporation of volatile low molecular weight fragments.

In the present study, the onset temperature of decomposition of benzimidazole under air was around 175 °C (Figure 5.7). The linking of two benzimidazole molecules with divinylsulfone (Compound **1**, Scheme 5.1) increased the onset temperature of decomposition to around 220 °C. However, the thermal induced oxidation of **1** obviously occurred in two major steps. The second onset temperature of the major thermo-oxidative decomposition under air was observed at around 480 °C.

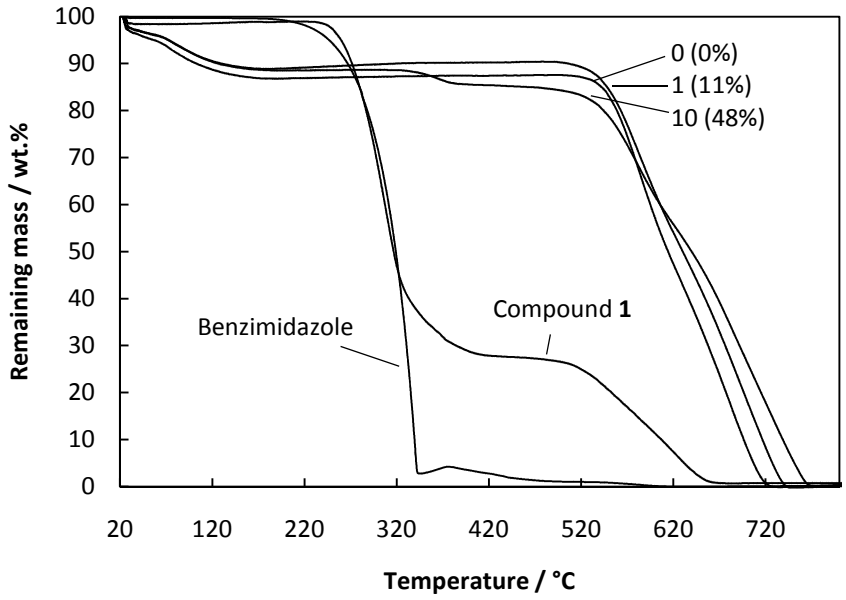

Figure 5.7 *Thermogravimetric curves of benzimidazole, compound **1** and PBI membranes treated with DVS. The initial DVS:PBI_{RU} molar ratios and the apparent degrees of crosslinking were as indicated.*

The PBI membrane with an apparent degree of crosslinking of 48% showed a similar two step thermal induced oxidation with a first onset temperature of the major decomposition at around 310 °C and a second one at close to 500 °C. The first onset temperature of decomposition at 310 °C was probably connected to the thermal induced oxidation of the sulfone linkages or the grafted groups. The second onset at 500 °C was most likely connected to the major thermo-oxidative decomposition of the polymer backbone. On the other hand, the linear PBI membrane and the membrane with an apparent degree of crosslinking of 11% showed only one apparent onset temperature of major decomposition at around 500 °C.

The weight loss of all membranes at temperatures up to 200 °C was obviously due to evaporation of water which had been absorbed from the atmosphere during storage since PBI is known to be highly hygroscopic. By defining the membrane water uptake from the atmosphere as the total weight loss at 200 °C, the water uptake of the linear PBI membrane (13%) was slightly higher compared with that of its crosslinked counterpart (11%).

5.3.7 Mechanical strength

Before phosphoric acid doping, the stress-strain curve of the crosslinked membrane with a linear average molecular weight of 44 kDa revealed no improvement in terms of Young´s modulus or engineering tensile stress at yield compared with its linear and non-doped counterpart, as shown in Figure 5.8.

At 180 °C the Young´s modulus and the engineering tensile stress at yield was about 300 MPa and 91 MPa, respectively, for both the linear reference membrane and its crosslinked counterpart with an apparent degree of crosslinking of 7%. However, the elongation at break of the crosslinked membrane was considerably lower. The crosslinked membrane showed less plastic deformation which indicated that it was more brittle than its linear counterpart. The increased brittleness also resulted in a slightly decreased engineering tensile stress at break from about 125 MPa to 100 MPa.

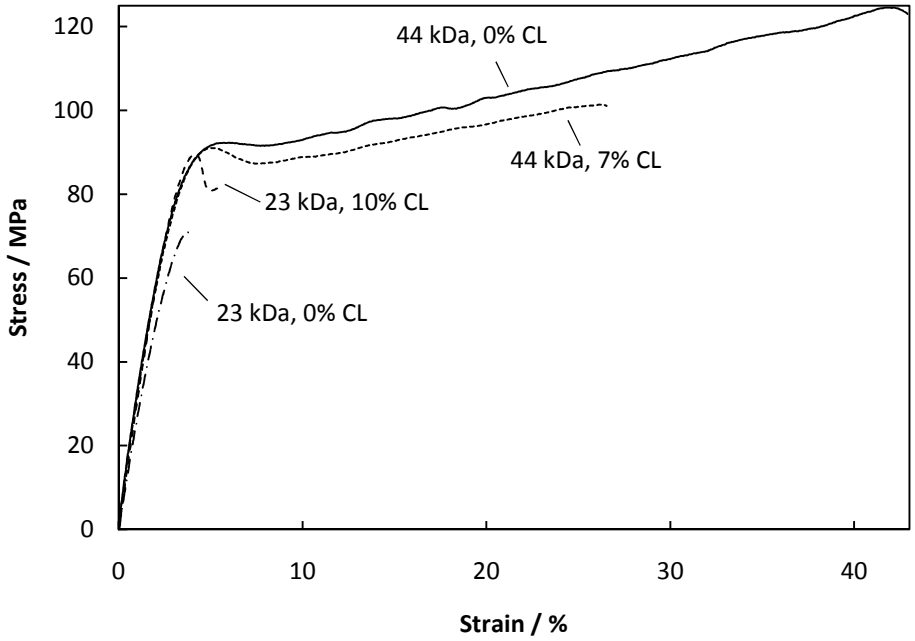

Figure 5.8 *Representative stress–strain curves at 180 °C of linear and post crosslinked membranes which were prepared from PBI with initial average molecular weights of 23 kDa and 44 kDa.*

In the low molecular weight range, on the other hand, a dramatic mechanical strength improvement with increasing average molecular weight can be expected for polymeric materials in general [103]. However, the mechanical strength dependence on the average molecular weight tends to level off in the higher molecular weight range. The expected mechanical toughening of the membrane after crosslinking would thus be more obvious for the membranes with a low linear average molecular weight. Hence, stress-strain curves of linear and crosslinked PBI membranes which had been prepared from a relatively low average molecular weight polymer (23 kDa) were recorded. The crosslinked membrane was obtained after post treatment in a solution with an initial DVS:PBI_{RU} molar ratio of 1, which resulted in an apparent degree of crosslinking of around 10%. After the post crosslinking of the membrane with a low linear average molecular weight of 23 kDa, the engineering tensile stress at break was found to increase from about 70 MPa to 87 MPa.

Similarly, the mechanical strength of phosphoric acid doped PBI membranes at a fixed acid doping level is well known to be highly dependent on the linear molecular weight of the polymer [183]. Phosphoric acid has a strong plasticizing effect on PBI which dramatically reduces the mechanical characteristics of the membrane in general, unless the acid doping level is less than or equal to 2 [78, 183]. Hence, if the membrane is doped with excess acid the intermolecular hydrogen bond interactions between the polymer chains are broken which results in a dramatic decay of the mechanical toughness. Stable covalent bonds between the linear PBI chains should thus considerably improve the mechanical characteristics, especially of the phosphoric acid doped membranes in the low linear average molecular weight range [100, 172].

As expected, after phosphoric acid doping the mechanical toughening of the crosslinked membrane was obvious, as shown in Figure 5.9. The membrane with a linear average molecular weight of 44 kDa and an apparent degree of crosslinking of 8% exhibited higher Young´s modulus as well as engineering tensile stress at break at 20 °C as well as at 180 °C compared with its linear counterpart of comparable phosphoric acid doping level. For example, the Young´s modulus at 20 °C increased from about 44 MPa for the linear PBI membrane to around 136 MPa for its crosslinked counterpart of comparable acid doping level.

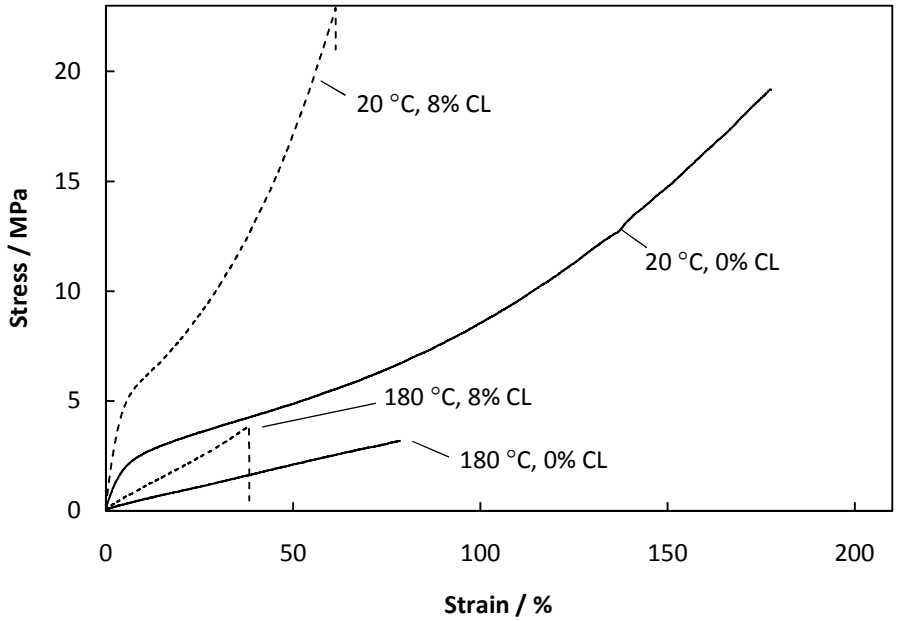

Figure 5.9 *Representative stress–strain curves of linear and crosslinked PBI membranes. The linear average molecular weight of PBI was 44 kDa. The PA doping level was about 10 for both membranes.*

Generally, the crosslinked membrane showed a much higher resistance to plastic deformation compared with the membrane based on linear PBI, as also illustrated by a lower elongation at break and higher engineering tensile stress at break. The increased toughness after post crosslinking was also illustrated by a considerably higher elastic modulus at 180 °C. Under these conditions the Young´s modulus after crosslinking was increased by 100% from 5 MPa to 10 MPa.

As seen from Table 5.3, the specific swelling per molecule of doping acid (total swelling divided by doping level) was 13.5, 12.0, 9.6 and 10.3 for the membranes with apparent degrees of crosslinking of 0%, 11%, 35%, and 48%, respectively. The lower specific swelling of the crosslinked membranes compared with their linear counterparts would in turn result a more coherent structure and thus a stronger resistance to deformation as illustrated in the stress-strain curve by a higher Young´s modulus in general of the crosslinked membranes.

5.3.8 In-plane conductivity

5.3.8.1 Phosphoric acid doped PBI

The presence of water improves the proton conductivity of phosphoric acid doped PBI membranes since water molecules actively participate in the proton conduction pathway [98], as described in more detail in Chapter 1.7.2. However, it is not as critical as for PFSA based membranes where the protons are transported through the membrane as hydrated complexes according to the vehicle mechanism [84].

For phosphoric acid doped PBI membranes with moderate doping levels of 3-6, reasonable proton conductivity in the 10^{-2} S cm^{-1} range can be obtained even under completely anhydrous conditions at temperatures up to 200 °C [98]. On the other hand, the proton conductivity of acid doped PBI membranes is strongly dependent on the acid doping level. For example, the proton conductivity of membranes with a phosphoric acid doping level above 20 prepared by the sol-gel methodology which

was originally developed by Xiao *et al.* [79] can reach as high as 0.25 S cm^{-1} at 180 °C, as also shown in Figure 1.11.

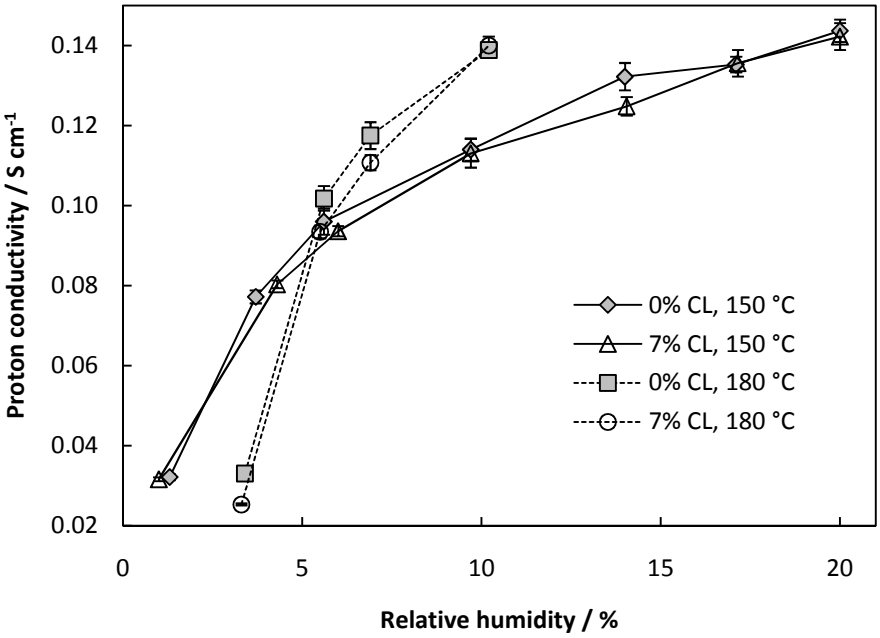

Figure 5.10 *In-plane proton conductivity at 150 °C and 180 °C of phosphoric acid doped membranes based on linear and post crosslinked PBI. The doping level of both membranes was about 10.*

Figure 5.10 shows the proton conductivity of a phosphoric acid doped linear PBI membrane and its crosslinked counterpart with an apparent degree of crosslinking of 7%. The linear and crosslinked membranes were doped in 85% H_3PO_4 at room temperature and at 50 °C, respectively, which resulted in phosphoric acid doping levels of around 10.

The proton conductivity data were in good agreement with previously reported conductivity data of an ionically crosslinked PBI based blend membranes of similar acid content which was measured under similar conditions [155]. The in-plane proton conductivity of both the linear membrane and its crosslinked counterpart in the present study reached 0.14 S cm^{-1} at 150 °C and 20% relative humidity and 0.14 S cm^{-1} at 180 °C and 10% relative humidity.

5.3.8.2 KOH doped PBI

It is well known that PBI membranes doped with aqueous alkali metal hydroxides exhibit hydroxide ion conductivity which makes them interesting as electrolyte materials for alkaline fuel cells. For example, Xing and Savadogo [230] reported hydroxide conductivity of KOH doped PBI in the 10^{-2} S cm^{-1} range. The hydroxide conductivity of the KOH doped PBI membrane was superior compared with that of the LiOH and NaOH doped PBI membranes and it was found to increase with temperature from about 0.02 S cm^{-1} at 25 °C to 0.095 S cm^{-1} at 70 °C. Furthermore, alkaline H_2/O_2 fuel cell tests were conducted at 50 °C based on these membranes in order to demonstrate the feasibility of the electrolyte material. The fuel cell based on the KOH doped PBI membrane showed initial performance comparable to that of a Nafion® 117 based fuel cell.

The pioneering work of Xing and Savadogo has stimulated further research activities devoted to the development of alkaline doped PBI membranes, mainly for direct ethanol fuel cells [234, 235]. However, the ethanol fed alkaline fuel cells based on KOH doped PBI suffer from severe durability

limitations due to the hydroxide ion conductivity decay over time. In addition, the carbonate formation rate within the MEA should be rather high.

In order to investigate the possibilities to operate a fuel cell based on a KOH doped PBI membrane at temperatures above 100 °C, conductivity measurements were conducted at 110 °C (85% relative humidity) as a function of time as shown in Figure 5.11. The PBI membrane was post-crosslinked with DVS to give an apparent degree of crosslinking of about 7% and subsequently doped in 6 mol L^{-1} KOH at 60 °C for 70 h [230].

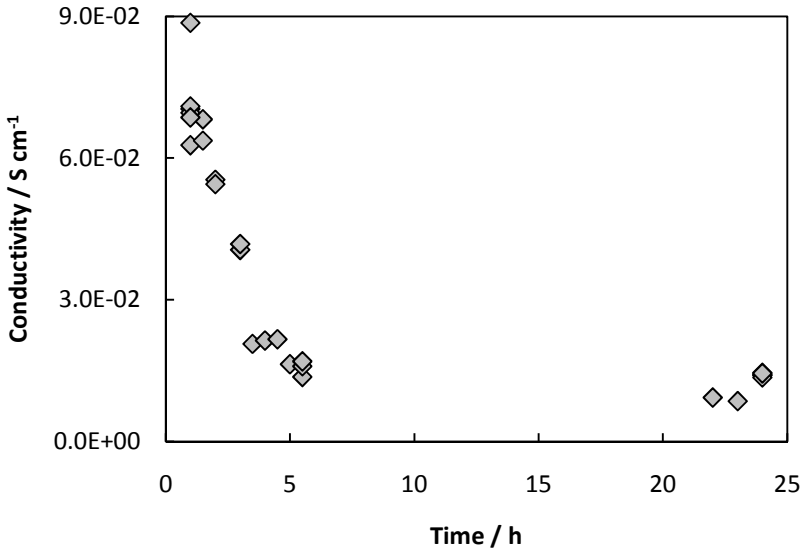

Figure 5.11 *Hydroxide conductivity of a KOH doped DVS crosslinked PBI membrane at 110 °C and 85% relative humidity.*

However, although the saturated vapor pressure of highly concentrated aqueous KOH is much lower than that of pure water at elevated temperatures [236] the hydroxide conductivity dropped due to the membrane dehydration from about 0.1 S cm^{-1} to 0.01 S cm^{-1} over a period of 24 h. Pressurization would thus be required in order to avoid dehydration and to maintain the high hydroxide ion conductivity at elevated temperatures.

5.3.9 Fuel cell tests

Figure 5.12 shows representative polarization curves at 150 °C and 180 °C of fuel cell MEAs based on the linear and post crosslinked phosphoric acid doped PBI membranes with a linear average molecular weight of about 44 kDa. Both membranes had a phosphoric acid doping level of around 10 and a membrane thickness of about 70 µm before the MEA hot-pressing.

In the low current density region where the catalytic activity of the electrodes is dominating the appearance of the polarization curve, no improvement was observed. However, it is interesting to note that the OCV of the fuel cell based on the crosslinked membrane was slightly higher than that of the cell based on the linear PBI membrane. This could probably be connected to decreased gas permeability of the crosslinked membrane due to the more coherent structure, as also illustrated by the lower specific volume swelling (Table 5.3). Reduced gas permeability should also give a higher fuel utilization coefficient which should allow for higher efficiency.

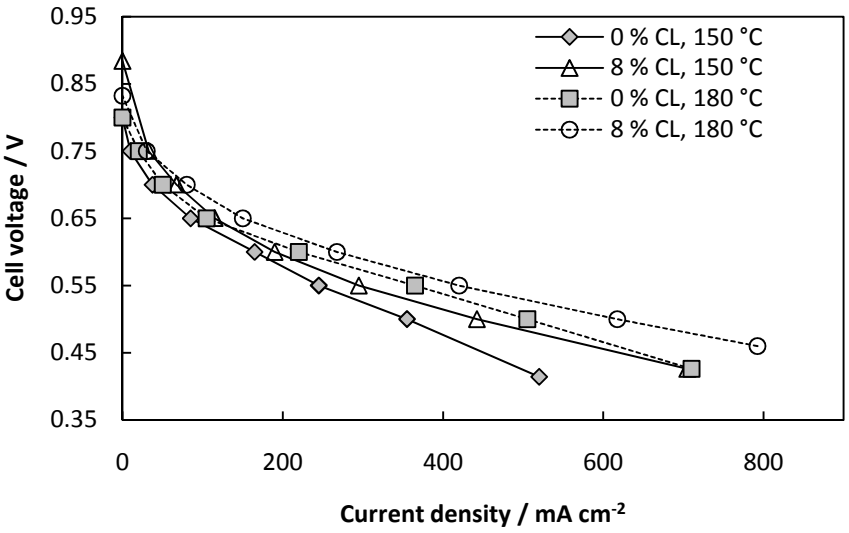

Figure 5.12 *Polarization curves of fuel cell MEAs based on linear and crosslinked PBI membranes operating with dry hydrogen and air at 150 °C and 180 °C.*

The fuel cell improvement was primarily achieved in the high current density region of the polarization curve. It should thus be connected to slightly lower overall ohmic resistance in cell based on the crosslinked PBI membrane. The slightly improved fuel cell performance of the MEA based on the post crosslinked PBI membrane is further illustrated in Figure 5.13 by higher power density in the high current density region.

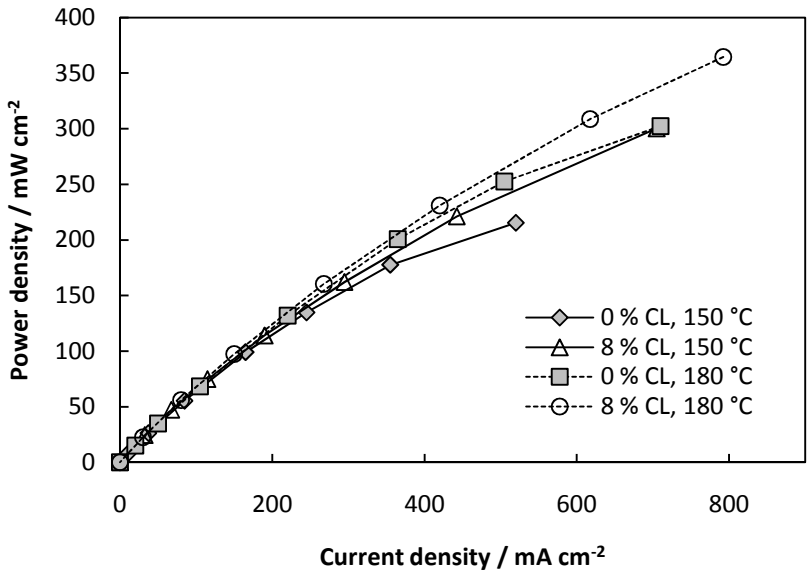

Figure 5.13 *Power density of fuel cells based on linear and crosslinked PBI membranes operating with dry hydrogen and air at various temperatures.*

The lower total ohmic resistance of the crosslinked PBI based fuel cell could eventually be explained by a slightly higher initial acid doping level of the membrane or better acid retention characteristics during the MEA preparation. Eventually, the higher hot-pressing temperature could give a better contact in the membrane electrode interface.

However, the better dimensional stability of the crosslinked PBI membrane should allow for even higher phosphoric acid doping levels without sacrificing the mechanical strength. It should thus allow for further reduced ohmic losses in the high current density range and thus higher efficiency. Additionally, the improved mechanical strength and the improved oxidative stability are expected to improve the long term durability of the fuel cell.

5.4 Summary

The PBI membrane post crosslinking chemistry with DVS was studied on a low molecular weight model system of benzimidazole and DVS, using methanol or aqueous potassium hydroxide as solvents. The stoichiometric reaction between benzimidazole and DVS in MeOH proceeded smoothly to give 1-[2-(2-(1*H*-benzimidazoyl)-ethanesulfonyl)-ethyl]-1*H*-benzoimidazole in 83% isolated yield after purification by flash column chromatography. On the other hand, if DVS was added in excess the mono-addition reaction was favored which indicated a risk for grafting of 2-methoxy-ethanesulfonyl groups on the PBI backbone rather than crosslinking.

The developed methodology for linking benzimidazole units with DVS was subsequently applied to crosslink PBI membranes in a post treatment procedure. PBI membranes were submerged in a MeOH solution containing DVS with DVS:PBI_{RU} molar ranging from 1 to 10. The effect of membrane thickness was also investigated which indicated that the crosslinking chemistry was limited by the diffusion of DVS into the bulk membrane. Hence, the apparent degree of crosslinking after DVS treatment was found to be dependent on the membrane thickness as well as the initial DVS:PBI_{RU} molar ratio. However, the apparent degree of crosslinking of the PBI membranes calculated from the weight gain after the DVS treatment corresponded well with the elemental analysis results with respect to the sulfur content.

The thermogravimetric curves of the crosslinked PBI membranes with high apparent degree of crosslinking showed an extra shoulder in the thermogram which was probably connected to the thermo-oxidative induced decomposition of the sulfone linkages or the graft 2-methoxy-ethanesulfonyl groups.

The oxidative stability of the membranes in the Fenton test was improved by crosslinking. The crosslinked membranes could tolerate higher weight losses before spontaneous membrane disintegration was observed. Additionally, the rate of weight loss decreased with increasing apparent degree of crosslinking.

Elevated doping temperatures were needed in order to reach sufficient acid doping levels of the crosslinked membranes for any practical use in PEM fuel cells. Under similar conditions and at the same acid doping level, the crosslinked membranes exhibited higher Young´s modulus and engineering tensile stress at break compared with their linear counterparts. Furthermore, the crosslinked membranes showed higher resistance to plastic deformation and reduced elongation at break after phosphoric acid doping.

At a phosphoric acid doping level of 10, the proton conductivity of the crosslinked membrane and its linear counterpart was similar. The proton conductivity reached above 0.1 S cm^{-1} under fully humid conditions. Conductivity measurements of the KOH doped crosslinked membranes at 110 °C showed a gradual decrease of the hydroxide conductivity due to membrane dehydration over time.

Fuel cell tests based on the phosphoric acid doped crosslinked membranes demonstrated the feasibility of the membranes as electrolyte materials. The OCV of the MEA based on the crosslinked PBI membrane was slightly higher than that of the MEA which was based on its linear counterpart, eventually indicating slightly lower gas permeability.

However, further efforts are needed with respect to electrode and MEA preparation procedures in order to improve the cell performance.

6 Thermal curing of PBI membranes for high temperature PEM fuel cells

The following chapter is devoted to the effect of thermal treatment of PBI membranes. The effect of thermal treatment and its correlation to the physiochemical membrane properties before and after phosphoric acid doping is discussed. The major parts of the data and discussion are also available in paper III which is available in the form of a manuscript in the appendix.

The fuel cell tests were conducted by Dr. Lars N. Cleemann at Technical University of Denmark, Kgs. Lyngby.

6.1 Background

Poly[2,2´(*m*-phenylene)-5,5´bibenzimidazole] (PBI or *m*-PBI, Figure 1.8 or Figure 6.1) has received most attention within the polybenzimidazole family of polymers, mainly due to its generally better processability characteristics relative to many of its structure analogues.

In addition to the excellent thermal and chemical stability of PBI, the polymer is characterized by its mechanical toughness. For example, among all known engineering plastics it has the highest reported compression strength [76]. As also discussed in the previous chapters, the mechanical properties of PBI membranes strongly depend on the doping level and the linear molecular weight of the polymer [183]. Although a high linear average molecular weight of PBI is desirable from a mechanical strength point of view, it dramatically limits the polymer processability possibilities. For example, as the linear molecular weight of the polymer increases, the solubility of the high molecular weight fraction is considerably reduced and the intrinsic viscosity [η] of the obtained polymer solution is dramatically increased. For this reason, the commercially available PBI (Celazole®, Celanese) has a low to medium linear molecular weight ranging from about 23-37 kDa corresponding to an intrinsic viscosity [η] of 0.55–0.80 dL g^{-1} [237]. Unfortunately, PBI in the lower region of this molecular weight range gives rather poor membranes in terms of mechanical stability and chemical resistance. Therefore, fractionation seems necessary before membrane casting in order to concentrate the high molecular weight fraction of the polymer batch [238].

In order to improve the processability of polybenzimidazoles, a pre-polymer approach was developed as reviewed by Neuse [74] and Levine [178]. The idea was to prepare a low molecular weight pre-polymer which could easily be processed by the available standard techniques. The pre-polymers exhibited fairly good solubility and contained open chain segments which were capable of ring closure and aromatization after subsequent heat treatment in the solvent-free state.

Covalent crosslinking is another approach which dramatically increases the molecular weight of the polymer, as also discussed in Chapter 5. Since a crosslinked polymeric material generally suffers from severe processability difficulties due to its tremendously high molecular weight, the crosslinking reactions have to be initiated after the processing. For example, different heat treatment procedures can be used to initiate the PBI crosslinking after membrane casting from a solution containing various types of crosslinking agents [100, 172, 221].

In addition to the molecular weight of the polymer, another factor which dramatically affects the macroscopic properties of polymer based materials in general is the degree of crystallinity. Materials of crystalline polymers are most often stiffer, tougher and less soluble than their amorphous or semi-crystalline counterparts [103]. For example, a certain degree of crystallinity is required for the PFSA

based electrolyte materials in order to obtain mechanically stable and water-insoluble membranes [59], which is also highlighted in Chapter 3.4.2.1.

PBI, on the other hand, is known to be more or less amorphous. Generally, the *meta* configuration of PBI effectively prevents crystallization of the polymer due to the wrinkled linear structure which results in poor polymer chain packing, as shown in Figure 6.1 [239]. This might also be the sole reason for the relatively good solubility of *m*-PBI in a limited number of highly polar aprotic organic solvents [73]. In contrast, the *para* analogue of PBI normally exhibits a considerably higher degree of crystallinity [240]. Consequently, it is less soluble which dramatically limits the polymer processability possibilities and thus its usability.

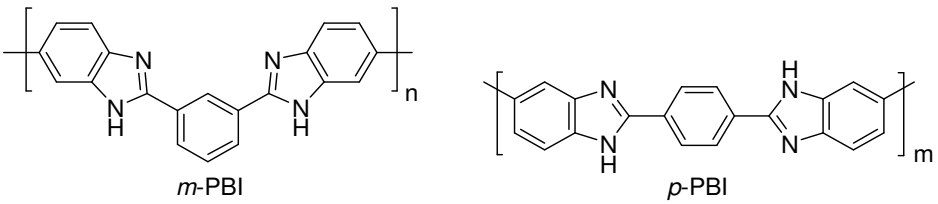

Figure 6.1 *Linear structure of m-PBI and p-PBI.*

Since the degree of crystallinity of different polybenzimidazoles highly depends on the polymer chain packing capability, it can thus be modified by tailoring the structure of the polymer backbone. For example, Scariah *et al.* [241] synthesized of set of *para* polybenzimidazole structure analogues containing flexibilizing spacers on the polymer backbone. The linear structure of the polymer dramatically affected the degree of crystallinity as well as its solubility. Furthermore, Aharaoni [242] indroduced alkyl spacers between the benzimidazole moieties in polybenzimidazole. After impregnation with phosphoric acid, it was found that crystalline polymeric salts were developed only when an even number of $–CH_2–$ spacing groups separated the benzimidazole moieties. Phosphoric acid doping of the polymers with an odd number of spacing $–CH_2–$ groups between the benzimidazole moieties resulted in completely amorphous polymeric salts. Employing a heat treatment procedure at temperatures up to 350 °C in combination with different aromatic reagents under pressure, Conciatori *et al.* [243] patented a process for increasing the crystallinity of various polybenzimidazole fibers. The degree of crystallinity of *m*-PBI and *p*-PBI can also be modified by careful tuning of the reaction parameters during the polycondensation as discussed by Kohama *et al.* [239].

The membrane casting procedure and the nature of the solvent are also known to affect the morphology of the obtained phosphoric acid doped membrane. For example, PBI membranes which are cast from mixtures of trifluoroacetic acid (TFA) and phosphoric acid are considerably more crystalline compared with the PBI membranes which are cast from DMAc followed by acid imbibing [244]. Furthermore, ABPBI membranes prepared by direct casting from methanesulfonic acid (MSA) and phosphoric acid are considerably more crystalline than the ABPBI membranes prepared by casting from MSA followed by phosphoric acid imbibing [245]. The relatively high degree of crystallinity of the TFA cast membranes was reported to result in a phosphoric acid doped membrane which was more rubbery and soft than the conventionally solution cast and acid imbibed membranes. The degree of crystallinity could be further increased by heat treatment. The membrane of higher degree of crystallinity also exhibited higher proton conductivity. It was suggested that the phosphoric acid was forced into the amorphous regions to give highly proton conducting pathways trough the membrane cross-section [78].

Heat treatment can often increase the degree of crystallinity of polymeric materials in general. For example, PFSA membranes generally require annealing in order to develop the crystalline regions which make them mechanically stable and insoluble in water [59]. Vogel and Marvel [73] observed that PBI becomes insoluble in all standard solvents after heat treatment at 500 °C. However, the

complete insolubility was not assigned to increased crystallinity of the polymer. It was suggested that crosslinking had occurred through free radical reactions which tremendously increased the molecular weight of the polymer. Gillham [246] further investigated the thermo-mechanical properties of PBI and confirmed that PBI changes from a thermoplastic polymer to a thermoset resin at about 450 °C. Based on spectroscopic evidence, the complete insolubility of the PBI after the heat treatment was assigned to crosslinking [240], as also discussed by Levine [178]. This was further illustrated on a macroscopic scale by Hwang *et al.* [247] who showed that heat treatment of spun ABPBI fibers at temperatures up to 540 °C increased the Young´s modulus by 153% and the engineering tensile strength by 63%. At the same time the elongation at break was considerably decreased, indicating considerable toughening of the material.

Based on extensive FTIR characterization the early stages of the PBI thermo-oxidative degradation was analyzed by Musto *et al.* [180], who also observed that the PBI membranes which had been heat treated under air atmosphere at even lower temperatures (350 °C) for 30 minutes were practically insoluble in DMAc. Shulman and Lochte [248] proposed a mechanism for the thermal oxidation of PBI at temperatures above 450 °C. It involved chain scission accompanied by crosslinking reactions, either by amide interchange or by benzene-biphenyl type coupling. The weakest link of the PBI backbone in a thermo-oxidative environment was obviously the nitrogen containing heterocyclic and the adjacent benzenoid rings [249, 250]. Later, Linkous [113] evaluated thermo-oxidatively crosslinked PBI as a potential electrolyte material for PEM steam electrolyzers operating at temperatures in the 200-400 °C temperature range. Unfortunately, the membranes based on the thermo-oxidatively crosslinked PBI as well as the pristine polymer were found to be susceptible to hydrolysis or further severe oxidation reactions at 300 °C under O_2/H_2O atmosphere.

In the present work, a heat treatment technique was investigated in order to modify the physiochemical characteristics of PBI membranes for high temperature PEM fuel cells. For this purpose, other effects than the change from a thermoplastic polymer to a thermoset have been considered including thermal degradation, oxidative chain scission and crystallization. Fuel cell tests were further conducted in order to demonstrate the feasibility and improved durability of the cured membranes.

6.2 Experimental

6.2.1 Membrane preparation

PBI with an average molecular weight ranging from about 23-64 kDa was supplied by Danish Power System ApS. The PBI was supplied either as powders or as membranes which were solution cast from DMAc through solvent evaporation. The PBI powders were dissolved in DMAc to give 5 wt.% solutions after filtering. PBI membranes were subsequently solution cast from the DMAc solution on glass substrates. All membranes were boiled in demineralized water for several hours and dried at temperatures up to 200 °C.

The heat treatments were conducted in a quarts glass lined tube furnace at temperatures ranging from 200-500 °C under air or argon atmosphere. For the membranes which were heat treated under argon atmosphere, the furnace was repeatedly evacuated and filled with argon at room temperature before the heat treatment procedure was started. During the heat treatment, argon was continuously purged through the furnace at a flow rate of about 100-200 mL min^{-1}.

Since the eventual chemical or physical effects on the membrane were assumed to be dependent on the thermal curing duration, two different standard curing procedures were established for the systematic membrane characterization. During the short thermal curing procedure, the sample was heated up to 350 °C over about 10 minutes under a continuous argon purge. When the furnace interior reached the target temperature, the membrane sample was treated isothermally for about 1 minute

before the power was switched off and the furnace was allowed to cool down to room temperature which took about 1.5-2 h. During the long thermal curing procedure, the sample was treated isothermally at 350 °C for 16 h under a continuous argon purge. The membranes obtained after the short and long curing procedures are hereafter referred to xx-Sh-C and xx-Lo-C, respectively, where xx corresponds to the initial linear average molecular of PBI in kDa. The non-cured reference membranes are hereafter referred to as xx-Ref, where xx corresponds to the linear average molecular weight of PBI in kDa.

Doping was achieved by submerging the membranes in 85% H_3PO_4 at temperatures ranging from room temperature to 100 °C. The acid doping levels were calculated on the dry polymer basis and the dry weights after phosphoric acid doping (dried at 150 °C until constant weight).

6.2.2 Characterization

Attenuated Total Reflectance Fourier Transform Infrared Spectroscopy (ATR-FTIR) was conducted using a Perkin Elmer Spectrum One FTIR spectrometer equipped with a universal ATR sampling accessory. The membrane samples were pre-dried at 200 °C before the spectra were recorded.

The TGA/DTA data were acquired using a Netzsch STA 409 PC. The samples were pre-dried at 250 °C *in vacuo* for 12 h in the chamber and thereafter cooled down to room temperature. The thermograms were recorded at a heating rate of 10 °C min^{-1} and argon was used as the purge gas.

The membrane samples (40 µm thick) were submerged in a 3% H_2O_2 (Merck) aqueous solution containing 4 ppm Fe(II) (added as $(NH_4)_2Fe(SO_4)_2 \cdot 6H_2O$) at 68 °C. After certain durations (maximum 20 h), the membrane samples were collected, rinsed with demineralized water and dried at 120 °C for at least 5 h. The dry weight was recorded and the membrane samples were submerged in freshly prepared Fenton solution for continuation of the test.

Wide angle X-ray diffraction (WAXD) data were recorded on a Huber D670 diffractometer equipped with a Cu-K α X-ray source.

Stress-strain curves were recorded at room temperature under ambient atmosphere.

In-plane proton conductivity was measured at temperatures ranging from 110-180 °C under anhydrous conditions. The membrane samples were conditioned at 180 °C for about 16 h before the first measurement. The temperature was then systematically lowered and the conductivity was recorded at intervals of 10 °C. The symmetric square wave current was supplied in a frequency range from 5-10 kHz.

6.2.3 MEA preparation and fuel cell testing

A platinum catalyst (56.2 wt.% Pt) supported on carbon black was used to prepare catalyst layers by spraying the catalyst dispersion onto carbon based non-woven gas diffusion layers, which were pre-coated with a micro-porous layer. PBI was used as the catalyst binder (0.1 mg cm^{-2}) which after the acid impregnation functioned as proton conducting phase in the electrode. The Pt loading of the final electrodes was 0.58 mg cm^{-2} at the cathode and 0.29 mg cm^{-2} at the anode.

The acid doped PBI membranes were sandwiched between two pieces of gas diffusion electrodes and hot-pressed at 200 °C under a pressure of about 4 MPa for 3 min.

The size of the active electrode area of the MEAs was 10 cm^2. The MEAs were tested in a single cell consisting of two graphite plates with simple parallel gas channels. Two aluminum end plates with attached heaters were used to clamp the graphite plates and a separate silver coated current collector was used to collect the current from the cell.

For fuel cell tests, dry hydrogen and air were used without pre-humidification at flow rates of 110 and 450 ml min^{-1}, respectively. Even at the maximum current densities, the gas flow rates were much higher than the consumption. In this way the fuel cell tests were performed in order to evaluate the materials but not to optimize the cell operation.

6.3 Results and discussion

6.3.1 ATR-FTIR

By definition, the thermo-oxidative stability of a material is connected to oxidation which is induced by heat. It can thus be evaluated by heat treating the material under an oxygen containing atmosphere, for example air. Thermal stability, on the other hand, is the heat resistance of a material in the absence of any oxidation agent. Thermal and thermo-oxidative stability are thus two completely different concepts which also might involve completely different degradation mechanisms.

After heat treatment of the PBI membrane under an oxygen containing atmosphere at temperatures above 300 °C for 16 h, the appearance of the FTIR spectrum was dramatically changed. As shown in Figure 6.2, the most pronounced difference was observed in the 1000-1800 cm^{-1} region of the spectrum which is mainly assigned to different vibration and breathing modes of the aromatic polymer backbone.

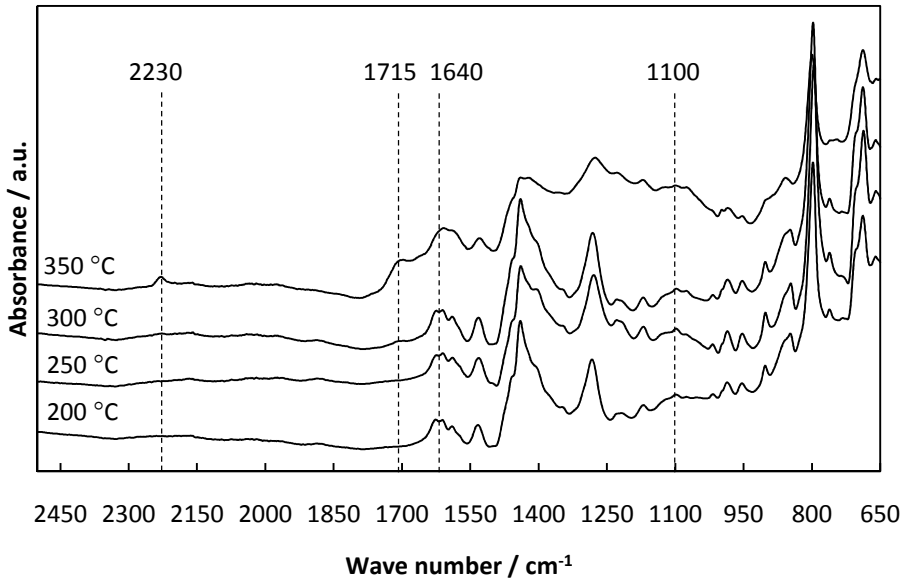

Figure 6.2 *ATR-FTIR spectra of membranes treated at temperatures ranging from 200-350 °C for 16 h under air atmosphere. The 2500-4000 cm^{-1} regions of the spectra are omitted for clarification.*

For example, the intense absorption bands which are centered around 1540 cm^{-1} and 1640 cm^{-1} in the FTIR spectrum of PBI have been assigned to stretching modes of C=C and C=N bonds in the aromatic backbone, respectively [109]. As previously reported [180], two new absorption bands at about 2230 cm^{-1} and 1715 cm^{-1} were observed in the FTIR spectrum of the PBI membrane which had been heat treated under air at 350 °C. The 2230 cm^{-1} absorption band was assigned to stretching vibrations of aromatic nitrile groups originating from the imidazole moieties whereas the absorption band at 1715 cm^{-1} was assigned to various carbonyl containing functionalities which were formed due to the extensive thermal oxidation of the polymer. Furthermore, in radical induced oxidation of PBI

membranes (Fenton test) a considerable intensity strengthening of the absorbance peak at around 1640 cm^{-1} was observed, indicating the formation of carbonyl functionalities [109]. A new wide absorption band which was assigned to various hydroxyl functionalities was also observed at around 1100 cm^{-1} after the Fenton test.

This data correlate well with the changed appearance of the FTIR spectrum of PBI after the heat treatment at 350 °C under air in the present study. Conclusively, the general broadening of the absorbance peaks in the 1000-1800 cm^{-1} region of the spectrum indicates severe thermal oxidation of the polymer backbone. The extensive thermal oxidation should ultimately result in polymer chain scission and thus a dramatic decrease of the linear molecular weight, as also previously reported for thermally oxidized PBI [180] or PBI membranes which had been subjected to radical induced oxidation in the Fenton test [109, 110].

On the other hand, according to the FTIR spectra of the PBI membranes which had been heat treated under an inert argon atmosphere showed considerable better stability at higher temperatures in general as shown in Figure 6.3.

When the samples were kept under a continuous argon flow, the PBI membranes could be treated at temperatures up to 400 °C for at least 16 h without affecting the visual appearances of the FTIR spectra. Up to this temperature no visual deviations which could be ascribed to any morphological changes or thermally induced decomposition or oxidation of the polymer matrix could be observed, for example carbonyl containing functionalities which should appear at around 1715 cm^{-1} in the FTIR spectrum.

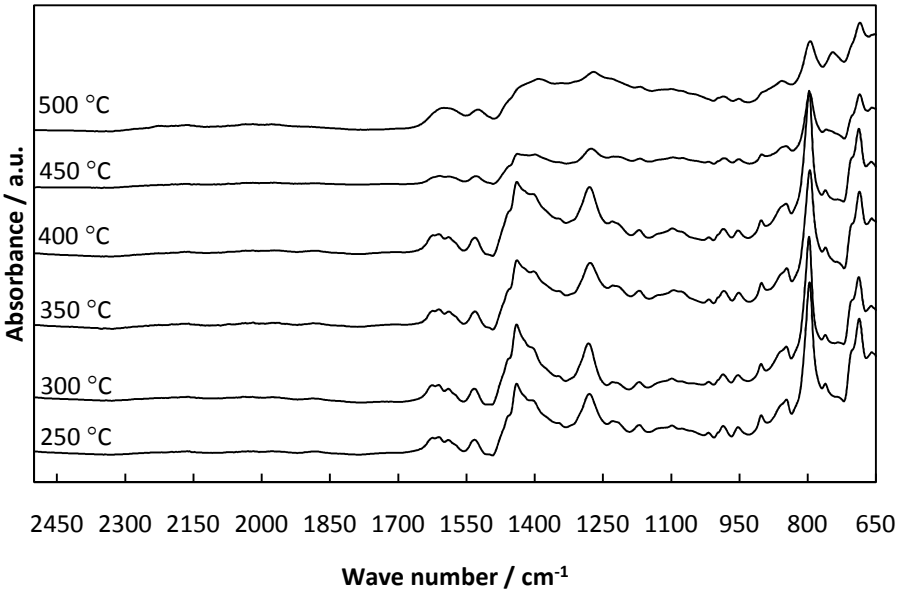

Figure 6.3 *ATR-FTIR spectra of membranes treated at temperatures ranging from 250-500 °C for 16 h under argon atmosphere. The 2500-4000 cm^{-1} regions of the spectra are omitted for clarification.*

However, the aim of the present study was not to investigate the thermal oxidation of PBI. The aim was to systematically investigate how the heat treatment affects the physiochemical characteristics of the membrane if thermal oxidation the polymer can be avoided. Therefore, a standard heat treatment temperature of 350 °C under argon, i.e. well below the thermal decomposition temperature of PBI, was defined.

6.3.2 Membrane preparation

The solubility of a polymer is generally highly dependent on the degree of crystallinity as well as on its linear molecular weight [103]. Hence, processes which dramatically increase the degree of crystallinity or the molecular weight of the PBI, such as crosslinking or linear growth, should considerably decrease the solubility of the polymer.

After heat treatment under argon at 350 °C the membranes were obviously almost completely insoluble in DMAc at 80 °C as shown in Figure 6.4 (64-Sh-C and 64-Lo-C). On the other hand, the non-cured reference membrane (64-Ref) readily dissolved completely in less than 20 minutes.

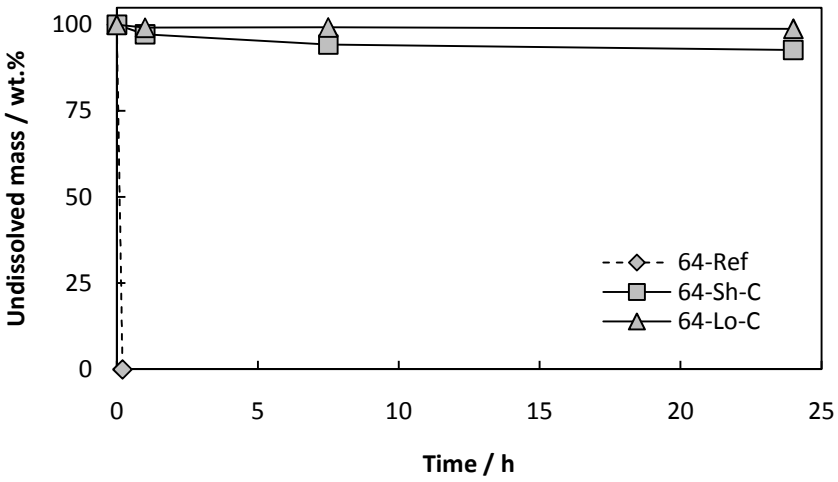

Figure 6.4 *Membrane solubility in DMAc at 80 °C.*

Previous studies on heat treated PBI at temperatures ranging from 350-500 °C have shown that the heat treatment results in an almost completely insoluble material [73, 180]. Based on thermo-mechanical measurements [246] and spectroscopic evidence [178, 240] the dramatically reduced solubility of PBI after heat treatment was assigned to a dramatic increase of the molecular weight through crosslinking. Based on the thermo-mechanical measurements, Gillham [246] demonstrated that PBI irreversibly cured during heat treatment at 450 °C which implies that it changed from a thermoplastic polymer to a thermoset. Furthermore, subsequent heat treatment of the processed PBI was also the key to increase the molecular weight of the polymer in the pre-polymer approach in order to improve its mechanical characteristics [74]. Complete insolubility is one of the fundamental characteristics of a thermoset due to its extremely high molecular weight.

6.3.3 Thermal analysis

Thermal analysis can be used to determine crosslinking temperatures of polymers since the crosslinking reactions are generally to some extent exothermic. For example, Han *et al.* [221] used DSC to determine the crosslinking temperature of PBI and an epoxy resin. It was identified by a small exotherm at about 160 °C.

Thermogravimetric analysis (TGA) and differential thermal analysis (DTA) data of the non-cured reference membrane 48-Ref and of the membrane which had been pre-cured at 350 °C for 16 h under argon (48-Lo-C) are shown in Figure 6.5. Both samples were pre dried *in vacuo* at 250 °C in the chamber in order to evaporate all solvent residuals the and absorbed moisture and other volatile impurities.

The non-cured reference membrane (48-Ref) showed a weight loss with an onset temperature at about 350 °C. This temperature was also used as the standard curing temperature of the PBI membranes in the present study and is highlighted in Figure 6.5 by a dashed line. The total weight loss of the non-cured reference membrane 48-Ref in the 350-450 °C temperature range was about 0.7%. On the other hand, this weight loss was not observed in the thermogram of the membrane which had been pre-cured at 350 °C (48-Lo-C) prior to the experiment. The onset of weight loss of the cured membrane 48-Lo-C did not start until the temperature reached about 430 °C. The small weight loss at 350 °C of the non-cured reference membrane 48-Ref could thus be associated with crosslinking reactions giving off volatile species as PBI changes from a thermoplastic polymer to a thermoset.

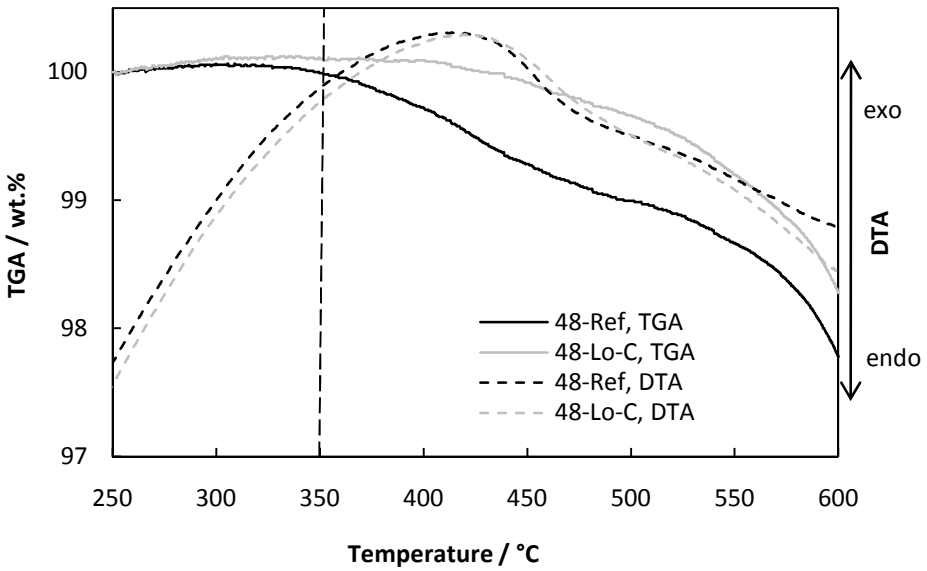

Figure 6.5 *TGA and DTA of the non-cured reference membrane (48-Ref) and of the membrane which had been cured a 350 °C for 16 h under argon prior to the experiment (48-Lo-C). The standard curing temperature is highlighted by a dashed line at 350 °C. Argon was used as purge gas and the heating rate was 10 °C min^{-1}.*

An exotherm was also observed in this temperature range which further indicates that chemical reactions, such as crosslinking, were taking place. However, although no obvious weight loss was recorded in this temperature range, the exotherm was also observed in the DTA of the membrane which had been cured at 350 °C for 16 h (48-Lo-C) before the experiment. The exotherm in the DTA of the 48-Lo-C membrane could indicate that further crosslinking reactions were taking place when the membrane was re-heated to 350 °C. However, the continuation of the thermal curing process obviously did not result in any volatile species since no obvious weight loss was recorded.

6.3.4 Fenton test

As also discussed in Chapter 3.3.7 and 5.3.3 the membrane degradation by radical induced oxidation has been identified as one of the major long term durability limitations of the conventional PFSA based PEM fuel cells [111] as well as of the phosphoric acid doped PBI [232] based high temperature PEM fuel cells. However, as also confirmed in Chapter 5.3.3 the radical-oxidative resistance of PBI can be considerably improved by covalent crosslinking [100, 172, 221] which should also improve the long term durability of the PBI based PEM fuel cells.

The relative chemical stability of the non-cured reference membrane (48-Ref) and of the membrane which had been cured at 350 °C for 16 h under argon (48-Lo-C) was evaluated in a Fenton test as summarized in Figure 6.6.

The average rate of weight loss of the non-cured reference membrane (48-Ref) during the first 77 h of the test was about 0.13 wt.% h^{-1}. The corresponding result of the membrane which had been cured at 350 °C for 16 h under argon (48-Lo-C) was about 0.05 wt.% h^{-1}. The rates of weight loss of the non-cured reference membrane (48-Ref) and of the cured membrane (48-Lo-C) were in good agreement with the rates of weight loss of the linear PBI membrane and the membrane with an apparent degree of crosslinking of 48% in Chapter 5.3.3, respectively.

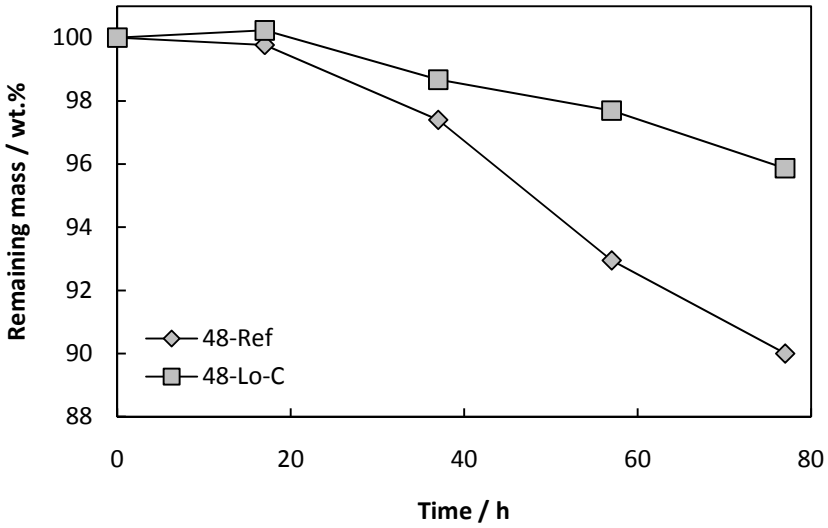

Figure 6.6 *Remaining membrane mass during the Fenton test of the non-cured reference membrane 48-Ref and of the membrane which had been cured at 350 °C for 16 h under argon (48-Lo-C).*

After about 80 h of effective Fenton test time the non-cured reference membrane 48-Ref started to spontaneously disintegrate after a weight loss of about 10%. In contrast, the membrane which had been cured at 350 °C for 16 h under argon (48-Lo-C) was still in one mechanically stable piece after 80 h which demonstrates the improved radical-oxidative resistance of the cured membrane. This is further illustrated in photographs of the membrane samples after the Fenton test, as shown in Appendix 1b.

6.3.5 Phosphoric acid doping

Phosphoric acid doping was achieved by submerging the membranes with different thermal history in 85% H_3PO_4 at temperatures ranging from 20-100 °C, as summarized in Table 6.1.

Table 6.1 *Phosphoric acid doping of the non-cured reference membrane (64-Ref) and of the membranes which had been cured at 350 °C under argon for 1 minute (64-Sh-C) and 16 h (64-Lo-C).*

Doping conditions	**Acid doping level**		
	64-Ref	**64-Sh-C**	**64-Lo-C**
Room temperature., 85% PA	10.2	1.2	0.1
70 °C, 85% PA	-	11.8	13.5
100 °C, 85% PA	Membrane dissolved	13.6	14.1

At room temperature a doping level of about 10 was obtained during doping of the non-cured reference membrane (64-Ref). It also corresponds well with the previously reported literature data for membranes based on linear PBI [171]. On the other hand, the phosphoric acid uptake at room temperature of the cured membranes 64-Sh-C and 64-Lo-C was very low and corresponded to acid doping levels of 1.2 and 0.1, respectively. It further indicates that the cured membranes exhibited strong resistance to swelling, which is also a fundamental characteristic of a covalently crosslinked structure.

In order to reach sufficient acid doping levels and thus sufficient proton conductivity for any practical use as electrolyte material in PEM systems, it is well known that covalently [100, 172] or ionically [101, 155] crosslinked PBI based membranes have to be doped at elevated temperatures, as also discussed in Chapter 3.3.5.1 and 5.3.3. Analogously, higher phosphoric acid doping levels were reached in the present study by elevating the doping temperature of the membranes which had been cured at 350 °C under argon.

During doping at 70 °C, phosphoric acid doping levels of 11.8 and 13.5 were obtained of the membranes which had been cured at 350 °C under argon for 1 min (64-Sh-C) and 16 h (64-Lo-C), respectively. After doping at this temperature the non-cured reference membrane 64-Ref was in swollen gel-like state which was highly mechanically unstable and could not be handled without breaking. By further doping at 100 °C the non-cured reference membrane 64-Ref was completely dissolved. On the other hand, after doping at 100 °C in 85% H_3PO_4 for 16 h, the membranes which had been cured at 350 °C under argon obtained phosphoric acid doping levels of around 14 and could easily be handled without breaking.

No visual color change was observed in the concentrated H_3PO_4 doping solution during doping at 100 °C of the membranes which had been cured at 350 °C under argon prior to the doping. This further illustrates the dramatically reduced solubility of the cured membranes and further confirms that PBI changed from a thermoplastic polymer to a thermoset during the heat treatment procedures.

The heavily doped membranes based on the cured PBI exhibited good flexibility and sufficient mechanical strength for the MEA preparation. After being submerged in 85% H_3PO_4 for one month at room temperature the acid doping levels of the cured membranes 64-Sh-C and 64-Lo-C slightly degreased to 12.1 and 13.9, respectively. It indicates a small gradual acid loss over time from the membranes to the phosphoric acid bulk solution when the temperature was decreased. This was probably a direct consequence of the cured membrane´s high resistance to swelling which resulted in a small contraction of the membranes when the temperature was lowered which physically pushed the phosphoric acid out from the polymer matrix. On the other hand, the acid doping level should still be high enough to provide sufficient proton conductivity to the membrane.

6.3.6 X-ray diffraction

6.3.6.1 Cured membranes

Different heat treatment procedures have previously been reported to induce crystallization of a wide range of structure analogues within the polybenzimidazole family of polymers [243, 247, 251]. For example, Arrieta *et al.* [251] heat treated PBI, Kevlar® and their blends at temperatures up to 320 °C for 1-15 days and found that the crystallinity of the polymer blend gradually increased during the heat treatment. The development of crystalline regions was also demonstrated to dramatically influence the physiochemical properties of the materials on a macroscopic scale.

ABPBI, which is the most simple structure analogue within the polybenzimidazole family, is known to exhibit a rather high degree of crystallinity. The degree of crystallinity can be further increased by heat treatment or by stretching the material in order to enhance the polymer chain orientation [252].

Krause and Haddock [253] determined the three dimensional crystallite size of heat treated ABPBI to be maximum 3 nm^3.

X-ray diffraction measurements were conducted in order to investigate how the heat treatment at temperatures up to 350 °C under argon affected the morphology of the PBI membranes in the present study. The X-ray diffractograms of the cured PBI membranes (64-Sh-C and 64-Lo-C) are compared with the X-ray diffractogram of the non-cured reference membrane 64-Ref in Figure 6.7.

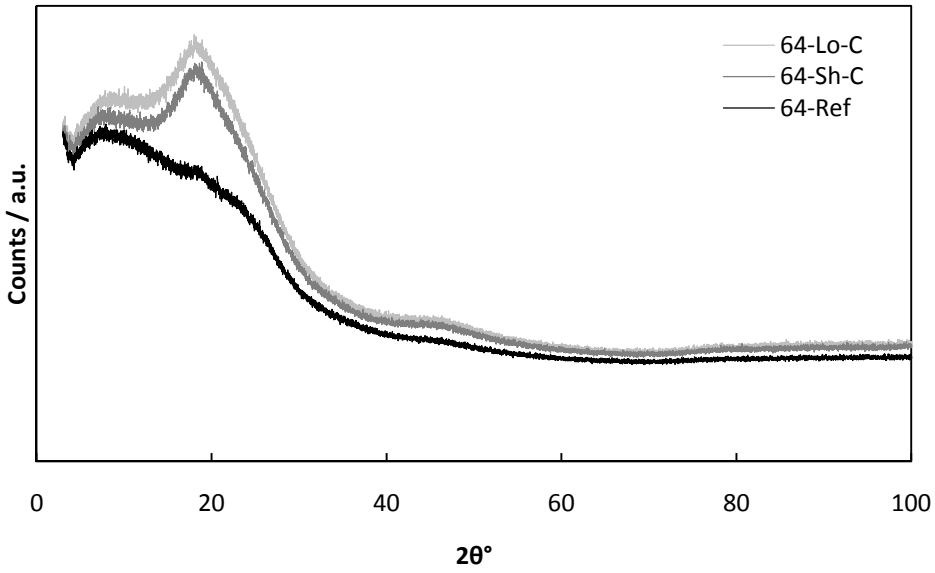

Figure 6.7 *X-ray diffractograms of the non-cured reference membrane 64-Ref and of the membranes which had been cured at 350 °C under argon for 1 min (64-Sh-C) and 16 h (64-Lo-C).*

As previously reported [73, 178], the non-cured reference PBI membrane (64-Ref) was found to be fully amorphous. However, after thermal curing at 350 °C under argon for 1 min (64-Sh-C) or 16 h (64-Lo-C) a broad reflection which was centered around 18° 2θ appeared in the diffractogram which indicated the development of regions in the polymer membranes with structural order. A similar broad reflection in the X-ray diffractogram was also reported for PBI precipitates which had been treated at temperatures up to 350 °C [239].

Cho *et al.* [254] recently showed that ABPBI membranes cast from EtOH/NaOH exhibit a crystalline uniplanar structure in which the aromatic rings are aligned parallel to the film surface. However, during doping in phosphoric acid most of the crystalline order in the membrane was lost due to the extensive volume swelling and the concomitant polymer chain separation. This was also confirmed in the present study. After acid doping the all membranes were apparently morphologically equal regardless of their thermal history, as shown in Figure 6.8.

The acid doping levels of the membranes varied between 10.2-14.1 depending on their thermal history and on the phosphoric acid doping conditions. The diffraction data of all the acid doped membranes showed a broad reflection centered around 23° 2θ which corresponded well with previously reported X-ray diffraction data of phosphoric acid doped PBI membranes with a phosphoric acid doping level of 4.8 [78].

For comparison, a PBI structure analogue with flexibilizing alkyl groups incorporated in the polymer backbone showed strong and relatively sharp reflections centered around 19.6° 2θ and 24.6° 2θ [242]. The phosphoric acid doping level of the polymer was equal to 2, meaning that all acid was bound to the polymer trough coulombic forces to form polymeric salt. The formation of the polymeric phosphate

salt subsequently resulted in increased crystallinity. Similarly, a maximum in the tensile modulus of PBI membranes was observed at an acid doping level equal to 2 which was explained by increased degree of crystallinity due to the polymeric phosphate salt formation [78].

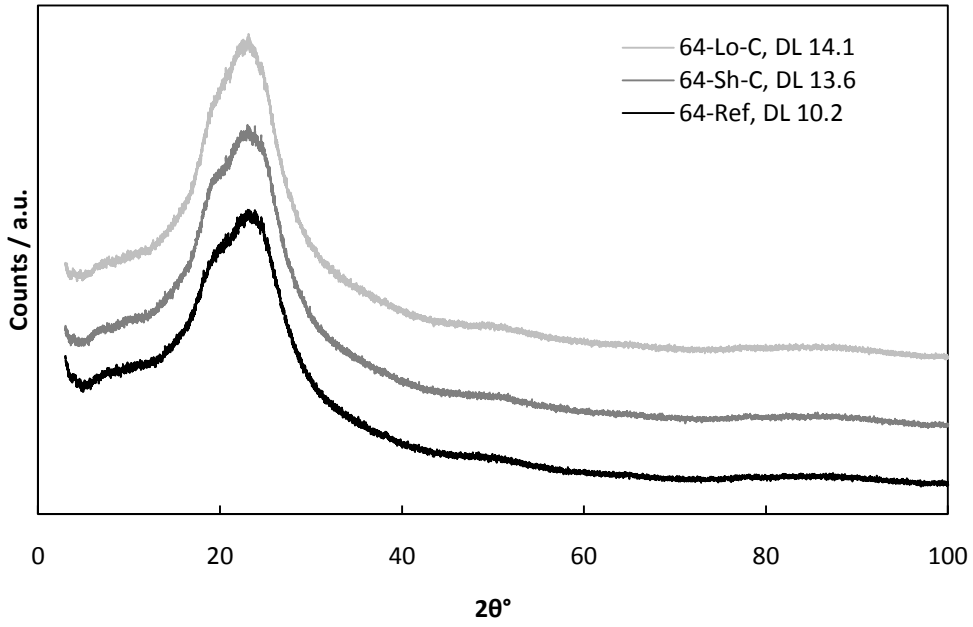

Figure 6.8 *X-ray diffractograms of the phosphoric acid doped non-cured reference membrane 64-Ref and of the phosphoric acid doped membranes which had been cured at 350 °C under argon for 1 min (64-Sh-C) and 16 h (64-Lo-C). The corresponding phosphoric acid doping levels (DL) of the membranes are indicated in the figure.*

The higher temperatures required in order to reach sufficient acid doping levels of the cured membranes could eventually partly be explained by their higher degree of crystallinity compared with their non-cured counterparts. Phosphoric acid uptake requires that the polymer chains are free to separate in order to allow for extensive volume swelling of the polymer matrix. Hence, the activation energy of phosphoric acid absorption in an ordered crystalline or semicrystalline structure which is characterized by strong intermolecular hydrogen bonding should be higher than that of a completely amorphous polymer structure.

6.3.6.2 Thermal aging of phosphoric acid doped non-cured PBI

During high temperature PEM fuel cell operating conditions the membrane is naturally subjected to temperatures in the 100-200 °C range for extended periods of time. Since high temperatures are known to induce partial crystallization of PBI, it is thus of interest to study the effect of high temperature on the morphology of phosphoric acid doped PBI membranes. X-ray diffractograms were therefore recorded of the phosphoric acid doped non-cured reference membrane (64-Ref) after anhydrous aging at 150 °C for up to about 6 weeks, as shown in Figure 6.9.

The X-ray diffractograms of the thermally aged membrane revealed a gradual development of two relatively sharp reflections at 18.5° 2θ and at 23.5° 2θ, which confirms that the thermal aging increases the structural order within the membrane.

On the other hand, water is formed within the MEA during fuel cell operation which most likely also will affect the membrane crystallization. In that case, the gradual crystallization of the membrane

should be dependent on the operating current density since it is a direct measure of the water formation rate.

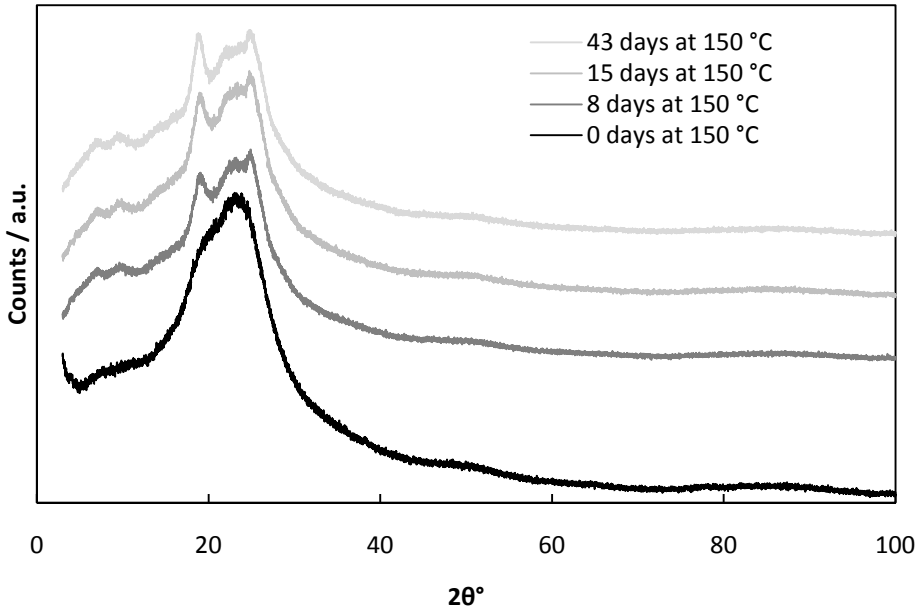

Figure 6.9 *X-ray diffractograms of the phosphoric acid doped non-cured reference membrane (64-Ref) with an acid doping level of 10.2 after anhydrous thermal aging at 150 °C for up to 43 days.*

6.3.7 Mechanical strength

6.3.7.1 The effect of the linear molecular weight

In order to study the correlation between the thermal history of PBI and the mechanical properties of the membranes after phosphoric acid doping, stress-strain curves were recorded at room temperature as shown in Figure 6.10. Since the mechanical properties of phosphoric acid doped PBI are known to be highly dependent on the linear average molecular weight of the polymer [183], the linear average molecular weight of PBI was varied from 23-44 kDa. The mechanical data are also summarized in Table 6.2. The doping levels were considerably higher than 2, meaning that the plasticizing effect of phosphoric acid highly influenced the appearance of the stress-strain curves [78, 244].

The phosphoric acid doped membranes based on PBI with a linear average molecular weight of 23 kDa which had been cured at 350 °C under argon for different durations (23-Sh-C and 23-Lo-C) were obviously tougher compared with their non-cured counterpart (23-Ref). For example, even though the acid doping level of the membrane which had been cured at 350 °C for 16 h (23-Lo-C) before acid doping was about 20% higher compared with that of its non-cured counterpart (23-Ref) the yield stress was almost twice as high. Furthermore, the elongation at break gradually decreased with increasing curing time from about 140% for the non-cured reference membrane 23-Ref to about 80% for the membrane which had been cured for 16 h (23-Lo-C), indicating reduced polymer chain mobility relative to each other. Additionally, the resistance to plastic deformation of the membranes which had been cured membrane 23-Lo-C was considerably higher than that of its non-cured counterpart (23-Ref) as indicated by a steeper slope of the stress-strain curve beyond the yield point. Despite the higher acid doping level, the cured membrane 23-Lo-C displayed nearly 3 times higher Young´s modulus compared with its phosphoric acid non-cured counterpart (23-Ref) as also shown in Figure 6.11.

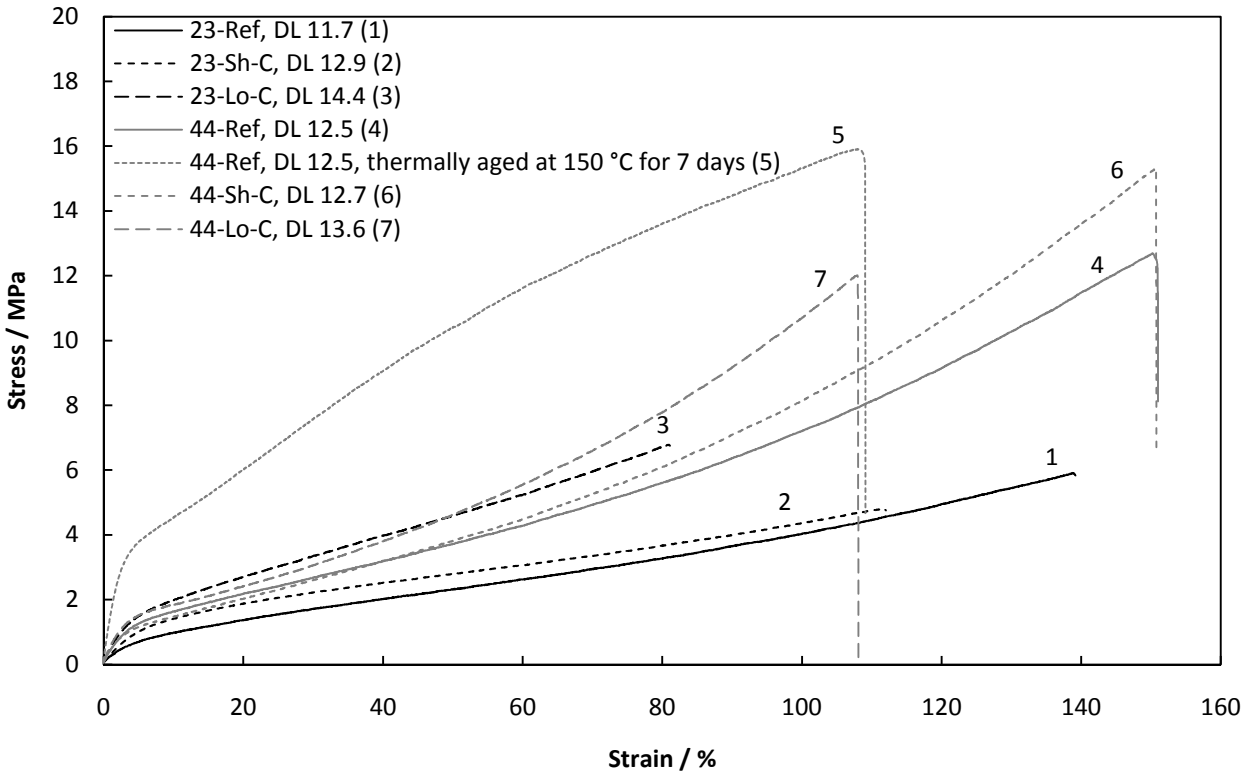

Figure 6.10 *Representative stress-strain curves at room temperature of membranes with different thermal history and initial linear average molecular weights of 23 kDa (23-Ref, 23-Sh-C and 23-Lo-C) and 44 kDa (44-Ref, 44-Sh-C and 44-Lo-C). The corresponding acid doping levels (DL) of the membranes are indicated in the figure. A representative stress-strain curve of the PA doped 44-Ref membrane which had been thermally aged at 150 °C for 7 days is also shown.*

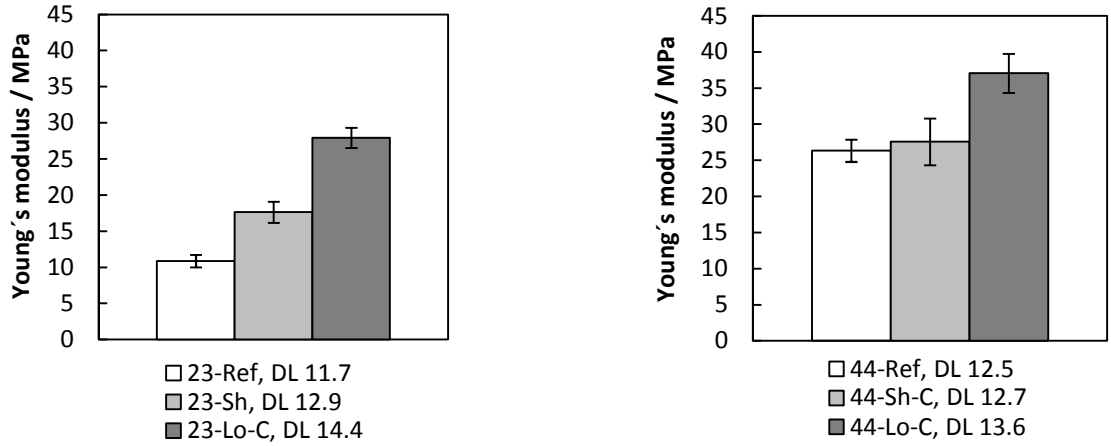

Figure 6.11 *Young´s modulus at room temperature of the phosphoric acid doped membranes with initial linear average molecular weight of 23 kDa (left) and 44 kDa (right). The corresponding acid doping levels (DL) are indicated in the figure.*

On the other hand, the mechanical toughening after the thermal induced curing of the membranes with an intermediate linear average molecular weight of 44 kDa was not as obvious, as also shown in Figure 6.10. However, as expected [183] the mechanical properties in terms of the engineering tensile stress at break as well as the Young´s modulus of the non-cured reference membrane 44-Ref were considerably improved when the initial linear average molecular weight of PBI was increased from 23 kDa to 44 kDa. For example, even though the acid doping level was slightly higher the Young´s modulus was nearly doubled when the linear average molecular weight was increased from 23 kDa (23-Ref) to 44 kDa (44-Ref). Furthermore, the Young´s modulus of the membrane with a low linear average molecular weight of 23 kDa which had been cured under argon at 350 °C for 16 h (23-Lo-C) was similar to that of the non-cured reference membrane with a high initial average molecular weight of 44 kDa (44-Ref). On the other hand, the Young´s modulus of the 44 kDa linear average molecular weight non-cured reference membrane (44-Ref) was considerably lower compared with that of the membrane with a similar linear average molecular weight but lower phosphoric acid doping level (Figure 5.9), which further illustrates the strong plasticizing effect of phosphoric acid.

Table 6.2 *Summary of the room temperature mechanical data.*

Membranes and conditions	Young´s modulus (MPa)	Engineering tensile stress at break (MPa)	Elongation at break (%)
23-Ref, DL 11.7	10.9 ± 0.9	5.7 ± 0.4	136 ± 11
23-Sh-C, DL 12.9	17.6 ± 1.5	4.7 ± 1.3	111 ± 37
23-Lo-C, DL 14.4	27.9 ± 1.4	5.7 ± 1.6	67 ± 21
44-Ref, DL 12.5	26.3 ± 1.5	13.3 ± 1.1	155 ± 7
44-Sh-C, DL 12.7	27.6 ± 3.2	14.4 ± 1.4	144 ± 8
44-Lo-C, DL 13.6	37.1 ± 2.7	12.1 ± 1.0	108 ± 5
44-Ref, DL 12.5 thermally aged at 150 °C for 7 days	113.8 ± 14.7	14.7 ± 0.9	96.4 ± 13.9

The cured membranes which were prepared from PBI with a linear average molecular weight of 44 kDa (44-Sh-C and 44-Lo-C) showed lower elongation at break and a steeper slope of the stress-strain curve beyond the yield point compared with its non-cured counterpart (44-Ref). It indicates increased resistance to plastic deformation and increasing rigidity in the rubbery region. Furthermore, the Young´s modulus of the membrane which had been cured for 16 h (44-Lo-C) was slightly higher compared with that of its non-cured counterpart (44-Ref), even though the acid doping level was about 9% higher.

Conclusively, the mechanical characteristics of the PBI membranes which had been cured under argon at 350 °C for different durations prior to the phosphoric acid doping resembled those of previously reported covalently crosslinked PBI membranes [100, 172] and what can be expected for a crosslinked structure. However, the degree of crosslinking was either very small or chemically rather non-uniform since no deviations could be observed in the FTIR spectrum of the cured membranes, as also discussed by Gillham [246].

On the other hand, mechanical toughening of a polymeric material can also be expected if the degree of crystallinity is increased [103]. However, the general toughening of the cured membranes in the present study cannot solely be explained by the higher degree of crystallinity since the membranes were apparently morphologically equal after the acid doping.

6.3.7.2 Thermally aged phosphoric acid doped PBI

As discussed in Chapter 6.1, crystalline materials are generally tougher and stiffer than their amorphous counterparts. For example, PBI membranes with an acid doping level of 2 exhibit

crystalline features due to the formation of polymeric salt which is illustrated on a macroscopic scale by an increased mechanical toughness [78].

As revealed by the X-ray diffractograms as shown in Figure 6.9 the degree of crystallinity was considerably increased after thermal ageing of the phosphoric acid doped non-cured reference membrane 44-Ref at 150 °C for up to 43 days. The effect of the increased degree of crystallinity on the mechanical properties after thermal aging is illustrated by the representative stress-strain curve in Figure 6.10.

It showed a significant toughening of the phosphoric acid doped membrane after thermal aging. For example, after thermal ageing at 150 °C the Young´s modulus was increased by more than 300% from about 26 MPa to around 114 MPa. Furthermore, the stress at yield was increased from 1.2 MPa to 3.7 MPa whereas the engineering tensile stress at break was slightly increased from 13.3 MPa to 14.7 MPa. The considerable membrane toughening was also illustrated by an increased resistance to plastic deformation as indicated by the slightly steeper slope of the stress-strain curve in the plastic deformation region.

The increased degree of structural order in the thermally aged membrane obviously affected its physiochemical properties which ultimately could result in a more brittle and fragile material. The gradual partial crystallization of the phosphoric acid doped membrane could thus result in a material which is more sensitive to mechanical or thermal stresses in the fuel cell which ultimately also could affect the durability of the MEA.

6.3.8 Proton conductivity

The anhydrous in-plane proton conductivity of the phosphoric acid doped membranes was recorded as a function of temperature, as shown in Figure 6.12.

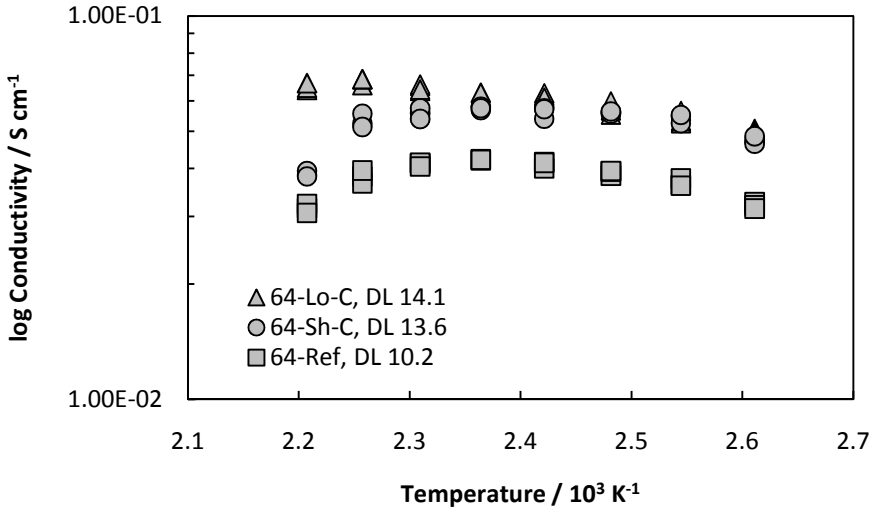

Figure 6.12 *Anhydrous proton conductivity of the phosphoric acid doped membranes based on cured PBI and of the phosphoric acid doped non-cured reference membrane. The corresponding doping levels are indicated in the figure.*

The anhydrous proton conductivity of the phosphoric acid doped cured membranes (64-Sh-C and 64-Lo-C) was somewhat higher compared with that of the phosphoric acid doped non-cured reference membrane 64-Ref, apparently due to their slightly higher phosphoric acid doping levels [98]. The conductivity of the membranes based on cured PBI (64-Sh-C and 64-Lo-C) with doping levels of

around 14 and of the non-cured reference membrane (64-Ref) with a lower acid doping level of around 10 reached about 0.06 S cm^{-1} and 0.04 S cm^{-1} at 150 °C, respectively. The data corresponded well with previously reported anhydrous conductivity data of covalently [100] or ionically [155] crosslinked PBI based membranes or PBI structure analogue based membranes [101] of similar phosphoric acid doping levels.

The proton conductivity of phosphoric acid solutions is strongly dependent on the water content. For example, at 20 °C the conductivity of 100% and 45% phosphoric acid was reported to differ by about an order of magnitude. It was increased from 0.025 S cm^{-1} to 0.22 S cm^{-1} when the H_3PO_4 concentration was reduced from 100% to 45% [107]. At temperatures around 170 °C and without active humidification, phosphoric acid dehydrates through condensation according to the completely reversible reaction in Equation 6.1 [99]. The dehydration results in the formation of pyrophosphoric acid or higher phosphoric acid oligomers which are less proton conducting than ortophosphoric acid.

$$2H_3PO_4 \rightleftharpoons H_4P_2O_7 + H_2O \qquad (6.1)$$

Hence, the conductivity at temperatures at or above 170 °C should be strongly dependent on the water content of the membrane. The phosphoric acid dehydration was illustrated in the present study by a gradual proton conductivity decay at temperatures above 160 °C. A similar effect has also been observed for phosphoric acid doped PBI membranes of low doping levels which were cast from TFA/PA [98] as well as for phosphoric acid doped PBI of very high acid doping levels which were prepared according to the sol-gel methodology [79].

6.3.9 Fuel cell tests

6.3.9.1 Polarization curves

Polarization curves were recorded after continuous fuel cell operation at a constant current load of 600 mA cm^{-2} for up to about 1800 h, as shown in Figure 6.13.

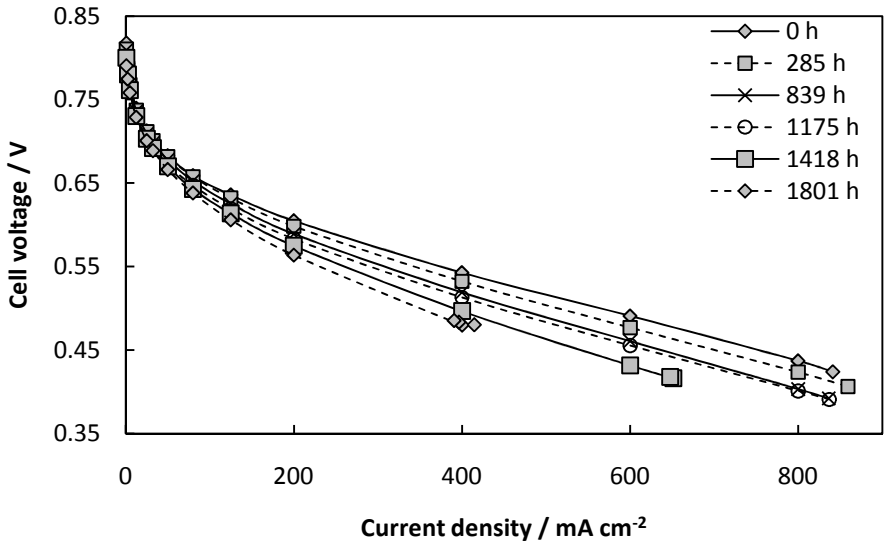

Figure 6.13 *Polarization curves of the MEA based on the PBI membrane which had been cured at 350 °C under argon for 16 h prior to the doping in 85% phosphoric acid at 100 °C (48-Lo-C). The polarization curves were recorded after fuel cell operation at a constant current load of 600 mA cm^{-2} for up to 1801 h.*

The OCV was slightly decreased during the first 1800 h of operation from 818 mV to 791 mV which was most likely due to the gradual increased gas permeability of the membrane. In the higher current density range the ageing of the MEA was illustrated by a steeper slope of the polarization curve in the linear region. The increased ohmic resistance over time could eventually be explained by the leakage of phosphoric acid trough steam distillation. It has previously been reported to be one of the major degradation mechanisms of phosphoric acid doped PBI based fuel cells, especially during high load operation when the water formation rate is high [255].

The gradual decrease of the fuel cell performance over time was also illustrated by a gradually reduced power density, especially in the high current density range as shown in Figure 6.14.

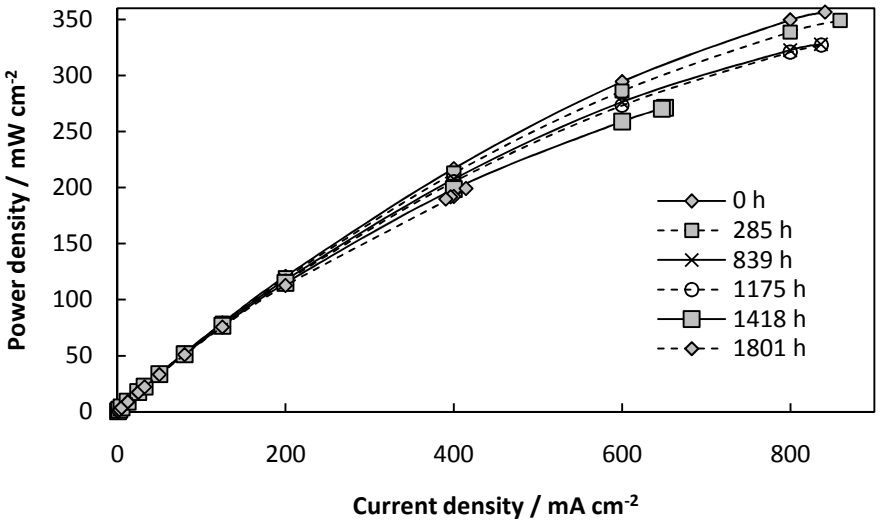

Figure 6.14 *Power density of the MEA based on the PBI membrane which had been cured at 350 °C under argon for 16 h prior to the doping in 85% phosphoric acid at 100 °C (48-Lo-C). The data were acquired after fuel cell operation at a constant load of 600 mA cm^{-2} for up to 1801 h.*

6.3.9.2 Durability

The long term durability is of primary concern for PEM fuel cells in general. Continuous steady state operation at a constant current load in the 150-160 °C temperature range is a mild mode for phosphoric acid doped PBI based fuel cells. The complete absence of liquid water minimizes the risk of the phosphoric acid wash-out, which is of critical concern for the long term durability of the cells since it would gradually reduce the membrane conductivity [255]. Furthermore, the cell voltage during steady state operation is considerably lower than the OCV which minimizes the oxidation rate of the carbon based catalyst support materials as well as the dissolution of the noble metal based catalyst materials. The catalyst degradation rate can thus be expected to be considerably reduced if fuel cell idling can be circumvented [256]. Operation at constant temperature will also minimize the stresses connected to thermal expansion and contraction of the cell components which could affect the membrane electrode interface. In other words, the major cause of failure of a PBI based fuel cell under the steady state operation mode is most likely connected to the membrane degradation.

A limited number of long term durability investigations of phosphoric acid doped PBI or PBI structure analogue based high temperature PEM fuel cells operated at constant current load or in load cycling mode have been published during the last decade [69, 79, 255, 257-261]. During the steady state tests the cells were generally operated at a rather low current load of 200 mA cm^{-2}. For example BASF-PEMEAS [69] has demonstrated a life time of over 20000 hours at 160 °C at a constant current load of 200 mA cm^{-2}. From the durability results, the average cell voltage decay rate was estimated to be about

5-6 µV h^{-1} when the cell was operated at a constant load of 200 mA cm^{-2}. Similar measurements were made by Yu *et al.* [255] under steady-state conditions, showing an average voltage decay rate of 4.9-6.3 µV h^{-1} at 160°C.

However, at higher current density the water formation rate at the cathode is high which might result in steam distillation of phosphoric acid and thus a continuous acid wash-out, especially at high operating temperatures in the 180-190 °C range [255]. The effect of operating temperature is further illustrated by the reduction of the demonstrated lifetime from 5000-20000 h at 150-160 °C to a few hundreds of hours at an operating temperature of 180-200 °C [262]. This was apparently due to the membrane degradation because the eventual death of the cell was accompanied by a sudden increase of the gas permeability.

Conclusively, the long lifetimes or the very low degradation rates which have been reported for the phosphoric acid doped PBI based fuel cells were typically achieved in the 120-160 °C temperature range and at a rather low current density of typically 200 mA cm^{-2}. In general, at higher current loads much higher average cell voltage decay rates were observed. For example, during steady state operation at a constant load of 400 mA cm^{-2} at 160 °C for 1150 h an average cell voltage decay rate of about 43 µV h^{-1} was observed [79]. Furthermore, Li and Scott [217] operated a PTFE reinforced phosphoric acid doped PBI based MEA in start/stop fuel cell mode with a maximum current load of 700 mA cm^{-2}. Under these conditions the MEA showed an obvious gradual decay of the cell voltage during 50 h of total operation time.

The low cell voltage decay rate during continuous fuel cell operation at 160 °C at a low current load of 200 mA cm^{-2} was confirmed in the present study, as shown in Figure 6.15.

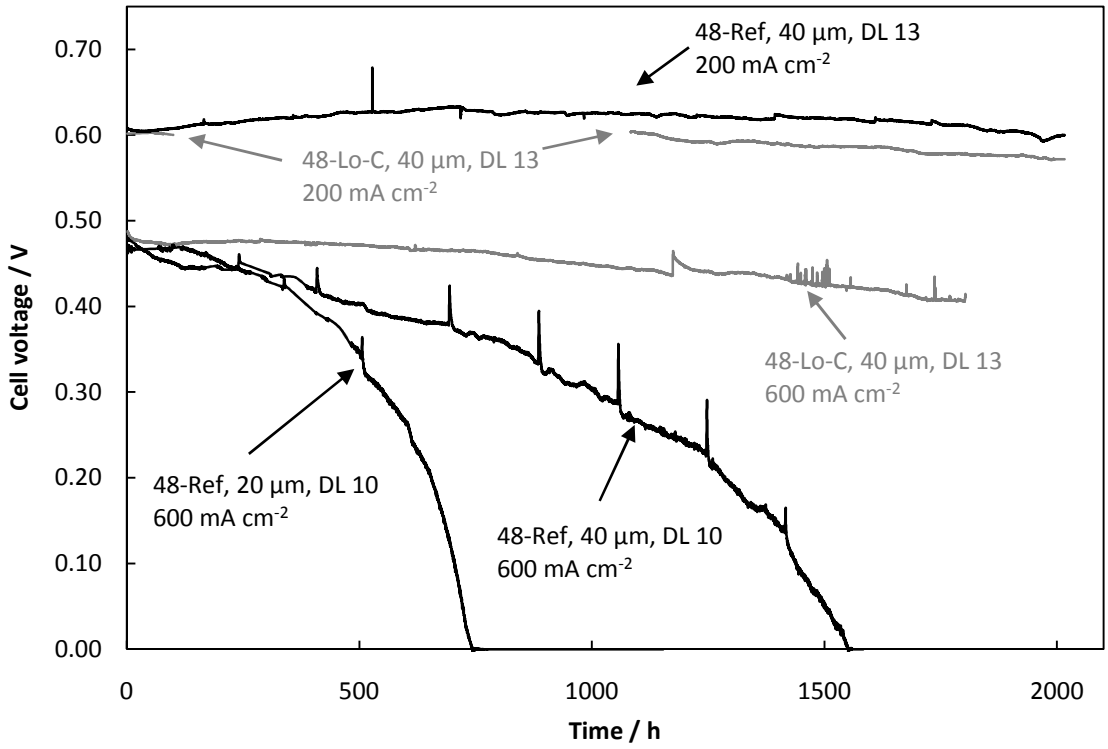

Figure 6.15 *Fuel cell voltages as functions of time of the MEAs based on non-cured PBI (48-Ref, black lines) and PBI which had been cured at 350 °C for 16 h under argon (48-Lo-C, grey lines) prior to the acid doping. The cells were operated at current loads of 200 mA cm^{-2} or 600 mA cm^{-2}. The corresponding membrane thicknesses and doping levels (DL) are indicated in the figure.*

Under these conditions the cell based on the non-cured reference membrane 48-Ref showed an average cell voltage decay rate of about 5-6 μV h^{-1} during about 2000 h of operation. The initial cell voltage of the MEA based on the cured membrane 48-Lo-C operating at 200 mA cm^{-2} (0.60 V) was practically identical with that of the MEA based on its non-cured counterpart (0.61 V). However, a current load malfunction of the cell based on the cured membrane 48-Lo-C occurred after about 100 h of operation which resulted in load cycling mode in the 100-1050 h range. During this period the current density varied between 0-200 mA cm^{-2} which implies that the cell voltage varied between OCV and about 0.6 V. This type of load cycling is well known to enhance the degradation rate of the MEA [69, 255] which was illustrated in the present study by a slightly higher average cell voltage decay rate of 13 μV h^{-1} during about 2000 h operation.

However, during continuous fuel cell operation at a considerably higher current load of 600 mA cm^{-2} the MEA based on the phosphoric acid doped cured PBI membrane 48-Lo-C showed a dramatically reduced degradation rate as compared with the non-cured reference membrane 48-Ref based MEA, as shown in Figure 6.15.

At a constant current load of 600 mA cm^{-2} the MEA based on the 20 μm thick non-cured reference membrane (48-Ref) showed an average cell voltage decay rate of about 630 μV h^{-1}. When the membrane thickness of the non-cured reference membrane (48-Ref) was doubled to 40 μm the average cell voltage decay rate was reduced to about 308 μV h^{-1}. The cell voltages of the two cells reached zero after about 750 h and 1550 h, respectively, which indicate complete membrane failure. Obviously, by reducing the thickness of the membrane by 50% the average cell voltage decay rate was doubled which further confirms that the cell voltage decay during operation at high current load is strongly connected to the membrane degradation. The MEA based on the PBI membrane which had been cured at 350 °C for 16 h under argon prior to doping in 85% H_3PO_4 at 100 °C (48-Lo-C), on the other hand, showed a considerably lower average cell voltage decay rate of 43 μV h^{-1} during the first 1800 h of operation. After 1800 h of continuous operation at a current load of 600 mA cm^{-2}, had decreased from about 0.49 V to 0.41 V.

The results confirm that the long term durability of PBI based high temperature PEM fuel cells is highly dependent on the membrane characteristics. The fuel cell durability at practical current load of 600 mA cm^{-2} could obviously be dramatically improved by introducing a thermal treatment step of the membrane prior to the phosphoric acid doping and the MEA manufacturing. In this way, the average cell voltage decay rate of the MEA could be reduced by as much as 86% which naturally should facilitate the commercial competitiveness of the technology.

6.4 Summary

Membranes of poly[2,2´(*m*-phenylene)-5,5' bibenzimidazole] (PBI) were prepared by solution casting from DMAc. The membranes were subsequently heat treated at temperatures up to 500 °C for up to 16 h under air or argon atmosphere in order to evaluate the thermo-oxidative or thermal stability of the membranes, respectively.

ATR-FTIR revealed considerable thermal oxidation of the membranes which had been heat treated under air atmosphere at temperatures above 300 °C, as indicated by enhanced absorbance in the 1000-1800 cm^{-1} region of the spectrum. Under an inert argon atmosphere, on the other hand, no obvious deviations in the FTIR spectra of the membranes which had been treated at temperatures up to 400 °C could be observed.

In order to evaluate the correlation between the thermal history of the membrane and its physiochemical characteristics after acid doping a heat treatment temperature of 350 °C under inert argon atmosphere was defined as the standard operating procedure. The heat treatment conditions were carefully chosen in order to circumvent the effects of thermal or thermo-oxidative degradation of the polymer. Since the physiochemical properties of phosphoric acid doped PBI membranes are highly

dependent on the linear average molecular weight of the polymer, the linear average molecular weight of the PBI used for the membrane preparation was varied between 23-64 kDa.

The membranes which had been heat treated at 350 °C under argon were almost completely insoluble in DMAc at 80 °C or in 85% H_3PO_4 at 100 °C, which further confirmed that PBI irreversibly cures and changes from a thermoplastic polymer to a thermoset during heat treatment at high temperatures.

Strong resistance to swelling is a fundamental characteristic of a crosslinked structure. Hence, in order to reach sufficient acid doping levels of the membranes which had been cured at 350 °C under argon for different durations, a doping temperature of 100 °C in 85% H_3PO_4 was required.

The thermogravimetric curves of the non-cured reference membrane showed a small weight loss with an onset temperature at about 350 °C. This weight loss was not observed in the thermogravimetric curve of the membrane which had been cured at 350 °C for 16 h under argon prior to the TGA experiment. The weight loss of the non-cured reference membrane in this temperature range could thus be connected to crosslinking reactions giving off volatile products. An exotherm with a maximum at about 410 °C was also observed in the DTA of the non-cured reference membrane and of the membrane which had been cured at 350 °C for 16 h under argon prior to the experiment. The exotherm could eventually be associated with the crosslinking reactions taking place in this temperature range which are responsible for irreversible curing of the membrane.

The wide angle X-ray diffraction measurements showed a considerable increase of the structural order of the membranes after the curing at 350 °C under argon. However, after phosphoric acid doping the membranes were morphologically equal (amorphous). On the other hand, anhydrous thermal aging of the phosphoric acid doped non-cured reference membrane at 150 °C for up to about 6 weeks showed a gradual development of relatively sharp reflections in the X-ray diffractograms over time, indicating partial crystallization of the membrane.

The general membrane toughening of the membranes which had been cured at 350 °C under argon prior to the phosphoric acid doping was most pronounced for the membrane with a low linear average molecular weight of PBI (23 kDa). The membrane toughening was apparently due to a dramatic increase of the molecular weight. This was illustrated on a macroscopic scale by increased engineering tensile stress at break and yield stress as well as a higher Young´s modulus. Furthermore, the decreased elongation at break and increased stress at yield in general of the cured membranes indicated increased brittleness which is a fundamental characteristic of a crosslinked polymer matrix. The increased brittleness of the cured membranes was also illustrated by the reduced plastic deformation. However, no indications of what could be ascribed to crosslinking could be observed in the ATR-FTIR spectra meaning that the degree of crosslinking should be either very small or chemically rather non-uniform.

The anhydrous proton conductivity of the cured and phosphoric acid doped membranes was higher compared with that of the non-cured reference membrane, apparently due to the higher phosphoric acid doping levels. At temperatures above 160 °C the anhydrous proton conductivity declined due to the dehydration of phosphoric acid.

The OCV of the MEA based on the membrane which had been cured at 350 °C for 16 h under argon slightly decreased from 818 mV to 791 mV during the first 1800 h of continuous operation at a constant load of 600 mA cm^{-2}. It indicates a gradual increase of the reactant permeability of the membrane over time. The slope of the linear part of the polarization curves in the high current density range gradually increased over the first 1800 h of the test. This was most likely due to the phosphoric acid leakage through steam distillation.

During continuous fuel cell operation at low current load of 200 mA cm^{-2} for 2000 h the MEA based on the non-cured reference membrane showed an average cell voltage decay rate of about 5-6 µV h^{-1}. The average cell voltage decay rate of the MEA based on the cured PBI membrane was slightly higher due

to the current load malfunction which resulted in load cycling mode between 0-200 mA cm^{-2} for about 900 h in the beginning of the durability test.

However, during continuous fuel cell operation at a current load of 600 mA cm^{-2} the average cell voltage decay rate of the MEA based on the membrane which had been cured at 350 °C for 16 h under argon prior to the phosphoric acid doping (43 µV h^{-1}) was dramatically reduced compared with that of the MEA which was based on the non-cured reference membrane (308 µV h^{-1}). The voltage decay rate was obviously connected to the membrane degradation since the MEA based on a 50% thinner non-cured reference membrane showed a much higher average voltage decay rate (630 µV h^{-1}). The results demonstrate that the membrane characteristics highly influence the long term durability of the phosphoric acid doped PBI high temperature PEM fuel cells, especially at high current loads. Their commercial viability could thus be strengthened by further improving and optimizing the membrane material.

7 Conclusions and outlook

7.1 Membranes for PEM water electrolysis

7.1.1 Steam electrolysis

Blend membranes of acidic and basic polymers have been widely investigated for PEM fuel cell applications during the last decade. However, the miscibility between polymers is generally poor due to their fundamental physiochemical differences. In this work a novel methodology was developed for the preparation of acid-base blend membranes based on Nafion® and PBI. The miscibility between the two polymers was found to be strongly dependent on the Nafion® counter cation. Based on the NH_4^+ ionomer form of Nafion®, homogenous blend membranes were prepared covering the whole composition range. The compatibilizing effect of the NH_4^+ cation was assigned to its moderate acidity in combination with its favorable hydrogen bond formation capability.

Inorganic proton conductors such as ZrP or phosphoric acid are commonly used as additives to pure PFSA and PBI membranes, mainly in order to improve their anhydrous proton conductivity. In this work, ZrP and phosphoric acid composites based on Nafion®, PBI and their blends covering the whole composition were prepared and extensively characterized with respect to their chemical and physiochemical properties. However, only the pristine phosphoric acid doped Nafion® and PBI membranes exhibited sufficient proton conductivity for steam electrolysis at 130 °C.

In steam electrolysis tests at 130 °C, the phosphoric acid doped Nafion® based MEA showed considerably better durability compared with the MEA which was based on phosphoric acid doped PBI. On the other hand, the steam electrolysis performance of the phosphoric acid doped Nafion® based MEA was rather moderate. The moderate performance could eventually be explained by a large membrane electrode interfacial contact resistance and uneven current distribution. This was most likely connected to the limited dimensional stability of the phosphoric acid doped Nafion® membrane under the operating conditions.

Aquivion™, on the other hand, is a low equivalent weight short side chain type PFSA membrane. Compared with the conventional Nafion® membranes, these types of materials exhibit better mechanical characteristics at elevated temperatures and higher elastic modulus which has previously been identified as the sole reason for their superior performance in H_2/O_2 PEM fuel cells. The superior dimensional stability of Aquivion™ compared with Nafion® at elevated temperatures was further confirmed in the present study. The high phosphoric acid uptake of Aquivion™ further allowed for high proton conductivity and thus improved steam electrolysis performance.

7.1.2 Liquid water electrolysis

PEM water electrolysis with a liquid water feed is a considerably more mature technology compared with PEM steam electrolysis. The liquid water feed allows for complete hydration and thus superior proton conductivity of the membrane. Pressurization in order to keep the feed water in the liquid phase also allows for elevated operating temperatures and thus a slightly reduced thermodynamic energy requirement for the water splitting reaction. Furthermore, system pressurization reduces the volume of the evolved gases at the electrodes which in turn reduces the ohmic resistance in the cell by improving the triple phase boundary contact in the electrodes.

In this work the dimensional stability of the membrane was identified as one important factor in order to reach good and stable electrolysis performance at temperatures above in the 120-130 °C range and at back pressures of 2-3 bar.

Nafion® based composite membranes with boron phosphate were developed in order to improve the membrane characteristics at elevated temperatures. The boron phosphate composite membranes exhibited slightly different spectroscopic and physiochemical characteristics compared with the pristine recast Nafion® membrane. Although the major fraction of the inorganic filler was dissolved and washed out during the membrane treatment as confirmed by solid state NMR, TGA and SEM-EDX the boron phosphate composites showed slightly higher conductivity and better water electrolysis performance compared with the pristine membrane.

Mechanical membrane reinforcement with highly porous PTFE was demonstrated to dramatically improve the proton conductivity as well as the water electrolysis performance at elevated temperatures and pressures. It was further confirmed that the dimensional stability of the membrane is of critical concern in order to reach good electrolysis performance. The MEA based on the PTFE reinforced membrane reached as high current density as 2500 mA cm^{-2} at a cell voltage of 1.95 V in liquid water electrolysis mode at 120 °C and 2 bar back pressure.

7.2 Membranes for high temperature PEM fuel cells

The anhydrous proton conductivity of phosphoric acid doped PBI membranes is highly dependent on the phosphoric acid content. A high acid doping level is crucial in order to minimize the ohmic resistance in PBI based high temperature PEM fuel cells. However, a compromise between the acid doping level and the mechanical strength generally has to be made due to the strong plasticizing effect of phosphoric acid.

In this work, novel procedures for tuning the chemical and physiochemical properties of phosphoric acid doped PBI membranes were developed. PBI membranes were solution cast from DMAc and post crosslinked with divinylsulfone or thermally cured at 350 °C under inert atmosphere. The divinylsulfone post crosslinking chemistry was studied in detail and optimized using a low molecular weight model system reaction.

The post crosslinking with divinylsulfone as well as the thermal curing of the PBI membranes improved the mechanical strength of the membranes after phosphoric acid doping, allowing for higher acid doping levels and thus improved proton conductivity. In addition to the improved mechanical strength after phosphoric acid doping, the crosslinked membranes exhibited improved radical-oxidative resistance.

High temperature PEM fuel cell tests were conducted in order to demonstrate the feasibility of the modified phosphoric acid doped PBI based membranes. The MEA based on the cured and phosphoric acid doped PBI membrane demonstrated a dramatic improvement of the long term durability in terms of the average cell voltage decay rate during operation at a constant current load of 600 mA cm^{-2} at 160 °C.

The results confirm that the long term durability of phosphoric acid doped PBI based high temperature PEM fuel cells is highly dependent on the membrane characteristics, especially during operation at high current loads.

It is also obvious that there is room for dramatic improvement of the long term durability of the high temperature PEM fuel cells by optimizing the membrane material. For example, an operationally simple heat treatment step before the acid doping of the membrane resulted in a dramatic reduced average cell voltage decay rate of 86% during continuous fuel cell operation at 160 °C and at a relatively high current load of 600 mA cm^{-2}.

7.3 Outlook

The developed methodology for the preparation of homogenous acid-base polymer blends by employing the counter cation as compatibilizer could eventually be applied on alternative acid-base polymer blend systems in order to extend the scope of the methodology.

Proof of concept was demonstrated for PEM steam electrolysis with phosphoric acid doped PFSA membranes. However, further research and development is needed in order to further improve the membrane and the membrane electrode interface as well as to optimize for the MEA preparation, cell design and the operational parameters. Further research should also be devoted to reducing the high anode overpotential of the cells operating in liquid water electrolysis mode.

Extensive knowledge about the membrane degradation mechanisms is the key to an intelligent design of novel, high-performing structures with high proton conductivity and further improved durability during operation in electrolysis mode as well as in fuel cell mode. Further work should thus be dedicated to *ex situ* accelerated membrane degradation tests as well as *in situ* tests in water or steam electrolyzer cells and fuel cells in combination with MEA post mortem analysis in order to unravel the mechanisms responsible for the membrane degradation.

8 References

[1] A. Hanslmeier, *Water in the Universe*, Springer Netherlands, Dordrecht, **2011**, pp. 1-24.
[2] H. Kaesz, P. Atkins, *Chem. Int.* **2003**, *25*, 14.
[3] R. Pohl, A. Antognini, F. Nez, F. D. Amaro, F. Biraben, J. M. R. Cardoso, D. S. Covita, A. Dax, S. Dhawan, L. M. P. Fernandes, A. Giesen, T. Graf, T. W. Hänsch, P. Indelicato, L. Julien, C.-Y. Kao, P. Knowles, E.-O. Le Bigot, Y.-W. Liu, J. A. M. Lopes, L. Ludhova, C. M. B. Monteiro, F. Mulhauser, T. Nebel, P. Rabinowitz, J. M. F. dos Santos, L. A. Schaller, K. Schuhmann, C. Schwob, D. Taqqu, J. F. C. A. Veloso, F. Kottmann, *Nature* **2010**, *466*, 213-216.
[4] A. L. Dicks, *J. Power Sources* **1996**, *61*, 113-124.
[5] A. Bauen, D. Hart, *J. Power Sources* **2000**, *86*, 482-494.
[6] N. Garland, DOE view of advanced materials for fuel cells. In *Advances in Materials for Proton Exchange Membrane Fuel Cell Systems 2011*, Pacific Grove, CA, USA, February 20-23 **2011**.
[7] L. E. Apodaca, *2008 Minerals Yearbook*, U.S. Geological Survey, **2010**, pp. 53.1-53.17.
[8] W. E. Winsche, K. C. Hoffman, F. J. Salzano, *Science* **1973**, *180*, 1325-1332.
[9] J. Verne, *The Mysterious Island*, Modern Library, New York, **2004** p. 379.
[10] G. Marbán, T. Valdés-Solís, *Int. J. Hydrogen Energy* **2007**, *32*, 1625-1637.
[11] M. Momirlan, T. N. Veziroglu, *Renewable Sustainable Energy Rev.* **2002**, *6*, 141-179.
[12] L. Schlapbach, A. Zuttel, *Nature* **2001**, *414*, 353-358.
[13] J. E. Funk, *Int. J. Hydrogen Energy* **2001**, *26* 185-190.
[14] G. Aylward, T. Findlay, *SI Chemical Data*, 5 ed., John Wiley & Sons Australia, Milton, **2002**, p. 150.
[15] A. Marshall, B. Borresen, G. Hagen, M. Tsypkin, R. Tunold, *Energy* **2007**, *32*, 431-436.
[16] P. H. Choi, D. G. Bessarabov, R. Datta, *Solid State Ionics* **2004**, *175*, 535-539.
[17] Q. Li, H. A. Hjuler, N. J. Bjerrum, *Electrochim. Acta* **2000**, *45*, 4219-4226.
[18] S. Sugawara, T. Maruyama, Y. Nagahara, S. S. Kocha, K. Shinohra, K. Tsujita, S. Mitsushima, K. Ota, *J. Power Sources* **2009**, *187*, 324-331.
[19] B. C. H. Steele, A. Heinzel, *Nature* **2001**, *414*, 345-352.
[20] M. Winter, R. J. Brodd, *Chem. Rev.* **2004**, *104*, 4245-4270.
[21] A. Volta, *Phil. Trans. R. Soc. London* **1800**, *90*, 403-431.
[22] J. Larminie, A. Dicks, *Fuel Cell Systems Explained*, 2 ed., John Wiley & Sons Ltd., Chichester, **2003**, pp. 67-226.
[23] M. L. Perry, T. F. Fuller, *J. Electrochem. Soc.* **2002**, *149*, S59-S67.
[24] F. T. Bacon, *Electrochim. Acta* **1969**, *14*, 569-585.
[25] W. T. Grubb, L. W. Niedrach, *J. Electrochem. Soc* **1960**, *107*, 131-135.
[26] W. T. Grubb (General Electric Company), US Patent 2913511, **1959**.
[27] R. F. Service, *Science* **1999**, *285*, 682-685.
[28] P. Costamagna, S. Srinivasan, *J. Power Sources* **2001**, *102*, 253-269.
[29] L. J. Nuttall, J. F. McElroy, *Int. J. Hydrogen Energy* **1983**, *8*, 609-615.
[30] S. Banerjee, D. E. Curtin, *J. Fluorine Chem.* **2004**, *125*, 1211-1216.
[31] K. D. Kreuer, *J. Membr. Sci.* **2001**, *185*, 29-39.
[32] Q. Li, R. H. He, J. O. Jensen, N. J. Bjerrum, *Chem. Mater* **2003**, *15*, 4896-4915.
[33] Q. Li, R. H. He, J. A. Gao, J. O. Jensen, N. J. Bjerrum, *J. Electrochem. Soc.* **2003**, *150*, A1599-A1605.
[34] Q. Li, H. A. Hjuler, C. Hasiotis, J. K. Kallitsis, C. G. Kontoyannis, N. J. Bjerrum, *Electrochem. Solid-State Lett.* **2002**, *5*, A125-A128.
[35] J. O. Jensen, Q. Li, C. Pan, A. P. Vestbø, K. Mortensen, H. N. Petersen, C. L. Sørensen, T. N. Clausen, J. Schramm, N. J. Bjerrum, *Int. J. Hydrogen Energy* **2007**, *32*, 1567-1571.
[36] R. Borup, J. Meyers, B. Pivovar, Y. S. Kim, R. Mukundan, N. Garland, D. Myers, M. Wilson, F. Garzon, D. Wood, P. Zelenay, K. More, K. Stroh, T. Zawodzinski, J. Boncella, J. E. McGrath, M. Inaba, K. Miyatake, M. Hori, K. Ota, Z. Ogumi, S. Miyata, A. Nishikata, Z. Siroma, Y. Uchimoto, K. Yasuda, K. I. Kimijima, N. Iwashita, *Chem. Rev.* **2007**, *107*, 3904-3951.
[37] S. Trasatti, *J. Electroanal. Chem.* **1999**, *476*, 90-91.
[38] R. de Levie, *J. Electroanal. Chem.* **1999**, *476*, 92-93.

[39] J. O. Jensen, V. Bandur, N. J. Bjerrum, S. H. Jensen, S. Ebbesen, M. Mogensen, N. Topshøj, L. Yde, Pre-investigation of water electrolysis, *PSO-F&U 2006-1-6287 project report* **2008**.
[40] R. J. Davenport, F. H. Schubert, D. J. Grigger, *J. Power Sources* **1991**, *36*, 235-250.
[41] A. Hauch, S. D. Ebbesen, S. H. Jensen, M. Mogensen, *J. Mater. Chem.* **2008**, *18*, 2331-2340.
[42] J. Nieminen, I. Dincer, G. Naterer, *Int. J. Hydrogen Energy* **2010**, *35*, 10842-10850.
[43] L. J. Nuttall, J. H. Russell, *Int. J. Hydrogen Energy* **1980**, *5*, 75-84.
[44] G. G. Scherer, T. Momose, K. Tomiie, *J. Electrochem. Soc.* **1988**, *135*, 3071-3073.
[45] S. Stucki, G. G. Scherer, S. Schlagowski, E. Fischer, *J. Appl. Electrochem.* **1998**, *28*, 1041-1049.
[46] F. Marangio, M. Santarelli, M. Calì, *Int. J. Hydrogen Energy* **2009**, *34*, 1143-1158.
[47] A. V. Nikiforov, I. M. Petrushina, E. Christensen, A. L. Tomás-García, N. J. Bjerrum, *Int. J. Hydrogen Energy* **2011**, *36*, 111-119.
[48] J. Xie, D. L. Wood, K. L. More, P. Atanassov, R. L. Borup, *J. Electrochem. Soc.* **2005**, *152*, A1011-A1020.
[49] P. Costamagna, S. Srinivasan, *J. Power Sources* **2001**, *102*, 242-252.
[50] G. Wu, K. L. More, C. M. Johnston, P. Zelenay, *Science* **2011**, *332*, 443-447.
[51] S. Trasatti, *J. Electroanal. Chem. Interfacial Electrochem.* **1972**, *39*, 163-184.
[52] A. Daghetti, G. Lodi, S. Trasatti, *Mater. Chem. Phys.* **1983**, *8*, 1-90.
[53] A. Marshall, B. Borresen, G. Hagen, M. Tsypkin, R. Tunold, *Mater. Chem. Phys.* **2005**, *94*, 226-232.
[54] A. V. Nikiforov, A. L. Tomás García, I. M. Petrushina, E. Christensen, N. J. Bjerrum, *Int. J. Hydrogen Energy* **2011**, *36*, 5797-5805.
[55] Q. Li, J. O. Jensen, R. F. Savinell, N. J. Bjerrum, *Prog. Polym. Sci.* **2009**, *34*, 449-477.
[56] P. Millet, F. Andolfatto, R. Durand, *Int. J. Hydrogen Energy* **1996**, *21*, 87-93.
[57] W. Grot, *Chem. Ind.* **1985**, 647-649.
[58] C. Heitner-Wirguin, *J. Membr. Sci.* **1996**, *120*, 1-33.
[59] G. Gebel, P. Aldebert, M. Pineri, *Macromolecules* **1987**, *20*, 1425-1428.
[60] K. A. Mauritz, R. B. Moore, *Chem. Rev.* **2004**, *104*, 4535-4585.
[61] M. A. Hickner, H. Ghassemi, Y. S. Kim, B. R. Einsla, J. E. McGrath, *Chem. Rev.* **2004**, *104*, 4587-4611.
[62] A. S. Aricò, A. Di Blasi, G. Brunaccini, F. Sergi, G. Dispenza, L. Andaloro, M. Ferraro, V. Antonucci, P. Asher, S. Buche, D. Fongalland, G. A. Hards, J. D. B. Sharman, A. Bayer, G. Heinz, N. Zandonà, R. Zuber, M. Gebert, M. Corasaniti, A. Ghielmi, D. J. Jones, *Fuel Cells* **2010**, *10*, 1013-1023.
[63] K. D. Kreuer, M. Schuster, B. Obliers, O. Diat, U. Traub, A. Fuchs, U. Klock, S. J. Paddison, J. Maier, *J. Power Sources* **2008**, *178*, 499-509.
[64] A. Ghielmi, P. Vaccarono, C. Troglia, V. Arcella, *J. Power Sources* **2005**, *145*, 108-115.
[65] G. Alberti, M. Casciola, *Annu. Rev. Mater. Res.* **2003**, *33*, 129-154.
[66] M. Martinez, Y. Molmeret, L. Cointeaux, C. Iojoiu, J.-C. Leprêtre, N. El Kissi, P. Judeinstein, J.-Y. Sanchez, *J. Power Sources* **2010**, *195*, 5829-5839.
[67] R. Savinell, E. Yeager, D. Tryk, U. Landau, J. Wainright, D. Weng, K. Lux, M. Litt, C. Rogers, *J. Electrochem. Soc.* **1994**, *141*, L46-L48.
[68] J. S. Wainright, J. T. Wang, D. Weng, R. F. Savinell, M. Litt, *J. Electrochem. Soc.* **1995**, *142*, L121-L123.
[69] T. J. Schmidt, J. Baurmeister, *J. Power Sources* **2008**, *176*, 428-434.
[70] J. Mader, L. Xiao, T. J. Schmidt, B. C. Benicewicz in *Advances in Polymer Science, Vol. 216* (Ed.: G. Scherer), Springer-Verlag, Berlin Heidelberg, **2008**, pp. 63-124.
[71] J. A. Asensio, E. M. Sanchez, P. Gomez-Romero, *Chem. Soc. Rev.* **2010**, *39*, 3210-3239.
[72] K. C. Brinker, I. M. Robinson (Du Pont de Nemours and Company), US Patent 2895948, **1959**.
[73] H. Vogel, C. S. Marvel, *J. Polym. Sci.* **1961**, *50*, 511-&.
[74] E. W. Neuse, *Adv. Polym. Sci.* **1982**, *47*, 1-42.
[75] Y. Iwakura, Y. Imai, K. Uno, *J. Polym. Sci., Part A: General Papers* **1964**, *2*, 2605-2615.
[76] T. S. Chung, *J. Macromol. Sci., Rev. Macromol. Chem. Phys.* **1997**, *C37*, 277-301.
[77] T. R. Hanley, T. E. Helminiak, C. L. Benner, *J. Appl. Polym. Sci.* **1978**, *22*, 2965-2978.
[78] M. Litt, R. Ameri, Y. Wang, R. Savinell, J. Wainright in *Solid State Ionics V, Vol. 548* (Eds.: G. A. Nazri, C. Julien, A. Rougier), Materials Research Society, Warrendale, **1999**, pp. 313-323.
[79] L. X. Xiao, H. F. Zhang, E. Scanlon, L. S. Ramanathan, E. W. Choe, D. Rogers, T. Apple, B. C. Benicewicz, *Chem. Mater.* **2005**, *17*, 5328-5333.
[80] R. F. Savinell (Case Western Reserve University), US Patent 5716727, **1998**.
[81] Z. Liu, Y.-M. Tsou, G. Calundann, E. De Castro, *J. Power Sources* **2011**, *196*, 1055-1060.
[82] K. D. Kreuer, *Chem. Mater.* **1996**, *8*, 610-641.
[83] T. Norby, *Nature* **2001**, *410*, 877-878.
[84] K. D. Kreuer, S. J. Paddison, E. Spohr, M. Schuster, *Chem. Rev.* **2004**, *104*, 4637-4678.

[85] T. A. Zawodzinski, C. Derouin, S. Radzinski, R. J. Sherman, V. T. Smith, T. E. Springer, S. Gottesfeld, *J. Electrochem. Soc.* **1993**, *140*, 1041-1047.
[86] P. Millet, D. Dragoe, S. Grigoriev, V. Fateev, C. Etievant, *Int. J. Hydrogen Energy* **2009**, *34*, 4974-4982.
[87] V. Antonucci, A. Di Blasi, V. Baglio, R. Ornelas, F. Matteucci, J. Ledesma-Garcia, L. G. Arriaga, A. S. Arico, *Electrochim. Acta* **2008**, *53*, 7350-7356.
[88] V. Baglio, R. Ornelas, F. Matteucci, F. Martina, G. Ciccarella, I. Zama, L. G. Arriaga, V. Antonucci, A. S. Arico, *Fuel Cells* **2009**, *9*, 247-252.
[89] S. A. Grigoriev, P. Millet, S. V. Korobtsev, V. I. Porembskiy, M. Pepic, C. Etievant, C. Puyenchet, V. N. Fateev, *Int. J. Hydrogen Energy* **2009**, *34*, 5986-5991.
[90] S. A. Grigoriev, V. I. Porembskiy, S. V. Korobtsev, V. N. Fateev, F. Auprêtre, P. Millet, *Int. J. Hydrogen Energy* **2011**, *36*, 2721-2728.
[91] N. Agmon, *Chem. Phys. Lett.* **1995**, *244*, 456-462.
[92] R. Bouchet, E. Siebert, *Solid State Ionics* **1999**, *118*, 287-299.
[93] R. Bouchet, S. Miller, M. Duclot, J. L. Souquet, *Solid State Ionics* **2001**, *145*, 69-78.
[94] J. R. P. Jayakody, S. H. Chung, L. Durantino, H. Zhang, L. Xiao, B. C. Benicewicz, S. G. Greenbaum, *J. Electrochem. Soc.* **2007**, *154*, B242-B246.
[95] C. E. Hughes, S. Haufe, B. Angerstein, R. Kalim, U. Mahr, A. Reiche, M. Baldus, *J. Phys. Chem. B* **2004**, *108*, 13626-13631.
[96] M. Kawahara, J. Morita, M. Rikukawa, K. Sanui, N. Ogata, *Electrochim. Acta* **2000**, *45*, 1395-1398.
[97] B. Z. Xing, O. Savadogo, *J. New Mater. Electrochem. Syst.* **1999**, *2*, 95-101.
[98] Y. L. Ma, J. S. Wainright, M. H. Litt, R. F. Savinell, *J. Electrochem. Soc.* **2004**, *151*, A8-A16.
[99] A. Schechter, R. F. Savinell, *Solid State Ionics* **2002**, *147*, 181-187.
[100] Q. Li, C. Pan, J. O. Jensen, P. Noyé, N. J. Bjerrum, *Chem. Mater.* **2007**, *19*, 350-352.
[101] Q. Li, H. C. Rudbeck, A. Chromik, J. O. Jensen, C. Pan, T. Steenberg, M. Calverley, N. J. Bjerrum, J. Kerres, *J. Membr. Sci.* **2010**, *347*, 260-270.
[102] R. H. He, Q. Li, J. O. Jensen, N. J. Bjerrum, *J. Polym. Sci., Part A: Polym. Chem.* **2007**, *45*, 2989-2997.
[103] M. P. Stevens, *Polymer Chemistry - An Introduction*, 3 ed., Oxford University Press, New York, **1999**, pp. 61-128.
[104] Y. Yuan, F. Johnson, I. Cabasso, *J. Appl. Polym. Sci.* **2009**, *112*, 3436-3441.
[105] A. Buckley, D. Stuetz, G. A. Serad in *Encyclopedia of Polymer Science and Engineering, Vol. 11* (Ed.: J. I. Kroschwitz), Wiley, New York, **1987**, pp. 572-601.
[106] K. R. Cooper, *ECS Trans.* **2009**, *25*, 995-1007.
[107] R. H. He, Q. Li, G. Xiao, N. J. Bjerrum, *J. Membr. Sci.* **2003**, *226*, 169-184.
[108] P. Wardman, L. P. Candeias, *Radiat. Res.* **1996**, *145*, 523-531.
[109] J. H. Liao, Q. F. Li, H. C. Rudbeck, J. O. Jensen, A. Chromik, N. J. Bjerrum, J. Kerres, W. Xing, *Fuel Cells*, doi: 10.1002/fuce.201000146.
[110] Z. Chang, H. Pu, D. Wan, L. Liu, J. Yuan, Z. Yang, *Polym. Degrad. Stab.* **2009**, *94*, 1206-1212.
[111] E. Endoh in *Handbook of Fuel Cells - Fundamentals, Technology and Applications, Vol. 5: Advances in Electrocatalysis, Materials, Diagnostics and Durability* (Eds.: W. Vielstich, H. Yokokawa, H. A. Gasteiger), Wiley, Chichester, **2009**, pp. 361-374.
[112] C. A. Linkous, H. R. Anderson, R. W. Kopitzke, G. L. Nelson, *Int. J. Hydrogen Energy* **1998**, *23*, 525-529.
[113] C. A. Linkous, *Int. J. Hydrogen Energy* **1993**, *18*, 641-646.
[114] P. L. Antonucci, A. S. Arico, P. Creti, E. Ramunni, V. Antonucci, *Solid State Ionics* **1999**, *125*, 431-437.
[115] M. Watanabe, H. Uchida, Y. Seki, M. Emori, P. Stonehart, *J. Electrochem. Soc.* **1996**, *143*, 3847-3852.
[116] P. Costamagna, C. Yang, A. B. Bocarsly, S. Srinivasan, *Electrochim. Acta* **2002**, *47*, 1023-1033.
[117] C. Yang, P. Costamagna, S. Srinivasan, J. Benziger, A. B. Bocarsly, *J. Power Sources* **2001**, *103*, 1-9.
[118] C. Yang, S. Srinivasan, A. S. Arico, P. Creti, V. Baglio, V. Antonucci, *Electrochem. Solid-State Lett.* **2001**, *4*, A31-A34.
[119] C. Yang, S. Srinivasan, A. B. Bocarsly, S. Tulyani, J. B. Benziger, *J. Membr. Sci.* **2004**, *237*, 145-161.
[120] F. Bauer, M. Willert-Porada, *Fuel Cells* **2006**, *6*, 261-269.
[121] F. Bauer, M. Willert-Porada, *J. Membr. Sci.* **2004**, *233*, 141-149.
[122] W. G. Grot, G. Rajendran (Du Pont de Nemours and Company), US Patent 5919583, **1999**.
[123] M. Casciola, D. Capitani, A. Comite, A. Donnadio, V. Frittella, M. Pica, *Fuel Cells* **2008**, *8*, 217-224.
[124] M. P. Rodgers, Z. Shi, S. Holdcroft, *Fuel Cells* **2009**, *9*, 534-546.
[125] S. K. Tiwari, S. K. Nema, Y. K. Agarwal, *Thermochim. Acta* **1998**, *317*, 175-182.
[126] F. Bauer, M. Willert-Porada, *Solid State Ionics* **2006**, *177*, 2391-2396.
[127] G. Alberti, M. Casciola, M. Pica, T. Tarpanelli, M. Sganappa, *Fuel Cells* **2005**, *5*, 366-374.

[128] J. A. Kerres, *Fuel Cells* **2005**, *5*, 230-247.
[129] J. Kerres, A. Ullrich, F. Meier, T. Häring, *Solid State Ionics* **1999**, *125*, 243-249.
[130] S. Krause, *Pure Appl. Chem.* **1986**, *58*, 1553-1560.
[131] J. Kerres, A. Ullrich, T. Häring, M. Baldauf, U. Gebhardt, W. Preidel, *J. New Mater. Electrochem. Syst.* **2000**, *3*, 229-239.
[132] J. Kerres, W. Zhang, A. Ullrich, C. M. Tang, M. Hein, V. Gogel, T. Frey, L. Jörissen, *Desalination* **2002**, *147*, 173-178.
[133] J. Kerres, C.-M. Tang, C. Graf, *Ind. Eng. Chem. Res.* **2004**, *43*, 4571-4579.
[134] J. Kerres, A. Ullrich, M. Hein, V. Gogel, K. A. Friedrich, L. Jörissen, *Fuel Cells* **2004**, *4*, 105-112.
[135] V. S. Silva, B. Ruffmann, S. Vetter, A. Mendes, L. M. Madeira, S. P. Nunes, *Catal. Today* **2005**, *104*, 205-212.
[136] V. S. Silva, S. Weisshaar, R. Reissner, B. Ruffmann, S. Vetter, A. Mendes, L. M. Madeira, S. Nunes, *J. Power Sources* **2005**, *145*, 485-494.
[137] S. M. J. Zaidi, *Electrochim. Acta* **2005**, *50*, 4771-4777.
[138] S. Mitovi, B. Vogel, E. Roduner, H. Zhang, X. Zhu, V. Gogel, L. Jörissen, M. Hein, D. Xing, F. Schönberger, J. Kerres, *Fuel Cells* **2006**, *6*, 413-424.
[139] S. Pasupathi, S. Ji, B. J. Bladergroen, V. Linkov, *Int. J. Hydrogen Energy* **2008**, *33*, 3132-3136.
[140] H. Zhang, X. Li, C. Zhao, T. Fu, Y. Shi, H. Na, *J. Membr. Sci.* **2008**, *308*, 66-74.
[141] O. D. Thomas, T. J. Peckham, U. Thanganathan, Y. Yang, S. Holdcroft, *J. Polym. Sci., Part A: Polym. Chem.* **2010**, *48*, 3640-3650.
[142] V. Deimede, G. A. Voyiatzis, J. K. Kallitsis, Q. Li, N. J. Bjerrum, *Macromolecules* **2000**, *33*, 7609-7617.
[143] C. Hasiotis, V. Deimede, C. Kontoyannis, *Electrochim. Acta* **2001**, *46*, 2401-2406.
[144] C. Hasiotis, Q. Li, V. Deimede, J. K. Kallitsis, C. G. Kontoyannis, N. J. Bjerrum, *J. Electrochem. Soc.* **2001**, *148*, A513-A519.
[145] C. Manea, M. Mulder, *Desalination* **2002**, *147*, 179-182.
[146] J. K. Kallitsis, N. Gourdoupi, *J. New Mater. Electrochem. Syst.* **2003**, *6*, 217-222.
[147] M. K. Daletou, N. Gourdoupi, J. K. Kallitsis, *J. Membr. Sci.* **2005**, *252*, 115-122.
[148] M. K. Daletou, J. K. Kallitsis, G. Voyiatzis, S. G. Neophytides, *J. Membr. Sci.* **2009**, *326*, 76-83.
[149] S. Feng, Y. Shang, S. Wang, X. Xie, Y. Wang, Y. Wang, J. Xu, *J. Membr. Sci.* **2010**, *346*, 105-112.
[150] A. Katzfuß, K. Krajinovic, A. Chromik, J. Kerres, *J. Polym. Sci., Part A: Polym. Chem.* **2011**, *49*, 1919-1927.
[151] F. Schönberger, M. Hein, J. Kerres, *Solid State Ionics* **2007**, *178*, 547-554.
[152] J. Kerres, D. M. Xing, F. Schönberger, *J. Polym. Sci., Part B: Polym. Phys.* **2006**, *44*, 2311-2326.
[153] D. Xing, J. Kerres, *Polym. Adv. Technol.* **2006**, *17*, 591-597.
[154] J. Kerres, F. Schönberger, A. Chromik, T. Häring, Q. Li, J. O. Jensen, C. Pan, P. Noyé, N. J. Bjerrum, *Fuel Cells* **2008**, *8*, 175-187.
[155] Q. Li, J. O. Jensen, C. Pan, V. Bandur, M. S. Nilsson, F. Schönberger, A. Chromik, M. Hein, T. Häring, J. Kerres, N. J. Bjerrum, *Fuel Cells* **2008**, *8*, 188-199.
[156] B. Kosmala, J. Schauer, *J. Appl. Polym. Sci.* **2002**, *85*, 1118-1127.
[157] K. Bouzek, S. Moravcová, Z. Samec, J. Schauer, *J. Electrochem. Soc.* **2003**, *150*, E329-E336.
[158] A. H. Haghighi, M. M. Hasani-Sadrabadi, E. Dashtimoghadam, G. Bahlakeh, S. E. Shakeri, F. S. Majedi, S. Hojjati Emami, H. Moaddel, *Int. J. Hydrogen Energy* **2011**, *36*, 3688-3696.
[159] R. Wycisk, J. K. Lee, P. N. Pintauro, *J. Electrochem. Soc.* **2005**, *152*, A892-A898.
[160] J. K. Lee, J. Kerres, *J. Membr. Sci.* **2007**, *294*, 75-83.
[161] Z. W. Bai, G. E. Price, M. Yoonessi, S. B. Juhl, M. F. Durstock, T. D. Dang, *J. Membr. Sci.* **2007**, *305*, 69-76.
[162] N. N. Krishnan, H.-J. Lee, H.-J. Kim, J.-Y. Kim, I. Hwang, J. H. Jang, E. A. Cho, S.-K. Kim, D. Henkensmeier, S.-A. Hong, T.-H. Lim, *Eur. Polym. J.* **2010**, *46*, 1633-1641.
[163] O. Acar, U. Sen, A. Bozkurt, A. Ata, *J. Mater. Sci.* **2010**, *45*, 993-998.
[164] O. Acar, U. Sen, A. Bozkurt, A. Ata, *Int. J. Hydrogen Energy* **2009**, *34*, 2724-2730.
[165] L. J. Hobson, Y. Nakano, H. Ozu, S. Hayase, *J. Power Sources* **2002**, *104*, 79-84.
[166] R. Wycisk, J. Chisholm, J. Lee, J. Lin, P. N. Pintauro, *J. Power Sources* **2006**, *163*, 9-17.
[167] A. Ainla, D. Brandell, *Solid State Ionics* **2007**, *178*, 581-585.
[168] Y. F. Zhai, H. M. Zhang, Y. Zhang, D. M. Xing, *J. Power Sources* **2007**, *169*, 259-264.
[169] X. Y. Lu, R. A. Weiss, *Macromolecules* **1992**, *25*, 6185-6189.
[170] Q. Li, H. A. Hjuler, N. J. Bjerrum, *J. Appl. Electrochem.* **2001**, *31*, 773-779.
[171] Q. Li, R. H. He, R. W. Berg, H. A. Hjuler, N. J. Bjerrum, *Solid State Ionics* **2004**, *168*, 177-185.
[172] P. Noyé, Q. Li, C. Pan, N. J. Bjerrum, *Polym. Adv. Technol.* **2008**, *19*, 1270-1275.
[173] A. S. Arico, P. Creti, P. L. Antonucci, V. Antonucci, *Electrochem. Solid-State Lett.* **1998**, *1*, 66-68.
[174] R. B. Dushin, V. N. Krylov, *Inorg. Mater.* **1978**, *14*, 216-218.

[175] A. Clearfield, J. R. Thomas, *Inorg. Nucl. Chem. Lett.* **1969**, *5*, 775-&.
[176] Z. X. Liang, W. M. Chen, J. G. Liu, S. L. Wang, Z. H. Zhou, W. Z. Li, G. Q. Sun, Q. Xin, *J. Membr. Sci.* **2004**, *233*, 39-44.
[177] Section 9: Molecular Structure and Spectroscopy. Infrared Correlation Charts in *CRC Handbook of Chemistry and Physics, 90th Edition (Internet Version 2010)* (Ed.: D. R. Lide), CRC Press/Taylor and Francis Boca Raton, FL.
[178] H. H. Levine in *Encyclopedia of Polymer Science and Technology, Vol. 11* (Eds.: N. M. Bikales, J. Conrad, A. Ruks, J. Perlman), Interscience, New York, **1969**, pp. 188-232.
[179] K. Y. Wang, Y. C. Xiao, T. S. Chung, *Chem. Eng. Sci.* **2006**, *61*, 5807-5817.
[180] P. Musto, F. E. Karasz, W. J. MacKnight, *Polymer* **1993**, *34*, 2934-2945.
[181] A. Ohma, S. Yamamoto, K. Shinohara, *J. Power Sources* **2008**, *182*, 39-47.
[182] M. Canagaratna, J. A. Phillips, H. Goodfriend, K. R. Leopold, *J. Am. Chem. Soc.* **1996**, *118*, 5290-5295.
[183] R. H. He, Q. Li, A. Bach, J. O. Jensen, N. J. Bjerrum, *J. Membr. Sci.* **2006**, *277*, 38-45.
[184] S. J. Osborn, M. K. Hassan, G. M. Divoux, D. W. Rhoades, K. A. Mauritz, R. B. Moore, *Macromolecules* **2007**, *40*, 3886-3890.
[185] K. A. Page, K. M. Cable, R. B. Moore, *Macromolecules* **2005**, *38*, 6472-6484.
[186] D. Hoel, E. Grunwald, *J. Phys. Chem.* **1977**, *81*, 2135-2136.
[187] R. B. Moore, C. R. Martin, *Macromolecules* **1989**, *22*, 3594-3599.
[188] G. A. Eisman, *J. Power Sources* **1990**, *29*, 389-398.
[189] P. Millet, R. Ngameni, S. A. Grigoriev, N. Mbemba, F. Brisset, A. Ranjbari, C. Etiévant, *Int. J. Hydrogen Energy* **2010**, *35*, 5043-5052.
[190] P. W. T. Lu, S. Srinivasan, *J. Appl. Electrochem.* **1979**, *9*, 269-283.
[191] J. P. Masson, R. Molina, E. Roth, G. Gaussens, F. Lemaire, *Int. J. Hydrogen Energy* **1982**, *7*, 167-171.
[192] S. Sawada, T. Yamaki, T. Maeno, M. Asano, A. Suzuki, T. Terai, Y. Maekawa, *Prog. Nucl. Energy* **2008**, *50*, 443-448.
[193] I.-Y. Jang, O.-H. Kweon, K.-E. Kim, G.-J. Hwang, S.-B. Moon, A.-S. Kang, *J. Membr. Sci.* **2008**, *322*, 154-161.
[194] I.-Y. Jang, O.-H. Kweon, K.-E. Kim, G.-J. Hwang, S.-B. Moon, A.-S. Kang, *J. Power Sources* **2008**, *181*, 127-134.
[195] J.-Y. Woo, K.-M. Lee, B.-C. Jee, C.-H. Ryu, C.-H. Yoon, J.-H. Chung, Y.-R. Kim, S.-B. Moon, A.-S. Kang, *J. Ind. Eng. Chem.* **2010**, *16*, 688-697.
[196] G. Wei, L. Xu, C. Huang, Y. Wang, *Int. J. Hydrogen Energy* **2010**, *35*, 7778-7783.
[197] W. Xu, K. Scott, S. Basu, *J. Power Sources*, doi: 10.1016/j.jpowsour.2010.12.039
[198] S. D. Mikhailenko, J. Zaidi, S. Kaliaguine, *J. Chem. Soc., Faraday Trans.* **1998**, *94*, 1613-1618.
[199] E. Montoneri, F. J. Salzano, E. Findl, F. Kulesa, *Solid State Ionics* **1986**, *18-9*, 944-1002.
[200] S. D. Mikhailenko, S. M. J. Zaidi, S. Kaliaguine, *Catal. Today* **2001**, *67*, 225-236.
[201] M. H. D. Othman, A. F. Ismail, A. Mustafa, *J. Membr. Sci.* **2007**, *299*, 156-165.
[202] S. M. J. Zaidi, S. U. Rahman, *J. Electrochem. Soc.* **2005**, *152*, A1590-A1594.
[203] P. Krishnan, J. S. Park, C. S. Kim, *J. Membr. Sci.* **2006**, *279*, 220-229.
[204] E. Cho, J. S. Park, S. H. Park, Y. W. Choi, T. H. Yang, Y. G. Yoon, C. S. Kim, W. Y. Lee, S. B. Park, *J. Membr. Sci.* **2008**, *318*, 355-362.
[205] Y. F. Liang, X. L. Zhu, X. G. Jian, *Solid State Ionics* **2008**, *179*, 1940-1945.
[206] S. Wen, C. L. Gong, W. C. Tsen, Y. C. Shu, F. C. Tsai, *Int. J. Hydrogen Energy* **2009**, *34*, 8982-8991.
[207] J. B. Moffat, J. F. Neeleman, *J. Catal.* **1973**, *31*, 274-277.
[208] J. B. Moffat, E. E. Chao, B. Nott, *J. Colloid Interface Sci.* **1978**, *67*, 240-246.
[209] G. Gebel, P. Aldebert, M. Pineri, *Polymer* **1993**, *34*, 333-339.
[210] A. Alentiev, J. Kostina, G. Bondarenko, *Desalination* **2006**, *200*, 32-33.
[211] F. M. Collette, C. Lorentz, G. Gebel, F. Thominette, *J. Membr. Sci.* **2009**, *330*, 21-29.
[212] G. A. Olah, US Patent 5110778, **1992**.
[213] S. Strella, *J. Appl. Polym. Sci.* **1963**, *7*, 569-579.
[214] S. Strella, *J. Appl. Polym. Sci.* **1963**, *7*, 1281-1289.
[215] R. Kannan, P. P. Aher, T. Palaniselvam, S. Kurungot, U. K. Kharul, V. K. Pillai, *J. Phys. Chem. Lett.* **2010**, *1*, 2109-2113.
[216] H. L. Lin, T. L. Yu, W. K. Chang, C. P. Cheng, C. R. Hu, G. B. Jung, *J. Power Sources* **2007**, *164*, 481-487.
[217] M. Li, K. Scott, *Electrochim. Acta* **2010**, *55*, 2123-2128.
[218] K. Y. Wang, Q. Yang, T. S. Chung, R. Rajagopalan, *Chem. Eng. Sci.* **2009**, *64*, 1577-1584.
[219] S. Yu, B. C. Benicewicz, *Macromolecules* **2009**, *42*, 8640-8648.
[220] N. Xu, X. X. Guo, J. H. Fang, H. J. Xu, J. Yin, *J. Polym. Sci., Part A: Polym. Chem.* **2009**, *47*, 6992-7002.

[221] M. Han, G. Zhang, Z. Liu, S. Wang, M. Li, J. Zhu, H. Li, Y. Zhang, C. M. Lew, H. Na, *J. Mater. Chem.* **2011**, *21*, 2187-2193.
[222] H. J. Davis, N. W. Thomas (Celanese Corporation), US Patent 4020142, **1977**.
[223] M. B. Sheratte (Acurex Corporation), US Patent 4154919, **1979**.
[224] J. E. Kuder, J. C. Chen (Celanese Corporation), US Patent 4634530, **1987**.
[225] B. S. Jorgensen, J. S. Young, B. F. Espinoza, US Patent 006946015B2, **2005**.
[226] J. S. Young, G. S. Long, B. F. Espinoza (The Regents of the University of California), US Patent 006997971B1, **2006**.
[227] L. Gubler, D. Kramer, J. Belack, O. Unsal, T. J. Schmidt, G. G. Scherer, *J. Electrochem. Soc.* **2007**, *154*, B981-B987.
[228] P. R. Sukumar, W. C. Wu, D. Markova, O. Unsal, M. Klapper, K. Mullen, *Macromol. Chem. Phys.* **2007**, *208*, 2258-2267.
[229] M. J. Sansone (Celanese Corporation), US Patent 4666996, **1987**.
[230] B. Xing, O. Savadogo, *Electrochem. Commun.* **2000**, *2*, 697-702.
[231] S. C. Kumbharkar, P. B. Karadkar, U. K. Kharul, *J. Membr. Sci.* **2006**, *286*, 161-169.
[232] A. D. Modestov, M. R. Tarasevich, V. Y. Filimonov, N. M. Zagudaeva, *Electrochim. Acta* **2009**, *54*, 7121-7127.
[233] S. R. Samms, S. Wasmus, R. F. Savinell, *J. Electrochem. Soc.* **1996**, *143*, 1225-1232.
[234] A. D. Modestov, M. R. Tarasevich, A. Y. Leykin, V. Y. Filimonov, *J. Power Sources* **2009**, *188*, 502-506.
[235] H. Hou, S. Wang, Q. Jiang, W. Jin, L. Jiang, G. Sun, *J. Power Sources* **2011**, *196*, 3244-3248.
[236] J. Balej, *Int. J. Hydrogen Energy* **1985**, *10*, 233-243.
[237] E. W. Choe, D. D. Choe in *Polymeric materials encyclopedia, Vol. 7* (Ed.: J. C. Salamone), CRC Press, New York, **1996**, pp. 5619-5638.
[238] J. S. Wainright, M. H. Litt, R. F. Savinell in *Handbook of fuel cells, Vol. 3* (Eds.: W. Vielstichm, A. Lamm, H. A. Gasteiger), John Wiley & Sons Ltd., Chichester **2003**, pp. 436-446.
[239] S.-i. Kohama, J. Gong, K. Kimura, S. Yamazaki, T. Uchida, K. Shimamura, K. Kimura, *Polymer* **2008**, *49*, 1783-1791.
[240] V. I. Kasatochkin, V. V. Korshak, V. V. Kurashev, Z. S. Smutkina, T. M. Frunze, T. M. Khrenkova, *Dokl. Chem. Technol.* **1964**, *159*, 843-846.
[241] K. J. Scariah, V. N. Krishnamurthy, K. V. C. Rao, M. Srinivasan, *J. Polym. Sci., Part A: Polym. Chem.* **1987**, *25*, 2675-2687.
[242] S. M. Aharoni, *J. Appl. Polym. Sci.* **1982**, *27*, 989-995.
[243] A. B. Conciatory, E. C. Chenevey, H. D. Noether, M. Dunay, US Patent 3495931, **1970**.
[244] R. F. Savinell, J. S. Wainright, M. Litt, *Electrochem. Soc. Proc.* **1999**, *98-27*, 81-87.
[245] J. A. Asensio, S. Borros, P. Gomez-Romero, *J. Membr. Sci.* **2004**, *241*, 89-93.
[246] J. K. Gillham, *Science* **1963**, *139*, 494-495.
[247] W. F. Hwang, D. R. Wiff, C. Verschoore, G. E. Price, T. E. Helminiak, W. W. Adams, *Polym. Eng. Sci.* **1983**, *23*, 784-788.
[248] G. P. Shulman, W. Lochte, *J. Macromol. Sci., Part A: Chem.* **1967**, *A1*, 413-428.
[249] R. A. Gaudiana, R. T. Conley, *Polym. Lett.* **1969**, *7*, 793-801.
[250] R. T. Conley, J. J. Kane, S. Ghosh, Mechanism of thermal oxidation of the benzimidazole system, *Technical Report AFML-TR-71-219* **1971**.
[251] C. Arrieta, E. David, P. Dolez, T. Vu-Khanh, *Polym. Compos.* **2011**, *32*, 362-367.
[252] W. F. Hwang, D. R. Wiff, C. L. Benner, T. E. Helminiak, *J. Macromol. Sci., Phys.* **1983**, *B22*, 231-257.
[253] S. J. Krause, T. Haddock, P. G. Lenhert, J. F. Obrien, T. E. Helminiak, W. W. Adams, *J. Polym. Sci., Part B: Polym. Phys.* **1986**, *24*, 1991-2016.
[254] J. Cho, J. Blackwell, S. N. Chvalun, M. Litt, Y. Wang, *J. Polym. Sci., Part B: Polym. Phys.* **2004**, *42*, 2576-2585.
[255] S. Yu, L. Xiao, B. C. Benicewicz, *Fuel Cells* **2008**, *8*, 165-174.
[256] Z. Qi, S. Buelte, *J. Power Sources* **2006**, *161*, 1126-1132.
[257] C. Wannek, B. Kohnen, H. F. Oetien, H. Lippert, J. Mergel, *Fuel Cells* **2008**, *8*, 87-95.
[258] T. J. Schmidt, J. Baurmeister, *ECS Trans.* **2006**, *3*, 861-869.
[259] J. A. Mader, B. C. Benicewicz, *Fuel Cells* **2011**, *11*, 222-237.
[260] J. A. Mader, B. C. Benicewicz, *Macromolecules* **2010**, *43*, 6706-6715.
[261] F. J. Pinar, P. Cañizares, M. A. Rodrigo, D. Úbeda, J. Lobato, *J. Power Sources* **2011**, *196*, 4306-4313.
[262] Q. Li, J. O. Jensen in *Membranes for Energy Conversion, Vol. 2* (Eds.: K. V. Peinemann, S. P. Nunes), WILEY-VCH Verlag GmbH & Co. KGaA, Weinheim, **2008**, pp. 61-96.

9 Abbreviations

2OH-PBI – Poly(2,2´-(dihydroxy-1,4-phenylene)5,5´-bibenzimidazole)
ABPBI – Poly(2,5-benzimidazole)
AFC – Alkaline fuel cell
CL – Crosslinking
DL – Doping level
DMAc – N,N-dimethylacetamide
DMF – N,N-dimethylformamide
DMFC – Direct methanol fuel cell
DMSO – Dimethylsulfoxide
DSC – Differential scanning calorimetry
DTA – Differential thermal analysis
DVS – Divinylsulfone
EDX – Energy-dispersive X-ray spectroscopy
EGDE – Ethylene glycol diglycidyl ether
F_6-PBI – Bis(trifluoromethyl) PBI
MCFC – Molten carbonate fuel cell
MEA – Membrane electrode assembly
NMP – N-methyl-2-pyrrolidone
OCV – Open circuit voltage
O-PBI – Ether containing PBI
PA – Phosphoric acid
PAFC – Phosphoric acid fuel cell
PBI or *m*PBI – Poly[2,2´-(*m*-phenylene)-5,5´-bibenzimidazole]
PEM – Proton exchange membrane (polymer electrolyte membrane)
PEMEC – Proton exchange membrane electrolyzer cell
PEMFC – Proton exchange membrane fuel cell
PEO – Poly(ethylene oxide)
PFSA – Perfluorosulphonic acid
POD – Poly(oxadiazole)
PPA – Polyphosphoric acid
PPO – Poly(phenylene oxide), especially poly(2,6-dimethyl-1,4-phenylene oxide)
*p*PBI- Poly[2,2´-(*p*-phenylene)-5,5´-bibenzimidazole]
PSF – Polysulfone
PSSA – Poly(styrene sulfonic acid)
PTA – Phosphotungstic acid
PTFE – Poly(tetrafluoroethylene)
PVPA – Poly(vinylphosphonic acid)
RH – Relative humidity
SEM – Scanning electron microscopy
sFPAE – Sulfonated partially fluorinated arylene polyethers
sFPAES – Sulfonated partially fluorinated poly(arylene ether sulfone)
sFPSO – Sulfonated partially fluorinated poly(arylene sulfone)
SOFC – Solide oxide fuel cell
SO_2-PBI – Sulphone containing PBI
sPAE – Sulfonated poly(arylene ether)
sPAES – Sulfonated poly(arylene sulfones)

$sP(E)_nK$ – Sulphonated poly((ether)$_n$) ketone)
sPAS – Sulfonated poly(arylene thioether)
sPASS – Sulfonated poly(arylenethioethersulfone)
sPES – Sulfonated poly(ether sulfone)
sPOP – Sulfonated poly(bis(phenoxy)phosphazene)
sPPENK – Sulfonated poly(phtalazinon ether nitrile ketone)
sPSF – Sulfonated polysulfone
SSC – Short side chain
TFA – Trifluoroacetic acid
TGA – Thermogravimetric analysis

10 Appendix 1: Photographs

a. Li^+

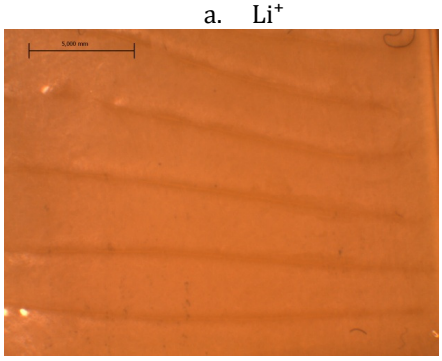

b. Na^+

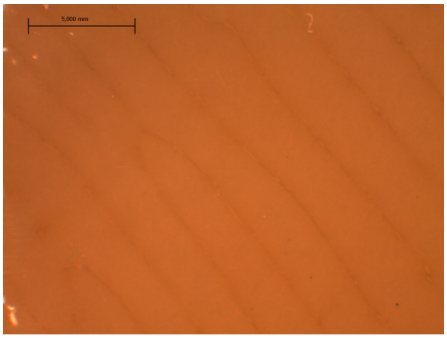

c. K^+

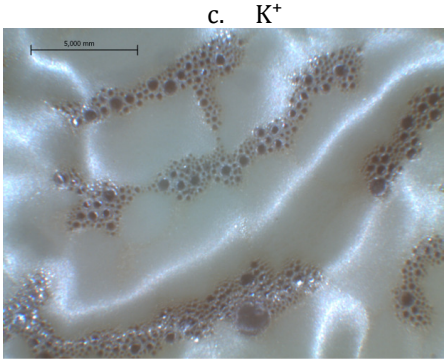

d. NH_4^+

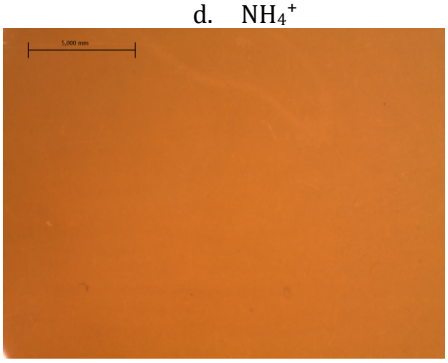

e. $N(CH_3)_4^+$

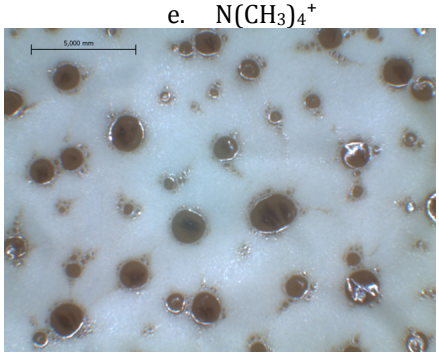

f. Rb^+

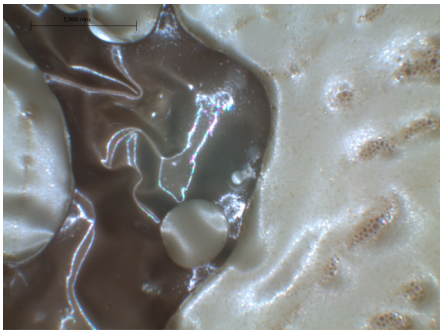

g. Cs^+

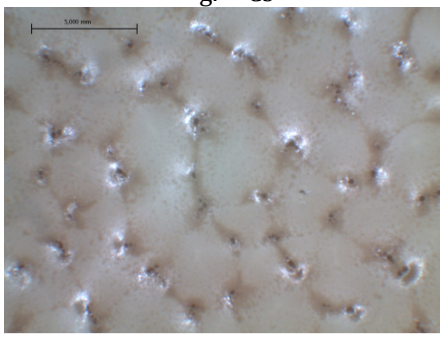

Appendix 1a *Microscope images of M088 (88 wt% Nafion® and 12 wt% PBI, Chapter 3) prepared from the Nafion® ionomers with different counter cations. The counter cations are indicated in the figure. All scale bars are 5.0 mm.*

a.

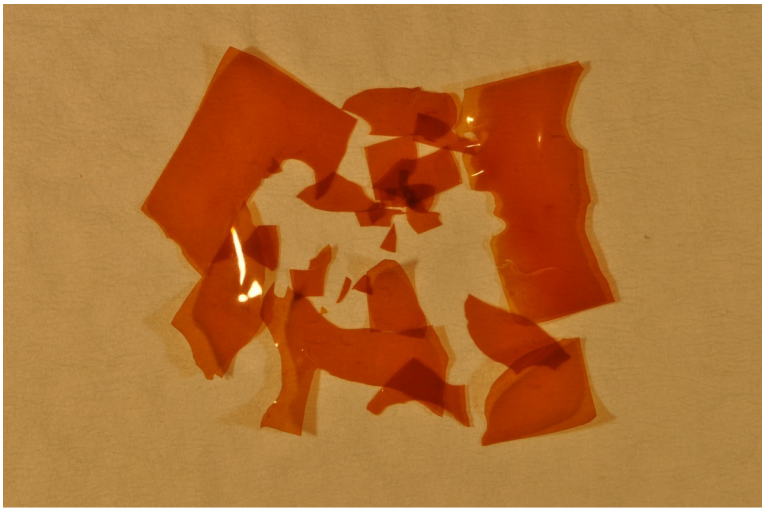

b.

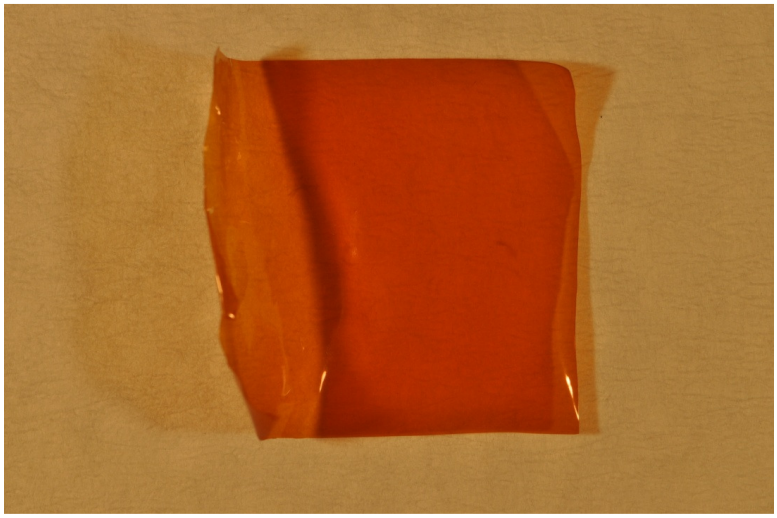

Appendix 1b *Photographs of the non-cured reference membrane 48-Ref (a) and of the membrane 48-Lo-C which had been cured at 350 °C for 16 h under argon (b) after 80 h Fenton test (Chapter 6).*

11 Appendix 2: Solid state NMR spectra

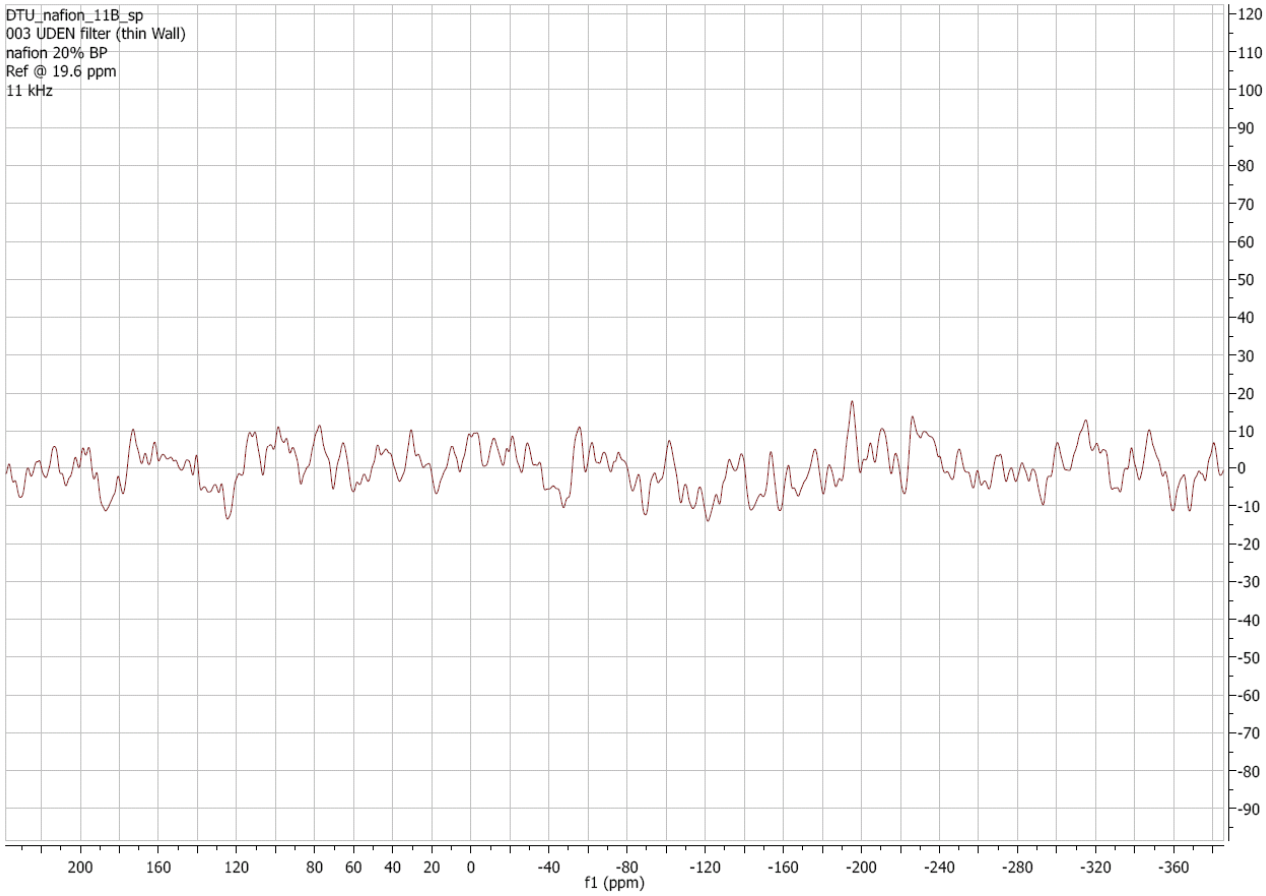

Appendix 2a *^{11}B solid state NMR spectrum of M20 (Chapter 4).*

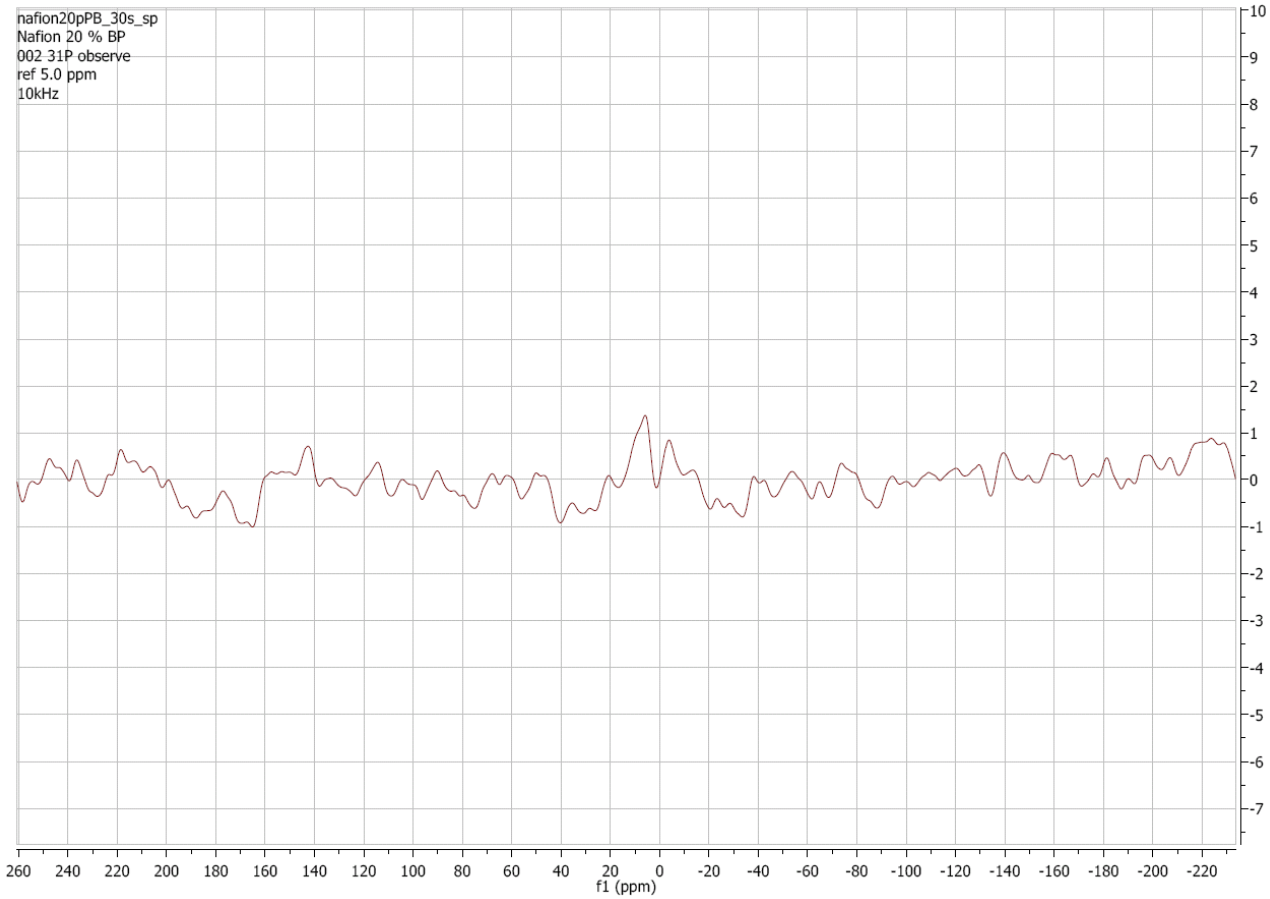

Appendix 2b *^{31}P solid state NMR spectrum of M20 (Chapter 4).*

12 Publications

I. **Phosphoric acid doped membranes based on Nafion®, PBI and their blends – Membrane preparation, characterization and steam electrolysis test**

D. Aili, M.K. Hansen, C. Pan, Q. Li, E. Christensen, J.O. Jensen, N.J. Bjerrum

Int. J. Hydrogen Energy **2011**, 36, 6985-6993

II. **Crosslinking of polybenzimidazole membranes by divinylsulfone post-treatment for high temperature proton exchange membrane fuel cell applications**

D. Aili, Q. Li, E. Christensen, J.O. Jensen, N.J. Bjerrum

Polym. Int. **2011**, 60, 1201-1207

III. **Thermal curing of PBI membranes for high temperature PEM fuel cells**

D. Aili, L.N. Cleemann, Q. Li, J.O. Jensen, E. Christensen, N.J. Bjerrum

Manuscript to be submitted to *J. Mater. Chem. (2011)*

IV. **Polybenzimidazoles – Synthesis, membranes and applications for energy conversion**

Q. Li, D. Aili, H.C. Rudbeck, J. Yang, J.O. Jensen, N.J. Bjerrum

Invited review book chapter. Manuscript to be submitted to High Performance Polymers, Nova Science Publishers, Inc. (2011)

I

Available at www.sciencedirect.com

ScienceDirect

journal homepage: www.elsevier.com/locate/he

Phosphoric acid doped membranes based on Nafion®, PBI and their blends – Membrane preparation, characterization and steam electrolysis testing

David Aili, Martin Kalmar Hansen, Chao Pan, Qingfeng Li, Erik Christensen, Jens Oluf Jensen, Niels J. Bjerrum*

Department of Chemistry, Kemitorvet 207, Technical University of Denmark, DK-2800 Lyngby, Denmark

ARTICLE INFO

Article history:
Received 9 January 2011
Received in revised form
7 March 2011
Accepted 10 March 2011
Available online 20 April 2011

Keywords:
Proton exchange membranes
Nafion®
Polybenzimidazole
Phosphoric acid
Steam electrolysis

ABSTRACT

Proton exchange membrane steam electrolysis at temperatures above 100 °C has several advantages from thermodynamic, kinetic and engineering points of view. A key material for this technology is the high temperature proton exchange membrane. In this work a novel procedure for preparation of Nafion® and polybenzimidazole blend membranes was developed. Homogeneous binary membranes covering the whole composition range were prepared and characterized with respect to chemical and physiochemical properties such as water uptake, phosphoric acid doping, oxidative stability, mechanical strength and proton conductivity. An MEA based on phosphoric acid doped Nafion® was operated at 130 °C at ambient pressure with a current density of 300 mA cm^{-2} at 1.75 V, with no membrane degradation observed during a test of 90 h. The PBI based MEAs showed better polarization curves (500 mA cm^{-2} at 1.75 V) but poor durability.

1. Introduction

Membranes of perfluorosulfonic acid (PFSA) have emerged as the state-of-the-art proton exchange membrane (PEM) material for fuel cells [1] as well as water electrolyzers [2] operating up to about 80 °C. Nafion® was developed in 1960s and is the most well known of this class of materials, consisting of a perfluorinated polymer backbone and branches with sulfonic acid terminal groups.

Nafion® has been extensively characterized with respect to its structure, properties and mechanism of proton conduction [3,4]. The proton conductivity of this material is strongly dependent on the presence of water and can reach above 0.1 S cm^{-1} under fully hydrous conditions. However, at ambient pressure the membrane dehydrates at temperatures above 80 °C, resulting in dramatic proton conductivity decay. In order to meet several technical challenges for both water electrolysers [5] and fuel cells [6], an operating temperature above 100 °C has been recognized as an attractive objective. This has resulted in an increasing demand for new PEM materials.

For PEM water electrolyzers, an elevated operating temperature offers several advantages from thermodynamic, kinetic and engineering points of view. At elevated temperatures, the electrode kinetics will be enhanced and therefore the overpotentials at both electrodes will be reduced Above 100 °C water is in the gaseous form and the electrolysis process is thermodynamically less energy demanding [7]. The reversible voltage of the water electrolysis cell is 1.23 V at room temperature (liquid) but only 1.14 V at 200 °C (steam). Of

* *Corresponding author*. Tel.: +45 45 25 23 18; fax: +45 45 88 31 36.
E-mail address: lqf@kemi.dtu.dk (Q. Li).

0360-3199/$ – see front matter
doi:10.1016/j.ijhydene.2011.03.058

course this part of the energy saving should be compensated by heat supply, which is expected to be covered by the waste heat from the cell Ohmic loss by means of e.g. evaporation and preheating of the feed water. From an engineering point of view this may further simplify the intensive cooling of the electrolyzer stacks especially when operating at higher current densities. Pressurized operation of PFSA based PEM water electrolysis systems, on the other hand, has been identified as a potential solution to improve the membrane hydration characteristics and thus the proton conductivity of the electrolyte [8,9], however at the expense of the enhance complexity of the balance of plant components [10]. The higher operational temperatures will additionally benefit the system pressurization and the subsequent gas compression.

An effective approach to improve the conductivity and the hydration characteristics of PFSA membranes at temperatures above 100 °C is to prepare composite membranes with inorganic fillers such as hygroscopic oxides (e.g. SiO_2 and TiO_2) [9,11–13], zirconium phosphates ($Zr(HPO_4)_2 \cdot nH_2O$, ZrP) [13,14], zirconium sulphophenylphosphates [15] and heteropolyacids [13]. It has also been demonstrated that the high ionic conductivity of Nafion® membranes can be maintained under dehydrating conditions if water is replaced by a less volatile proton solvent, such as ionic liquids [16] or phosphoric acid (PA) [17]. It has been shown that a PA doped Nafion® membrane exhibit proton conductivity of around 10^{-2} S cm^{-1} at 120–175 °C [17] as well as improved kinetics for the oxygen reduction reaction (ORR) in the fuel cell mode [18]. However, no successful PEM fuel cell or water electrolysis tests based on PA doped PFSA membranes have to our knowledge yet been demonstrated.

During the last 15 years, on the other hand, PA doped poly [*m*-phenylene-bis(5,5′-benzimidazole)] (PBI) has evolved as a promising PEM material for applications in fuel cells operating at temperatures of up to 200 °C [19,20]. PBI is a basic polymer with good chemical as well as thermal stability due to its rigid aromatic backbone. In PBI/PA systems the proton conductivity is strongly dependent on the acid doping level [21,22], which is defined as the number of PA molecules per repeating unit of the polymer.

Several approaches have been investigated aiming at improving the properties of PBI/PA membranes, including synthesis of PBI structure analogues [23], preparation of PBI composites [24] or covalently cross-linked structures [25,26]. Another approach is to prepare ionically cross-linked membranes from mixtures of PBI and acidic polymers like sulfonated poly(etheretherketone) [27], sulfonated polysulfone [28,29] or sulfonated partially fluorinated arylene polyethers [30,31]. Such blend membranes exhibits improved mechanical strength and chemical stability, allowing for higher acid doping levels and therefore high conductivity and better fuel cell performance. Coating of Nafion® membranes with PBI has been demonstrated as a successful approach in order to decrease the methanol permeability in Nafion® [32,33]. Wycisk et al. used the partially Na^+ cation exchanged Nafion® ionomer to prepare Nafion®/PBI blend membranes with PBI contents of up to 8 wt.% [34]. Furthermore, Zhai et al. obtained a transparent and strong film when the neutral Na^+ ionomer of Nafion® was employed for casting a Nafion®/PBI blend membrane with 80 wt.% Nafion® and 20 wt.% PBI [35]. The membrane was subsequently doped with PA and evaluated in fuel cell tests at 150 °C, showing improved durability compared with PA doped PBI membranes. However, the reported procedures for Nafion®/PBI blend membrane preparation are rather limited in terms of composition range – most likely due to miscibility problems between the two polymers.

In the present paper the miscibility of Nafion® and PBI was first investigated by using different salt forms of the Nafion® ionomer. Membranes covering the whole composition range were prepared based on the NH_4^+ cation exchanged Nafion® ionomer and characterized with respect to chemical and physiochemical properties including water uptake, PA doping, proton conductivity and thermal, mechanical and chemical stability. Based on the membranes exhibiting sufficient proton conductivity, membrane electrode assemblies (MEAs) were prepared and single cell steam electrolysis tests were conducted at 130 °C at ambient pressure.

2. Experimental

2.1. Membrane preparation

The Nafion® ionomers of Li^+, Na^+, K^+, NH_4^+, $N(CH_3)_4^+$, Rb^+ and Cs^+ were prepared by neutralization of the as received Nafion® dispersion (DuPont) with aqueous solutions of the corresponding hydroxides. After solvent evaporation at 90 °C *in vacuo*, the solid residues were collected and dissolved in dimethylacetamide (DMAc, Merck) to give a 5 wt.% solution. PBI with a number average molecular weight of 66 kDa was supplied by Danish Power Systems ApS and dissolved in DMAc to obtain a 5 wt.% solution after filtration.

The cation exchanged Nafion® ionomer solution was mixed with the PBI/DMAc solution to give polymer blends of Nafion®/PBI with weight ratios of 97/3, 94/6, 88/12, 82/18, 70/30, 40/60, 5/95. The polymer blend solutions were sonicated for 1 h, followed by casting on pre-heated Petri-dishes (95 cm^2) and drying in a pre-heated furnace at 120 °C. Pure Nafion® and PBI membranes were prepared according to the same procedure. The membranes were subsequently boiled in 0.1 M H_2SO_4 for 1 h in order to restore the H^+ form of Nafion® and finally boiled in demineralized water for 4 h. The obtained blend membranes are referred to as Mxxx according to their Nafion® content in wt.%, i.e. M088 for a blend membrane containing 88 wt.% Nafion® and 12 wt.% PBI. The pure Nafion® and PBI membranes are referred to as M100 and M000, respectively.

PA doping was achieved by soaking the membranes in 85% PA at temperatures ranging from 50 to 150 °C for at least 16 h in an open flask covered with a glass plate. The membranes were dried until a constant weight was reached at 100 °C *in vacuo* before and after acid doping. The amount of absorbed PA was calculated based on the weight gains.

2.2. Membrane characterization

Fourier Transform InfraRed (FTIR) spectra were recorded on a Perkin–Elmer 1710 Infrared Fourier Transform spectrometer under ambient atmosphere on 5–10 μm thick membrane

samples. The spectra were integrated using Spectrum 2.0 software.

Thermogravimetric analysis (TGA) was performed on a Netzsch STA 409 PC equipped with a Netzsch QMS 403 C mass spectrometer. Synthetic air was used as purge gas and the samples were heated from room temperature to 1000 °C at a rate of 10 °C min^{-1}.

For evaluation of the relative chemical stability, membrane samples (approximately 1 g) were immersed in 100 mL 3% H_2O_2 (Merck) aqueous solutions containing 4 ppm Fe(II) (added as $(NH_4)_2Fe(SO_4)_2 \cdot 6H_2O$) at 68 °C. After a certain period of time (maximum 20 h), the membrane samples were collected, rinsed with demineralized water and dried at 110 °C for at least 5 h. The dry weight was measured and the membrane samples were immersed in freshly prepared solution for continuation of the experiment. The reported results are the average numbers from two parallel measurements.

Stress-strain curves were recorded at 130 °C under ambient humidity, i.e. without humidity control at a rate of 10.00 mm min^{-1}. The equipment used was a modified universal materials testing machine (Testometric Micro 350). The membrane sample, together with grips, was contained in a metallic chamber equipped with heating elements.

Through-plane conductivity was measured by sandwiching the membrane between two gas diffusion electrodes, consisting of a layer of Pt/C catalyst and a porous carbon substrate, as described elsewhere [24]. The relative humidity was controlled by pumping water into a steam generator by means of an infusion pump and converged with an airflow into the conductivity cell. The symmetric square wave current was supplied with a frequency ranging from 6 to 7 kHz.

2.3. Electrolysis tests

The anode catalyst (IrO_2) was prepared by the Adam fusions method, as described by Marshall et al. [36] but scaled up to 10 times the amount of the precursor salt ($H_2IrCl_6 \cdot 4H_2O$). The calcination time for the salt-oxide mixture was extended to 5 h at 500 °C. The cathode catalyst (Pt/C) was prepared by chemical reduction of H_2PtCl_6 by formic acid in the presence of Vulcan XC-72R powder (Cabot) [18]. The final composition of the catalyst was 40 wt.% Pt on carbon.

The anodes were prepared for each MEA by spraying a catalyst ink directly to the gas diffusion layer (GDL). The GDL was made of a tantalum coated (Tantaline®) stainless steel felt (Swiit Metallic Fiber Co. Ltd). The catalyst was sprayed onto the substrate manually at 130 °C from an ink consisting of IrO_2, Nafion® dispersion (DuPont) and ethanol. The IrO_2 loading was around 4 mg cm^{-2}. For the cathode, a 600 cm^2 sheet was prepared by spraying the catalyst ink (Pt/C, PBI, PA and formic acid) onto a non-woven carbon cloth GDL (Freudenberg). The catalyst loading was 0.7 mg Pt cm^{-2}.

The tests were performed in a round single cell with an active electrode area of 10 cm^2. The flow pattern was an asymmetric spiral with inlet and outlet in the outer perimeter. The flow plates were made of tantalum coated stainless steel (Tantaline®) and fixed to aluminum end plates containing heating elements.

The electrolysis tests were performed at a typical cell temperature of 130 °C at ambient pressure. The steam was fed through an evaporator at 180 °C. The cell was first heated to the operating temperature before steam was supplied to the cell in order to avoid condensation of water in the cell. Current step potentiometry was performed and the steady-state potential was recorded 10 min after each current was set.

3. Results and discussion

3.1. Membrane preparation

3.1.1. Nafion®/PBI binary membranes

When Nafion® in its protonated form (Nafion®–H) was mixed with a PBI/DMAc solution, a turbid suspension was formed as a result of the instant acid-base reaction between Nafion® (pK_a −6 [37]) and PBI (pK_{aH} 5.5 [22]). A set of experiments was designed where the Nafion® counter-cation was systematically varied during membrane casting, since it is well known that polymer miscibility can be strongly dependent on the present cations [28]. Membrane composition M088 was used for the ionomer screening. The resulting membranes were subsequently evaluated according to their visual appearances as listed in Table 1.

Complete phase separation occurred during membrane casting when any of the K^+, $N(CH_3)_4^+$, Rb^+ or Cs^+ Nafion® ionomers were used. The resulting membranes had agglomerates of PBI dispersed in a continuous opaque Nafion® phase. The Na^+ and Li^+ ionomers gave transparent blend membranes. However, texture and irregularities were observed in the membranes indicating miscibility problems.

As the ion size increases from H^+, Li^+ and Na^+ to K^+, Rb^+ or Cs^+, the Lewis acidity and therefore the charge coordination ability of the cations decreases. The H^+ form of Nafion® is involved in a strong acid-base interaction with PBI forming insoluble polymeric salt from which a membrane cannot be cast. K^+, Rb^+ or Cs^+ Nafion® ionomers are non-acidic and forms stable solutions when mixed with PBI. However, phase separation occurred during membrane casting. Compared with K^+, Rb^+ and Cs^+, Li^+ and Na^+ are weakly acidic allowing for limited charge coordination.

In this context, NH_4^+ is special. It has an ionic radius similar to that of K^+ but is significantly more acidic (pK_{aH} 9.2). In addition, NH_4^+ has the inherent potential to form hydrogen

Table 1 – Visual appearances of M088 (88 wt% Nafion® and 12 wt% PBI) prepared from different cation exchanged Nafion® ionomers.

Nafion® ionomer	H^+	Li^+	Na^+	K^+	NH_4^+	$N(CH_3)_4^+$	Rb^+	Cs^+
Membrane visual appearance	Poor	Reasonable	Reasonable	Poor	Homogeneous	Poor	Poor	Poor

bonds with imine groups in the benzimidazole rings of PBI and O atoms in the sulfonic acid groups of Nafion®.

The weak acidity and the hydrogen bond formation capability of NH_4^+ facilitate the coordination between Nafion® and PBI. The interaction is not strong enough to form precipitation, which means that the polymer blends are soluble and stable in DMAc. This discussion seems supported by the observation that complete phase separation occurred during casting when the Nafion® ionomer with a completely non-acidic and aprotic cation ($N(CH_3)_4^+$) was employed.

Based on these results, blend membranes covering the whole composition range could easily be cast from the Nafion®–NH_4 ionomers. After casting, the membranes were boiled in dilute H_2SO_4 and treated with boiling water in order to wash out NH_4^+ and to restore the protonated form of Nafion® to give an ionically cross-linked blend membrane. A schematic illustration of the ionic cross-linking of the polymer blend is given in Figure 1.

The degree of ionic cross-linking was dependent on membrane composition. In M088 the amount of acidic groups in Nafion® equals the amount of basic groups in PBI, which according to Eq. (1) results in complete neutralization. 1100 corresponds to the equivalent weigh of Nafion® and 308 to the molecular weight per PBI repeating unit.

$$\text{Acidic groups per PBI repeating unit} = \left(\text{Wt. fraction Nafion}^{®}/1100\right)\Big/\left(\text{Wt. fraction PBI}/308\right) \quad (1)$$

It should be noted that each PBI repeating unit has 2 basic sites. Hence, M094, M097 and M100 membranes are acidic while M082, M060, M030, M005 and M000 have an excess of basic groups. The blend membrane casting procedure based on Nafion®–NH_4 could without modifications be scaled up to prepare 800 cm^2 homogeneous membranes throughout the whole composition range.

3.1.2. *PA doping*

PA doping was performed at temperatures ranging from 50 to 150 °C. The PA doping results are summarized in Fig. 2. The membranes with an excess of basic groups were partly soluble in phosphoric acid at temperatures higher than 50 °C. Those PBI-rich membranes displayed lower doping level at 80 °C than at 50 °C, apparently due to the loss of the polymer. The PA uptake for membrane M000 (pure PBI) doped at 50 °C corresponds to around 11 PA molecules per PBI repeating unit, whereas the PA uptake for membrane M100 (pure Nafion®) doped at 150 °C corresponds to around 5 PA molecules per sulfonic acid group. These results corresponds well with previously reported results for pristine PA doped PBI and Nafion® membranes treated under similar conditions [17,38]. A minimum in PA uptake was observed for M088, which could be explained by the complete ionic cross-linking reaction between the two polymers. The very coherent polymer matrix exhibits very high resistance to swelling. Since Nafion® is a stronger acid than PA, the ionic interaction between Nafion® and PBI will not be affected by PA and the Nafion®/PBI complex will remain intact.

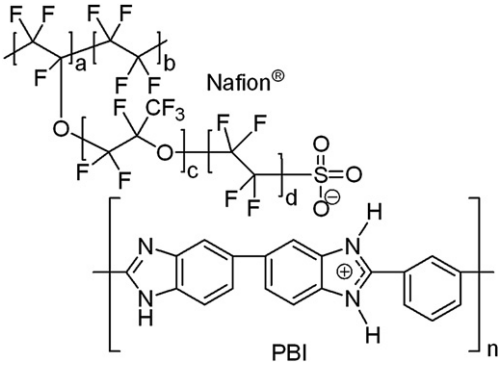

Fig. 1 – –Illustration of ionically cross-linked recast Nafion®/PBI complex.

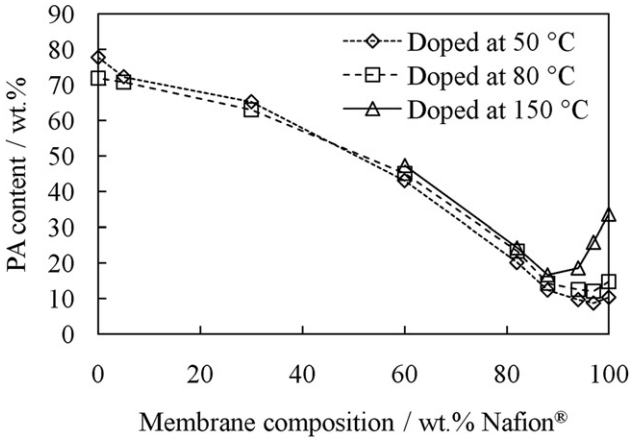

Fig. 2 – The PA uptake for Nafion®/PBI blend membranes doped in 85 % PA at different temperatures.

3.2. *FTIR spectra*

FTIR spectra were recorded for membranes covering the whole composition range (Fig. 3), and the band assignments for the two polymers are summarized in Table 2.

A broad absorption band (1100–1370 cm^{-1}) was observed for the M100 and M094 membranes, which was assigned to C–F and sulfonic acid end group stretching. Two distinct absorption peaks were developed at 1230 cm^{-1} and 1160 cm^{-1} for the neutral membrane (M088) and for the blend

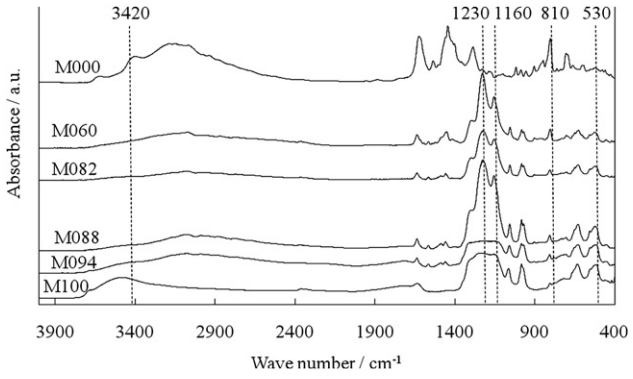

Fig. 3 – FTIR spectra for Nafion®/PBI blend membranes. The weight percentages of Nafion® in the blend membranes are indicated in the figure.

Table 2 – FTIR spectra and absorption band assignments for Nafion®, PBI and their blends.

Wave number (cm^{-1})	Assignment		
	Nafion® [40,41]	PBI [28,41]	Nafion®/PBI blends [41]
530	CF_2–O–CF_2		
640	CF_2–O–, –CF_2–		
710		Benzene ring C–H bending	
810		Benzene ring C–H bending	
980 (s)	C–F stretching (–CF(CF_3))		
	C–O–C stretch		
1070 (m)	S–O stretch		
1100–1370(s, broad)	CF_2 and CF_3 stretch, S–O stretch		
1160 (s, broad)			Ionic sulfonate
1230 (vs, broad)			Ionic sulfonate
1300 (s)		N–H	
1450 (vs)		Aromatic C–C stretch	
1630 (vs)		C=C/C=N imine stretch	
3160 (broad)		Hydrogen bonded N–H	
3420 (broad)		Non-hydrogen bonded N–H	
3500 (broad)	O–H stretch		

membranes with an excess of basic groups (M082 and M060). The appearance of these bands has previously been reported to be very sensitive to the local environment of the sulfonate group [28,39]. The changed appearance of the absorbance bands to a more distinct shape was likely due to formation of ionic sulfonate groups as a consequence of the acid-base reaction between Nafion® and PBI.

The high frequency FTIR showed an absorption band at 3420 cm^{-1} for M000 which was assigned to non-hydrogen bonded N–H stretching. It has previously been reported that this band experiences a slight red shift to lower frequencies when PBI is blended with sulfonated polysulfone, indicating a more pronounced hydrogen bonding present [28]. For the Nafion®/PBI blend membranes (M094-M060) the intensity of the 3420 cm^{-1} absorption band was very low while the 3160 cm^{-1} absorption band was still present. This indicates, just like expected, that the fraction of free non-hydrogen bonded N–H protons is very low in the Nafion®/PBI membranes since they are participating in the ionic cross-linking between the two polymers.

Two characteristic absorption peaks in the FTIR fingerprint region (810 cm^{-1} for PBI and 530 cm^{-1} for Nafion®) were chosen and integrated in order to obtain the area under the peaks. The relative areas are plotted as a function of the membrane composition in Fig. 4. A linear correlation between the relative peak intensity and blend membrane composition was observed, which confirmed the blend membrane composition homogeneity after casting and washing.

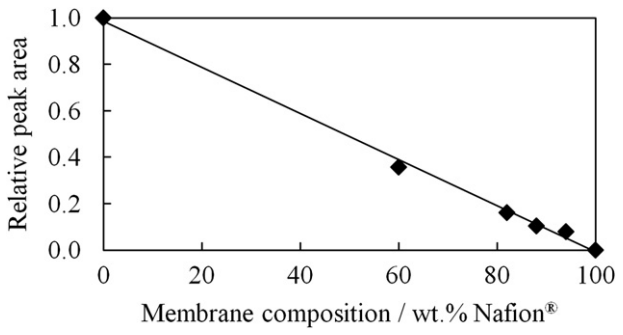

Fig. 4 – Relative peak areas for the absorption bands at 810 cm^{-1} and 530 cm^{-1} in Figure 3.

3.3. TGA

Onset temperatures of decomposition and water uptake data for non-doped membranes were obtained from TGA measurements. The water uptake was calculated from the total weight loss at 250 °C on the dry polymer basis. Water uptake data and onset temperature of the major decomposition are plotted as functions of membrane composition in Fig. 5. Mass-spectrometry confirmed that the major weight loss at temperatures of up to 250 °C was due to evaporation of water. The hydrophilicity of PBI is due to intermolecular hydrogen bonding between water and N and N–H groups in PBI [38]. In this work PBI and recast Nafion® showed water uptakes of 22% and 33%, respectively, which was in agreement with previously reported results for solution cast PBI and Nafion® 117 [42]. The water uptake decreased from 33% for M100 to around 18% for M097. It reached a minimum at the neutral composition (M088) which could possibly be explained by the lack of free hydrogen bonding sites and reduced swelling capability. Going toward

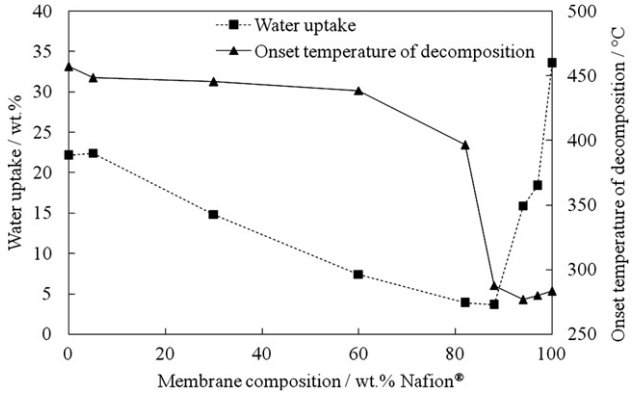

Fig. 5 – Water uptake and onset temperature of major decomposition.

higher PBI contents (membranes M082-M000) increased the amount of hydrophilic N or N–H sites available for hydrogen bond interaction with water, resulting in increased water uptake. The water uptake showed a trend that was similar to the PA uptake during membrane doping.

The onset temperature of the major decomposition was around 280 °C for the membranes with an excess of acid groups (M100-M094). At the neutral composition (M088) the onset temperature was found to be slightly higher (288 °C). For blend membranes with an excess of basic groups (M082, M060, M030, M005 and M000), the onset temperature of the major decomposition increased to above 400 °C.

3.4. *Mechanical strength*

Mechanical data at 130 °C and ambient humidity for pristine as well as PA doped membranes is summarized in Table 3. For the non-doped membranes the resistance to deformation was improved as the PBI content in the membranes increased, indicated by a Young's modulus increase from 2.9 MPa for M100 (pure Nafion®) to about 2,700 MPa for M000 (pure PBI). The engineering tensile stress at break data followed the same trend and increased gradually from about 0 for M100 to about 126 MPa for M000. This corresponds well to previously reported mechanical data for PBI membranes [43]. The measuring temperature was above the glass-transition temperature of Nafion® which explains the very poor mechanical properties for M100. The elongation at break was more than 800% for M100 and dropped to 9% for M082 and then increased to about 40% for M000. This further illustrates how the acid-base interactions between the two polymers make the polymer matrix very coherent.

Stress-strain curves were also recorded for the PA doped membranes. Membranes M100, M094, M088 and M082 were doped in 85% PA at 150 °C whereas membrane M060 and M000 were doped at 50 °C. It is well known that PBI membranes suffer from poor mechanical stability at high acid doping levels due to the plasticizing effect of PA [43]. This was also confirmed in this investigation and illustrated by a dramatic decrease in Young's modulus as well as engineering tensile stress at break and an increase in elongation at break. On the other hand, the mechanical properties for the pure recast Nafion® membrane (M100) were improved after acid doping. This could eventually be connected to a shift in the glass-transition temperature after PA doping. After acid doping, a minimum in elongation at break and a maximum in Young's modulus and stress at break were observed close to the neutral composition (M088). This could primarily be explained by the lower PA doping level for these membranes. On the other hand, the lower PA doping level for these membranes originates from the strong acid-base interaction between the two polymers.

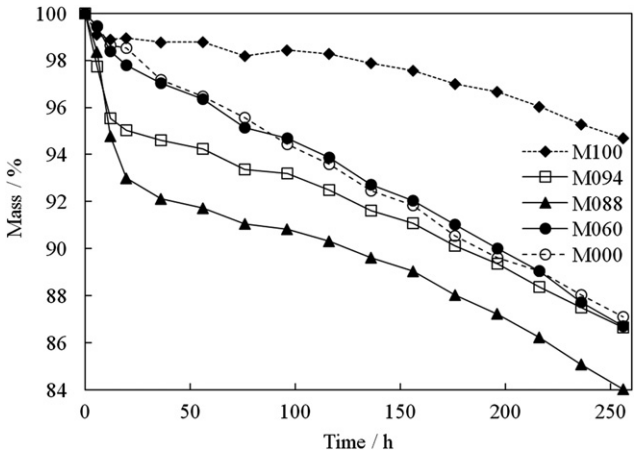

Fig. 6 – Chemical degradation expressed as the membrane remaining mass after certain durations.

3.5. *Fenton test*

The relative chemical stability of the membranes was evaluated in an accelerated degradation test (Fig. 6). The polymer samples were immersed in aqueous solutions of hydrogen peroxide (3 wt.%) and 4 ppm Fe(II) to catalyze the decomposition of hydrogen peroxide into hydroxyl radicals.

The chemical degradation mechanism of Nafion® has been subject for extensive investigation. Radical attack on the sulfonic acid end groups have been suggested as a starting point, followed by an unzipping mechanism according to Equations (2) and (3) [44].

$$-(CF_2)SO_3^- + R^\cdot \rightarrow -(CF_2)SO_3^\cdot + R^\cdot \quad (2)$$

$$-(CF_2)SO_3^\cdot \rightarrow -(CF_2)^\cdot + SO_3 \quad (3)$$

Table 3 – Summary of Young's modulus, elongation at break and engineering tensile stress at break for Nafion®/PBI blend membranes at 130 °C and ambient relative humidity. The PA contents for the doped membranes are indicated in parentheses.

Membrane	Young's modulus (MPa)		Elongation at break (%)		Engineering tensile stress at break (MPa)	
	Pristine	PA doped	Pristine	PA doped	Pristine	PA doped
M100 (34%)	2.9 ± 0.5	5.5 ± 0.8	>800	732 ± 49	≈0	2.3 ± 0.2
M094 (19%)	64.5 ± 8.7	59.0 ± 3.4	70.8 ± 9.9	192 ± 29.3	5.1 ± 0.9	3.6 ± 0.4
M088 (17%)	313 ± 12.4	200 ± 13.7	14.1 ± 2.1	19.8 ± 5.0	16.9 ± 0.3	9.1 ± 0.7
M082 (24%)	722 ± 25.6	272 ± 11.7	9.3 ± 1.7	64.5 ± 11.0	30.9 ± 2.7	13.2 ± 0.5
M060 (43%)	1596 ± 145	127 ± 15.8	16.4 ± 6.5	109 ± 8.8	68.7 ± 3.4	8.4 ± 0.6
M000 (78%)	2708 ± 510	5.8 ± 1.7	39.8 ± 8.6	113 ± 17.8	126 ± 16.9	1.8 ± 0.2

SO_3 will in turn form an adduct ($^+OH_2 \bullet SO_3^-$) with water followed by deprotonation to form sulfuric acid. SO_3 has also been reported to form zwitterionic adducts with ammonia ($^+NH_3 \bullet SO_3^-$) with low energy barrier of formation [45]. The electron donating sites in PBI may form adducts with SO_3 in the same manner as ammonia and hence promote Nafion® oxidation by shifting the reaction towards the SO_3 formation. In this way PBI could act as a catalyst for the initiation of Nafion® oxidation. This could also explain why the highest initial rate of oxidation in the Fenton test was observed for the membrane with equimolar amounts of acidic and basic groups (M088).

On the other hand Kerres et al. reported improved chemical resistance for ionically cross-linked blend membranes of PBI and sulfonated partially fluorinated arylene polyethers [30]. These contradicting results could possibly be explained by a major distinction in the degradation mechanism between Nafion® and the sulfonated partially fluorinated arylene polyethers.

3.6. *Through-plane conductivity*

The through-plane conductivity data for the PA doped membranes is shown in Fig. 7. The measurements were made at 130 °C with a relative humidity in the 16–18% range. The blend membranes with Nafion® contents of 88% (M088), 94% (M094) and 100% (M100) were doped in 85% PA at 150 °C for about 16 h, while the blend membranes with Nafion® contents of 0% (M000) and 60% (M060) were doped in 85% PA at 50 °C. The PA contents of these membranes are indicated in the figure, also as shown in Fig. 2. It should be remembered that it is not straightforward to compare these results because of the large variation of the PA content. For M000 with an acid content of 78 wt.%, corresponding to an acid doping level of around 11, the conductivity was about 0.09 S cm^{-1}. For pure Nafion® membranes with an acid content of 34 wt.%, the conductivity was found to be 0.03–0.04 S cm^{-1}. Both are in good agreement with the literature data [17,23]. For the blend membranes, the conductivity was considerably lower. This is most likely due to the low PA content, which is apparently a major contributor to the proton conductivity in the membranes. More efforts are being made to improve the acid doping of these membranes.

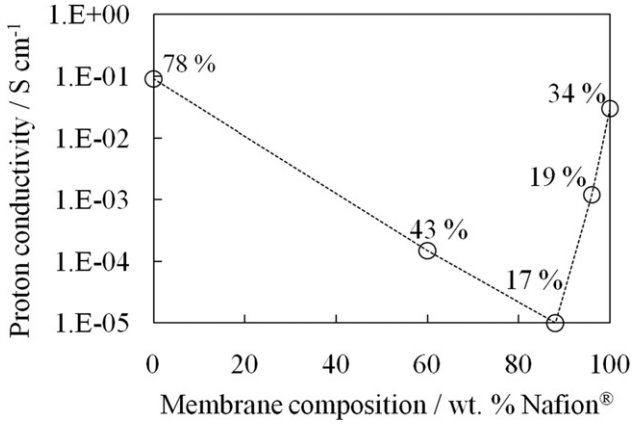

Fig. 7 – Proton conductivity of PA doped membranes at 130°C and relative humidity of 16–18%. The PA contents of the membranes are indicated in the figure.

3.7. *Electrolysis test*

It is well known that a membrane proton conductivity of at least 10^{-2} S cm^{-1} is required for high temperature PEM fuel cells in order to get a reasonable performance [20]. Consequently, this should also be valid when the cell is operated in the electrolysis mode. Based on the results from the through-plane conductivity measurements it was clear that only the pure PA doped Nafion® (M100) and PBI (M000) membranes could fulfill the conductivity requirements for the electrolyte material. Hence, the tested membranes were PBI (M000) and Nafion® (M100 and 212) doped in 85% PA at 50 °C and 150 °C, respectively. The single cells were assembled directly from anode, cathode and membrane without previous hot pressing. Fig. 8 shows a set of typical polarization curves for three cells. It can be seen that at low current densities the voltages for the three different kinds of cells were more or less identical, indicating that the major difference in the cell performance was not due to a difference in the catalytic activity of the electrodes but rather a difference in the conductivity of the membranes.

The performances of the two different Nafion® cells were more or less identical. For the MEA based on PA doped M100 the current density reached 300 mA cm^{-2} at 1.75 V. The current density was significantly higher for the PBI/PA (M000) MEA at 1.75 V (500 mA cm^{-2}). This can be compared with about 450 mA cm^{-2} at 1.75 V for a Nafion®-SiO_2 based cell, obtained at 120 °C under ambient pressure by Antonucci et al. [9]. However, poor durability was observed for the MEA based on PA doped PBI. Most of the tested PBI/PA based MEAs lasted only for a couple of hours. The durability problems were apparently connected to severe membrane failure since a decrease in the cell voltage under a constant current, accompanied by a reduction of the gas evolution (both hydrogen and oxygen) was observed. On the other hand, fuel cell durability tests with acid doped PBI membranes have been demonstrated for more than 20,000 h with a degradation rate of 5–10 μV h^{-1} [20,46]. The mechanism of PBI/PA membrane degradation under the electrolysis conditions is not understood and further efforts are being made in studies of it.

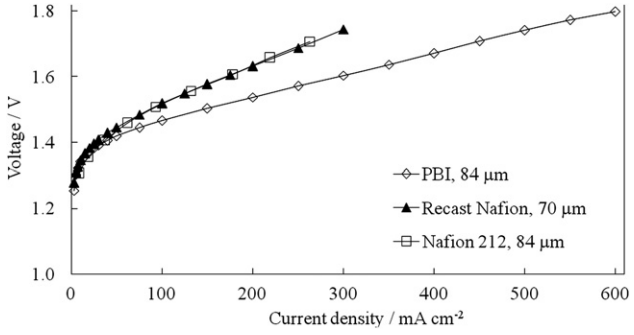

Fig. 8 – Polarization curves for steam electrolysis cells with different membranes. The type of membranes and the corresponding membrane thickness are indicated in the figure.

Nafion®/PA membranes exhibited better durability compared with PBI/PA membranes. During a continuous test of 90 h, the current density under a constant cell voltage of 1.7 V was varied with temperature and steam pumping, however, no evident membrane degradation was observed from the polarization as well as gas production at both electrodes.

Due to the insufficient proton conductivity of the blend membranes, polarization curves could not be recorded for the MEAs based on these membranes. Work is in progress to optimize the acid doping procedure in order to improve proton conductivity and the cell performance for steam electrolysis .

4. Conclusions

A novel procedure for solution casting of homogeneous Nafion®/PBI blend membranes was developed based on the Nafion®–NH_4 salt form. The moderate acidity of NH_4^+ in combination with its inherent ability to form hydrogen bonds prevented Nafion®/PBI phase separation during membrane casting. The homogeneity of the blend membranes through the whole composition range was confirmed by FTIR. FTIR further indicated a decreased fraction of non-hydrogen bonded N–H groups in the Nafion®/PBI blend membranes. The water uptake and the onset temperature of polymer decomposition of the blend membranes showed a strong dependence on the composition of the binary blend membranes, with a minimum at around 88 wt.% Nafion® and 12 wt.% PBI, where the complete neutralization occurs between the acidic Nafion® and basic PBI. Mechanical strength at 130 °C, i.e. the Young's modulus and tensile stress at break, of the non-doped blend membranes showed a gradual increase as the PBI content increased. The composition corresponding to the neutral blend membrane showed the highest weight loss as well as the highest initial rate of weight loss in the Fenton test. This indicated a chemical incompatibility between the two polymers in the oxidizing environment. The PA uptake during doping was strongly dependent on the membrane composition, exhibiting a minimum for the neutral blend membrane. A similar trend was observed for the water uptake of the pristine blend membranes and the proton conductivity of the PA doped membranes. Preliminary steam electrolysis tests were made at 130 °C, showing reasonable performance and stability for MEAs based on PA doped Nafion® membranes.

Acknowledgments

Danish Power Systems ApS is thanked for providing PBI. Financial supports are acknowledged from the European Commission within the 7th Framework Programme (WELTEMP project 212903) and the Danish Council for Strategic Research (HyCycle).

REFERENCES

[1] Banerjee S, Curtin DE. Nafion® perfluorinated membranes in fuel cells. J Fluorine Chem 2004;125:1211–6.

[2] Millet P, Andolfatto F, Durand R. Design and performance of a solid polymer electrolyte water electrolyzer. Int J Hydrogen Energy 1996;21:87–93.

[3] Heitner-Wirguin C. Recent advances in perfluorinated ionomer membranes: structure, properties and applications. J Memb Sci 1996;120:1–33.

[4] Mauritz KA, Moore RB. State of understanding of Nafion. Chem Rev 2004;104:4535–85.

[5] Linkous CA, Anderson HR, Kopitzke RW, Nelson GL. Development of new proton exchange membrane electrolytes for water electrolysis at higher temperatures. Int J Hydrogen Energy 1998;23:525–9.

[6] Li Q, He R, Jensen JO, Bjerrum NJ. Approaches and recent development of polymer electrolyte membranes for fuel cells operating above 100 °C. Chem Mater 2003;15:4896–915.

[7] Hauch A, Ebbesen SD, Jensen SH, Mogensen M. Highly efficient high temperature electrolysis. J Mater Chem 2008;18:2331–40.

[8] Millet P, Dragoe D, Grigoriev S, Fateev V, Etievant C. GenHyPEM: a research program on PEM water electrolysis supported by the European commission. Int J Hydrogen Energy 2009;34:4974–82.

[9] Antonucci V, Di Blasi A, Baglio V, Ornelas R, Matteucci F, Ledesma-Garcia J, et al. High temperature operation of a composite membrane-based solid polymer electrolyte water electrolyser. Electrochim Acta 2008;53:7350–6.

[10] Grigoriev SA, Millet P, Korobtsev SV, Porembskiy VI, Pepic M, Etievant C, et al. Hydrogen safety aspects related to high-pressure polymer electrolyte membrane water electrolysis. Int J Hydrogen Energy 2009;34:5986–91.

[11] Antonucci PL, Arico AS, Creti P, Ramunni E, Antonucci V. Investigation of a direct methanol fuel cell based on a composite Nafion®-silica electrolyte for high temperature operation. Solid State Ionics 1999;125:431–7.

[12] Watanabe M, Uchida H, Seki Y, Emori M, Stonehart P. Self-humidifying polymer electrolyte membranes for fuel cells. J Electrochem Soc 1996;143:3847–52.

[13] Alberti G, Casciola M. Composite membranes for medium-temperature PEM fuel cells. Annu Rev Mater Res 2003;33:129–54.

[14] Costamagna P, Yang C, Bocarsly AB, Srinivasan S. Nafion® 115/zirconium phosphate composite membranes for operation of PEMFCs above 100 °C. Electrochim Acta 2002;47:1023–33.

[15] Alberti G, Casciola M, Pica M, Tarpanelli T, Sganappa M. New preparation methods for composite membranes for medium temperature fuel cells based on precursor solutions of insoluble inorganic compounds. Fuel Cells 2005;5:366–74.

[16] Doyle M, Choi SK, Proulx G. High-temperature proton conducting membranes based on perfluorinated ionomer membrane-ionic liquid composites. J Electrochem Soc 2000;147:34–7.

[17] Savinell R, Yeager E, Tryk D, Landau U, Wainright J, Weng D, et al. A polymer electrolyte for operation at temperatures up to 200 °C. J Electrochem Soc 1994;141:L46–48.

[18] Li Q, Hjuler HA, Bjerrum NJ. Oxygen reduction on carbon supported platinum catalysts in high temperature polymer electrolytes. Electrochim Acta 2000;45:4219–26.

[19] Wainright JS, Wang JT, Weng D, Savinell RF, Litt M. Acid-doped polybenzimidazoles – a new polymer electrolyte. J Electrochem Soc 1995;142:L121–123.

[20] Li Q, Jensen JO, Savinell RF, Bjerrum NJ. High temperature proton exchange membranes based on polybenzimidazoles for fuel cells. Prog Polym Sci 2009;34:449–77.

[21] He R, Li Q, Jensen JO, Bjerrum NJ. Doping phosphoric acid in polybenzimidazole membranes for high temperature proton exchange membrane fuel cells. J Polym Sci Part A Polym Chem 2007;45:2989–97.

[22] Ma YL, Wainright JS, Litt MH, Savinell RF. Conductivity of PBI membranes for high-temperature polymer electrolyte fuel cells. J Electrochem Soc 2004;151:A8–16.
[23] Li Q, Rudbeck HC, Chromik A, Jensen JO, Pan C, Steenberg T, et al. Properties, degradation and high temperature fuel cell test of different types of PBI and PBI blend membranes. J Memb Sci 2010;347:260–70.
[24] He R, Li Q, Xiao G, Bjerrum NJ. Proton conductivity of phosphoric acid doped polybenzimidazole and its composites with inorganic proton conductors. J Memb Sci 2003;226:169–84.
[25] Li Q, Pan C, Jensen JO, Noyé P, Bjerrum NJ. Cross-linked polybenzimidazole membranes for fuel cells. Chem Mater 2007;19:350–2.
[26] Noyé P, Li Q, Pan C, Bjerrum NJ. Cross-linked polybenzimidazole membranes for high temperature proton exchange membrane fuel cells with dichloromethyl phosphinic acid as a cross-linker. Polym Adv Technol 2008; 19:1270–5.
[27] Kerres J, Ullrich A, Meier F, Häring T. Synthesis and characterization of novel acid-base polymer blends for application in membrane fuel cells. Solid State Ionics 1999; 125:243–9.
[28] Deimede V, Voyiatzis GA, Kallitsis JK, Li Q, Bjerrum NJ. Miscibility behavior of polybenzimidazole/sulfonated polysulfone blends for use in fuel cell applications. Macromolecules 2000;33:7609–17.
[29] Hasiotis C, Li Q, Deimede V, Kallitsis JK, Kontoyannis CG, Bjerrum NJ. Development and characterization of acid-doped polybenzimidazole/sulfonated polysulfone blend polymer electrolytes for fuel cells. J Electrochem Soc 2001;148: A513–519.
[30] Kerres J, Schönberger F, Chromik A, Häring T, Li Q, Jensen JO, et al. Partially fluorinated arylene polyethers and their ternary blend membranes with PBI and H_3PO_4. Part I. Synthesis and characterisation of polymers and binary blend membranes. Fuel Cells 2008;8:175–87.
[31] Li Q, Jensen JO, Pan C, Bandur V, Nilsson MS, Schönberger F, et al. Partially fluorinated arylene polyethers and their ternary blends with PBI and H_3PO_4. Part II. Characterisation and fuel cell tests of the ternary membranes. Fuel Cells 2008;8:188–99.
[32] Hobson LJ, Nakano Y, Ozu H, Hayase S. Targeting improved DMFC performance. J Power Sources 2002;104:79–84.
[33] Ainla A, Brandell D. Nafion®-polybenzimidazole (PBI) composite membranes for DMFC applications. Solid State Ionics 2007;178:581–5.
[34] Wycisk R, Chisholm J, Lee J, Lin J, Pintauro PN. Direct methanol fuel cell membranes from Nafion-polybenzimidazole blends. J Power Sources 2006;163:9–17.
[35] Zhai YF, Zhang HM, Zhang Y, Xing DM. A novel H_3PO_4/Nafion-PBI composite membrane for enhanced durability of high temperature PEM fuel cells. J Power Sources 2007;169:259–64.
[36] Marshall A, Borresen B, Hagen G, Tsypkin M, Tunold R. Preparation and characterisation of nanocrystalline $Ir_xSn_{1-x}O_2$ electrocatalytic powders. Mater Chem Phys 2005; 94:226–32.
[37] Yang YS, Siu A, Peckham TJ, Holdcroft S. Structural and morphological features of acid-bearing polymers for PEM fuel cells. In: Scherer GG, editor. Adv polym sci. Berlin Heidelberg: Springer Verlag; 2008. p. 55–126.
[38] Li Q, He R, Berg RW, Hjuler HA, Bjerrum NJ. Water uptake and acid doping of polybenzimidazoles as electrolyte membranes for fuel cells. Solid State Ionics 2004;168:177–85.
[39] Lu XY, Weiss RA. Specific interactions and ionic aggregation in miscible blends of nylon-6 and zinc sulfonated polystyrene ionomer. Macromolecules 1992;25:6185–9.
[40] Liang ZX, Chen WM, Liu JG, Wang SL, Zhou ZH, Li WZ, et al. FT-IR study of the microstructure of Nafion® membrane. J Memb Sci 2004;233:39–44.
[41] Section 9: molecular structure and spectroscopy. Infrared correlation charts. In: Lide DR, editor. CRC handbook of chemistry and physics. 90th ed. Boca Raton, FL: CRC Press/ Taylor and Francis; 2010. Internet version.
[42] Li Q, Hjuler HA, Bjerrum NJ. Phosphoric acid doped polybenzimidazole membranes: physiochemical characterization and fuel cell applications. J Appl Electrochem 2001;31:773–9.
[43] He R, Li Q, Bach A, Jensen JO, Bjerrum NJ. Physicochemical properties of phosphoric acid doped polybenzimidazole membranes for fuel cells. J Memb Sci 2006;277:38–45.
[44] Endoh E. Highly durable PFSA membranes. In: Vielstich W, Yokokawa H, Gasteiger HA, editors. Handbook of fuel cells – fundamentals, technology and applications. Chichester: Wiley; 2009. p. 361–74.
[45] Canagaratna M, Phillips JA, Goodfriend H, Leopold KR. Structure and bonding of the sulfamic acid zwitterion: microwave spectrum of $^{+}H_3N{-}SO_3^{-}$. J Am Chem Soc 1996; 118:5290–5.
[46] Schmidt TJ, Baurmeister J. Properties of high-temperature PEFC Celtec®-P 1000 MEAs in start/stop operation mode. J Power Sources 2008;176:428–34.

II

Research Article

Received: 24 September 2010 Revised: 15 November 2010 Accepted: 1 December 2010 Published online in Wiley Online Library: 28 March 2011

(wileyonlinelibrary.com) DOI 10.1002/pi.3063

Crosslinking of polybenzimidazole membranes by divinylsulfone post-treatment for high-temperature proton exchange membrane fuel cell applications

David Aili, Qingfeng Li,* Erik Christensen, Jens Oluf Jensen and Niels J Bjerrum

Abstract

Phosphoric acid-doped polybenzimidazole (PBI) has been suggested as a promising electrolyte for proton exchange membrane fuel cells operating at temperatures up to 200 °C. This paper describes the development of a crosslinking procedure for PBI membranes by post-treatment with divinylsulfone. The crosslinking chemistry was studied and optimized on a low-molecular-weight model system and the results were used to optimize the crosslinking conditions of PBI membranes. The crosslinked membranes were characterized with respect to chemical and physiochemical properties, showing improved mechanical strength and oxidative stability compared with their linear analogues. Fuel cell tests were further conducted in order to demonstrate the feasibility of the crosslinked membranes.

Keywords: polybenzimidazole; divinylsulfone; crosslinking; proton exchange membranes; fuel cells

INTRODUCTION

The conventional proton exchange membrane (PEM) fuel cell technology is based on perfluorosulfonic acid (PFSA) membranes, e.g. DuPont's Nafion®, as electrolytes.[1] The proton conductivity of PFSA membranes is strongly dependent on the presence of water which limits the operating temperature to around 80 °C for ambient pressure systems.

An operating temperature above 100 °C has been suggested as a promising solution to meet several technical and system engineering challenges for PEM fuel cells.[2] Improved electrocatalyst CO tolerance,[3] simplified water management and cooling systems as well as better possibilities for heat recovery[4] are some of the main arguments for an elevated operating temperature, as recently reviewed.[5] The aim for a higher PEM fuel cell operating temperature has resulted in an increased demand for new electrolyte materials.

Phosphoric acid (PA) doped poly[*m*-phenylene-bis(5,5′-benzimidazole)] (PBI) membranes were first suggested as electrolyte for PEM fuel cells operating at temperatures of up to 200 °C by Wainright *et al*. in 1995.[6] PA/PBI electrolytes have received much attention since then and have been extensively characterized.[5,7,8] PA/PBI membranes exhibit good thermal, mechanical and chemical stability and can maintain proton conductivity in the region of 10^{-2} S cm^{-1} under anhydrous conditions. The molecular weight of one PBI repeat unit (PBI_{RU}) is 308 g mol^{-1} and the structure is shown in Fig. 1.

PBI can be doped with PA either by soaking a solution-cast PBI membrane in a PA solution[9] or by casting a membrane directly from a polyphosphoric acid polycondensation solvent according to a sol–gel procedure developed by Xiao *et al*.[10] The conductivity of PA-doped PBI is strongly dependent on the acid doping level,[7,9] which is defined as the number of PA molecules per PBI_{RU}. Alkaline-doped PBI membranes have also been suggested as electrolytes for PEM fuel cells,[11] but have not been as extensively investigated as PA-doped PBI membranes.

Much research effort has been devoted to the improvement of, for example, mechanical properties or proton conductivity of PBI membranes by fibre reinforcement[12] or by the preparation of composite membranes with porous polytetrafluoroethylene[13] or inorganic fillers.[14]

Crosslinking has also been suggested as one way to tailor the properties of PBI membranes. Ionically crosslinked blend membranes of PBI and partially fluorinated and sulfonated arylene polyethers have recently been reported to exhibit improved chemical stability compared with pristine PBI and to have sufficient mechanical strength for membrane electrode assembly (MEA) preparation even at PA doping levels as high as 10–13.[15–17] Dichloro-*p*-xylene has been used for the preparation of crosslinked PBI nanofiltration membranes.[18,19] Recently, dibromo-*p*-xylene[20] and dichloromethylphosphinic acid[21] were demonstrated to crosslink PBI after heat treatment at temperatures of up to

* *Correspondence to: Qingfeng Li, Department of Chemistry, Kemitorvet 207, Technical University of Denmark, DK-2800 Lyngby, Denmark. E-mail: lqf@kemi.dtu.dk*

Department of Chemistry, Kemitorvet 207, Technical University of Denmark, DK-2800 Lyngby, Denmark

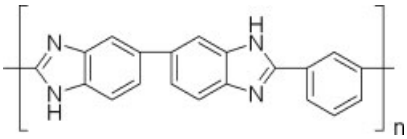

Figure 1. Chemical structure of PBI repeat unit.

300 °C. Pendant amino groups on the PBI backbone were recently introduced and used as handles for further crosslinking reactions.[22] Additionally, several patents describing PBI functionalization or crosslinking procedures for varying applications have been granted over the years.[23–29] Divinylsulfone (DVS) was first suggested as a crosslinking agent for PBI in a US patent filed in 1987.[29] The crosslinking reaction was assumed to be a Michael-type addition and alkali metal alkoxides or quaternary ammonium hydroxides were employed as catalysts. However, little detailed investigation of the covalent crosslinking chemistry has yet been reported and generally complete reaction between the crosslinker and two active sites of the polymer is assumed when the degree of crosslinking is calculated.

In this paper we describe a novel procedure for crosslinking PBI membranes by post-treatment with DVS. A low-molecular-weight model system was designed in order to optimize the polymer membrane post-treatment conditions. The crosslinked PBI membranes were characterized with respect to chemical and physiochemical properties and tested in fuel cells.

EXPERIMENTAL

Model system reaction

All chemicals were used as received without further purification. The reactions were performed under ambient atmosphere. NMR spectra were recorded on a Varian Mercury 300 spectrometer, using deuterated dimethylsulfoxide (DMSO-d_6) as solvent. The chemical shifts are given in ppm relative to the solvent residual peaks at 2.50 ppm (^{1}H NMR) and 39.52 ppm (^{13}C NMR). Assignments were accomplished by coupling pattern and integrals. Thin-layer chromatography (TLC) was performed using Merck pre-coated aluminium TLC plates coated with silica gel 60 F_{254}, visualized in UV light (254 nm). Flash column chromatography was carried out with silica gel (0.04–0.063 mm) for purification of products. Evaporation and concentration refers to the use of a rotary evaporator under reduced pressure. The reported yields are isolated yields.

Reaction in MeOH

Benzimidazole (359.8 mg, 3.05 mmol (Table 1, entry 1); 358.8 mg, 3.04 mmol (Table 1, entry 2)) was dissolved in MeOH (20 mL). DVS (174.8 mg, 1.48 mmol (Table 1, entry 1); 353.1 mg, 2.99 mmol (Table 1, entry 2)) was added at room temperature under stirring. After stirring at 50 °C for 70 h, the reaction mixture was concentrated and purification was achieved using flash column chromatography (SiO_2; 19 : 1 CH_2Cl_2:MeOH) to give product **1** as a white solid (R_f = 0.27) and product **2a** as a colourless oily liquid (R_f = 0.33). The yields are listed in Table 1.

Reaction in aqueous KOH

Benzimidazole (379.5 mg, 3.21 mmol) was dissolved in 1 mol L^{-1} aqueous KOH (20 mL). DVS (187.3 mg, 1.59 mmol) was added at room temperature, resulting in instant precipitation of a white solid. The reaction mixture was further stirred at room temperature for 1 h. Product **1** was isolated from the mother liquor as a white solid (153.9 mg, 27%) by filtration.

Table 1. Yields and products of the model system reaction in MeOH

Entry	Benzimidazole (eq.)	DVS (eq.)	Yield (**1**)	Yield (**2a** + trace amounts of **2b**)
1	1	0.5	83%	7%
2	1	1	36%	58%

NMR spectral data

1-[2-(2-(1*H*-benzimidazoyl)ethanesulfonyl)ethyl]-1*H*-benzoimidazole (**1**). ^{1}H NMR (300 MHz, DMSO-d_6; δ, ppm): 8.21 (2H, s), 7.64 (2H, dd, J = 7.8, 0.9 Hz), 7.57 (2H, dd, J = 7.2, 1.2 Hz), 7.23 (4H, m), 4.69 (4H, t, J = 7.0 Hz), 3.77 (4H, t, J = 7.0 Hz). ^{13}C NMR (75 MHz, DMSO-d_6; δ, ppm): 145.9, 144.0, 134.0, 123.2, 122.4, 120.2, 111.1, 52.2, 49.9.

1-[2-(2-Methoxyethanesulfonyl)ethyl]-1*H*-benzoimidazole (**2a**). ^{1}H NMR (300 MHz, DMSO-d_6; δ, ppm): 8.23 (1H, s), 7.65 (1H, dd, J = 8.4, 0.6 Hz), 7.61 (1H, dd, J = 7.8, 0.9 Hz), 7.24 (2H, m), 4.69 (2H, t, J = 6.6 Hz), 3.68 (2H, t, J = 6.6 Hz), 3.66 (2H, t, J = 5.1 Hz), 3.41 (2H, t, J = 5.1 Hz), 3.21 (3H, s). ^{13}C NMR (75 MHz, DMSO-d_6; δ, ppm): 145.0, 144.1, 134.0, 123.1, 122.4, 120.2, 111.0, 66.1, 58.8, 53.4, 49.9, 38.2.

Membrane preparation and PA doping

PBI powder with a weight-average molecular weight of 44 kDa (intrinsic viscosity) was supplied by Danish Power Systems A/S. The PBI powder was dissolved in dimethylacetamide (DMAc) at 80 °C to give a 5 wt% solution after filtering. PBI membranes were cast from the PBI/DMAc solution on a glass substrate and dried at temperatures of up to 120 °C. The residual solvent was removed by boiling the membranes in water and MeOH for several hours followed by drying at 200 °C for at least 15 h. The dry membranes were weighed and soaked in MeOH with a fixed PBI : MeOH mass ratio, followed by addition of varying amounts of DVS to give DVS : PBI_{RU} molar ratios of 0, 1, 5 and 10. The reaction mixtures were stirred at 50 °C for 70 h and the membranes were thereafter treated with boiling water and then MeOH for several hours, followed by drying at 200 °C and weighing. From the weight gains the apparent degrees of crosslinking were calculated. PA doping of the pristine and crosslinked PBI membranes was achieved by soaking the membranes in 85% PA at various temperatures and for various durations.

Elemental analysis

Elemental analysis (H, N, C, S) was performed on three parallel samples by Mikroanalytisches Laboratorium, Universität Wien.

Fourier transform infrared (FTIR) spectra

FTIR spectra were recorded on a PerkinElmer 1710 spectrometer under ambient atmosphere. The membranes were pre-dried at 200 °C for 20 h.

Thermogravimetric analysis

TGA was performed using a Netzsch STA 409 PC equipped with a Netzsch QMS 403 C mass spectrometer. Synthetic air was used as the purge gas and the samples were heated to 1000 °C at a heating rate of 10 °C min^{-1}.

Chemical stability

Membrane samples (30–40 μm thick) were immersed in a 3% H_2O_2 (Merck) aqueous solution containing 4 ppm Fe(II) (added as $(NH_4)_2Fe(SO_4)_2{\cdot}6H_2O$) at 68 °C. Every 20 h, the membrane samples were collected, rinsed with demineralized water and dried at 120 °C for at least 5 h. The dry weight was measured and the membrane samples were immersed in freshly prepared Fenton solution for continuation of the tests.

Mechanical strength

Stress–strain curves were recorded using a modified universal materials testing machine (Testometric Micro 350) at a rate of 10.00 mm min^{-1}. The membrane samples, together with grips, were contained in a metallic chamber equipped with heating elements.

In-plane proton conductivity

In-plane conductivity was measured at 150 and 180 °C as a function of relative humidity at ambient pressure. The measurements were carried out using a four-probe conductivity cell. A symmetric square wave current in the frequency range 5–10 kHz was applied through platinum foils and the voltage drop was measured via platinum probes fixed at a distance of 1.0 cm apart. The PA-doped membrane samples were pre-dried at 180 °C for 2 h before the dimensions were measured.

Fuel cell tests

A platinum catalyst (40 wt% Pt) supported on carbon black (Vulcan 72R, Cobat) was prepared using a solution reduction method. The catalyst powders were dispersed in a mixture of formic acid, PA and PBI (0.5 wt% PBI). The ink was sonicated for 30 min and sprayed onto non-woven gas diffusion layers (carbon cloth). On the final gas diffusion electrodes the platinum loading was about 0.7 mg Pt cm^{-2}. The PBI loading was about 0.14 mg cm^{-2}, and the catalyst layer was doped with PA at a level of 1.2 mg cm^{-2}. Pristine and crosslinked (8% apparent crosslinking) PBI membranes (70 μm thick) were doped in 85% PA at 20 and 50 °C, respectively, for at least 24 h to give acid doping levels of about 10. The membranes were sandwiched between two pieces of gas diffusion electrodes and hot-pressed under a pressure of about 10 MPa for 10 min. The hot-pressing temperature was 150 °C for non-crosslinked PBI. For crosslinked PBI, the acid-doped membranes were stiffer (with much higher Young's modulus); the hot-pressing temperature was therefore elevated to 200 °C with no systematic optimization. The size of the active electrode area of the MEAs was 4 cm^2. Dry hydrogen and air at flow rates of 100 and 200 mL min^{-1}, respectively, were supplied to the fuel cell without pre-humidification. These gas flow rates were much higher than the stoichiometry even at the maximum current measured. In this way the fuel cell test was performed in order to evaluate the materials but not to optimize the cell operation. Polarization curves were obtained using a current step potentiometer with the steady-state potential recorded 2 min after each current was set.

RESULTS AND DISCUSSION

Model system reaction in MeOH

A low-molecular-weight model system reaction was designed in order to study the linking of benzimidazole groups with DVS in detail (Scheme 1). When benzimidazole is reacted with DVS in stoichiometric amount the reaction proceeds smoothly and the desired product **1** is formed in 83% yield (Table 1, entry 1). When DVS is added in excess (Table 1, entry 2), **2a** is the major product and is isolated in 58% yield. This indicates that grafting of 2-methoxyethanesulfonyl groups could be favoured instead of crosslinking if a PBI membrane is post-treated with excess DVS. In this reaction the solvent competes with benzimidazole as nucleophile, and it is likely that the reaction with benzimidazole goes via a dimethoxylated sulfone intermediate, followed by a substitution reaction. However, it must be kept in mind that the model system reaction is very different from the PBI membrane post-treatment reaction. The local concentration of benzimidazole units in a PBI membrane is far higher than it is in the model system reaction, and the degrees of freedom are very much limited in the membrane.

Reaction in aqueous base

When a stoichiometric amount of DVS is added to benzimidazole in aqueous KOH, product **1** is formed and precipitates from the mother liquor in 27% yield after 1 h at room temperature. PBI doped with KOH has previously been demonstrated to exhibit ionic conductivity in the region of 10^{-2} S cm^{-1},[11] which makes it an interesting electrolyte for alkaline PEM fuel cell applications. The results from the alkaline model system reaction indicate that it could be possible to combine an operationally simple and fast post-crosslinking procedure for PBI membranes with alkaline doping for fuel cell applications. This is, however, out of the scope of the present work.

Post-crosslinking of PBI membrane

A schematic of the crosslinking procedure by post-treatment is shown in Scheme 2. After the post-treatment with DVS, the membranes are visually homogeneous and insoluble in DMAc at 80 °C. From the weight gains after the DVS treatment the weight percentages of sulfur in the membranes were calculated. As seen from Table 2, the calculated results are in good agreement with the sulfur contents determined by elemental analysis.

It is likely that membranes treated with DVS contain a certain amount of graft 2-methoxyethanesulfonyl groups together with crosslinks. The risk for grafting is also confirmed in the model system investigation when DVS is added in excess. Hence, the apparent degree of crosslinking calculated from the membrane weight gain could be different from the real degree of crosslinking. In Fig. 2(a) the apparent degree of crosslinking after the DVS treatment of a 30 μm thick PBI membrane is plotted *versus* the initial DVS : PBI_{RU} molar ratios. At a DVS : PBI_{RU} ratio of 1, the degree of crosslinking would be 100% by assuming complete reaction between one DVS molecule and two PBI reactive sites, which would give the membrane a weight gain of 38%. The measured weight gain after the DVS treatment is, however, 2.1%. This corresponds to an apparent degree of crosslinking of 11%, as shown in Fig. 2(a). The fraction of the graft 2-methoxyethanesulfonyl is unknown, which obviously would be higher at higher initial DVS : PBI_{RU} molar ratios.

It is well known that PBI membranes are dense and exhibit very low gas permeability.[30] During the post-treatment the reaction between DVS and PBI should start on the membrane surface and the obtained apparent degree of crosslinking would therefore be dependent on the membrane thickness. This was studied by treating a set of membranes with varying thicknesses in a solution with an initial DVS : PBI_{RU} molar ratio of 1 (Fig. 2(b)). It reveals

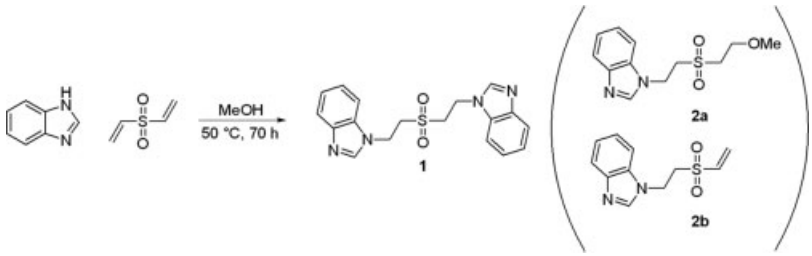

Scheme 1. Model system reaction in MeOH.

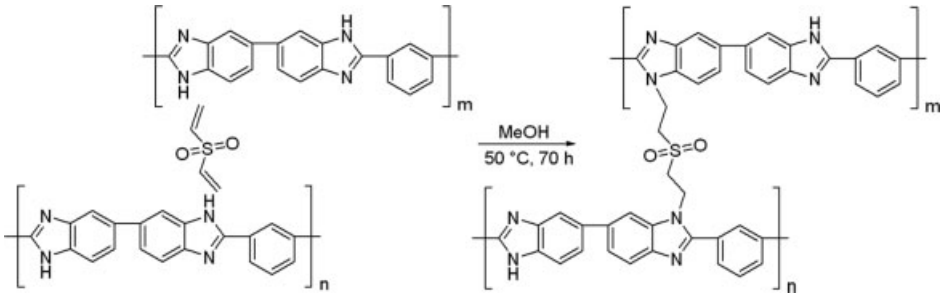

Scheme 2. Schematic of PBI crosslinking by post-treatment with DVS.

Table 2. Calculated and analyzed sulfur content of the cross-linked membranes

Initial DVS : PBI_{RU} molar ratio	1	5	10
Calculated sulfur content from weight gain, wt.%	0.060	0.43	0.99
Found sulfur content, wt.% (elemental analysis)	0.053	0.45	0.94

a correlation between the membrane thickness and apparent degree of crosslinking. The apparent degree of crosslinking increases from about 5% for a 150 µm thick membrane to about 13% for a 20 µm thick membrane, indicating that the post-treatment crosslinking reaction is limited by the diffusion of DVS into the bulk membrane. As a result, the crosslinking reaction would be influenced by the morphology of the membrane surface. In the present study, however, membranes from solution casting were used with no further surface treatment.

PA doping

PBI membranes can be readily doped with PA. As previously reported, an acid doping level of *ca* 11 was achieved in 85% PA.[31] This is confirmed by the present study, as evident from Table 3. At 50 °C the linear reference membrane is partly dissolved, as indicated by a slightly coloured doping solution.

As evident from Table 3, in 85% PA at room temperature, the acid doping level for a crosslinked membrane with an apparent degree of crosslinking of 35%, for example, is as low as 0.7 and the corresponding volume swelling is only 5%. As previously reported,[20,21] crosslinked PBI membranes need to be doped at elevated temperature in order to get a sufficient doping level, since the crosslinks reduce the swelling capability of the membrane. At 50 °C the doping level is increased to 7.4 for the same crosslinked membrane, which is accompanied by an increase in the volume swelling of 71%. In addition, the doping acid solution remains clear during the doping, indicating the insolubility of crosslinked membranes in the doping acid.

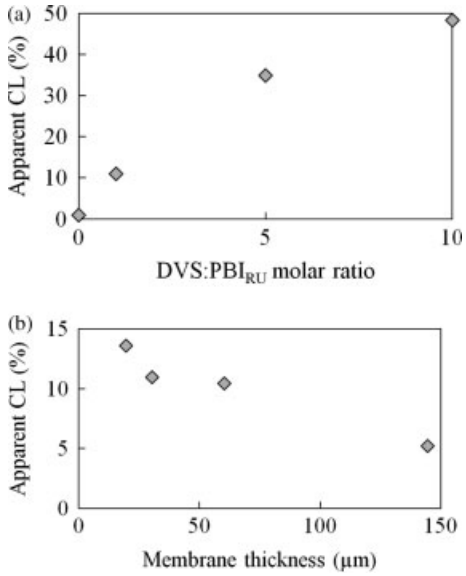

Figure 2. Apparent degree of crosslinking (CL) as a function of (a) the initial DVS : PBI_{RU} molar ratio for a constant membrane thickness of 30 µm and (b) the membrane thickness for a constant initial DVS : PBI_{RU} molar ratio of 1.

FTIR spectral analysis

The FTIR spectra of membranes with varying apparent degrees of crosslinking are shown in Fig. 3. Pristine PBI shows all characteristic absorption bands,[18] and two new absorption bands are observed at *ca* 1140 and 1324 cm^{-1} for the membranes post-treated with DVS. These bands are assigned to sulfone group absorption[32] and originate from DVS molecules reacted with the polymer. The absorption bands are more pronounced for membranes treated with higher DVS : PBI_{RU} molar ratios, indicating an increased concentration of sulfone groups. Furthermore, an obvious decrease of the 3420 cm^{-1} absorption band intensity is observed for the membranes with very high apparent degrees

Table 3. PA doping of PBI membranes of different apparent cross-linking degrees in 85% PA

Initial DVS : PBI_{RU} molar ratio (apparent CL degree in parenthesis)	0 (0%)		1 (11%)		5 (35%)		10 (48%)	
Doping temperature (°C)	20	50	20	50	20	50	20	50
Doping level (PA/PBI_{RU})	10.6	–	3.2	8.3	0.7	7.4	0.4	6.0
Volume swelling (%)	143	–	33	110	5	71	6	62

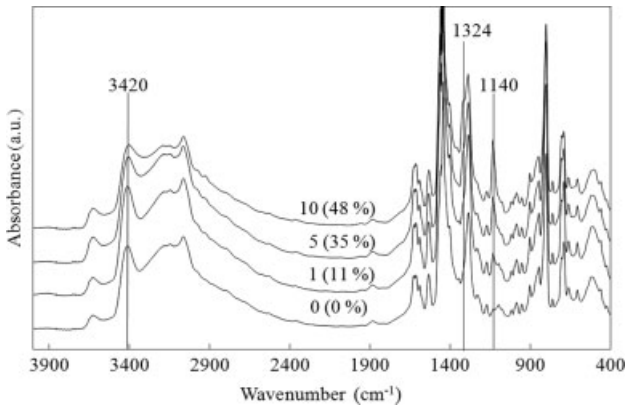

Figure 3. FTIR spectra of pristine PBI and PBI membranes treated with DVS. The initial DVS : PBI_{RU} molar ratios are as indicated together with the apparent degrees of crosslinking in parentheses.

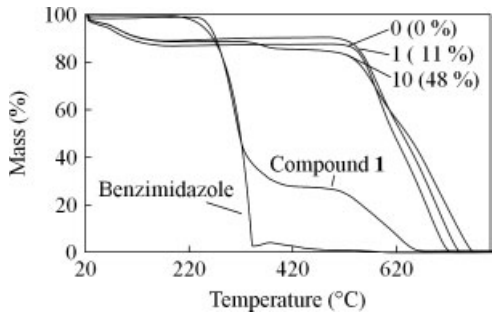

Figure 4. Thermograms for benzimidazole, compound **1** and PBI membranes treated with DVS. The initial DVS : PBI_{RU} molar ratios are as indicated together with the apparent degrees of crosslinking in parentheses.

of crosslinking. This absorption band is associated with N–H stretching vibrations in the imidazole moieties.[18] As new N–C bonds are formed during the post-treatment reaction, the number of N–H bonds is reduced. Since the intensity of the absorption band is directly proportional to the concentration of N–H in the sample, the effect should be more pronounced for the samples with high apparent degrees of crosslinking.

Thermogravimetric analysis

The onset temperature of decomposition for benzimidazole in air is *ca* 175 °C (Fig. 4). The linking of two benzimidazole molecules with DVS (compound **1**, Scheme 1) increases the onset temperature of decomposition to *ca* 220 °C. The thermal oxidation of **1** occurs in two steps. The second onset temperature of decomposition is observed at *ca* 480 °C. Concerning PBI, the membrane with an apparent degree of crosslinking of 48% shows a similar two-step thermal oxidation with the first onset temperature at *ca* 310 °C and the second one at *ca* 500 °C. The first onset at 310 °C is probably connected to thermal decomposition of sulfone linkages or graft groups, whereas the second onset at 500 °C is connected to decomposition of the polymer backbone. The linear PBI membrane and the membrane with an apparent degree of crosslinking of 11% show only one onset temperature of decomposition at *ca* 500 °C. The weight loss at temperatures of up to 200 °C is due to evaporation of water absorbed from the atmosphere by the hygroscopic polymer membranes. By defining the membrane water uptake from the atmosphere as the total weight loss at 200 °C, the water uptake is slightly higher for the linear PBI (13%) compared with its crosslinked analogue (11%).

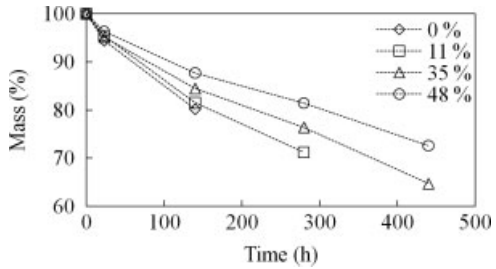

Figure 5. Membrane remaining masses during the Fenton test for membranes of various apparent degrees of crosslinking.

Chemical stability

The relative chemical stability of the membranes with apparent degrees of crosslinking of 0, 11, 35 and 48% was evaluated using the Fenton test. In the Fenton test hydroxyl radicals are generated by Fe(II)-catalysed decomposition of hydrogen peroxide. Membrane degradation by radical-induced oxidation has been identified as one of the major PEM fuel cell durability issues for Nafion® -based[33] as well as PA/PBI-based[34] PEM fuel cells. The generation of hydrogen peroxide or hydroxyl radicals has been suggested to occur on platinum deposited in the membrane during operation of fuel cells at high potentials.[35]

In this investigation, the linear PBI reference membrane starts to spontaneously disintegrate after 140 h in the Fenton test solution after a 20% weight loss (Fig. 5). In contrast, the membrane with an apparent degree of crosslinking of 11% lasts for 280 h and can take a 29% weight loss before it spontaneously starts to disintegrate. The corresponding result for the membrane with an apparent degree of crosslinking of 35% is 440 h and 35% weight loss. When the experiment is terminated after 440 h, the membrane with an apparent degree of crosslinking of 48% is still intact. A general trend is that the rate of weight loss decreases with increasing degree of crosslinking, which is in agreement with previously reported results for crosslinked PBI membranes.[20,21]

Mechanical strength

Stress–strain curves were recorded for a non-doped linear PBI membrane and a PBI membrane with an apparent degree of

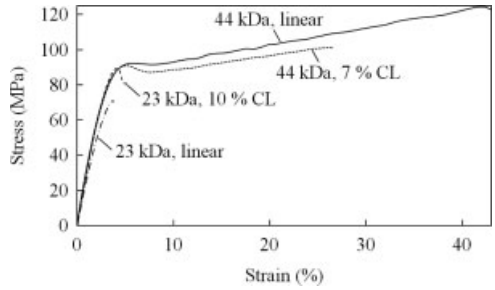

Figure 6. Typical stress–strain curves at 180 °C for linear and crosslinked membranes prepared from PBI of high and low molecular weight. (CL, degree of crosslinking).

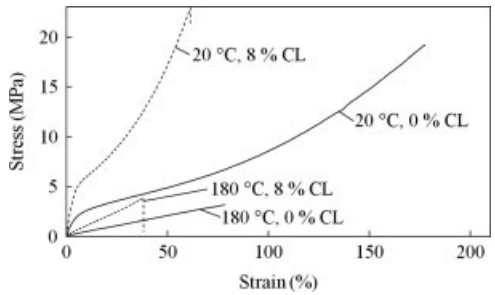

Figure 7. Typical stress–strain curves for linear and crosslinked PBI membranes. The PA doping level was about 10 for both membranes. (CL, degree of crosslinking).

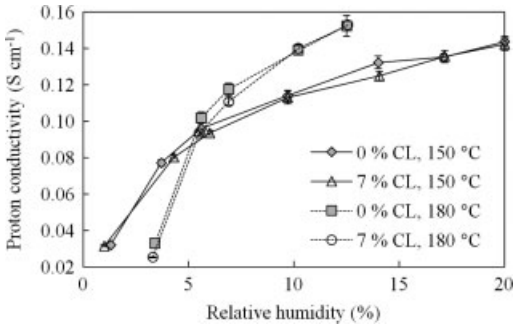

Figure 8. In-plane conductivity for PA-doped linear and DVS-treated PBI membranes at 150 and 180 °C. The PA doping level was about 10 for both membranes. (CL, degree of crosslinking).

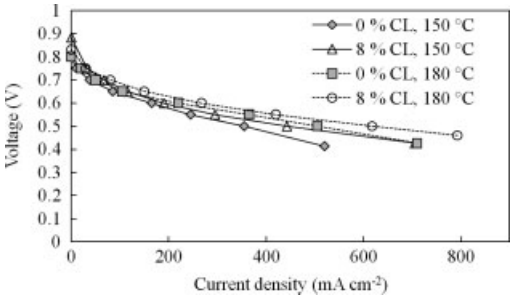

Figure 9. Polarization curves of fuel cells based on linear and crosslinked PBI membranes operating with dry hydrogen and air at various temperatures. (CL, degree of crosslinking).

crosslinking of 7%. At 180 °C no improvement in terms of Young's modulus or stress at yield is apparent for the crosslinked membrane compared with the linear membrane (Fig. 6). The Young's modulus is about 3 GPa and the stress at yield about 91 MPa for both membranes. However, the elongation at break is less for the membrane post-treated with DVS. In the low-molecular-weight range, significant improvement in the mechanical strength with increasing molecular weight can be expected, as reported for PA-doped PBI membranes.[8] This mechanical strength dependence on molecular weight would level off in the higher molecular weight ranges.[36] Stress–strain curves were also recorded for the PBI membranes prepared from low-molecular-weight polymer (23 kDa) and its crosslinked analogue obtained after the post-treatment with a DVS : PBI_{RU} ratio of 1, which gives an apparent degree of crosslinking of 10%. The stress at break is found to increase from about 70 MPa for the linear membrane to about 87 MPa for the crosslinked analogue.

After PA doping the mechanical strengthening of the DVS-treated membranes is obvious (Fig. 7). Membranes with an apparent degree of crosslinking of 8% exhibit higher Young's modulus as well as tensile stress at break at 20 and 180 °C compared with the linear PBI of similar PA doping level. The Young's modulus at 20 °C increases from 44 MPa for the linear PBI membrane to 136 MPa for the crosslinked membrane. At 180 °C the Young's modulus increases from 5 MPa to 10 MPa. The poorer mechanical properties in general for the acid-doped membranes compared with the non-doped ones can be explained by the plasticizing effect of PA, i.e. reduced intermolecular hydrogen bonding between –N═and –NH– groups after PA doping. As seen from Table 3, the specific swelling per molecule of doping acid (total swelling divided by doping level) is 13.5, 12.0, 9.6 and 10.3 for membranes with apparent degrees of crosslinking of 0, 11, 35 and 48%, respectively. This would result in a stronger resistance to deformation, and thus a higher Young's modulus.

In-plane proton conductivity

It is known that PA/PBI membranes exhibit anhydrous proton conductivity at elevated temperatures, even though the presence of water improves the proton conductivity. The dependence of the conductivity on the water content is, however, not as critical as for PFSA membranes. A reasonable conductivity in the region of 10^{-2} S cm^{-1} can be obtained even under completely dry conditions for PA/PBI membranes with moderate doping levels of 3–6.[7] In contrast, the conductivity is strongly dependent on the PA doping level and can reach as high as 0.25 S cm^{-1} at 180 °C for membranes with a PA doping level above 20 prepared by the sol–gel procedure.[10] Fig. 8 shows the proton conductivity for a PA-doped linear PBI membrane and a membrane with an apparent degree of crosslinking of 7%. The linear PBI membrane was doped in 85% PA at room temperature whereas the DVS-treated membrane was doped in 85% PA at 50 °C. The relatively low apparent degree of crosslinking for the DVS-treated membrane results in a high doping level of around 10. The proton conductivity data are in line with previously reported results for ionically crosslinked PBI-based blend membranes of similar doping levels measured at similar temperature and relative humidity.[16] The conductivity reaches 0.14 S cm^{-1} at 150 °C and 20% relative humidity and 0.15 S cm^{-1} at 180 °C and 13% relative humidity for both the linear membrane and the crosslinked analogue.

Fuel cell tests

Figure 9 shows polarization curves of fuel cells based on linear and crosslinked PBI membranes at 150 and 180 °C. The acid doping

level is about 10 PA per PBI_{RU} and the membrane thickness is about 70 μm. It is interesting to note that the open circuit voltage of the fuel cell based on the crosslinked membrane is slightly higher than that of the cell with the linear PBI membrane, probably due to decreased gas permeability of the crosslinked membrane. This could be the reason why the cell based on the crosslinked membrane shows slightly better performance. The improvement is primarily achieved in the high current density region, i.e. due to the increased membrane conductivity. As expected, in the low current density region where the catalytic activity of the electrodes dominates, no improvement in the polarization curves is observed. It should be remarked that the fuel cells with crosslinked membranes were only tested for 2 days with no visible performance decay. The improved mechanical strength and chemical stability are expected to improve the fuel cell durability, which is under evaluation by the authors' group.

CONCLUSIONS

Crosslinking of PBI membranes by post-treatment with DVS was investigated. The crosslinking chemistry was studied for a low-molecular-weight model system of benzimidazole and DVS in MeOH or aqueous potassium hydroxide as solvents. The non-catalysed reaction in MeOH indicated a risk for grafting of 2-methoxyethanesulfonyl groups on the PBI backbone instead of crosslinking when DVS was added in excess. The apparent degree of crosslinking of PBI membranes calculated from the weight gain after DVS treatment fitted well with the results from elemental analysis. The apparent crosslinking after DVS treatment was found to be dependent on the membrane thickness as well as the initial DVS : PBI_{RU} molar ratio. TGA results for crosslinked PBI membranes with high apparent degrees of crosslinking showed an extra shoulder in the mass loss curves, probably connected to the decomposition of sulfone linkages. The oxidative stability of membranes under Fenton test conditions was improved by crosslinking. During further acid doping, elevated doping temperatures were needed for the crosslinked membranes. For a similar acid doping level, the crosslinked membranes showed improved Young's modulus and tensile stress at break compared with the linear membrane. The proton conductivity was in the same range for membranes with a similar doping level, regardless of being crosslinked or not. Preliminary fuel cell tests demonstrated the feasibility of the membranes. However, further efforts are needed to improve cell performance with respect to electrode and MEA preparation and to evaluate cell durability.

ACKNOWLEDGEMENTS

Financial support is gratefully acknowledged from the European Commission within the 7th Framework Programme (WELTEMP project 212903) and the ForskEL programme (HotMEA, 010221).

REFERENCES

1 Costamagna P and Srinivasan S, *J Power Sources* **102**:242–252 (2001).
2 Li Q, He RH, Jensen JO and Bjerrum NJ, *Chem Mater* **15**:4896–4915 (2003).
3 Li Q, He RH, Gao JA, Jensen JO and Bjerrum NJ, *J Electrochem Soc* **150**:A1599–A1605 (2003).
4 Jensen JO, Li Q, Pan C, Vestbo AP, Mortensen K, Petersen HN, *et al*, *Int J Hydrogen Energy* **32**:1567–1571 (2007).
5 Li Q, Jensen JO, Savinell RF and Bjerrum NJ, *Prog Polym Sci* **34**:449–477 (2009).
6 Wainright JS, Wang JT, Weng D, Savinell RF and Litt M, *J Electrochem Soc* **142**:L121–L123 (1995).
7 Ma YL, Wainright JS, Litt MH and Savinell RF, *J Electrochem Soc* **151**:A8–A16 (2004).
8 He RH, Li Q, Bach A, Jensen JO and Bjerrum NJ, *J Membr Sci* **277**:38–45 (2006).
9 He RH, Li Q, Jensen JO and Bjerrum NJ, *J Polym Sci A: Polym Chem* **45**:2989–2997 (2007).
10 Xiao LX, Zhang HF, Scanlon W, Ramanathan LS, Choe EW, Rogers D, *et al*, *Chem Mater* **17**:5328–5333 (2005).
11 Xing B and Savadogo O, *Electrochem Commun* **2**:697–702 (2000).
12 Lu YH, Chen JM, Cui HX and Zhou HD, *Compos Sci Technol* **68**:3278–3284 (2008).
13 Lin HL, Yu TL, Chang WK, Cheng CP, Hu CR and Jung GB, *J Power Sources* **164**:481–487 (2007).
14 He RH, Li Q, Xiao G and Bjerrum NJ, *J Membr Sci* **226**:169–184 (2003).
15 Kerres J, Schönberger F, Chromik A, Häring T, Li Q, Jensen JO, *et al*, *Fuel Cells (Weinheim)* **8**:175–187 (2008).
16 Li Q, Jensen JO, Pan C, Bandur V, Nilsson MS, Schönberger F, *et al*, *Fuel Cells (Weinheim)* **8**:188–199 (2008).
17 Li Q, Rudbeck HC, Chromik A, Jensen JO, Pan C, Steenberg T, *et al*, *J Membr Sci* **347**:260–270 (2010).
18 Wang KY, Xiao YC and Chung TS, *Chem Eng Sci* **61**:5807–5817 (2006).
19 Wang KY, Yang Q, Chung TS and Rajagopalan R, *Chem Eng Sci* **64**:1577–1584 (2009).
20 Li Q, Pan C, Jensen JO, Noyé P and Bjerrum NJ, *Chem Mater* **19**:350–352 (2007).
21 Noyé P, Li Q, Pan C and Bjerrum NJ, *Polym Adv Technol* **19**:1270–1275 (2008).
22 Xu N, Guo XX, Fang JH, Xu HJ and Yin J, *J Polym Sci A: Polym Chem* **47**:6992–7002 (2009).
23 Davis HJ and Thomas NW, Chemical modification of polybenzimidazole semipermeable. US Patent 4020142 (1977).
24 Sheratte MB, Linear and crosslinked polybenzimidazoles. US Patent 4154919 (1979).
25 Kuder JE and Chen JC, Chemical modification of preformed polybenzimidazole semipermeable membrane. US Patent 4634530 (1987).
26 Onishi Y, Iura K, Maeno A, Itoh T and Tsuji K, Varnish-coated electric wire and method of producing the same. European Patent Application 0566148A1 (1993).
27 Jorgensen BS, Young JS and Espinoza BF, Crosslinked polybenzimidazole membranes for gas separation. US Patent 006946015B2 (2005).
28 Young JS, Long GS and Espinoza BF, Crosslinked polybenzimidazole membrane for gas separation. US Patent 006997971B1 (2006).
29 Sansone MJ, Crosslinking of polybenzimidazole polymer with divinyl sulfone. US Patent 4666996 (1987).
30 Kumbharkar SC, Karadkar PB and Kharul UK, *J Membr Sci* **286**:161–169 (2006).
31 Li Q, He RH, Berg RW, Hjuler HA and Bjerrum NJ, *Solid State Ionics* **168**:177–185 (2004).
32 Lide DR (ed.), Molecular structure and spectroscopy section 9, infrared correlation charts, in *CRC Handbook of Chemistry and Physics*, 90th edition (Internet version). CRC Press/Taylor and Francis, Boca Raton, FL (2010).
33 Sugawara S, Maruyama T, Nagahara Y, Kocha SS, Shinohra K, Tsujita K, *et al*, *J Power Sources* **187**:324–331 (2009).
34 Modestov AD, Tarasevich MR, Filimonov VY and Zagudaeva NM, *Electrochim Acta* **54**:7121–7127 (2009).
35 Ohma A, Yamamoto S and Shinohara K, *J Power Sources* **182**:39–47 (2008).
36 Stevens MP, *Polymer Chemistry: An Introduction*, 3rd edition. Oxford University Press, New York, pp. 100–106 (1999).

III

Journal Name

Dynamic Article Links ►

Cite this: DOI: 10.1039/c0xx00000x

www.rsc.org/xxxxxx

ARTICLE TYPE

Thermal curing of PBI membranes for high temperature PEM fuel cells

David Aili,[a] Lars N. Cleemann,[a] Qingfeng Li,*[a] Jens Oluf Jensen,[a] Erik Christensen[a] and Niels J. Bjerrum[a]

Received (in XXX, XXX) Xth XXXXXXXXX 20XX, Accepted Xth XXXXXXXXX 20XX

DOI: 10.1039/b000000x

Phosphoric acid doped polybenzimidazole (PBI) has emerged as one of the most promising electrolyte materials for PEM fuel cells operating under anhydrous conditions at temperatures up to 200 °C. However, the limited long term durability of the membrane electrode assemblies (MEAs) is currently hampering the commercial viability of the technology. In the present study, thermal treatment of PBI membranes under inert atmosphere at temperatures up to 350 °C prior to the acid doping was investigated aiming at improving the physiochemical characteristics of the membranes. The systematic membrane characterization with respect to solubility, phosphoric acid doping, radical-oxidative resistance and mechanical strength indicated that the PBI membranes irreversibly cured during the heat treatment at 350 °C under argon atmosphere. After curing, the PBI membranes demonstrated features which are fundamental characteristics of a thermoset resin including complete insolubility, high resistance to swelling and improved mechanical toughness. Additionally, the thermal treatment was found to increase the degree of crystallinity of the membranes. The improved physiochemical characteristics of the membranes after curing were further illustrated by a dramatically improved long term durability of the corresponding fuel cell MEAs. During continuous operation for 1800 h at 160 °C and 600 mA cm^{-2} the average cell voltage decay rate of the MEA based on the cured membrane was 43 μV h^{-1}. This should be compared with an average cell voltage decay rate of 308 μV h^{-1} which was recorded for the MEA based on its non-cured counterpart.

Introduction

During the last decades, phosphoric acid (PA) doped poly[2,2´(*m*-phenylene)-5,5´bibenzimidazole] (PBI, Figure 1) has evolved as one of the most promising electrolyte materials for proton exchange membrane (PEM) fuel cells operating under anhydrous conditions at temperatures up to 200 °C.[1,2] As a fully aromatic heterocyclic polymer, PBI possesses a very high glass transition temperature (T_g) of 425-436 °C and excellent thermal and chemical stability. PBI is also characterized by its mechanical toughness. For example, among all known engineering plastics it has the highest reported compression strength.[3]

The first published synthetic route to PBI was based on melt condensation polymerization of an equimolar mixture of 3,3´-diaminobenzidine and diphenyl isophtalate.[4] However, the melt condensation polymerization gave a rather poorly defined polymer. From a polymerization point of view the most critical issue is to achieve a linear growth of the macromolecular chain with sufficiently minimized side reactions in order to maintain the structure purity. Chain branching and/or crosslinking are among the side reactions of primary concern.[5] Homogenous solution polymerization in polyphosphoric acid (PPA) at 170-200 °C, on the other hand, gives a better control of the reaction which also results in a more well defined polymer and minimized side reactions.[6]

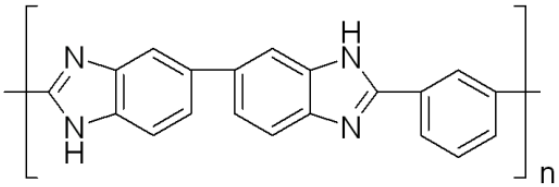

Fig. 1 Chemical structure of PBI.

The high T_g of PBI excludes the conventional polymer processing techniques such as thermoforming, moulding or melt extrusion. PBI only exhibits sufficient solubility in a few organic solvents which can be used for fiber extrusion and membrane casting. However, the solubility of PBI and the intrinsic viscosity [η] of the obtained solutions highly depend on the linear molecular weight of the polymer. Therefore, the commercially available PBI (Celazole®, Celanese) has a low to medium linear molecular weight ranging from about 23-37 kDa corresponding to an intrinsic viscosity [η] of 0.55–0.80 dL g^{-1}.[7] PBI in the lower region of this molecular weight range gives rather poor membranes in terms of mechanical stability and oxidative resistance and fractionation seems necessary before membrane casting in order to concentrate the high molecular weight fraction of the polymer batch.[8]

The proton conductivity of the PA doped PBI membrane is

highly dependent on the acid doping level (DL) of the membrane which is defined as the number of PA molecules per repeating unit of the polymer. For example, under anhydrous conditions at 180 °C the conductivity increases from about 0.03 S cm^{-1} to 0.25 S cm^{-1} when the doping level is increased from 6 to 32.[9,10]

Unfortunately, the mechanical strength of the PA doped PBI membrane is dramatically reduced as the PA doping level is increased due to the strong plasticizing effect of PA.[11] The mechanical characteristics of PBI membranes at high doping levels can thus be considerably improved by increasing the linear average molecular weight of the polymer[11] or by covalent[9,12-15] or ionic crosslinking.[16-19]

Although a high linear average molecular weight of PBI is desirable from a mechanical strength point of view it obviously causes processability difficulties since the solubility is dramatically reduced and the intrinsic viscosity [η] of the obtained polymer solution is increased as the linear molecular weight is increased. In order to improve the processability of polybenzimidazoles a pre-polymer approach was developed, as reviewed by Neuse[5] and Levine.[20] The idea was to prepare a low molecular weight pre-polymer which could easily be processed using standard techniques. The pre-polymers exhibited fairly good solubility and contained open chain segments which were capable of ring closure and aromatization after subsequent heat treatment in the solvent-free state.

After heat treatment at 500 °C, Vogel and Marvel[4] observed that PBI becomes completely insoluble in all standard solvents. Apart from the linear chain growth through continued polycondensation, it was suggested that crosslinking had occurred through free radical reactions. Gillham[21] further investigated the thermo-mechanical properties of PBI and confirmed that PBI changes from a thermoplastic polymer to a thermoset resin at about 450 °C. Based on spectroscopic evidence it was also confirmed that crosslinking had occurred,[22] as also discussed by Levine.[20] This was further illustrated on a macroscopic scale by Hwang *et al.*,[23] who showed that heat treatment of spun ABPBI fibers at temperatures up to 540 °C increased the Young´s modulus by 153% and the engineering tensile strength by 63%. At the same time the elongation at break was considerably decreased.

Based on extensive FTIR characterization the early stages of the PBI thermo-oxidative degradation was analyzed by Musto *et al.*,[24] who also observed that the PBI membranes which had been heat treated under air at even lower temperatures (350 °C) for 30 minutes were practically insoluble in DMAc. Shulman and Lochte[25] proposed a mechanism for the thermal oxidation of PBI at temperatures above 450 °C. It involved chain scission accompanied by crosslinking reactions, either by amide interchange or by benzene-biphenyl type coupling. The weakest link of the PBI backbone in a thermo-oxidative environment was obviously the nitrogen containing heterocyclic and the adjacent benzenoid rings.[26,27] Later, Linkous[28] evaluated the thermo-oxidatively crosslinked PBI membranes as a potential electrolyte material for PEM steam electrolyzers.

In the present work, the post heat treatment technique was investigated to process the preformed PBI membranes for high temperature PEM fuel cells. In order to avoid thermal or thermo-oxidative degradation of the polymer, spectroscopic characterization (ATR-FTIR) in combination with TGA/DTA was used to define the curing temperature and conditions. The cured PBI membranes were further characterized with respect to their chemical and physiochemical properties such as solubility, radical-oxidative resistance, phosphoric acid doping, morphology, mechanical strength and proton conductivity. Fuel cell tests were further conducted in order to demonstrate the feasibility and the improved durability of the cured membranes.

Experimental

Membrane preparation

PBI with an average molecular weight ranging from about 23-64 kDa was supplied by Danish Power System ApS. The weight average molecular weights were determined by viscometry measurement in concentrated sulfuric acid using the empirical Mark-Houwink constants $K = 1.94 \times 10^{-4}$ dL g^{-1} and $\alpha = 0.791$.[29] The PBI was supplied either as powders or as membranes which had been solution cast from DMAc through solvent evaporation. The PBI powders were dissolved in DMAc to give 5 wt.% solutions after filtering. PBI membranes were subsequently solution cast from the DMAc solution on glass substrates. All membranes were boiled in demineralized water for several hours and dried at temperatures up to 200 °C.

The heat treatments were conducted in a quarts glass lined tube furnace at temperatures ranging from 200-500 °C under air or argon atmosphere. For the membranes which were heat treated under argon atmosphere, the furnace was repeatedly evacuated and filled with argon at room temperature before the heat treatment procedure was started. During the heat treatment, argon was continuously purged through the furnace at a flow rate of about 100-200 mL min^{-1}.

Since the eventual chemical or physical effects on the membrane were assumed to be dependent on the thermal curing duration, two different standard curing procedures were established for the systematic membrane characterization. During the short thermal curing procedure, the sample was heated up to 350 °C over about 10 minutes. When the furnace interior reached the target temperature, the membrane sample was treated isothermally for about 1 minute before the power was switched off and the furnace was allowed to cool down to room temperature which took about 1.5-2 h. During the long thermal curing procedure, the sample was treated isothermally at 350 °C for 16 h. The membranes obtained after the short and long curing procedures are hereafter referred to xx-Sh-C and xx-Lo-C, respectively, where xx corresponds to the initial linear average molecular weight of PBI in kDa. The non-cured reference membranes are hereafter referred to as xx-Ref, where xx corresponds to the linear average molecular weight of PBI in kDa.

Doping was achieved by submerging the membranes in 85% H_3PO_4 at temperatures ranging from 20-100 °C. The acid doping levels were calculated on the dry polymer basis and the dry weights after phosphoric acid doping (dried at 150 °C until constant weight).

Membrane characterization

Attenuated Total Reflectance Fourier Transform Infrared Spectroscopy (ATR-FTIR) was conducted using a Perkin Elmer

Spectrum One FTIR spectrometer equipped with a universal ATR sampling accessory. The membrane samples were pre-dried at 200 °C for 4 h before the spectra were recorded.

The TGA/DTA data were acquired using a Netzsch STA 409 PC. The samples were pre-dried at 250 °C *in vacuo* for 12 h in the chamber and thereafter cooled down to room temperature. The thermograms were recorded at a heating rate of 10 °C min^{-1} and argon was used as the purge gas.

For the Fenton test, the membrane samples (40 µm thick) were submerged in a 3% H_2O_2 (Merck) aqueous solution containing 4 ppm Fe(II) (added as $(NH_4)_2Fe(SO_4)_2{\cdot}6H_2O$) at 68 °C. After certain durations (maximum 20 h), the membrane samples were collected, rinsed with demineralized water and dried at 120 °C for at least 5 h. The dry weight was recorded and the membrane samples were submerged in freshly prepared Fenton solution for continuation of the test.

Wide angle X-ray diffraction (WAXD) data were recorded on a Huber D670 diffractometer equipped with a Cu-K α X-ray source.

Stress-strain curves were recorded under ambient conditions using a sample length of 30 mm and a grip separation rate of 10.00 mm min^{-1}. The equipment used was a modified universal materials testing machine (Testometric Micro 350).

In-plane proton conductivity was measured at temperatures ranging from 110-180 °C under anhydrous conditions. The membrane samples were pre-conditioned at 180 °C for about 16 h before the sample dimensions were determined. The temperature was then systematically lowered and the conductivity was recorded at intervals of 10 °C. The measurements were carried out using a four-probe conductivity cell. A symmetric square wave current was supplied through platinum foils in the 5-10 kHz frequency range. The voltage drop was measured via platinum probes which were fixed at a distance of 1.0 cm apart.

MEA preparation and fuel cell testing

A platinum catalyst (56.2 wt.% Pt) supported on carbon black was used to prepare catalyst layers by spraying the catalyst dispersion onto carbon based non-woven gas diffusion layers, which had been pre-coated with a micro-porous layer. PBI was used as the catalyst binder (0.1 mg cm^{-2}) which after the acid impregnation functioned as proton conducting phase in the electrode. The Pt loading of the final electrodes was 0.58 mg cm^{-2} at the cathode and 0.29 mg cm^{-2} at the anode.

The acid doped PBI membranes were sandwiched between two pieces of gas diffusion electrodes and hot-pressed at 200 °C under a pressure of about 4 MPa for 3 min.

The size of the active electrode area of the MEAs was 10 cm^2. The MEAs were tested in single cells consisting of two graphite plates with simple parallel gas channels. Two end plates made of aluminium with attached heaters were used to clamp the graphite plates and a separate silver coated current collector was used to collect the current from the cell.

For the fuel cell tests, dry hydrogen and air were used without pre-humidification at flow rates of 110 and 450 ml min^{-1}, respectively. Even at the maximum current densities, the gas flow rates were much higher than the consumption. In this way the fuel cell tests were performed in order to evaluate the materials but not to optimize the cell operation.

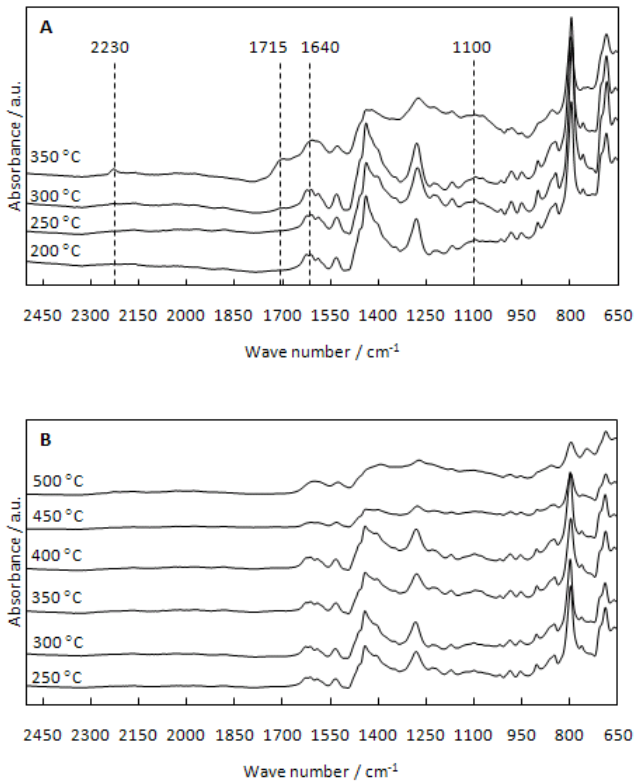

Fig. 2 ATR-FTIR spectra of the PBI membranes which had been treated at different temperatures for 16 h under air (A) or argon (B) atmosphere. The 2500-4000 cm^{-1} regions of the spectra are omitted for clarification.

Results and discussion

ATR-FTIR

After heat treatment of the PBI membrane for 16 h under an oxygen containing atmosphere at temperatures above 300 °C, the appearance of the FTIR spectrum was dramatically changed. As shown in Figure 2A, the most pronounced difference was observed in the 1000-1800 cm^{-1} region of the spectrum which is mainly assigned to different vibration and breathing modes of the aromatic backbone. For example, the intense absorption bands centred around 1540 cm^{-1} and at about 1640 cm^{-1} have been assigned to stretching modes of C=C and C=N bonds in the aromatic backbone, respectively.[30] As previously reported, two new absorption bands at about 2230 cm^{-1} and 1715 cm^{-1} were observed in the FTIR spectrum of the PBI membrane which had been heat treated under air at 350 °C.[24] The 2230 cm^{-1} absorption band was assigned to stretching vibrations of aromatic nitrile groups originating from the imidazole moieties whereas the absorption band at 1715 cm^{-1} was assigned to various carbonyl containing functionalities which were formed due to the extensive thermal oxidation of the polymer. In the radical induced oxidation of PBI membranes (Fenton test) a considerable intensity strengthening of the absorbance peak at around 1640 cm^{-1} was observed, indicating the formation of carbonyl functionalities.[30] A new wide absorption band was also observed at around 1100 cm^{-1} which was assigned to hydroxyl functionalities.

The literature data of oxidized PBI were in good agreement with the changed appearance of the FTIR spectrum of the PBI membrane after the heat treatment under air at 350 °C in the

present study. Conclusively, the general broadening of the absorbance bands in the 1000-1800 cm^{-1} region of the spectrum indicates severe thermally induced oxidation of the polymer backbone. The extensive thermally induced oxidation should ultimately result in polymer chain scission and thus a dramatic decrease of the linear molecular weight, as also confirmed for thermally oxidized PBI[24] or PBI membranes which had been subjected to radical induced oxidation in the Fenton test.[30,31]

On the other hand, the PBI membranes which had been heat treated under inert argon atmosphere showed considerably better stability at higher temperatures in general, as shown in Figure 2B. Under a continuous argon flow the PBI membranes could be heat treated at temperatures up to 400 °C for at least 16 h without affecting the visual appearance of its FTIR spectrum.

TGA/DTA

Thermal analysis can be used to determine crosslinking temperatures of polymers since the crosslinking reactions are generally exothermic to some extent. For example, Han *et al.*[15] used DSC to determine the crosslinking temperature of PBI and an epoxy resin which was identified as a small exotherm at about 160 °C.

Thermogravimetric analysis (TGA) and differential thermal analysis (DTA) data of the non-cured reference membrane (48-Ref) and the membrane which had been pre-cured at 350 °C for 16 h under argon (48-Lo-C) are shown in Figure 3. The samples were pre-dried *in vacuo* at 250 °C for 16 h in the chamber before the measurement was started in order to completely evaporate the solvent residuals and absorbed moisture.

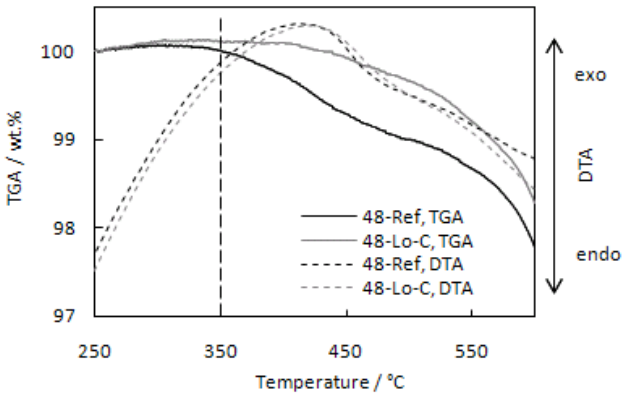

Fig. 3 TGA and DTA of the non-cured reference membrane (48-Ref) and of the membrane which had been pre-cured at 350 °C for 16 h under argon (48-Lo-C). The standard curing temperature is highlighted by a dashed line at 350 °C.

The non-cured reference membrane (48-Ref) showed a weight loss with an onset temperature at about 350 °C, which was also the standard curing temperature of the PBI membranes in the present study. The total weight loss in the 350-450 °C temperature range was about 0.7%. On the other hand, this weight loss was not observed in the thermogram of the membrane which had been pre-cured at 350 °C (48-Lo-C). The onset of weight loss of the pre-cured membrane 48-Lo-C did not start until the temperature reached about 430 °C. The small weight loss at 350 °C of the non-cured membrane 48-Ref could thus be associated with crosslinking reactions giving off volatile species as PBI changes from a thermoplastic polymer to a thermoset resin.

An exotherm was also observed in this temperature range which further indicates that chemical reactions, such as crosslinking, were taking place. However, although no obvious weight loss was recorded in this temperature range, the exotherm was also observed in the DTA of the membrane which had been cured at 350 °C for 16 h (48-Lo-C) before the experiment. The exotherm in the DTA of the 48-Lo-C membrane could indicate that further crosslinking reactions were taking place when the membrane was re-heated to 350 °C. However, the continuation of the thermal curing process obviously did not result in any volatile species since no weight loss was recorded.

Solubility

Previous studies on heat treatment of PBI at temperatures of 350-500 °C have shown that the thermal treatment results in an almost completely insoluble material.[4,24] Based on thermo-mechanical measurements[21] and spectroscopic evidence[20,22] the complete insolubility was assigned to a dramatic increase of the molecular weight through crosslinking.

The complete insolubility of PBI after thermal treatment at 350 °C was also confirmed in the present study, as shown in Figure 4. After the thermal treatment procedure the membranes were obviously almost completely insoluble in DMAc at 80 °C (64-Sh-C and 64-Lo-Cu) whereas the non-cured reference membrane (64-Ref) readily dissolved completely in less than 20 minutes.

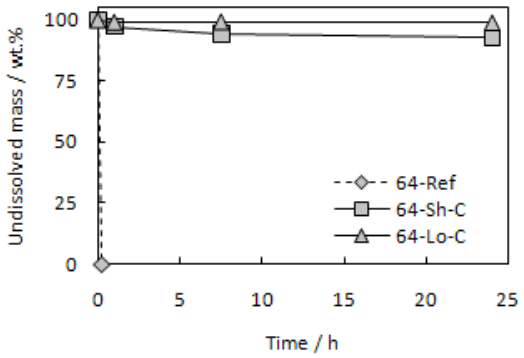

Fig. 4 Membrane solubility in DMAc at 80 °C.

Fenton test

The membrane degradation by radical induced oxidation has been identified as one of the major long term durability limitations of the PA doped PBI based high temperature PEM fuel cells.[32] However, the oxidative resistance of PBI membranes can be dramatically improved by covalent crosslinking[9,12,13,15] which also should improve the long term durability of the PBI based PEM fuel cells.

As shown in Figure 5, the average rate of weight loss of the non-cured reference membrane 48-Ref during the 80 h of effective Fenton test in the present study was about 0.13 wt.% h^{-1}. The corresponding result of the cured membrane 48-Lo-C was about 0.05 wt.% h^{-1}. The rates of weight loss of the cured membrane 48-Lo-C and its non-cured counterpart 48-Ref corresponded well with the rates of weight loss of PBI with an apparent degree of crosslinking of 48% and its linear counterpart, respectively.[13]

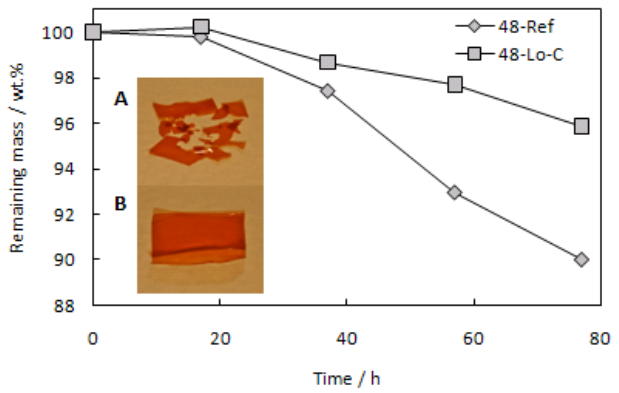

Fig. 5 Remaining membrane mass after certain durations of the Fenton test of the non-cured reference membrane (48-Ref) and of the membrane which had been cured at 350 °C for 16 h under argon (48-Lo-C). Photographs of 48-Ref (A) and 48-Lo-C (B) after 80 h Fenton test.

After a weight loss of about 10%, the non-cured reference membrane 48-Ref started to spontaneously disintegrate after about 80 h in the Fenton solution (photography A, Figure 5). In contrast, the cured membrane 48-Lo-C was still in one mechanically stable piece (photography B, Figure 5) after 80 h which further confirmed the improved radical-oxidative resistance of crosslinked PBI.

Phosphoric acid doping

PA doping was achieved by submerging the membranes in 85% H_3PO_4 at temperatures ranging from room temperature (rt) to 100 °C, as summarized in Table 1.

At room temperature a doping level of about 10 was obtained during doping of the non-cured reference membrane 64-Ref which is in good agreement with the previously reported literature data.[33] On the other hand, the phosphoric acid uptake at room temperature of the thermally cured membranes 64-Sh-C and 64-Lo-C was very low and corresponded to acid doping levels of 1.2 and 0.1, respectively. It further confirms the strong resistance to swelling of the cured membranes, which is also a fundamental characteristic of a covalently crosslinked structure.[9,12,13] It is well known that elevated doping temperatures are required during doping of crosslinked PBI membranes in order to reach sufficient acid doping levels for any practical use in fuel cells. Analogously, higher PA doping levels could be reached by elevating the doping temperature of the cured membranes in the present study.

During doping at 70 °C, PA doping levels of 11.8 and 13.5 were obtained of the cured membranes 64-Sh-C and 64-Lo-C, respectively. After doping at this temperature the non-cured reference membrane 64-Ref was in a swollen gel-like state which was highly mechanically unstable and could not be handled. By further doping at 100 °C the non-cured reference membrane 64-Ref was completely dissolved. On the other hand, after doping at 100 °C in 85% H_3PO_4 for 16 h, the cured membranes 64-Sh-C and 64-Lo-C obtained PA doping levels of around 14 and could easily be handled without breaking. The heavily doped cured membranes exhibited good flexibility and sufficient mechanical strength for the MEA preparation.

No visual color change was observed in the concentrated H_3PO_4 solution during doping of the cured membranes at 100 °C. This further illustrates the very limited membrane solubility and further indicates that PBI changed from a thermoplastic polymer to a thermoset during the thermal treatment.

Table 1 PA doping of the non-cured reference membrane 64-Ref and of the cured membranes 64-Sh-C and 64-Lo-C.

Doping conditions	PA doping level		
	64-Ref	**64-Sh-C**	**64-Lo-C**
rt, 85% PA	10.2	1.2	0.1
70 °C, 85% PA	-	11.8	13.5
100 °C, 85% PA	Membrane dissolved	13.6	14.1

X-ray diffraction

Materials of crystalline polymers are most often stiffer, tougher and less soluble than their amorphous or semi-crystalline counterparts. For example, membranes of perfluorosulfonic acid (PFSA) such as Nafion® generally require annealing in order to develop the crystalline regions which makes them mechanically stable and insoluble in water.[34]

PBI, on the other hand, is known to be more or less amorphous. Generally, the *meta* configuration of PBI effectively prevents crystallization of the polymer due to the wrinkled linear structure which results in poor polymer chain packing.[22,35] This might also be the sole reason for the relatively good solubility of *m*-PBI in a limited number of highly polar aprotic organic solvents.[4]

The morphology of polybenzimidazoles can be modified by careful tuning of the reaction parameters during the polycondensation or by tailoring the structure of the polymer backbone.[35] For example, Scariah *et al.*[36] synthesized of set of *para* polybenzimidazole structure analogues containing flexibilizing spacers in the polymer backbone. The linear structure of the polymer dramatically affected the degree of crystallinity and thus its solubility. Employing a heat treatment procedure at temperatures up to 350 °C in combination with different aromatic reagents under pressure, Conciatori *et al.*[37] patented a process for increasing the crystallinity of various polybenzimidazole fibers. Furthermore, Arrieta *et al.*[38] heat treated PBI, Kevlar® and their blends at temperatures up to 320 °C for 1-15 days and the X-ray diffraction measurements showed a gradual increase of the crystallinity of the polymer blend during the heat treatment.

The wide angle X-ray diffractograms (WAXD) of the PBI membranes in the present study and their PA doped counterparts are shown in Figure 6A. As previously reported,[4,20] the pristine PBI membrane (64-Ref) was found to be fully amorphous. However, after a short heat treatment at 350 °C under inert atmosphere (64-Sh-C) a broad reflection centred around 18° was developed confirming an increase of the structural order within the membrane. For comparison, a similar broad reflection was reported for PBI precipitates which had been treated at temperatures up to 350 °C.[35]

The choice of membrane casting procedure and the nature of the solvent are also known to affect the morphology of the obtained PA doped membrane. For example, PBI membranes cast from mixtures of trifluoroacetic acid (TFA) and PA are considerably more crystalline compared with acid imbibed PBI membranes which have been cast from DMAc.[39] Furthermore, ABPBI membranes prepared by direct casting from methanesulfonic acid (MSA) and PA are considerably more

crystalline than the ABPBI membranes prepared by casting from MSA followed by PA imbibing.[40] The relatively high degree of crystallinity of the TFA cast membranes was reported to result in a PA doped membrane which was more rubbery and soft than the conventionally solution cast and acid imbibed membranes. The degree of crystallinity of the PA doped membranes could be further increased by heat treatment. Additionally, the membrane of higher crystallinity exhibited higher proton conductivity. It was suggested that the PA was forced into the amorphous regions, thus creating highly proton conducting pathways through the membrane cross-section.[41]

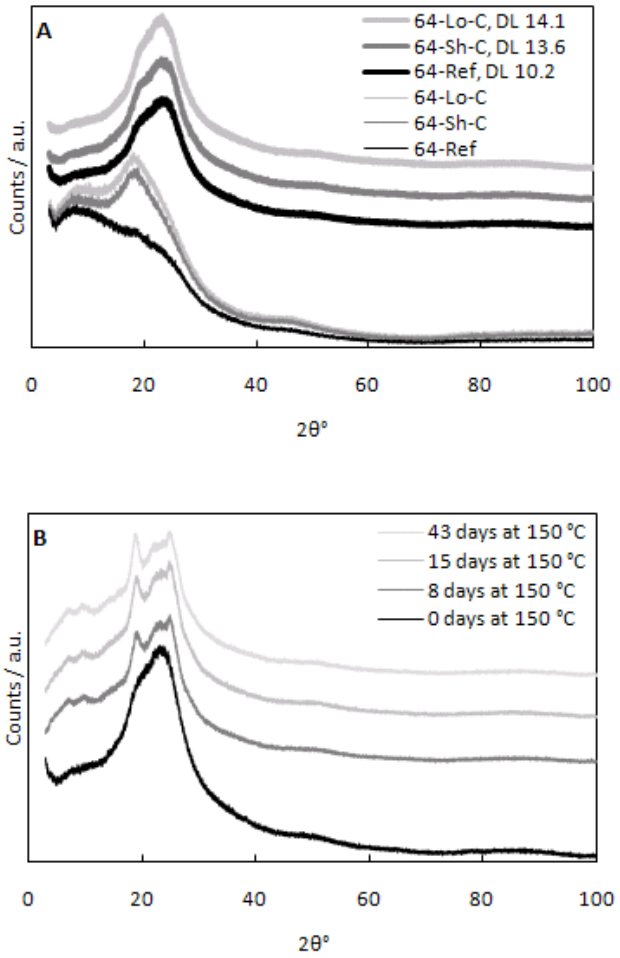

Fig. 6 X-ray diffractograms of the non-cured reference membrane 64-Ref and the cured membranes 64-Sh-C and 64-Lo-C before and after acid doping (A). The corresponding PA doping levels (DL) are indicated in the figure. X-ray diffractograms of the PA doped non-cured reference membrane 44-Ref (DL 12.5) after anhydrous thermal aging at 150 °C for up to 43 days (B).

ABPBI, which is the most simple structure analogue within the polybenzimidazole family, is known to exhibit a rather high degree of crystallinity. The degree of crystallinity can be further increased by heat treatment or by stretching the material in order to enhance the polymer chain orientation.[42] Cho *et al.*[43] showed that ABPBI membranes cast from EtOH/NaOH exhibit a crystalline uniplanar structure in which the aromatic rings are aligned parallel to the film surface. However, during doping in PA most of the crystalline order in the membrane was lost due to the extensive volume swelling and the concomitant polymer chain separation.

This was also confirmed in the present study. After PA doping all the membranes were apparently morphologically equal regardless of their thermal history. However, the acid doping levels varied between 10.2-14.1 depending on the thermal history of the membranes and the doping conditions. The diffraction data showed a broad reflection centred around 23° of all the acid doped membranes which corresponded well with the previously reported X-ray diffraction data of PA doped PBI membranes with a doping level of 4.8.[41]

During high temperature PEM fuel cell operating conditions the PA doped membrane is naturally subjected to temperatures in the 100-200 °C range for extended periods of time. It is thus of interest to study the effect of high temperatures on the morphology of PA doped PBI membranes. X-ray diffractograms were therefore recorded of the non-cured PA doped reference membrane (64-Ref) after anhydrous aging at 150 °C for up to about 6 weeks, as shown in Figure 6B. As also observed by Savinell *et al.*,[39] heat treatment of the PA doped PBI membrane resulted in a gradual increase of the degree of crystallinity. This was illustrated by the development of two relatively sharp reflections at 18.5° and at 23.5° during the thermal aging. For comparison, after PA impregnation of polybenzimidazoles containing alkyl spacers it was found that crystalline polymeric salts were developed only when an even number of $–CH_2–$ spacing groups separated the benzimidazole moieties. The X-ray diffractograms of the crystalline polymeric salt showed strong and relatively sharp reflections centered around 19.6° and 24.6°,[44] which is in good agreement with the diffraction pattern of the thermally aged membrane in the present study.

Mechanical strength

In order to study the correlation between the thermal history of PBI and the mechanical properties of the membranes after PA doping, stress-strain curves were recorded at room temperature as shown in Figure 7. The linear average molecular weight of PBI was also varied from 23-44 kDa since the mechanical properties of PA doped PBI membranes are known to be highly dependent on the linear average molecular weight of the polymer.[11] The mechanical data are also summarized in Table 2.

The PA doped membranes based on PBI with a linear average molecular weight of 23 kDa which had been cured at 350 °C under argon for different durations were obviously tougher compared with their non-cured counterpart of similar linear average molecular weight. For example, even though the PA doping level of the cured membrane 23-Lo-C was about 20% higher compared with that of its non-cured counterpart (23-Ref) the yield stress was almost twice as high. Furthermore, the elongation at break gradually decreased with increasing curing time from about 140% for the non-cured reference membrane 23-Ref to about 80% for the membrane which had been cured for 16 h (23-Lo-C), indicating reduced polymer chain mobility. Additionally, the resistance to plastic deformation of the PA doped cured membrane 23-Lo-C was considerably higher than that of its non-cured counterpart (23-Ref) as indicated by a steeper slope of the stress-strain curve beyond the yield point.

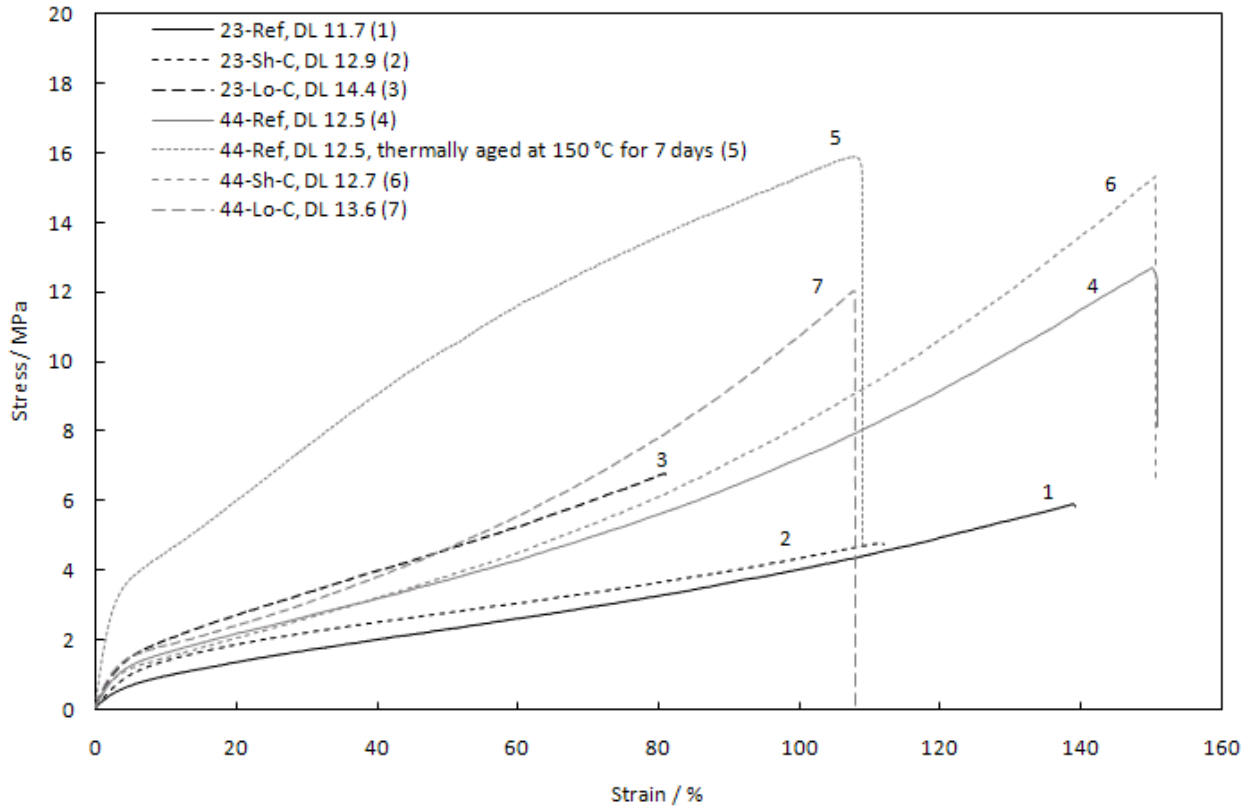

Fig. 7 Representative stress-strain curves at room temperature of membranes with different thermal history and initial linear average molecular weights of 23 kDa (23-Ref, 23-Sh-C and 23-Lo-C) and 44 kDa (44-Ref, 44-Sh-C and 44-Lo-C). The corresponding acid doping levels (DL) are indicated in the figure. A representative stress-strain curve of the PA doped 44-Ref membrane which had been thermally aged at 150 °C for 7 days is also shown.

Table 2 Summary of the mechanical data at room temperature. The membrane types and the corresponding PA doping levels are indicated in the table. The reported values are the average values of at least 5 samples and the errors represent the corresponding standard deviations.

Membrane type	Young´s modulus (MPa)	Engineering tensile stress at break (MPa)	Elongation at break (%)
23-Ref, DL 11.7	10.9 ± 0.9	5.7 ± 0.4	136 ± 11
23-Sh-C, DL 12.9	17.6 ± 1.5	4.7 ± 1.3	111 ± 37
23-Lo-C, DL 14.4	27.9 ± 1.4	5.7 ± 1.6	67 ± 21
44-Ref, DL 12.5	26.3 ± 1.5	13.3 ± 1.1	155 ± 7
44-Sh-C, DL 12.7	27.6 ± 3.2	14.4 ± 1.4	144 ± 8
44-Lo-C, DL 13.6	37.1 ± 2.7	12.1 ± 1.0	108 ± 5
44-Ref, DL 12.5, Thermally aged at 150 °C for 7 days	113.8 ± 14.7	14.7 ± 0.9	96.4 ± 13.9

Despite the higher PA doping level, the Young´s modulus of the cured membrane 23-Lo-C was nearly 3 times higher compared with that of its non-cured counterpart (23-Ref). The mechanical toughening after the thermal induced curing of the membranes having an intermediate linear average molecular weight of 44 kDa was not as obvious. However, as expected[11] the mechanical properties in terms of the engineering tensile stress at break as well as the Young´s modulus of the non-cured reference membrane were considerably improved when the initial linear average molecular weight of PBI was increased from 23 kDa (23-Ref) to 44 kDa (44-ref). For example, even though the PA doping level was slightly higher the Young´s modulus was nearly doubled when the linear average molecular weight was increased from 23 kDa (23-Ref) to 44 kDa (44-Ref). The Young´s modulus of the cured membrane 23-Lo-C was similar to that of the non-cured reference membrane with a higher initial average molecular weight of 44 kDa (44-Ref). On the other hand, the Young´s modulus of the 44 kDa linear average molecular weight non-cured reference membrane (44-Ref) was considerably lower compared with that of the membrane with a similar linear average molecular weight but lower phosphoric acid doping level,[13] which further illustrates the strong plasticizing effect of PA.

The cured membranes which were prepared from PBI with a linear average molecular weight of 44 kDa (44-Sh-C and 44-Lo-C) showed lower elongation at break and a steeper slope of the stress-strain curve beyond the yield point compared with its non-cured counterpart (44-Ref). It indicates increased resistance to plastic deformation and increasing rigidity in the rubbery region. Furthermore, the Young´s modulus of the cured membrane 44-Lo-C was slightly higher compared with that of its non-cured counterpart (44-Ref), even though the PA doping level was about 9% higher.

Conclusively, the mechanical characteristics of the PBI membranes which had been cured under argon at 350 °C for

different durations prior to the PA doping resembled those of previously reported covalently crosslinked and PA doped PBI membranes[9,12,13] and what can be expected for a crosslinked structure. However, the degree of cure was either relatively small or chemically rather non-uniform since no deviations could be observed in the FTIR spectrum of the cured membranes which could be assigned to crosslinking, as also discussed by Gillham.[21]

On the other hand, mechanical toughening of a polymeric material can also be expected if the degree of crystallinity is increased.[45] As previously reported[39] and as revealed by the X-ray diffraction data in Figure 6B the degree of crystallinity was considerably increased during thermal ageing of the PA doped membranes. The increased crystallinity of the thermally aged PA doped membrane 44-Ref in the present study was illustrated on a macroscopic scale by a 300% increased elastic modulus from about 26 MPa to around 114 MPa after 7 days at 150 °C. Furthermore, the stress at yield was increased from 1.2 MPa to 3.7 MPa whereas the engineering tensile stress at break was slightly increased from 13.3 MPa to 14.7 MPa.

Proton conductivity

As shown in Figure 8, the anhydrous proton conductivity of the PA doped cured membranes (64-Sh-C and 64-Lo-C) was somewhat higher than that of the PA doped non-cured reference membrane 64-Ref, apparently due to the slightly higher PA contents.[46] At 150 °C it varied between 0.04-0.06 S cm^{-1} depending on the acid doping level of the membrane. The conductivity data were in good agreement with that of covalently[9,12,13] or ionically[17] crosslinked PBI based membranes or PBI structure analogue based membranes[18] of similar doping levels.

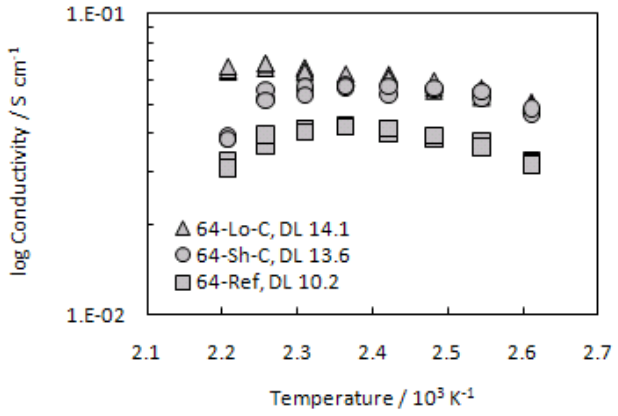

Fig. 8 Anhydrous proton conductivity of the PA doped non-cured reference membrane 64-Ref and of the cured membranes 64-Sh-C and 64-Lo-C. The corresponding doping levels (DL) are indicated in the figure.

The proton conductivity of PA solutions is strongly dependent on the water content. For example, at 20 °C the conductivity of 100% and 45% PA was reported to differ by about an order of magnitude. It was increased from 0.025 S cm^{-1} to 0.22 S cm^{-1} when the H_3PO_4 concentration was reduced from 100% to 45%.[47] At temperatures around 170 °C and without active humidification, H_3PO_4 dehydrates to pyrophosphoric or higher phosphoric acid oligomers which are less proton conducting than ortophosphoric acid.[48] Hence, the conductivity at temperatures at or above 170 °C should be strongly dependent on the water content of the membrane. The phosphoric acid dehydration was illustrated in the present study by a proton conductivity decay at temperatures above 160 °C. A similar effect has also been observed for PA doped PBI membranes of low doping levels cast from TFA/PA[46] as well as for PA doped PBI with very high acid doping levels prepared according to the sol-gel methodology.[10]

Fuel cell test

Continuous steady state operation at a constant load in the 150-160 °C temperature range is a mild mode for PA doped PBI based fuel cells. The complete absence of liquid water minimizes the risk for the PA wash-out, which is of critical concern for the long term durability of the cells since it would gradually reduce the membrane conductivity.[49] The constant temperature also minimizes the stresses connected to thermal expansion or contraction of the different layers in the MEA and therefore the deterioration of the membrane electrode interface. Furthermore, the cell voltage during steady state operation is considerably lower than the OCV which minimizes the oxidation rate of the carbon based catalyst support materials as well as the dissolution of the noble metals which is very much potential dependent. The catalyst degradation rate can thus be expected to be considerably reduced if fuel cell idling can be circumvented.[50] In other words, the major cause of failure of a PBI based fuel cell under the steady state operation mode is most likely connected to the membrane degradation.

Polarization curves of the MEA based on the cured membrane 48-Lo-C were recorded after continuous fuel cell operation at a constant current load of 600 mA cm^{-2} for up to about 1800 h, as shown in Figure 9. The OCV was slightly decreased during the first 1800 h of operation from 818 mV to 791 mV which was most likely due to the gradual increased gas permeability of the membrane. In the higher current density range the ageing of the MEA was illustrated by a steeper slope of the polarization curve in the linear region. The increased ohmic resistance over time could eventually be explained by the leakage of PA through steam distillation. It has previously been reported to be one of the major degradation mechanisms of PA doped PBI based fuel cells, especially during high load operation when the water formation rate is high.[49] The gradual decrease of the fuel cell performance over time was also illustrated by a reduced power density, especially in the high current density range.

Several long term durability investigations of PA doped PBI or PBI structure analogue based high temperature PEM fuel cells operated at constant load or in load cycling mode have been published during the last decade.[10,49,51-56] However, during the steady state tests the cells were generally operated at a rather low current load of 200 mA cm^{-2}. For example, BASF-PEMEAS[53] has demonstrated a life time exceeding 20000 hours at 160 °C and at a constant current load of 200 mA cm^{-2}. The average cell voltage decay rate during operation was estimated to about 5-6 µV h^{-1}. Similar measurements were made by Yu *et al.* [49] under steady-state conditions, showing an average voltage decay rate of 4.9-6.3 µV h^{-1} at 160°C. The water formation rate at the cathode naturally increases with the current density which also dramatically increased the PA loss due to steam distillation, especially at high operating temperatures in the 180-190 °C range. The effect of operating temperature was further illustrated by the reduction of the demonstrated lifetime of 5000-20000 h to

a few hundreds of hours when the operating temperature was increased from 150-160 °C to 180-200 °C.[57] This was apparently due to membrane failure because the eventual death of the cell was accompanied by a sudden increase of the gas permeability.

Conclusively, the long lifetimes or the very low voltage decay rates reported for the PA doped PBI based fuel cells were typically achieved during continuous operation at 120-160 °C and at rather low current loads of typically 200 mA cm^{-2}. At higher current densities much higher voltage decay rates have been reported. For example, during steady state operation at a constant current load of 400 mA cm^{-2} at 160 °C for 1150 h the average cell voltage decay rate was about 43 μV h^{-1}.[10] Furthermore, Li and Scott[58] operated a PTFE reinforced PA doped PBI based MEA in start/stop fuel cell mode at a constant load of 700 mA cm^{-2}, showing an obvious gradual decay of the cell voltage during 50 h.

The low cell voltage decay rate during continuous fuel cell operation at 160 °C at a low current load of 200 mA cm^{-2} was confirmed in the present study, as shown in Figure 10. Under these conditions the cell based on the non-cured reference membrane 48-Ref showed an average voltage decay rate of about 5-6 μV h^{-1} during about 2000 h of operation. The initial cell voltage of the MEA based on the cured membrane 48-Lo-C operating at 200 mA cm^{-2} (0.60 V) was practically identical with that of the MEA based on its non-cured counterpart (0.61 V). However, a current load malfunction of the cell based on the cured membrane 48-Lo-C occurred after about 100 h of operation which resulted in load cycling mode in the 100-1050 h range. During this period the current density varied between 0-200 mA cm^{-2} which implies that the cell voltage varied between OCV and about 0.6 V. This type of load cycling is well known to enhance the degradation rate of the MEA[49, 53] which was illustrated in the present study by a slightly higher average cell voltage decay rate of 13 μV h^{-1} during about 2000 h operation.

At a constant current load of 600 mA cm^{-2} the MEA based on the 20 μm thick non-cured reference membrane (48-Ref) showed an average cell voltage decay rate of about 630 μV h^{-1}. When the membrane thickness of the non-cured reference membrane (48-Ref) was doubled to 40 μm the average cell voltage decay rate was reduced to about 308 μV h^{-1}. The cell voltages of the two cells reached zero after about 750 h and 1550 h, respectively, which indicate complete membrane failure. Obviously, by reducing the thickness of the membrane by 50% the average cell voltage decay rate was doubled which further confirms that the cell voltage decay during operation at high current load is strongly connected to the membrane degradation. The MEA based on the PBI membrane which had been cured at 350 °C for 16 h under argon prior to doping in 85% H_3PO_4 at 100 °C (48-Lo-C), on the other hand, showed a considerably lower average cell voltage decay rate of 43 μV h^{-1}. After 1800 h of continuous operation at a current load of 600 mA cm^{-2}, the cell voltage had decreased from about 0.49 V to 0.41 V.

The results confirm that the long term durability of PBI based high temperature PEM fuel cells is highly dependent on the membrane characteristics. The fuel cell durability at practical load of 600 mA cm^{-2} could obviously be dramatically improved by introducing a thermal treatment step of the membrane before acid doping and the MEA manufacturing. In this way, the average fuel cell voltage decay rate could be reduced by as much as 86% which naturally should facilitate the commercial competitiveness of the technology.

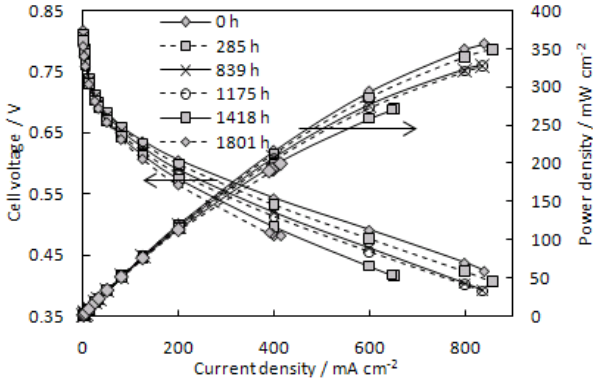

Fig. 9 Polarization data of the MEA based on the membrane which had been cured at 350 °C for 16 h under argon (48-Lo-C) prior to the acid doping. The polarization curves were recorded after fuel cell operation at a constant load of 600 mA cm^{-2} for up to 1801 h.

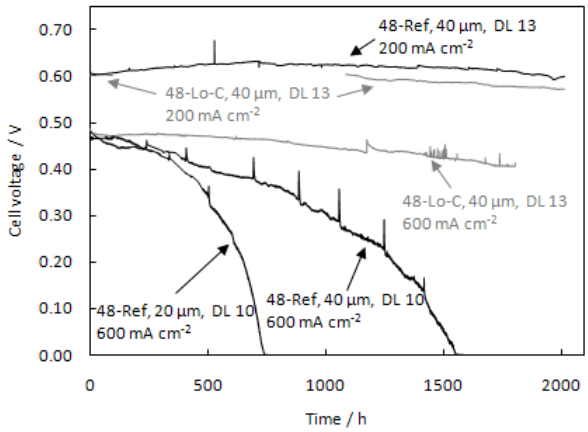

Fig. 10 Fuel cell voltages as functions of time of the MEAs based on non-cured PBI (48-Ref, black lines) and PBI which had been cured at 350 °C for 16 h under argon (48-Lo-C, grey lines) prior to the acid doping. The cells were operated at current loads of 200 mA cm^{-2} or 600 mA cm^{-2}. The corresponding membrane thicknesses and doping levels (DL) are indicated in the figure.

Conclusions

The thermochemical properties of PBI were investigated using ATR-FTIR in combination with TGA/DTA. PBI was found to irreversibly cure during heat treatment at 350 °C under argon atmosphere. The change from a thermoplastic to a thermoset was illustrated by a dramatically reduced solubility and improved radical-oxidative stability. The thermal treatment also increased the structural order within the membrane as confirmed by X-ray diffraction. After PA doping, all membranes were apparently morphologically equal. The PA doped cured PBI membranes were considerably tougher than their non-cured counterparts even though the acid doping levels were higher. During continuous fuel cell operation at 160 °C for 2000 h at a low current load of 200 mA cm^{-2} the average cell voltage decay rate of the MEA based on the non-cured membrane was 5-6 μV h^{-1}.Under similar operating conditions but at a considerably higher current load of 600 mA cm^{-2} the average cell voltage decay rates of the MEAs

based on the non-cured membrane and the cured membrane were 308 μV h^{-1} and 43 μV h^{-1}, respectively. The results confirm that the long term durability of PBI based high temperature PEM fuel cells is highly dependent on the membrane characteristics, especially at high current loads.

Acknowledgements

Danish Power Systems ApS is gratefully acknowledged for donating materials. Funding of this work is acknowledged from the Danish ForskEL programme, the Danish National Research Foundation and the Danish Energy Agency.

References

1 J. S. Wainright, J. T. Wang, D. Weng, R. F. Savinell and M. Litt, *J. Electrochem. Soc.*, 1995, **142**, L121-L123.
2 Q. Li, J. O. Jensen, R. F. Savinell and N. J. Bjerrum, *Prog. Polym. Sci.*, 2009, **34**, 449-477.
3 T. S. Chung, *J. Macromol. Sci., Rev. Macromol. Chem. Phys.*, 1997, **C37**, 277-301.
4 H. Vogel and C. S. Marvel, *J. Polym. Sci.*, 1961, **50**, 511-&.
5 E. W. Neuse, *Adv. Polym. Sci.*, 1982, **47**, 1-42.
6 Y. Iwakura, Y. Imai and K. Uno, *J. Polym. Sci., Part A: General Papers*, 1964, **2**, 2605-2615.
7 E. W. Choe and D. D. Choe, in *Polymeric Materials Encyclopedia*, ed. J. C. Salamone, CRC Press, New York, 1996, vol. 7, pp. 5619-5638.
8 J. S. Wainright, M. H. Litt and R. F. Savinell, in *Handbook of Fuel Cells: Fundamentals, Technology and Applications*, eds. W. Vielstich, A. Lamm and H. A. Gasteiger, John Wiley & Sons Ltd, Chichester, 2003, vol. 3, pp. 436-446.
9 Q. Li, C. Pan, J. O. Jensen, P. Noyé and N. J. Bjerrum, *Chem. Mater.*, 2007, **19**, 350-352.
10 L. X. Xiao, H. F. Zhang, E. Scanlon, L. S. Ramanathan, E. W. Choe, D. Rogers, T. Apple and B. C. Benicewicz, *Chem. Mater.*, 2005, **17**, 5328-5333.
11 R. H. He, Q. Li, A. Bach, J. O. Jensen and N. J. Bjerrum, *J. Membr. Sci.*, 2006, **277**, 38-45.
12 P. Noyé, Q. Li, C. Pan and N. J. Bjerrum, *Polym. Adv. Technol.*, 2008, **19**, 1270-1275.
13 D. Aili, Q. Li, E. Christensen, J. O. Jensen and N. J. Bjerrum, *Polym. Int.*, 2011, **60**, 1201-1207.
14 S. Yu, H. Zhang, L. Xiao, E. W. Choe and B. C. Benicewicz, *Fuel Cells*, 2009, **9**, 318-324.
15 M. Han, G. Zhang, Z. Liu, S. Wang, M. Li, J. Zhu, H. Li, Y. Zhang, C. M. Lew and H. Na, *J. Mater. Chem.*, 2011, **21**, 2187-2193.
16 J. Kerres, F. Schönberger, A. Chromik, T. Häring, Q. Li, J. O. Jensen, C. Pan, P. Noyé and N. J. Bjerrum, *Fuel Cells*, 2008, **8**, 175-187.
17 Q. Li, J. O. Jensen, C. Pan, V. Bandur, M. S. Nilsson, F. Schönberger, A. Chromik, M. Hein, T. Häring, J. Kerres and N. J. Bjerrum, *Fuel Cells*, 2008, **8**, 188-199.
18 Q. Li, H. C. Rudbeck, A. Chromik, J. O. Jensen, C. Pan, T. Steenberg, M. Calverley, N. J. Bjerrum and J. Kerres, *J. Membr. Sci.*, 2010, **347**, 260-270.
19 D. Aili, M. K. Hansen, C. Pan, Q. Li, E. Christensen, J. O. Jensen and N. J. Bjerrum, *Int. J. Hydrogen Energy*, 2011, **36**, 6985-6993.
20 H. H. Levine, in *Encyclopedia of Polymer Science and Technology* eds. N. M. Bikales, J. Conrad, A. Ruks and J. Perlman, Interscience New York, 1969, vol. 11, pp. 188-232.
21 J. K. Gillham, *Science*, 1963, **139**, 494-495.
22 V. I. Kasatochkin, V. V. Korshak, V. V. Kurashev, Z. S. Smutkina, T. M. Frunze and T. M. Khrenkova, *Dokl. Chem. Technol.*, 1964, **159**, 843-846.
23 W. F. Hwang, D. R. Wiff, C. Verschoore, G. E. Price, T. E. Helminiak and W. W. Adams, *Polym. Eng. Sci.*, 1983, **23**, 784-788.
24 P. Musto, F. E. Karasz and W. J. MacKnight, *Polymer*, 1993, **34**, 2934-2945.
25 G. P. Shulman and W. Lochte, *J. Macromol. Sci., Part A: Chem.*, 1967, **A1**, 413-428.
26 R. A. Gaudiana and R. T. Conley, *Polym. Lett.*, 1969, **7**, 793-801.
27 R. T. Conley, J. J. Kane and S. Ghosh, *Mechanism of thermal oxidation of the benzimidazole system*, Technical Report AFML-TR-71-219, Department of Chemistry, Wright State University, Dayton, 1971.
28 C. A. Linkous, *Int. J. Hydrogen Energy*, 1993, **18**, 641-646.
29 A. Buckley, D. Stuetz and G. A. Serad, in *Encyclopedia of Polymer Science and Engineering*, ed. J. I. Kroschwitz, Wiley, New York, 1987, vol. 11, pp. 572-601.
30 J. H. Liao, Q. F. Li, H. C. Rudbeck, J. O. Jensen, A. Chromik, N. J. Bjerrum, J. Kerres and W. Xing, *Fuel Cells*, 2011, doi: 10.1002/fuce.201000146.
31 Z. Chang, H. Pu, D. Wan, L. Liu, J. Yuan and Z. Yang, *Polym. Degrad. Stab.*, 2009, **94**, 1206-1212.
32 A. D. Modestov, M. R. Tarasevich, V. Y. Filimonov and N. M. Zagudaeva, *Electrochim. Acta*, 2009, **54**, 7121-7127.
33 Q. Li, R. H. He, R. W. Berg, H. A. Hjuler and N. J. Bjerrum, *Solid State Ionics*, 2004, **168**, 177-185.
34 G. Gebel, P. Aldebert and M. Pineri, *Macromolecules*, 1987, **20**, 1425-1428.
35 S.-i. Kohama, J. Gong, K. Kimura, S. Yamazaki, T. Uchida, K. Shimamura and K. Kimura, *Polymer*, 2008, **49**, 1783-1791.
36 K. J. Scariah, V. N. Krishnamurthy, K. V. C. Rao and M. Srinivasan, *J. Polym. Sci., Part A: Polym. Chem.*, 1987, **25**, 2675-2687.
37 *US Pat.*, 3 495 931, 1970.
38 C. Arrieta, E. David, P. Dolez and T. Vu-Khanh, *Polym. Compos.*, 2011, **32**, 362-367.
39 R. F. Savinell, J. S. Wainright and M. Litt, *Electrochem. Soc. Proc.*, 1999, **98-27**, 81-87.
40 J. A. Asensio, S. Borros and P. Gomez-Romero, *J. Membr. Sci.*, 2004, **241**, 89-93.
41 M. Litt, R. Ameri, Y. Wang, R. Savinell and J. Wainright, in *Solid State Ionics V*, eds. G. A. Nazri, C. Julien and A. Rougier, Materials Research Society, Warrendale, 1999, vol. 548, pp. 313-323.
42 W. F. Hwang, D. R. Wiff, C. L. Benner and T. E. Helminiak, *J. Macromol. Sci., Phys.*, 1983, **B22**, 231-257.
43 J. Cho, J. Blackwell, S. N. Chvalun, M. Litt and Y. Wang, *J. Polym. Sci., Part B: Polym. Phys.*, 2004, **42**, 2576-2585.
44 S. M. Aharoni, *J. Appl. Polym. Sci.*, 1982, **27**, 989-995.
45 M. P. Stevens, *Polymer Chemistry - An Introduction*, Oxford University Press, New York, 3rd edn., 1999, pp. 79-83.
46 Y. L. Ma, J. S. Wainright, M. H. Litt and R. F. Savinell, *J. Electrochem. Soc.*, 2004, **151**, A8-A16.
47 R. H. He, Q. Li, G. Xiao and N. J. Bjerrum, *J. Membr. Sci.*, 2003, **226**, 169-184.
48 A. Schechter and R. F. Savinell, *Solid State Ionics*, 2002, **147**, 181-187.
49 S. Yu, L. Xiao and B. C. Benicewicz, *Fuel Cells*, 2008, **8**, 165-174.
50 Z. Qi and S. Buelte, *J. Power Sources*, 2006, **161**, 1126-1132.
51 C. Wannek, B. Kohnen, H. F. Oetien, H. Lippert and J. Mergel, *Fuel Cells*, 2008, **8**, 87-95.
52 T. J. Schmidt and J. Baurmeister, *ECS Trans.*, 2006, **3**, 861-869.
53 T. J. Schmidt and J. Baurmeister, *J. Power Sources*, 2008, **176**, 428-434.
54 J. A. Mader and B. C. Benicewicz, *Fuel Cells*, 2011, **11**, 222-237.
55 J. A. Mader and B. C. Benicewicz, *Macromolecules*, 2010, **43**, 6706-6715.
56 F. J. Pinar, P. Cañizares, M. A. Rodrigo, D. Úbeda and J. Lobato, *J. Power Sources*, 2011, **196**, 4306-4313.
57 Q. Li and J. O. Jensen, in *Membranes for Energy Conversion*, eds. K. V. Peinemann and S. P. Nunes, WILEY-VCH Verlag GmbH & Co. KGaA, Weinheim, 2008, vol 2, pp. 61-96.
58 M. Li and K. Scott, *Electrochim. Acta*, 2010, **55**, 2123-2128.

Notes and references

[a] *Technical University of Denmark, Department of Chemistry, Kemitorvet 207, Kgs. Lyngby, Denmark. Fax: +45 4588 3136; Tel: +45 45 25 23 18; E-mail: lqf@kemi.dtu.dk*